Assessments of roles for calreticulin in antigen presentation

by

Natasha Del Cid

A dissertation submitted in partial fulfillment
of the requirements for the degree of
Doctor of Philosophy
(Immunology)
in The University of Michigan
2012

Doctoral Committee:

Professor Malini Raghavan, Chair
Professor Robert S. Fuller
Professor Kyung-Dall Lee
Professor Yang Liu
Assistant Professor Yasmina Laouar

Acknowledgments

I would like to first thank my family for all their support. Their complete and unwavering confidence in me has made me believe that anything truly is possible in this life.

I am additionally thankful for all the scientific support and guidance that Malini Raghavan has given me throughout these years. The training during my graduate career was the foundation of my scientific career and all things to come.

I would like to thank Rob Peters for all his companionship throughout this phase in my life. Our scientific conversations were invaluable and have helped shaped me into the scientist I am today. I can also confidently call myself a true athlete and a better person because of Rob Peters. He was my confidant at all hours of the day and night, and for that I will forever be grateful. My graduate school career and thesis will forever be tied to Rob Peters.

I am grateful for my boyfriend turned husband, Chris, for all his support and for infusing so much love, music, food, travel and culture into our lives. I would also like to thank all my friends with whom I have had endless conversations with about everything and nothing. In no specific order, Jennifer Oliver, Cailin Wilke, Beth Lubeck, Phil Lapinski, Phil King, Joel Swanson, Chris Perria, Elise Jeffery, Tim Bauler, Ericca Stamper, Sanjeeva Wijeyesakere, Monem Rizvi, Sukhmani Bedi, and Suzanne Speck.

I would also like to acknowledge Zarinah Aquil for always having smiles for me and for all of her hard work. We are all so grateful for having you with us.

I would also like to thank my committee and collaborators for all of their suggestions and support in the form of ideas and reagents.

Finally, I would like to acknowledge all the mice that gave their lives for these experiments.

Table of Contents

List of Figures

List of Abbreviations

APC Antigen presenting cell

β2m β2 microglobulin

BMDC Bone marrow-derived DC

BM Mϕ Bone marrow-derived Mϕ

DC Dendritic cell

ER Endoplasmic Reticulum

ERAD ER-associated degradation

G1M3 Glcα1–3Manα1– 2Manα1–2Man-OH

HSP Heat shock protein

LLO Listeriolysin O

Mϕ Macrophage

MEF Mouse embryonic fibroblast

MHC Major Histocompatibility Complex

NEM *N*-Ethylmaleimide

OVA Ovalbumin

PLC Peptide loading complex

PS Phosphatidylserine

TAP Transporter associated with antigen processing

TCR T cell receptor

Abstract

MHC class I molecules are important glycoproteins of the adaptive immune response. Assembly of MHC class I molecules occurs in the endoplasmic reticulum (ER) of cells. A group of proteins termed the MHC class I peptide-loading-complex (PLC) facilitate the assembly of MHC class I molecules. Calreticulin, a member of the PLC, is a soluble ER chaperone that aids in the folding of nascent glycoproteins via a glycan-binding site contained within a globular lectin-like domain. Calreticulin also interacts with ERp57, a thiol-oxidoreductase that facilitates disulfide isomerization in calreticulin-associated glycoproteins. Although it is widely accepted that calreticulin utilizes its lectin-like domain to chaperone glycoproteins, calreticulin can also suppress aggregation of non-glycosylated substrates *in vitro* under conditions of ER-stress. Thus, the cellular modes of substrate binding by calreticulin remain unclear and somewhat controversial. To this end, we focus on characterizing requirements for calreticulin recruitment into the PLC and identifying substrates of calreticulin within the PLC. Although calreticulin is typically ER-localized, under conditions of cell-stress, tumorigenesis, or cell-death, calreticulin migrates to the cell-surface where it acts as a pro-phagocytic signal. Soluble extracellular calreticulin is also suggested to mediate endocytosis of associated antigen. Thus, we investigated whether calreticulin-mediated phagocytosis or endocytosis translates to enhanced presentation of exogenous antigen to CD8 T-cells. In sum, we assess mechanisms relevant to calreticulin-mediated protein folding in the ER, and impacts of extracellular calreticulin upon presentation of exogenous antigen to CD8 T-cells.

We show that calreticulin recruitment into the PLC is mediated via glycan and ERp57-dependent interactions. Additionally tapasin, an assembly factor for MHC class I molecules, is a key substrate for calreticulin recruitment into the PLC, and tapasin itself is a calreticulin substrate. We also show that the pro-phagocytic/endocytic role of calreticulin *per se* does not impact CD8 T-cell

responses against cell-associated, peptide, bead-associated, or fused antigen. We investigate factors that may have rendered calreticulin-mediated phagocytosis non-essential, including impacts of innate stimulation and alternative modes of antigen transfer. Together, these findings allow for a better understanding of the chaperone function of calreticulin in the ER and mechanisms relevant to inducing CD8 T-cell responses against soluble and cell-associated antigens.

Chapter 1
Introduction

MHC class I antigen presentation to CD8 T cells

Major histocompatibility complex (MHC) class I molecules are expressed on the surface of all nucleated cells (Figure 1.1). These molecules typically present peptides derived from intracellular proteins to T cell receptors (TCR) of CD8 T cells. The MHC class I molecule – TCR interaction (Figure 1.2) is crucial for the development, maintenance, tolerance and activation of CD8 T cells (Ernst et al., 1999; Goldrath and Bevan, 1999; Kieper and Jameson, 1999; Koller et al., 1990; Luckashenak et al., 2008).

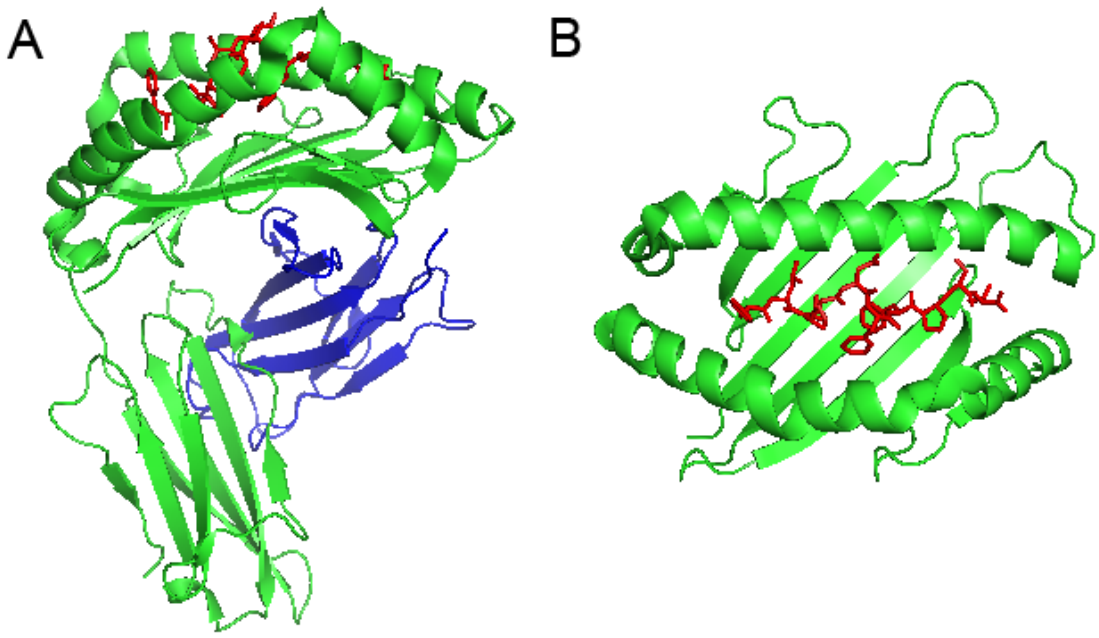

Figure 1.1. Crystal structure of a human MHC class I molecule in complex with a peptide [PDB ID 3OXR; (Liu et al., 2011)]. (A) MHC class I heavy chain (depicted in green) in shown in complex with the light chain β2m (depicted in blue). The heavy chain is made up of three domains: a membrane bound immunoglobulin-like domain (α_3) and the folded α_1 and α_2 domains, which form the peptide binding groove. The light chain (β2m) is composed of an immunoglobulin-like domain and is non-covalently bound to the heavy chain. (B) Top view of the MHC class I peptide binding groove. The peptide sitting within the binding groove is depicted in red in both *A* and *B*.

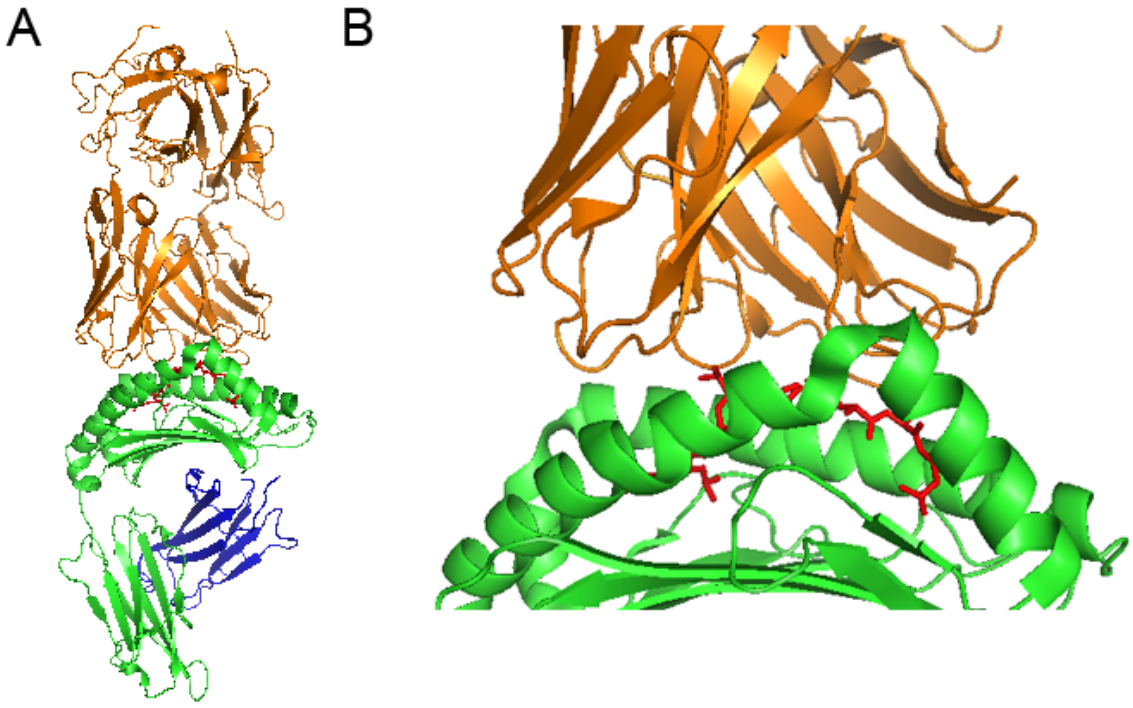

Figure 1.2. Crystal structure of a TCR binding to a MHC class I–peptide complex [PDB ID 3O4L; (Miles et al., 2010)]. (A, B) The TCR (depicted in orange) simultaneously binds residues of the MHC class I heavy chain (depicted in green) and peptide (depicted in red). β2m is depicted in blue. A close up of the interaction between TCR and MHC class I – peptide complex is shown in *B*.

The activation of CD8 T cells by antigen presenting cells (APC) occurs primarily in secondary lymphoid organs (lymph nodes and spleen) and requires two signals (Figure 1.3). Signal 1 involves signaling through the TCR; this signal is provided by a MHC class I molecule – peptide complex against which the TCR is specific. This interaction alone will not result in the activation of the CD8 T cell. If a CD8 T cell receives TCR stimulation in the absence of Signal 2, the T cell will become unable to further respond to stimulation (anergy). Anergy is thought to prevent the activation of self-reactive CD8 T cells and contribute to maintaining peripheral tolerance. Cell surface molecules on the APC that are upregulated in response to pathogens or inflammatory environment provide

signal 2. The best-characterized molecules that provide signal 2 (co-stimulatory molecules) on APCs are B7.1 (CD80) and B7.2 (CD86), which interact with CD28 on the CD8 T cell.

Under steady-state conditions, MHC class I molecules on APCs are loaded with self-derived peptides. Additionally, surface levels of MHC class I and other co-stimulatory molecules are relatively low. When APCs are exposed to foreign pathogens or inflammatory cytokines, the APCs undergo a process called maturation, which includes the up-regulation MHC and co-stimulatory molecules. The phagocytic capacity of mature APCs is diminished and APC efforts are diverted to processing of antigen and loading it onto MHC molecules to stimulate T cell activation. As the APCs migrate to the nearest draining lymph node, maturation continues. Pathogenic material acquired via phagocytosis or direct infection is processed into smaller peptides to be loaded onto MHC molecules. In the draining lymph node, the migrating APCs (and resident lymph node APCs that have been exposed to the foreign pathogen) activate naïve CD8 T cells that bind APCs via interactions mediated by the TCR and MHC class I – pathogen derived peptide complexes [reviewed in (Sille et al., 2005)]. Depending on the pathogen and extent of inflammation within the lymph node, CD4 T cell help may be required for the activation of CD8 T cells. MHC class II molecules present peptides derived from extracellular proteins to CD4 TCR. MHC class II molecules are highly similar in structure to MHC class I molecules. The most notable differences between the two are that 1) the ends of the peptide binding cleft of MHC class II molecules are open, permitting the loading of longer peptides, and 2) MHC class II molecules are made up of two membrane bound dimers (the α and β chain) whereas MHC class I is made up of a membrane bound α chain and soluble β2m [reviewed in (Wolf and Ploegh, 1995)]. CD4 T cell help comes in the form of cytokines and ligands that activate APCs. Activated CD4 T cells secrete inflammatory IFNγ and upregulate cell surface CD40L, the latter of which binds to CD40 on the APC. The CD40L-CD40 interaction and IFNγ both induce the upregulation of co-stimulatory molecules on the APC, which provides Signal 2 to the CD8 T cell. Once a CD8 T cell is activated, it clonally expands and migrates out of the lymph node to the site of infection. In addition to TCR and CD28 signaling,

inflammatory cytokines such as IL-12 help in expanding the antigen-specific CD8 T cell population in the lymph node.

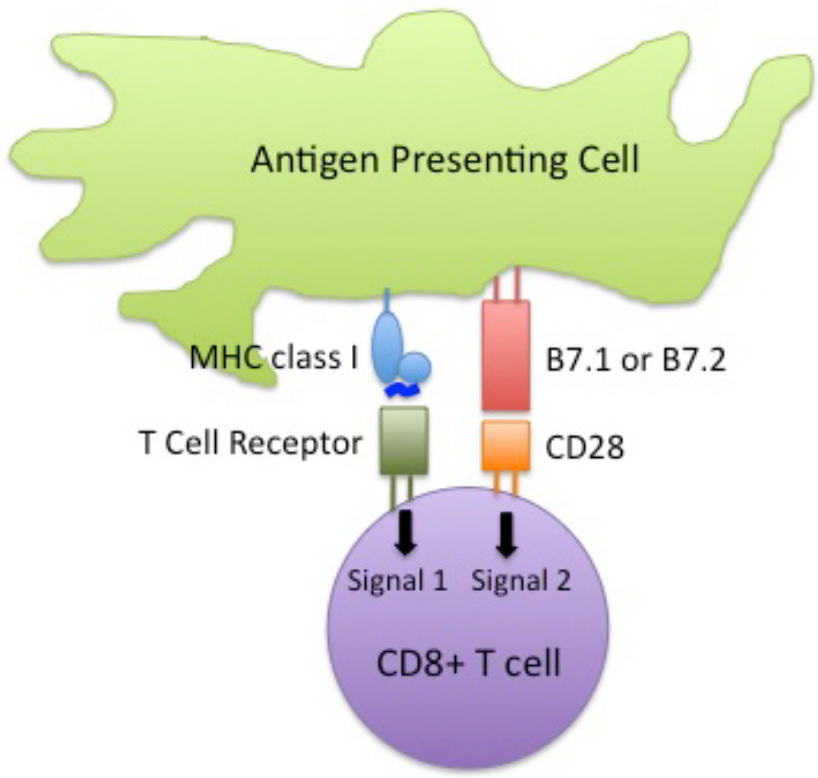

Figure 1.3. Naïve CD8 T cells require two signals provided by APCs for activation. Upon exposure to pathogens, inflammatory cytokines or CD40 engagement on the APC by CD40L expressed on activated CD4 T helper cells, APCs upregulate the co-stimulatory molecules B7.1 and B7.2. These molecules provide Signal 2 to the naïve CD8 T cell. TCR signaling via MHC class I-peptide engagement provides Signal 1 to the naïve CD8 T cell. Upon receiving both signals, naïve CD8 T cells clonally expand and differentiate into cytotoxic effector T cells.

In the periphery, the CD8 T cell engages with cellular MHC class I molecule – peptide complexes of the same specificity as that which caused initial activation of the CD8 T cell. At this stage, only Signal 1 is needed to initiate the effector function of activated CD8 T cells. Upon engagement, the cytotoxic T cell kills the infected cells by one of two, or both, mechanisms. Cytotoxic T cells are able to kill target cells via interactions between Fas ligand and the Fas receptor on the cytotoxic T cell and target cell, respectively. Engagement of the Fas receptor induces programmed cell death

(apoptosis) of the target cell. The cytotoxic T cell can also induce apoptosis of the target cell by secreting granules containing perforin and granzymes directly at the target cell (Figure 1.4). Perforin is a pore-forming protein and granzymes are a family of pro-apoptotic serine proteases. Perforin is essential for the delivery of granzymes into the cytosol. However, whether perforin forms pores on the cell surface of the target cell or within endosomal compartments of the target cell is not yet completely understood. Once in the cytosol, the granzymes act on number of different substrates. The cleavage of these substrates results in the initiation of apoptosis. The secretory granules do not affect the cytotoxic T cell. Rather, after initiating apoptosis in the infected target cell, the cytotoxic T cell disengages from the target cell and continues surveillance of the periphery for other infected cells. In addition to inducing apoptosis in infected cells, cytotoxic T cells also release the pro-inflammatory cytokines IFNγ and TNFα at the site of infection. Finally, to inhibit peripheral tissue injury, the immunosuppressive cytokine IL-10 is secreted by cytotoxic T cells. [reviewed in (Hoves et al., 2010) and (Zhang and Bevan, 2011)].

Thus, MHC class I molecules are crucial for the activation and peripheral effector function of CD8 T cells. We addressed a number of outstanding questions in the field of MHC class I antigen presentation and CD8 T cell activation. Our findings contribute to the fields of MHC class I assembly and the antigen presentation of soluble and cell-associated antigens.

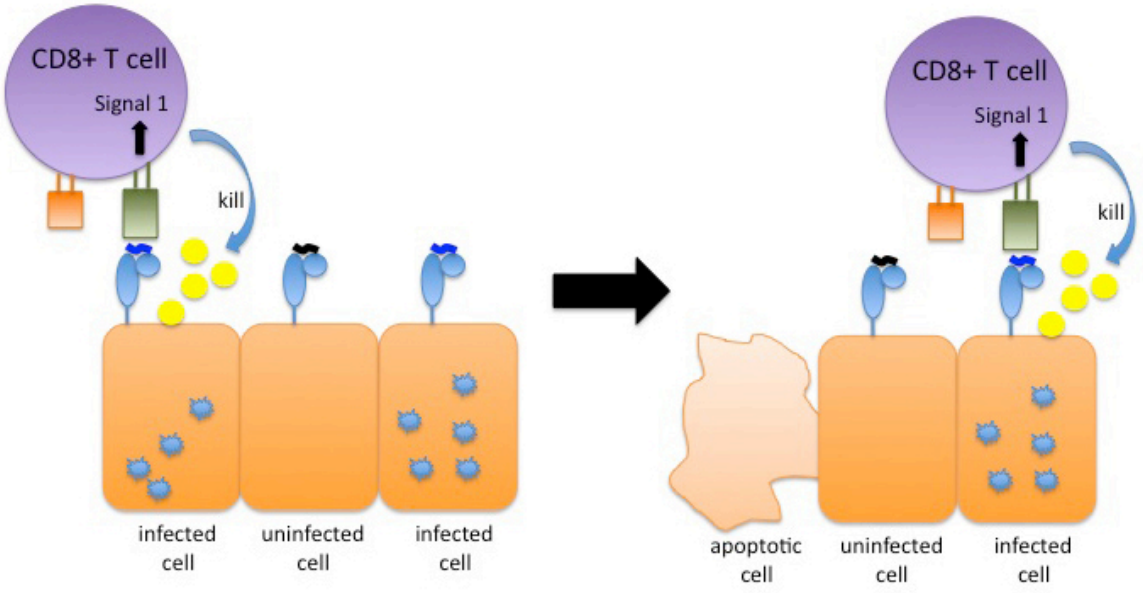

Figure 1.4. Activated CD8 T cells require only Signal 1 to induce effector function. Upon engagement with a MHC class I molecule – peptide complexes of the same specificity as that which caused initial activation of the cytotoxic T cell, the target cell is killed. Depicted here is the secretion of granules containing perforin and granzymes. The pore-forming protein (perforin) will facilitate the entry of the granzymes into the cytosol of the infected cell. Once in the cytosol, the granzymes will cleave a number of substrates. The cleavage of the substrates will initiate apoptosis in the infected cell. The cytotoxic T cell continues to survey the peripheral environment for additional infected cells.

MHC class I peptide loading complex

MHC class I molecules are composed of a heavy chain, a light chain (β2m), and a peptide of about 8-10 amino acids in length (Figure 1.1) (Bjorkman et al., 1987). This trimeric protein is assembled in the lumen of the endoplasmic reticulum (ER) by a group of chaperones and assembly factors termed the MHC class I peptide loading complex (PLC). This complex consists of the transporter associated with antigen processing (TAP), tapasin, the lectin-like chaperone calreticulin and the thiol oxidoreductase ERp57 (Figure 1.5). Upon translation, MHC class I heavy chains fold with the help of the membrane bound homologue of calreticulin, calnexin, and its partner ERp57. MHC class I heavy chains may undergo disulfide bond isomerization at this

stage, which is facilitated by ERp57. β2m forms complexes with the heavy chains, and MHC class I heterodimers associate with the PLC. Within the PLC, the MHC class I molecules are loaded with optimal peptides, which helps stabilize the MHC class I molecules. Stable MHC class I molecules are transported to the cell surface where the TCR – MHC class I-peptide interaction occurs. MHC class I molecules loaded with sub-optimal peptide are unstable on the cell-surface, which reduces the efficiency of the TCR – MHC class I-peptide interaction (Garbi et al., 2000). Thus, maintaining quality control of MHC class I molecules is vital for the development and function of CD8 T cells.

Peptides that bind to MHC class I molecules are typically derived from the cytosol. In the cytosol, a large multi subunit called the proteosome degrades proteins into peptides [reviewed in (Sijts and Kloetzel, 2011)]. The derived peptides are extended at the N-terminus while the C-terminus is compatible for binding to the MHC class I peptide groove. TAP is a transmembrane ABC-transporter, and the cytoplasmic side of TAP binds to these extended peptides and transports them into the ER in an ATP hydrolysis dependent manner [reviewed in (Procko and Gaudet, 2009)]. Within the ER lumen, the aminopeptidade ERAAP (ERAAP in mice; ERAP1 in humans) trims the N-terminally extended peptides to generate peptides of 8-10 amino acids in length, which fit into the groove of MHC class I molecule. ERAAP deficiency disrupts the stability of MHC class I-peptides complexes, vastly changes the peptide repertoire, and reduces CD8 T cell responses in mice (Hammer et al., 2006).

Tapasin, ERp57 and calreticulin work cooperatively to assemble stable MHC class I molecules that are loaded with optimal peptides [reviewed in (Raghavan et al., 2008) and (Cresswell et al., 2005)]. The absence of any one of the PLC components results in reduced surface expression and sub-optimal assembly of MHC class I (Gabathuler et al., 1994; Gao et al., 2002; Garbi et al., 2000; Garbi et al., 2006). Within the PLC, TAP binds to tapasin (Lehner et al., 1998; Sadasivan et al., 1996). Tapasin stabilizes TAP, which allows for a greater flow of peptides into the ER (Lehner et al., 1998). In addition, the TAP-tapasin interaction concentrates the influx of peptides around folding MHC class I molecules. Tapasin also interacts with ERp57 via a stable disulfide bond (Peaper et al., 2005). MHC class I also interacts directly with tapasin (Bangia et al., 1999; Rizvi and Raghavan, 2006). Thus, tapasin functions as the bridge between MHC

class I and TAP. Calreticulin binds directly to ERp57 via residues in the calreticulin P domain (Frickel et al., 2002). Calreticulin also binds MHC class I, and this interaction is reduced in cells treated with the glucosidase I and II inhibitor castanospermine, which inhibits the trimming of the 3 terminal glucose residues on N-linked glycans (Sadasivan et al., 1996). The interactions of calreticulin with substrates containing N-linked glycans are dependent on the ability of calreticulin to interact with monoglucosylated glycans on the glycoprotein substrate. Castanospermine treatment inhibits the generation of glycans containing single terminal glucose residues. Hence, the finding that castanospermine treatment of cells reduced MHC class I - calreticulin interactions (Sadasivan et al., 1996) suggested that calreticulin – MHC class I binding is dependent on a glycan interaction.

Tapasin is suggested to be the "peptide editor" of the PLC [reviewed in (Wearsch and Cresswell, 2008)]. In doing so, tapasin displaces low affinity peptides bound to the MHC class I peptide binding groove and facilitates the exchange for high affinity peptides (Howarth et al., 2004). Tapasin is also believed to have the ability to detect the presence of empty MHC class I heterodimers or those loaded with sub-optimal peptides and prevent the export of these unstable MHC class I molecules from the ER. The functions of ERp57 and calreticulin within the PLC are not fully understood, however both are required to generate stably loaded MHC class I molecules. [reviewed in (Peaper and Cresswell, 2008)]. ERp57 appears to have a structural role in the PLC, as the redox activity of ERp57 is not required for the stabilization of the PLC or for the generation of stable MHC class I molecules (Zhang et al., 2009). In this study, we investigated modes of calreticulin recruitment to the PLC and function of calreticulin within the MHC class I assembly complex.

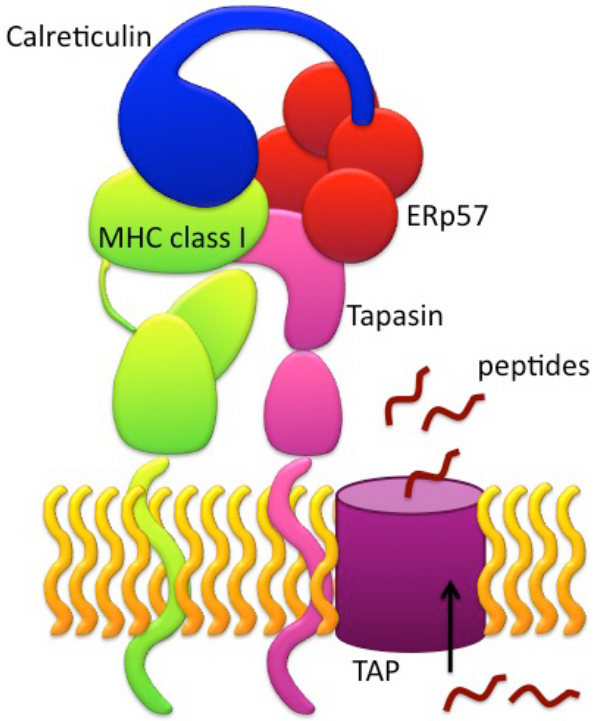

Figure 1.5. The MHC class I PLC. Tapasin binds TAP and MHC class via non-covalent interactions. Tapasin also forms a stable disulfide bond with ERp57. Via interactions through its P domain, calreticulin interacts with ERp57. Studies described in Chapter 2 contributed to a better understanding of how calreticulin is recruited to the PLC.

Calreticulin

Calreticulin is a soluble calcium binding ER resident chaperone that aids in the folding of nascent glycoproteins [reviewed in (Michalak et al., 2009)] Calreticulin is composed of three domains, and each domain serves a role in the protein's various functions. The domains are: a globular domain, P-domain, and acidic C-terminal domain (Figure 1.6A).

The globular domain of calreticulin is composed of both the N- and C- terminal regions. These regions come together to form a β-strand sandwich and a C-terminal helix that spans both the globular and acidic C-terminal domains. The glycan binding site is located within the globular domain (Figure 1.6B) (Kozlov et al., 2010). The glycan binding site play an important role in calreticulin substrate recognition as discussed below. Calreticulin also contains calcium-binding sites. One of these sites, the high affinity site, resides in the globular domain (Figure 1.6B). This site binds a calcium ion with an affinity of ~16 μM. The C-terminal acidic domain of calreticulin contains

multiple low affinity calcium binding sites (binding affinity of ~590 μM) (Wijeyesakere et al., 2011). It is suggested that calreticulin binds about 50% of the calcium stored in the ER (Nakamura et al., 2001). Accordingly, calreticulin deficiency results in embryonic lethality in mice due to impairments in cardiac development. This is caused by alterations in calcium signaling that impact cardiac development (Mesaeli et al., 1999). Calreticulin-deficient mouse embryonic fibroblasts (MEF) have been utilized to understand the various functions of calreticulin [reviewed in (Michalak et al., 2009)]. MHC class I assembly is impaired in calreticulin-deficient MEFs, and MHC classs I molecules that do traffic to the surface of the cell are unstable. Importantly, the antigen presentation by calreticulin-deficient MEFs is compromised compared to their wild-type counterparts (Gao et al., 2002). Calreticulin has also been shown to play a positive role in cell adhesion, wound healing and apoptosis (Fadel et al., 1999; Nakamura et al., 2000; Nanney et al., 2008). Calcium release from the ER is involved in the initiation of certain types of apoptosis. Thus, increased calreticulin expression results in increased apoptosis, as increased calreticulin levels enhance the calcium concentration in the ER. On the other hand, calreticulin-deficiency results in a resistance to apoptosis, as calcium levels in the ER are reduced [reviewed in (Michalak et al., 2009)].

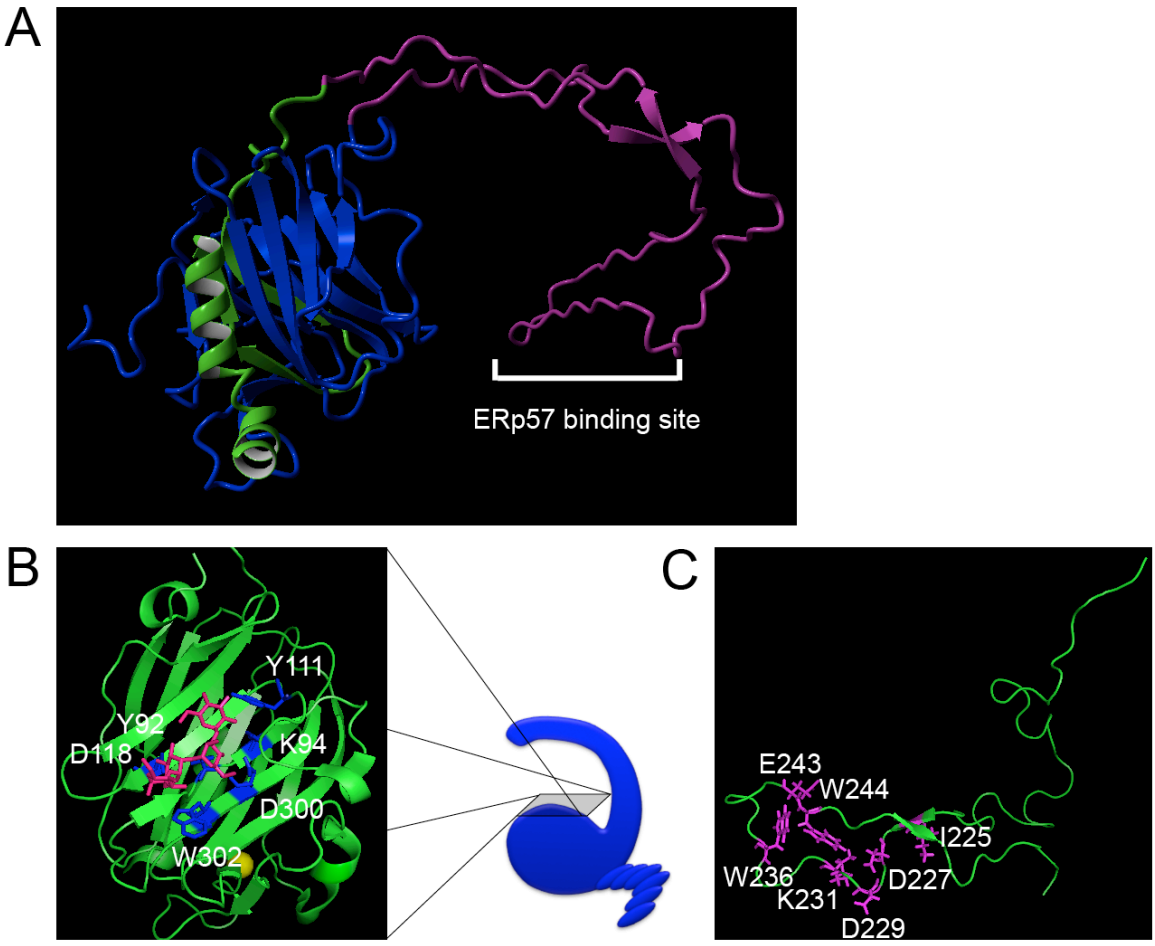

Figure 1.6. Structure of calreticulin. A. Homology model of calreticulin based on the crystal structure of the calreticulin globular domain (PDB ID 3O0V) and calnexin (PDB ID 1JHN) (Kozlov et al., 2010; Schrag et al., 2001). The globular domain is depicted in blue (N-terminus of calreticulin) and green (C-terminus of calreticulin). The P domain, which contains an ERp57 binding site, is depicted in purple. The C-terminal acidic domain is not included in the model. This model combining the globular and P domain was built by Sanjeeva J. Wijeyesakere. B. Putative glycan-binging residues of calreticulin domain [(PDB ID 3O0W) (Kozlov et al., 2010)] are highlighted in purple, and the region of the calreticulin model corresponding to the glycan binding site is boxed. The Glc_1Man_3 ligand is depicted in pink. The high affinity calcium binding site is occupied by a calcium ion (depicted as a yellow sphere). Mutagenesis studies and recent crystal structure studies have implicated highlighted residues (blue) in glycan binding. C. NMR structure of the P domain of calreticulin (PDB ID 1K9C) (Ellgaard et al., 2002). ERp57 binding sites are highlighted in purple based on NMR studies using calreticulin and ERp57 (Frickel et al., 2002).

Both calreticulin and its membrane bound homologue calnexin bind ERp57 through residues at the tip of the hook-shaped, proline-rich P-domain (Frickel et al., 2002) (Figure 1.6C). In cooperation with ERp57, calreticulin and calnexin aid in the folding of nascent glycoproteins. This process is dependant on the recognition by calreticulin or calnexin of modified glycans on nascent glycoproteins. Upon translation in the ER, an N-linked glycan with three terminal glucose residues ($Glc_3Man_9GlcNAc_2$, Figure 1.7) is attached to nascent glycoproteins. ER localized α-glucosidase I cleaves the first glucose and α-glucosidase II cleaves second glucose. What remains is a monoglucosylated N-linked glycan ($Glc_1Man_9GlcNAc_2$, Figure 1.7). Calreticulin and calnexin bind to monoglucosylated N-linked glycans through a glycan-binding site located within their globular domains (Kozlov et al., 2010; Peterson et al., 1995; Spiro et al., 1996; Ware et al., 1995) (Figure 1.6B). Calreticulin/calnexin bind glycoprotein substrates, and ERp57 facilitates isomerization of disulfide bonds within the substrates. Upon cleavage of the terminal glucose residue by α-glucosidase II, release of substrate from calreticulin/calnexin is thought to be initiated. If folded correctly, the glycoproteins can proceed through the secretory pathway. A soluble enzyme, UDP-Glucose:glycoprotein glucosyltransferase (UGGT), senses improperly folded glycoproteins. UGGT re-glucosylates the N-linked glycan of the misfolded glycoproteins. The misfolded glycoprotein is now tagged for re-entry into the calreticulin/calnexin cycle. In this model, UGGT is the protein-folding sensor, and calreticulin and calnexin bind substrate via glycan-based interactions and initiate the interaction between substrate and ERp57 [reviewed in (Rutkevich and Williams, 2011)]. Hence, calreticulin and calnexin are key players in ER quality control.

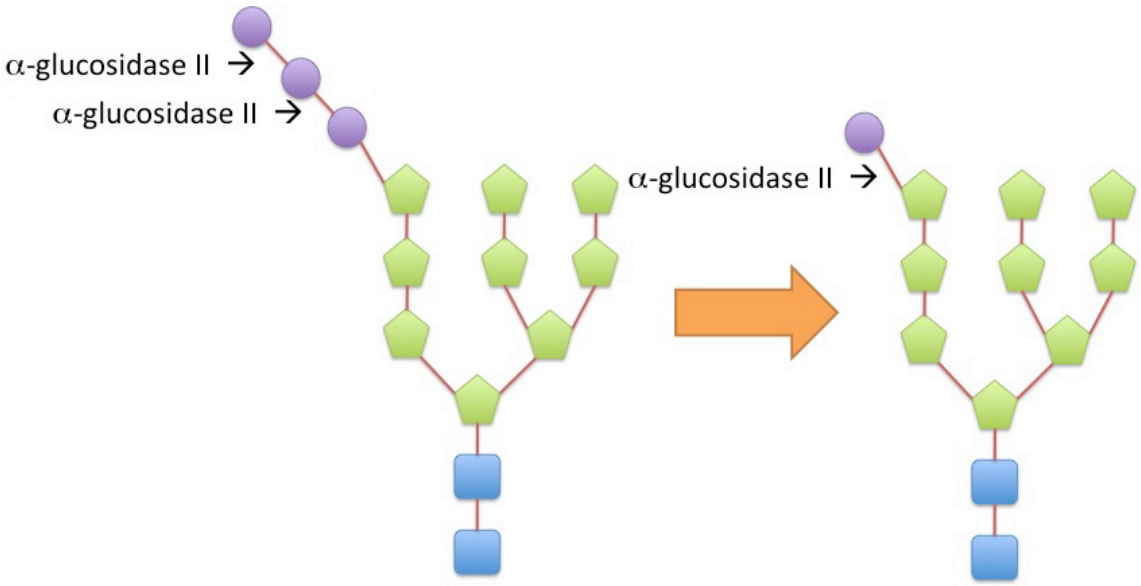

Figure 1.7. N-linked glycan modification. (A) A core glycan consisting of 2 N-acetylglucosamines (depicted as blue squares), 9 mannoses (depicted as green pentagons), and 3 glucoses (depicted as purple circles) are attached to nascent glycoproteins in the ER. α-glucosidase I cleaves the terminal glucose residue, and α-glucosidase II cleaves the second glucose residue. What remains is a monoglucosylated N-linked glycan residue (B), to which calreticulin and calnexin bind via sites located in their globular domains. α-glucosidase II can also cleave the terminal glucose residue if this residue becomes fully exposed.

In 1999, it was demonstrated that calreticulin also has the ability bind and inhibit the thermal aggregation of non-glycosylated misfolded polypeptide substrates *in vitro* (Saito et al., 1999). Subsequently, within cells, calreticulin was shown to bind de-glycosylated MHC class I heavy chains under ER stress conditions (tunicamycin treatment) (Rizvi et al., 2004). Thus, once it was recognized that calreticulin can also bind and chaperone non-glycosylated polypeptide substrates, the questions arose whether calreticulin recruitment into the PLC is based on polypeptide, rather than glycan-based, interactions with MHC class I. Evidence to support both models – (a) calreticulin recruitment into the PLC via ERp57 and MHC class I glycan-based interactions and (b) calreticulin recruitment into the PLC via MHC class I polypeptide-based interactions – have been proposed (Dong et al., 2009; Sadasivan et al., 1996; Zhang et al., 2009). In Chapter 2, we undertook experiments to examine impacts of mutations within the glycan

and ERp57 binding sites of calreticulin on MHC class I assembly and calreticulin recruitment to the PLC.

MHC class I antigen cross-presentation

APCs typically present endogenously synthesized peptides (both self and foreign) in the context of MHC class I molecules to CD8 T cells. APCs can also present exogenously derived peptides in the context of MHC class I. This process, termed cross-presentation, is important for initiating cytotoxic responses against many intracellular pathogens and tumor cells as well as for maintaining peripheral tolerance [(Luckashenak et al., 2008) and reviewed in (Amigorena and Savina, 2010)]. As described above, conventional MHC class I antigen presentation involves the degradation of proteins in the cytosol into smaller peptides. After being transported into the ER by TAP, the peptides are trimmed and loaded onto folding MHC class I molecules. MHC class I antigen cross-presentation involves the uptake of both soluble and cell-associated antigens by the general mechanisms of endocytosis and phagocytosis by APC. In addition to being targeted for MHC class II presentation to CD4 T cells, peptides generated from the exogenously acquired proteins are loaded onto MHC class I molecules for presentation to CD8 T cells.

Mechanisms of MHC class I antigen cross-presentation

There are several models proposed for the mechanism by which cross-presentation occurs (Figure 1.8) [reviewed in (Raghavan et al., 2008)]. They can be divided into two main categories: one that is dependent on TAP and the proteosome and one that is independent of these two factors. TAP-independent cross-presentation has been termed the "vacuolar pathway" (Figure 1.7a) Upon uptake into an endosome, an antigen degraded into smaller peptides by cysteine proteases such as cathepsin S. The peptides are loaded onto recycling MHC class I molecules within the endosome, and the new MHC class I – peptide complex is trafficked to the surface of the cell. TAP and proteosome dependant mechanisms require that the exogenous protein reach the cytosol. One mechanism depicted in Figure 1.8b involves the retrograde transport of antigen from the extracellular environment to the ER. Within the ER, the antigen is transported to the cytosol via Sec61, which is a putative translocon channel thought to function in the transport of substrates from the ER → cytosol. Sec61 plays a role in ER-associated degradation (ERAD) (Schafer and Wolf, 2009), which exports terminally misfolded

proteins out of the ER into the cytoplasm for degradation. In the cytoplasm, the exogenously derived protein is processed via the conventional MHC class I pathway. The antigen is degraded by the proteosome, and the peptides are transported into the ER by TAP. The second TAP and proteosome dependant pathway is depicted in Figure 1.8c. Via this pathway, the exogenous antigen is transported into the cytosol directly from a phagosome. This pathway is somewhat controversial [reviewed in (Amigorena and Savina, 2010)], as the presence of ERAD machinery within phagosomes has been highly debated. Finally, it has also been proposed that TAP itself is recruited to early endosomes via TLR4/MyD88 signaling (Burgdorf et al., 2008). This pathway (Figure 1.8d) proposes that exogenous antigens are first translocated from the endosome to the cytosol, where the antigen is degraded by the proteosome. The peptides are then translocated back into the endosome via TAP. The peptide products are loaded onto recycling MHC class I molecules and transported back to the surface of the cell, similarly to the vacuolar pathway (Figure 1.8a). As mentioned above, ERAP plays a role in trimming N-terminally extended peptides that are transported into the ER by TAP. Another aminopeptidase, insulin-regulated aminopeptidase (IRAP), has been implicated in cross-presentation by its ability to trim N-terminally extended peptides within endosomes (Saveanu et al., 2009).

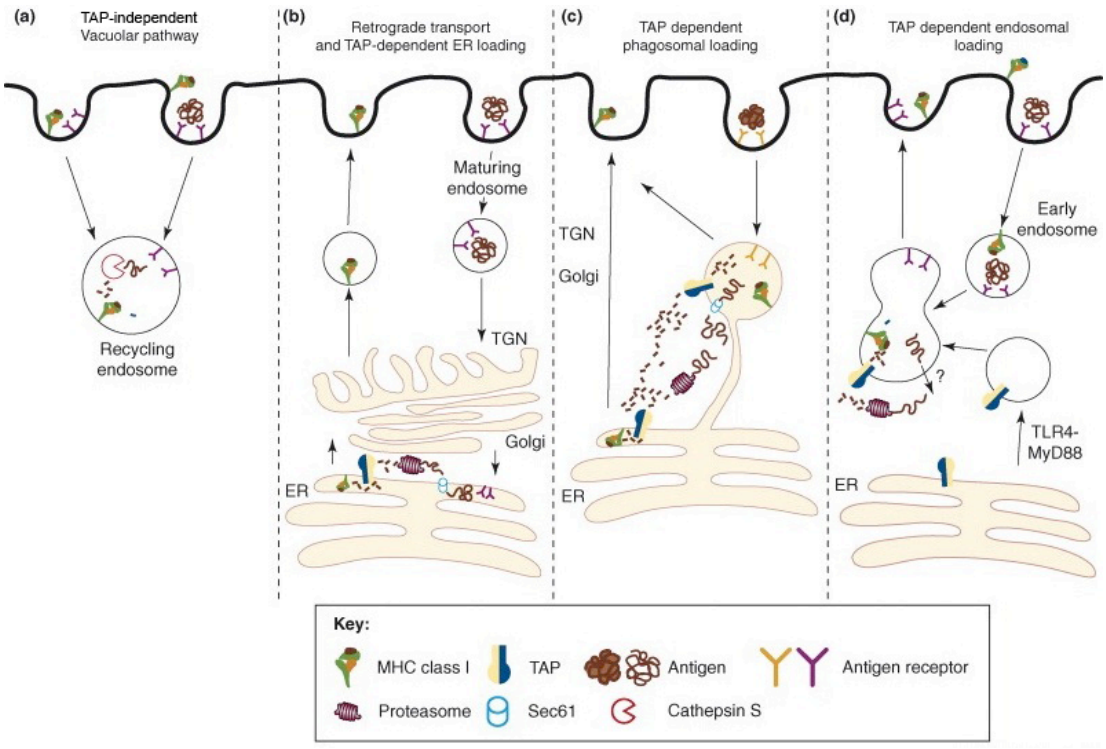

Figure 1.8. Proposed pathways for MHC class I antigen cross-presentation. (a) TAP-independent vacuolar pathway; endocytosed antigens are proteolytically processed by cysteine proteases such as cathepsin S. Peptide is loaded onto recycling MHC class I molecules within the endosome, and the newly formed MHC class I-peptide complex traffics back to the plasma membrane. (b) The retrograde translocation model proposes that some soluble antigens are directly targeted to the ER following retro-trafficking through the trans-Golgi network and Golgi. Once in the ER, the antigen is retro-translocated into the cytosol by ERAD machinery (Sec61) and processed similarly to an endogenous protein for MHC class I presentation. (c) The TAP-dependent phagosomal pathway; phagocytosed antigens use the Sec61 channel to egress out of the phagosome, are proteasomally processed and are reimported into the phagosome for loading onto MHC class I molecules within the phagosome. Once the MHC class I molecules are loaded, they traffic to the plasma membrane. Phagocytosed antigens that have egressed into the cytoplasm could also follow the classical ER-routed MHC class I pathway for endogenous proteins. (d) The TAP-dependent endosomal pathway proposes that TAP is recruited to an early endosome through TLR4/MyD88 signaling. Antigen egresses from the endosome by an unknown transporter and after proteasomal proteolysis, processed peptides are shuttled back into endosomes by recruited TAP and loaded onto recycling MHC class I molecules. This figure is adapted from (Burgdorf and Kurts, 2008) and redrawn.

APC subsets and receptors involved in MHC class I cross-presentation

Antigen uptake by receptors has been closely examined in the context of cross-presentation. Most notably, cross-presentation of soluble ovalbumin (OVA) has been shown to be dependant on the mannose receptor, which is a C-type lectin receptor. Mannose receptor mediated uptake traffics OVA to early endosomes, which are favorable for cross-presentation onto MHC class I molecules (pathway depicted in Figure 1.8d). However, uptake via scavenger receptors traffics OVA to lysosomes, which are favorable for MHC class II presentation, but not for MHC class I presentation (Burgdorf et al., 2007; Burgdorf et al., 2008). The requirement for the mannose receptor in the cross-presentation of OVA remains a controversial issue (Burgdorf et al., 2010; Segura et al., 2009). F_c receptors and a number of other C-type lectin receptors have also been shown to support the cross-presentation of exogenous proteins [reviewed in (Kurts et al., 2010)].

The relevant APC that cross-primes a CD8 T cell is dependant on a number of factors. For example, subcutaneously delivered apoptotic cells are cross-presented by CD169+ macrophages (Mϕ). This is largely due to the location of the Mϕ within the draining lymph node (Asano et al., 2011). Dendritic cells (DC) *are* able to cross-present the same apoptotic cells *in vitro*, but do not have access to the cells *in vivo* due to the architecture of the lymph node. However, when apoptotic cells are injected intravenously, extracted CD8α+ lymphoid (CD11b-) DC have the ability cross-prime CD8 T cells *in vitro*, whereas myeloid (CD11b+) CD8α- DC or Mϕ do not (den Haan et al., 2000). A later study implicating DCs in the cross-priming of CD8 T cells *in vivo* did so by ablating all CD11c+ cells (Jung et al., 2002). Various antigens (cell-associated OVA, the bacterium *Listeria monocytogenes*, and *Plasmodium yoelii* sporozoites) in that study were delivered intravenously. Further support for a role of CD8 DC in cross-priming CD8 T cells has been generated by selectively ablating CD8 DC by cytochrome c administration. Mice treated with cytochrome C are shown to be impaired in cross-priming CD8 T cells against intravenously delivered cell-associated OVA (Lin et al., 2008). Recently, a subset within the CD8 DC population located in the marginal zone of lymph nodes has been implicated in tolerizing CD8 T cell responses against apoptotic cell-associated antigens (Qiu et al., 2009). Finally, steady-state and activated CD8 DC are both shown to be competent for cross-priming soluble OVA, but different pathways are utilized depending

on whether or not CD8 DCs are activated (Segura et al., 2009). Thus, it appears that there may be a number of factors involved in determining what APC subset is responsible for cross-presenting antigen to CD8 T cells. These factors may include mode of delivery, size of antigen, inflammatory environment, and the extent of pathogen load.

The ability of an APC to preserve antigen within a phagosome enhances the efficiency of cross-presentation of antigen-derived peptides. Neutral pH and low phagosomal proteolytic activity within the first few hours after phagocytosis are thought to favor cross-presentation by bone marrow-derived DC (BMDC) (Mantegazza et al., 2008; Savina et al., 2009). The recruitment of NADPH oxidase (NOX2) to the phagosomes/endosomes is important for maintaining a neutral pH in the phagosomal lumen, thus inhibiting rapid degradation of antigens. Interestingly, CD8 splenic DC, but not CD8- splenic DC, alkalinize their phagosomes/endosomes in a NOX2 dependant manner (Savina et al., 2009).

Finally, exploring factors that determine the induction of tolerance or activation of CD8 T cell responses against apoptotic cell-associated antigens is an emerging area in the field of antigen cross-presentation. The mode of administration is one determinant of ensuing CD8 T cell fate. Whereas intravenous delivery of antigen bearing apoptotic cells induces CD8 T cell tolerance (Qiu et al., 2009), subcutaneous injection of apoptotic cells induces an effector response (Asano et al., 2011; Obeid et al., 2007b). However, not all modes of cell death are immunogenic (Obeid et al., 2007b). Determining what types of cell death are immunogenic and the mechanism behind the immunogenicity is of great relevance for the chemotherapeutic treatment of solid tumors (reviewed in (Kepp et al., 2011)).

Role of heat shock proteins in the cross-presentation of soluble antigen

Heat shock proteins (HSP), including calreticulin, gp96, HSP90 and HSP70, bind immunogenic peptides (Basu and Srivastava, 1999; Binder and Srivastava, 2005). Exogenously delivered HSP-peptide complexes enhance the cross-presentation of associated peptides to CD8 T cells (Basu et al., 2001; Basu and Srivastava, 1999). Additionally, immunizing mice with HSPs isolated from tumor cells results in protection from a subsequent live tumor challenge (Basu and Srivastava, 1999; Binder and Srivastava, 2004; Nair et al., 1999). The advantage to this immunization method is that

specific antigenic tumor peptides do not need to be identified. Clinical trials have been undertaken using autologous HSP from patients with established tumors. Vitespan (aka Prophage), an autologous tumor-derived HSP gp96-peptide complex vaccine, showed promise in Phase III clinical trials for treatment of Stage IV melanoma (Testori et al., 2008). Notably, this treatment has already been approved in Russia to treat patients who are at an intermediate risk for disease (kidney cancer) recurrence. In addition to HSPs isolated from tumor cells, the engineered surface expression of gp96 on tumor cells or secretion of gp96 from cells has been shown to elicit a more potent immune response against the cells compared to cells that do secrete or express surface gp96 [reviewed in (Tsan and Gao, 2009)].

The immunogenicity of autologous HSPs derived from established tumors is attributed to the binding of HSPs including gp96, calreticulin and HSP70 to the APC receptor CD91 (Basu et al., 2001). It is hypothesized that HSPs target associated peptides directly to APCs via CD91. CD91-mediated uptake of the HSP facilitates the enhanced uptake and cross-presentation of HSP-associated peptides. In addition to CD91, HSPs have been shown to bind to other scavenger receptors. LOX-1 has been shown to bind and facilitate the cross-presentation of HSP70 associated antigen (Delneste, 2004). Scavenger receptor-A and scavenger receptor expressed by endothelial cell-I (SREC-I) have been shown to mediate the internalization of gp96 and calreticulin (Berwin et al., 2004; Berwin et al., 2003). SREC-I has also been shown to internalize and cross-present HSP90 associated antigen (Murshid et al., 2010). It is apparent that there are a number of different phagocytic receptors that facilitate the uptake of a number of different HSPs. It is therefore not surprising that cross-priming of CD8 T cells was not negatively impacted when a single HSP (gp96) was knocked down *in vivo* (Lev et al., 2009). All together, these studies suggest redundancy in HSPs and their receptors.

The success of HSP-based vaccines may also be attributed to the ability of the HSPs to protect the associated peptides from rapid degradation in the extracellular environment, thus preserving antigen for cross-presentation. Alternatively, the ability of HSPs to signal through CD91 and induce the activation of pro-inflammatory cytokines may be the factor determining the immunogenicity of HSP-peptide complexes (Pawaria and Binder, 2011) rather than their enhanced cross-presentation. It has been suggested

that HPSs directly activate APCs, inducing them to secrete a wide array of pro-inflammatory cytokines and upregulate co-stimulatory molecules. In this model, HSPs serve as "danger signals." However, when controlled for specific TLR stimuli, stimulatory effects of HSPs are lost [reviewed in (Tsan and Gao, 2009)].

We assessed whether calreticulin enhances the cross-presentation of an associated soluble antigen. In Chapter 3, we accomplished this by assessing whether proliferation of naïve CD8 T cells *in vitro* and *in vivo* was *enhanced* in response to a calreticulin-associated antigen (fusion or bead-associated) compared to the antigen alone.

Role of calreticulin in the efferocytosis of cells

Receptors, ligands and pathways involved in the uptake of apoptotic cells are different than those involved in phagocytosis of antibody-mediated opsonized particles or cells. Hence, the phagocytosis of dying cells has been termed "efferocytosis" to distinguish it from other types of phagocytosis [reviewed in (Gardai et al., 2006)]. Apoptotic cells express a number of cell-surface phagocytic molecules that distinguish them from live cells. These molecules are termed "eat me" signals, as they induce the uptake and clearance of apoptotic cells (reviewed in (Erwig and Henson, 2008) and (Gardai et al., 2006)). The most widely characterized of these molecules is phosphatidylserine (PS). PS is normally located on the inner leaflet of the plasma membrane. However, it is found on the outer leaflet of apoptotic cells due to the inhibition of a translocase that normally localizes PS to the outer leaflet and the scrambling of the lipid bilayer (Bratton et al., 1997; Verhoven et al., 1995). A number of bridging molecules have been shown to bind PS and bridge apoptotic cells to receptors on efferocytes (cells that phagocytose apoptotic cells) [reviewed in (Ravichandran, 2011)]. Calreticulin has also been identified as an "eat me" signal on apoptotic and pre-apoptotic cells; CD91 is the proposed receptor that binds calreticulin on the cell-surface (Gardai et al., 2005; Kuraishi et al., 2007; Obeid et al., 2007b). Collectins have also been shown to bind to and opsonize apoptotic cells to mediate efferocytosis. Interestingly, C1q (a member of the collected family) has been shown to bind calreticulin. It is possible that C1q binds calreticulin on apoptotic cells, enhancing the number of "eat me" signals on the apoptotic cell or that a C1q coated apoptotic cell binds low levels of surface calreticulin on efferocytes. "Don't eat me" molecules are typically present on live cells

and downregulated or redistributed on apoptotic cells. CD47 is the best-characterized "don't eat me" signal, binding SIRPα on the phagocyte (Gardai et al., 2005; Oldenborg et al., 2000). The balance between "eat me" and "don't eat me" signals determines the phagocytic fate of a cell (Figure 1.9). In addition, clustering of "eat me" signals in patches removed of "don't eat me" signals may be an additional mechanism to mediate uptake of apoptotic cells [reviewed in (Gardai et al., 2006)].

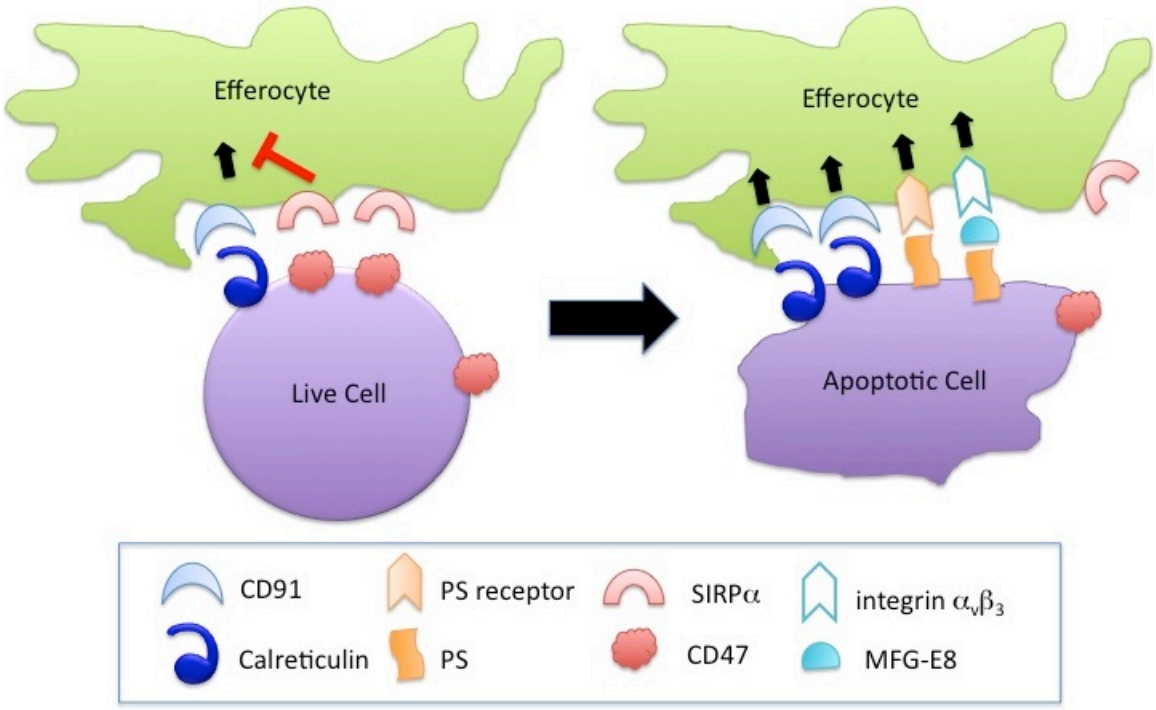

Figure 1.9. Surface ligands on cells mediate their removal. Live healthy cells express low levels of the "eat me" signals calreticulin and PS and high levels of the "don't eat me" signal CD47. Apoptotic cells upregulate both calreticulin and PS and downregulate CD47. The balance is shifted towards "eat me," and the dying cell is engulfed by an efferocyte. CD91 and SIRPα are known receptors for calreticulin and CD47, respectively. A number of receptors recognize PS directly including TIM-4, BAI1 and Stabilin-2. Soluble extracellular bridging molecules, such as MFG-E8, can also bind PS and facilitate uptake of apoptotic cells by binding to receptors on effectocytes [reviewed in (Ravichandran, 2011)].

Immunogenicity of cell-surface and extracellular calreticulin

Calreticulin is upregulated on apoptotic murine cells and is redistributed on Drosophila cells in response to UV-irradiation. Both the upregulation and redistribution of calreticulin result in calreticulin-dependant phagocytosis of the treated cells (Gardai et al., 2005; Kuraishi et al., 2007). Calreticulin is also upregulated on the surface of pre-apoptotic (cells that have yet not upregulated PS) tumor cells treated with anthracyclins, oxaliplatin or ionizing radiation (Obeid et al., 2007a; Obeid et al., 2007b; Tesniere et al., 2010). These treatments induce immunogenic tumor cell death, which is partially dependant on calreticulin (reviewed in (Kepp et al., 2011)). Specifically, mice immunized with calreticulin deficient tumor cells treated with drug form tumors at high frequencies in subsequent live tumor challenges compared to mice immunized with calreticulin sufficient drug-treated cells (Obeid et al., 2007b). Thus, the presence of calreticulin in the immunizing cell population enhances the generation of an anti-tumor immune response. The immunogenicity of tumor cells induced by anthracyclins, oxaliplatin and ionizing radiation is linked to: (1) the upregulation of surface calreticulin (an "eat me signal") and (2) the secretion of HMGB1 and ATP (both "danger signals"). It is suggested that the ability of calreticulin to facilitate uptake of the tumor cells treated with drug enhances antigen delivery to APCs, thus enhancing CD8 T cell cross-priming against tumor cell-associated antigens. However, this possibility has not been directly demonstrated.

In Chapter 3, we evaluated the impact of calreticulin induction on the surface of an antigen donor cell upon CD8 T cell proliferation in response to cell-associated antigen.

Effect of innate signaling on the cross-presentation of cell-associated antigen

The effect of innate signaling on antigen presentation has just recently been explored. Within an APC, each phagosome is autonomous, and only those that contain a TLR ligand mature and load exogenously derived peptides on MHC class II molecules. Hence, naïve murine CD4 T cells do not proliferate or secrete IFNγ in response to apoptotic cell-associated antigens, even in the presence of bacteria because the phagosomes containing apoptotic cells lack TLR ligands that are necessary for efficient MHC class II antigen presentation (Blander and Medzhitov, 2006). Surprisingly, in contrast to CD4 T cells, CD8 T cells proliferate and are activated in response to apoptotic cell-associated antigen

(Frleta et al., 2009). However, proliferation and cytotoxicity are inhibited when the apoptotic cell expresses a TLR ligand. The observed CD8 T cell inhibition suggests that CD8 T cell activation against apoptotic cell-associated antigen is inhibited the presence TLR stimuli.

Studies examining T cell responses to apoptotic cell-associated antigen in the presence of TLR ligands have mostly been performed *in vitro*. The *in vivo* T cell response to apoptotic cell-associated antigen in the presence of innate signaling is not well characterized. In Chapter 3 we examined the proliferation of naïve CD8 T cells to cell-associated antigen in the presence of lipopolysaccharide (LPS).

In summary, we posed a number of questions relating to the functions of calreticulin in antigen presentation. First, we investigated the relevant mode of calreticulin recruitment into the PLC (as MHC class I molecules are the best-characterized substrates of calreticulin). To this end, understanding the interactions that mediate calreticulin recruitment into the PLC would elucidate mechanisms for MHC class I assembly and mechanisms of the general chaperone function of calreticulin. Following this, we sought to determine the role of calreticulin in antigen cross-presentation. It is expected that a more complete understanding of the role of calreticulin in antigen cross-presentation would be a valuable initial step towards the development of effective cancer therapies and vaccines.

Chapter 2

Modes of calreticulin recruitment to the Major Histocompatibility Complex Assembly pathway

Abstract

MHC class I molecules are ligands for TCRs of CD8 T cells and inhibitory receptors of natural killer cells. Assembly of the heavy chain, light chain, and peptide components of MHC class I molecules occurs in the ER. Specific assembly factors and generic ER chaperones, collectively called the MHC class I PLC, are required for MHC class I assembly. Calreticulin has an important role within the PLC and induces MHC class I cell surface expression, but the interactions and mechanisms involved are incompletely understood. We show that interactions with the thiol oxidoreductase ERp57 and substrate glycans are important for the recruitment of calreticulin into the PLC and for its functional activities in MHC class I assembly. Additionally, we show that β2m promotes calreticulin and ERp57 stabilization within the PLC through direct or indirect interactions. The glycan and ERp57 binding sites of calreticulin contribute directly or indirectly to complexes between calreticulin and the MHC class I assembly factor tapasin and are important for maintaining steady-state levels of both tapasin and MHC class I heavy chains. A number of destabilizing conditions and mutations induce generic polypeptide binding sites on calreticulin and contribute to calreticulin-mediated suppression of misfolded protein aggregation in vitro. We show that generic polypeptide binding sites *per se* are insufficient for stable recruitment of calreticulin to PLC substrates in cells. However, such binding sites could contribute to substrate stabilization in a step that follows the glycan and ERp57-dependent recruitment of calreticulin to the PLC.

Introduction

Calreticulin is a soluble protein of the ER, where it functions in calcium binding and as a molecular chaperone (Michalak et al., 2009). Calreticulin binds to monoglucoslyated N-linked oligosaccharides on newly synthesized glycoproteins and maintains quality control of glycoprotein folding in the ER. A structural model for calreticulin was derived (Figure 2.1A) using the crystal structure of the calreticulin globular domain (Kozlov et al., 2010) and the crystal structure of the closely related protein, calnexin (Schrag et al., 2001). Calreticulin contains three structural domains. The first is a large globular domain comprising the N- and C-terminal regions of the protein that form a β-stranded sandwich and a C-terminal helix (Figure 2.1A, green, dark blue, and light blue). The glycan binding site is located within this domain (Figure 2.1B). A second hook- shaped P-domain forms a β-stranded hairpin structure inserted in the middle of the globular domain (Figure 2.1A, purple). The tip of this domain forms a binding site for ERp57 (Frickel et al., 2002), an ER oxidoreductase that works cooperatively with calreticulin and calnexin in glycoprotein folding (Oliver et al., 1999). A third C-terminal domain, rich in acidic amino acids, is functional as a low affinity/high capacity calcium coordination site (Michalak et al., 2009). This region is not present in the luminal domain of calnexin.

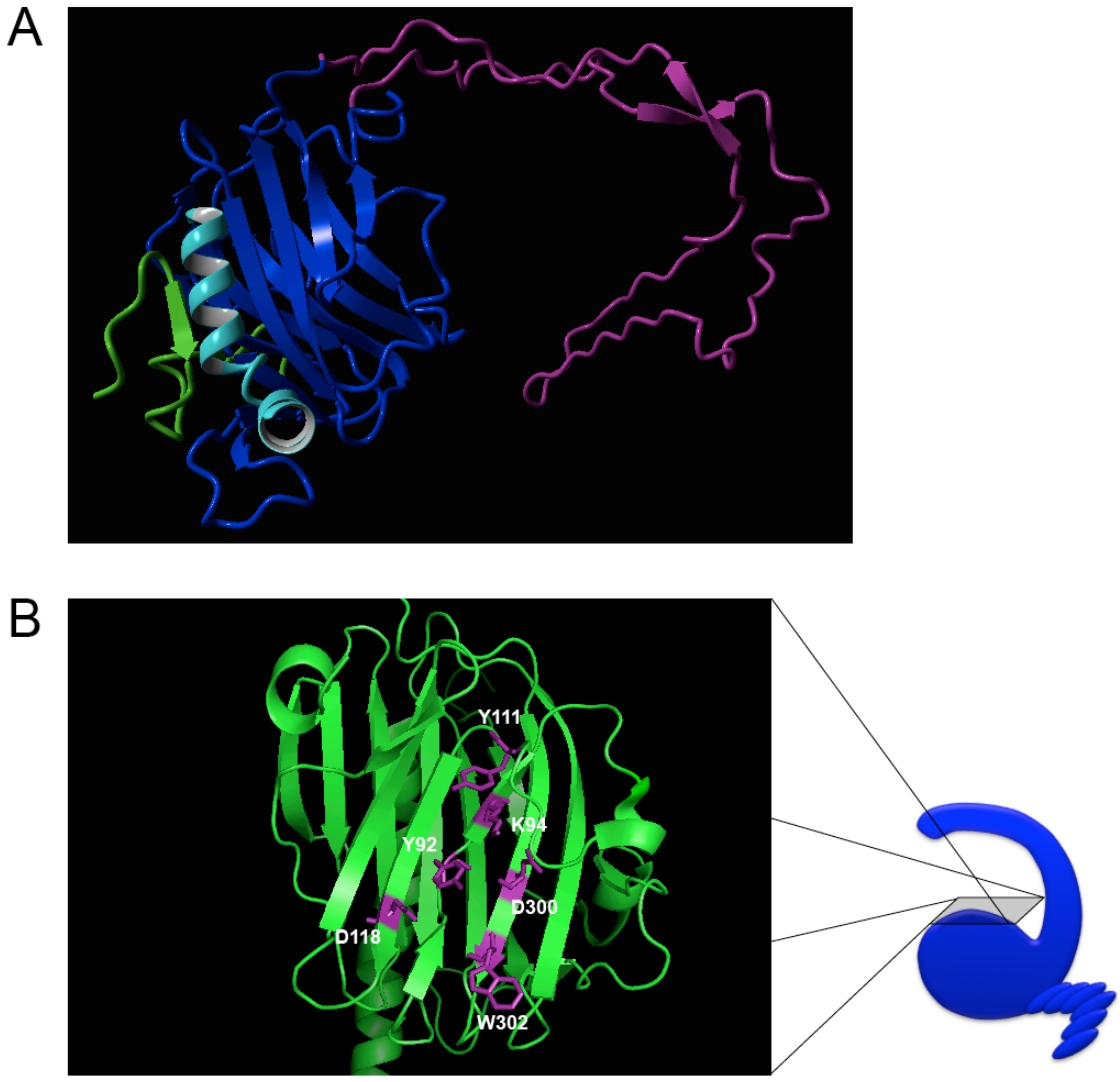

Figure 2.1. Structural model for calreticulin and depiction of truncation mutants and glycan-binding site. (A) A model for the calreticulin structure was based on the crystal structure of the calreticulin globular domain (PDB ID 3O0V) (Kozlov et al., 2010) and calnexin (PDB ID 1JHN) (Schrag et al., 2001). Calreticulin residues 1-32 are depicted in green. The C-terminal helix is depicted in light blue, and the core calreticulin structure in shown in dark blue. The P-domain is depicted in purple. The C-terminal acidic domain is not included in the model. This model was built by Sanjeeva J. Wijeyesakere. (B) Putative glycan-binding residues of calreticulin are highlighted in purple, and the region of the calreticulin model corresponding to the glycan binding site is boxed. This model was based on the crystal structure of the calreticulin globular domain (PDB ID 3O0V). Mutagenesis studies and recent crystal structure studies (Gopalakrishnapai et al., 2006; Kapoor et al., 2004; Kozlov et al., 2010) have implicated highlighted residues (purple) in glycan binding.

In vitro studies have shown that calreticulin can bind to misfolded non-glycosylated polypeptides and suppress their irreversible aggregation (Saito et al., 1999). This activity is induced by various conditions associated with ER stress, including calcium depletion and heat shock (Rizvi et al., 2004). These conditions also induce calreticulin oligomerization (Jorgensen et al., 2003; Rizvi et al., 2004). Much remains to be understood about the one or more binding sites on calreticulin that are used to suppress substrate aggregation, as well as the relevance of this activity to calreticulin-mediated protein folding under physiological non-stress conditions.

Calreticulin is a key player in the MHC class I assembly pathway (Gao et al., 2002). The MHC class I-dedicated assembly factors, TAP and tapasin, as well as the generic ER-folding factors ERp57 and calreticulin, form a large complex with MHC class I molecules, collectively called the PLC. TAP provides a major source of peptides for MHC class I molecules, whereas tapasin, ERp57, and calreticulin facilitate assembly of MHC class I molecules with peptides [reviewed in (Raghavan et al., 2008)]. Calreticulin is a component of the PLC, and calreticulin-deficient cells express reduced cell surface MHC class I molecules (Gao et al., 2002). The mechanisms by which calreticulin contributes to enhanced MHC class I assembly are not well understood.

Early studies with glycosylation inhibitors, MHC class I mutants, and *in vitro* binding analyses suggested that glycan-based interactions with MHC class I molecules recruit calreticulin into the PLC (Harris et al., 1998; Sadasivan et al., 1996; Wearsch et al., 2004). More recent studies with calreticulin mutants that are defective for glycan or ERp57 binding have suggested that calreticulin can be recruited into the PLC in the absence of interactions with both ERp57 and substrate glycans and that polypeptide-based interactions are important for calreticulin recruitment (Ireland et al., 2008; Zhang et al., 2009). However, partial truncation of the P-domain of calreticulin (including residues mediating ERp57 binding) impacted calreticulin recruitment to the PLC (Zhang et al., 2009), and ERp57- and tapasin-deficient cells have impaired recruitment of calreticulin into the PLC (Garbi et al., 2006; Grandea et al., 2000). Thus, although MHC class I molecules are one of the best-characterized substrates of calreticulin, the precise mechanism by which calreticulin is recruited into the PLC remains unclear. Furthermore, whereas numerous studies involving glycosylation inhibitors and substrates lacking

glycans have shown that the presence of monoglucosylated glycans on substrate glycoproteins are important for calreticulin binding and ER quality control, whether or not substrate glycans alone are sufficient for calreticulin recruitment is not well understood, and neither is the molecular basis for differences in substrate profiles between calnexin and calreticulin. Additionally the roles of ERp57, polypeptide-based, and other interactions in substrate recruitment to calreticulin have not been well studied.

To address some of these questions, various truncation mutants targeting different domains of calreticulin and point mutants targeting glycan and ERp57 binding residues were generated. These constructs were used to understand the impacts of truncations and mutations on calreticulin structure and stability, to investigate modes of calreticulin binding to PLC components, and to examine reconstitution of MHC class I assembly in calreticulin-deficient cells. With these mutants we were able to show that calreticulin recruitment into the PLC is largely dependant on glycan- and ERp57-based interactions. Additionally, tapasin and MHC class I glycan mutants were generated and expressed in tapasin deficient and MHC class I deficient cells, respectively, to show that the glycan of tapasin influences calreticulin recruitment into the PLC more so than that of the MHC class I heavy chain.

Results

C- and N-terminal Truncations Destabilize Monomers of Calreticulin

The first 32 residues of the calreticulin globular domain lack significant predicted secondary structure, with the exception of a short β-strand. Near the calreticulin C terminus, preceding the acidic domain is an α-helix, the major predicted helix in the calreticulin structure (Figure 2.1). Based on these predicted structural features, we made truncated versions of calreticulin using Ala-1 and Val-33 as start sites, and Asp-318, Gln-339, Glu-362, and Leu-399 as stop sites. Asp-318 truncates the protein prior to the C-terminal helix, Gln-339 truncates the protein following the C-terminal helix and just prior to the acidic region, whereas Glu-362 extends the calreticulin sequence several residues into the C-terminal acidic domain and just prior to the end of the C-terminal helix. A construct in which the entire P-domain of calreticulin was deleted (amino acids 187–283) and replaced by two glycine residues was also generated.

Following protein expression in *E. coli* and purification on a nickel column, gel-

filtration analysis indicated that full-length calreticulin, $mCRT_{1–399}$ (mCRT(WT)), was present largely in the monomeric form (Sp1, Figure 2.2A), as expected. Native PAGE analysis of purified protein verified that mCRT(WT) (12 μM) was largely monomeric at 4 °C, in the presence of 1 mM $CaCl_2$ (Figure 2.2D, lane 1). As previously described (Jorgensen et al., 2003; Rizvi et al., 2004), the formation of dimers and oligomers of mCRT(WT) was induced by heat treatment or calcium depletion (Figure 2.2D, lane 1 compared with lanes 2–4). C-terminal deletion constructs $mCRT_{1–362}$ and $mCRT_{1–339}$ (mCRT(ΔC)) were also largely monomeric, although the extent of oligomeric forms of these proteins was enhanced relative to mCRT(WT) (Figure 2.2A). In response to heat treatment or calcium depletion, dimeric and oligomeric structures were enhanced for $mCRT_{1–362}$ and $mCRT_{1–339}$ (mCRT(ΔC)), relative to mCRT(WT) (Figure 2.2, compare D–F). Additional deletion of the C-terminal helix ($mCRT_{1–318}$) dramatically affected calreticulin structure (Figure 2.2A). No monomers were recovered from the purification (Figure 2.2, A and G), and the major peak migrated in the column void volume. This construct was not used further in this study.

N-terminal truncation of calreticulin ($mCRT_{33–362}$) also impacted calreticulin structure (Figure 2.2B). Oligomeric species were recovered, and monomers were absent. Different oligomeric forms were classified based on the gel-filtration chromatograms and native PAGE analyses as: Sp3, consisting largely of the dimeric form of the protein and Sp4 and Sp5, consisting of higher order oligomeric forms (Figure 2.2, A, B, G, and H).

The calreticulin ΔP mutant (mCRT(ΔP)) was recoverable as monomers following purification, as were mCRT(ΔC), $mCRT_{1–362}$, and mCRT(WT) (Figure 2.2C). The oligomerization phenotype for mCRT(ΔP) resembled that of mCRT(WT) (Figure 2.2I).

A thermostability assay was next used to compare heat-induced unfolding of mCRT constructs. A fluorescent dye (Sypro Orange) was used that displays enhanced binding to proteins following thermal unfolding. CD studies at 280 nm have previously revealed the occurrence of a conformational change in human calreticulin, which has a transition midpoint (T_m) value of 46.4 °C in the presence of 1 mM $CaCl_2$ (Li et al., 2001). A similar T_m value was measured for mCRT(WT) in the Sypro Orange-based thermostability assay (T_m value 47.96 +/- 0.21 °C) (Figure 2.2J). In the presence of the calreticulin-binding glycan Glcα1–3Manα1– 2Manα1–2Man-OH (G1M3), the T_m value was significantly

right-shifted to 51.08 +/- 0.18°C indicating that the glycan had slightly stabilized calreticulin. Both mCRT(ΔP) and mCRT(ΔC) displayed fluorescence profiles similar to those obtained with mCRT(WT), and both were right-shifted by G1M3 (Figure 2.2, K and L). However, the T_m value measured for mCRT(ΔC) was 44.29 +/- 0.44 °C in the absence of G1M3, and 46.91 +/- 0.17 °C in the presence of G1M3. These findings indicate that mCRT(ΔC) is less resistant to heat-induced structural changes than mCRT(WT). However, mCRT(ΔC) was able to bind to and be stabilized by G1M3, as was mCRT(ΔP) (Table 2.1). Different species of the oligomeric $mCRT_{33–362}$ construct did not display thermostability profiles resembling those of mCRT(WT) and did not bind G1M3 as indicated by the thermostability-shift assays (data not shown) and, therefore, are not described further in this study.

A Biacore-based assay was used to measure ERp57 binding to the monomeric truncation constructs. mCRT(WT) and mCRT(ΔC) bound to ERp57, whereas binding was essentially undetectable with mCRT(ΔP), as expected (Frickel et al., 2002) (Figure 2.2M). Calculated K_D values were 0.55 +/- 0.26 μM and 1.2 +/- 0.8 μM, respectively, for mCRT(WT) and mCRT(ΔC) (Figure 2.2N).

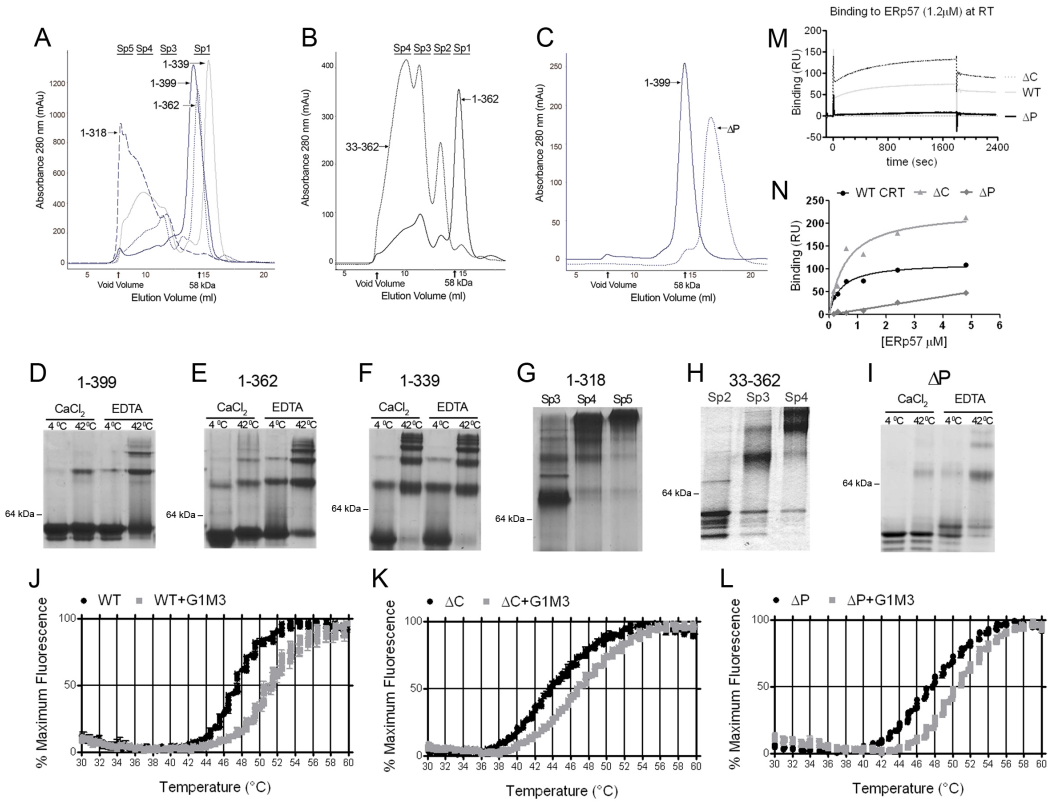

Figure 2.2. Impacts of calreticulin domains on structure and functional activities. Analytical gel-filtration chromatography of C-terminal (A), N-terminal (B), and P-domain (C) truncation mutants of mCRT. All constructs were directly analyzed following nickel affinity chromatography, except mCRT(ΔP) for which monomers were first isolated by gel filtration and then re-analyzed by a second analytical gel-filtration step shown. Following gel-filtration chromatography, peak fractions were analyzed by native-PAGE following protein (12 μM) incubations for 1 h in 1 mM $CaCl_2$ or 10 mM EDTA at 4 or 42 °C (D–F and I). Fractions corresponding to the indicated oligomeric species (Sp2–Sp5) of $mCRT_{1–318}$ or $mCRT_{33–362}$ were directly analyzed by native PAGE (1 mM $CaCl_2$, 4 °C) (G and H). One representative analysis is shown of two or more independent analyses. J–L, monomeric mCRT constructs were incubated with the fluorophore SYPRO Orange and subjected to a thermal stability analysis using a real-time PCR machine. Normalized fluorescence data (mean of triplicate wells ±S.E.) for one of three independent experiments are shown. Compiled T_m values for all constructs discussed in this report are shown in Table 2.1. M and N, mCRT constructs were immobilized on a Biacore CM5 chip to response unit (RU) values of 438, 426, and 480 (respectively, for WT, ΔP, and ΔC), and human ERp57 was injected over each surface or a control bovine serum albumin surface. Representative sensorgrams following subtraction of corresponding sensorgrams from the bovine serum albumin surface are shown in M. Dose-response graphs for binding constant calculations are shown in N. One representative of two (ΔC and ΔP) or five (WT) independent analyses of N are shown. Analyses shown in 2.2A, B, and D-H were performed by Ericca Stamper. Analyses shown in 2.2J-L were performed by Elise Jeffery. Analyses shown in 2.2M and N were performed by Syed Monem Rizvi.

Constructs	Protein			Protein + G1M3			Protein + ATP		
	T_m	SEM	n	T_m	SEM	n	T_m	SEM	n
mCRT(WT)	47.96	± 0.21	5	51.08	± 0.18	5	46.24	± 0.02	2
mCRT(ΔC)	44.29	± 0.44	3	46.91	± 0.17	3	---		
mCRT(ΔP)	47.63	± 0.07	3	51.00	± 0.27	3	45.49	± 0.13	2
mCRT(Y92A)	45.90	± 0.31	2	46.23	± 0.28	2	---		
mCRT(W244A)	46.59	± 0.46	2	50.74	± 0.03	2	---		
mCRT(Y92AW244A)	42.96	± 0.55	2	43.82	± 0.01	2	---		
mCRT(W302A)	44.82	± 0.55	3	45.67	± 0.55	3	---		

Table 2.1. Thermostability analyses of calreticulin constructs from SYPRO Orange binding assays. Indicated mCRT constructs (left column) were incubated with the fluorophore SYPRO Orange and subjected to a thermal stability analysis using a real time PCR machine. Proteins (16 μM) were incubated alone (Protein), with 48 μM G1M3 (Protein + G1M3), or with 3 mM ATP (Protein + ATP). Each condition was analyzed in triplicate within an experiment. For each experiment, mean % maximum fluorescence values from triplicate wells were plotted as a function of temperature, and T_m values were estimated as the temperatures at which 50% of the maximum fluorescence was observed. T_m values shown are the averaged T_m values from n independent experiments for each condition, SEM represents the standard error of the estimated mean T_m values. Analyses shown in Table 2.1 were performed by Elise Jeffery.

Compared with mCRT(WT), $mCRT_{1–339}$ (ΔC) and mCRT(ΔP) Have Reduced Abilities to Mediate MHC Class I Assembly in $CRT^{-/-}$ Cells

Calreticulin-deficient cells (K42) express reduced cell surface MHC class I, which can be restored by expression of wild-type calreticulin (Gao et al., 2002). Impacts of mCRT(ΔC) and mCRT(ΔP) truncations upon this activity were next assessed. The pMSCV-puro and pMSCV-ires-GFP viral vectors were utilized for stable and transient expressions, respectively. A small but reproducible induction of surface MHC class I (K^b) molecules was observed when K42 cells were infected with viruses encoding mCRT(WT) compared with those infected with viruses lacking the calreticulin DNA (Figure 2.3A). Using the pMSCV-puro viral vector system, mCRT(ΔP) was significantly impaired in the ability to induce the surface expression of the MHC class I allele H2-K^b relative to mCRT(WT) (Figure 2.3A; p-values of 0.0160 and 0.0089 were obtained using the antibodies Y3 and AF6, respectively). An impairment was also observed in the ability of mCRT(ΔP) to induce the surface expression of the MHC class I allele H2-D^b compared to mCRT(WT), however the impairment did not reach statistical significance (Figure 2.3A; p=0.0823). Additionally, using the pMSCV-ires-GFP viral vector system, mCRT(ΔP) was impaired in the ability to induce the surface MHC class I allele H2-K^b relative to mCRT(WT), however the impairment did not reach significance (Figure 2.3A; p=0.0566). Using both vector systems, a reduction in MHC class I cell-surface expression was also observed in the context of mCRT(ΔC) compared to mCRT(WT), although the reduction did not reach significance (Figure 2.3A).

Additional assays were developed to compare functional activities of the different calreticulin constructs. We noted that steady-state levels of tapasin and MHC class I heavy chains were significantly reduced in cells lacking mCRT compared with cells expressing mCRT(WT) (Figure 2.3B, lysates panels). This was a consistent phenotype in the lysate analyses. Cells expressing mCRT(ΔP) and mCRT(ΔC) also displayed lower steady-state levels of tapasin and MHC class I heavy chains, a phenotype that was more pronounced for mCRT(ΔP) compared with mCRT(ΔC) (Figure 2.3B, lysates panels and tapasin and MHC class I blots). Lower steady-state protein level was not a general phenotype of all ER proteins in K42 cells that lacked calreticulin. For example, ERp57 levels appeared enhanced rather than reduced in the absence of calreticulin (Figure 2.3B,

lysates panels and ERp57 blots).

To assess interactions between PLC components, immunoprecipitations were first performed with a calreticulin-specific antibody, and immunoblotting analyses were undertaken with antibodies directed against different PLC components (Figure 2.3B, CRT IP). A strong signal for tapasin was observed with mCRT(WT) and mCRT(ΔC), whereas tapasin binding to mCRT(ΔP) was impaired (Figure 2.3B, CRT IP and tapasin blot). ERp57 binding to mCRT(WT) and mCRT(ΔC) was weakly detected in some assays (for example, Figure 2.3B, CRT IP and ERp57 blot), and undetectable in other assays (Figure 2.4, ERp57 blot), whereas ERp57 binding to mCRT(ΔP) was undetectable in all analyses. These results suggest that the known P domain-dependent calreticulin-ERp57 interaction (Frickel et al., 2002) was at the detection threshold of these immunoprecipitation reactions. Tapasin forms a disulfide-linked heterodimer with ERp57, an interaction that is observable only if thiol-modifying agents are included during cell lysis (Peaper et al., 2005). Thiol-modifying agents modify free cysteines, thus preventing the disruption of pre-formed disulfide bonds (tapasin-ERp57). A thiol-modifying agent, *N*-Ethylmaleimide (NEM), was not required to observe the calreticulin-tapasin interaction (Figure 2.3B, tapasin blot, compare signals +/- NEM). MHC class I molecules were not detectable in the anti-calreticulin immunoprecipitations (Figure 2.4, MHC class I blot), indicating that glycan-based interactions between MHC class I and calreticulin *per se* are insufficient for stable detection of complex formation between these proteins.

Anti-TAP1 immunoprecipitations revealed incorporation of mCRT(ΔC) into the MHC class I PLC and a deficiency in mCRT(ΔP) incorporation, when expressed at levels similar to mCRT(ΔC) (Figure 2.3C, CRT blot and lanes 2, 3, 9, and 10). Tapasin was incorporated into the PLC of all cells (Figure 2.3C, tapasin blot and lanes 8 –11). Levels of MHC class I detectable within the PLC were reflective of steady-state levels of MHC class I, most readily detectable with mCRT(WT), and very weakly detectable with mCRT(ΔP) or cells expressing the control vector (Figure 2.3C, MHC class I blot and lanes 8 –11). Thus, although PLCs are observable in calreticulin-deficient cells as previously noted (Gao et al., 2002), the efficiency of incorporation of MHC class I molecules is significantly impacted by calreticulin deficiency.

Immunoprecipitations with an anti-MHC class I antibody revealed that MHC class I binding to tapasin was most readily detectable in the context of mCRT(WT), with significant reductions noted in other cells (Figure 2.3D, tapasin blot and lane 8 compared with lanes 9 –11), reflective of alterations in steady-state levels of tapasin. Additionally, ERp57 binding to MHC class I was also most readily detectable in the context of mCRT(WT) (Figure 2.3D, ERp57 blot and lane 8 compared with lanes 9 –11). A very weak signal for mCRT(WT) was observed in the anti-MHC class I immunoprecipitations in two of four experiments (Figure 2.3D, CRT blot and lane 8; a nonspecific band is visualized just below this band), indicating this was also a weak interaction at the detection threshold. Neither of the two mutant calreticulin constructs was observable in these assays.

Together the results in Figure 2.3 indicated that calreticulin deficiency reduced steady-state levels of tapasin and MHC class I heavy chains and cell surface expression of MHC class I. Tapasin-calreticulin binding was readily detectable and abolished by the mCRT(ΔP) mutation, which also negatively impacted calreticulin and MHC class I incorporation into the PLC. Furthermore, the mCRT(ΔC) mutation reduced steady-state levels of PLC components.

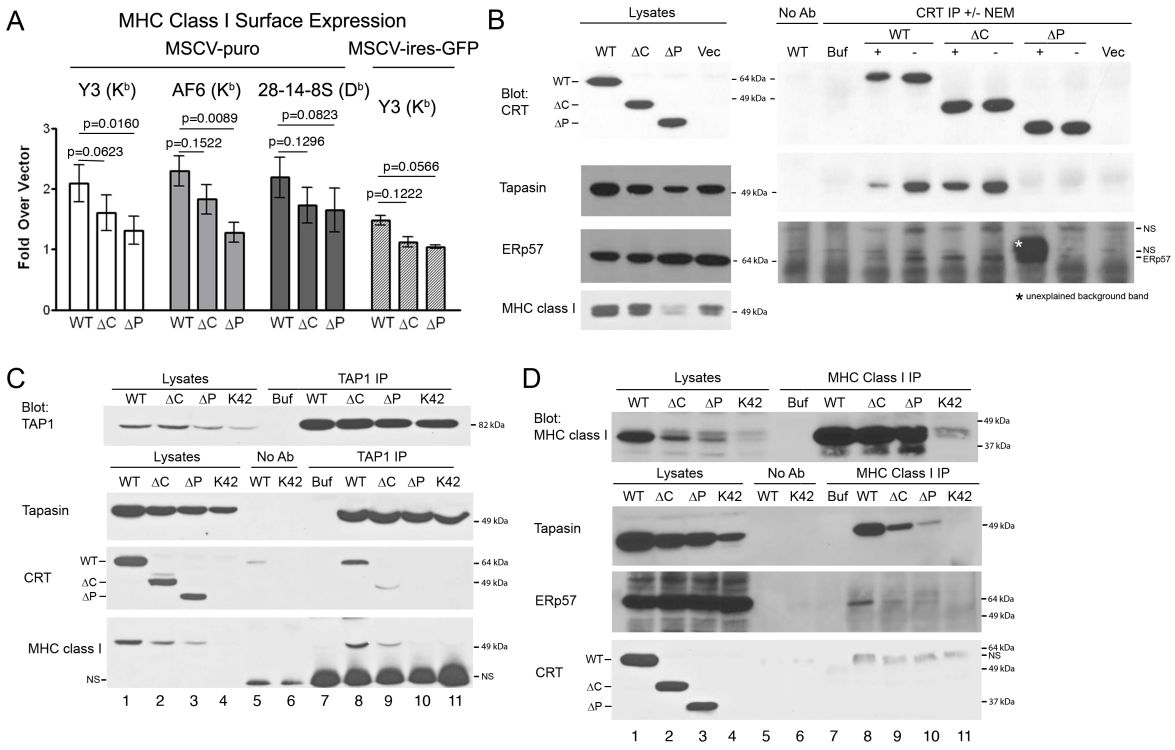

Figure 2.3. mCRT(ΔC) and mCRT(ΔP) have reduced abilities to mediate MHC class I assembly in calreticulin-deficient (K42) cells. A, flow cytometric analyses of cell surface expression of MHC class I on K42 cells infected with retroviruses generated with pMSCV-puro (left three sets of bar graphs) or pMSCV- ires-GFP (bar graph set on the extreme right) encoding indicated mCRT constructs or control virus lacking CRT. The -fold induction of mean fluorescence relative to parallel control infections with vector alone is indicated. Y3 (anti-H2-K^b), AF6 (anti-H2-K^b), or 28-14-8S (anti-H2-D^b) antibodies were used in the analyses as indicated. Data are averaged over seven independent analyses from four separate infection (Y3, left (MSCV-puro) panel), six independent analyses from two separate infection (AF6 and 28-14-8S panels), and three independent analyses from two separate infections (Y3, right (MSCV-IRES-GFP) panel). A pair-wise student t-test was used for statistical analysis. Mean ± s.e.m. is shown. B–D, immunoprecipitations from cells expressing indicated mCRT constructs or control vector-infected cells with anti-calreticulin (B) anti-TAP1 (C) or anti-MHC class I (D). Immunoblotting analyses of indicated cell lysates or immunoprecipitates were undertaken with antibodies directed against various PLC components. Lysates were generated in the presence or absence of NEM (B). Data are representative of five, two, or three independent analyses, respectively, for B–D. No antibody (No Ab) controls were performed by incubating indicated lysates with beads, and Buffer (Buf) indicates signals obtained with antibody alone (without lysates). NS indicates nonspecific bands.

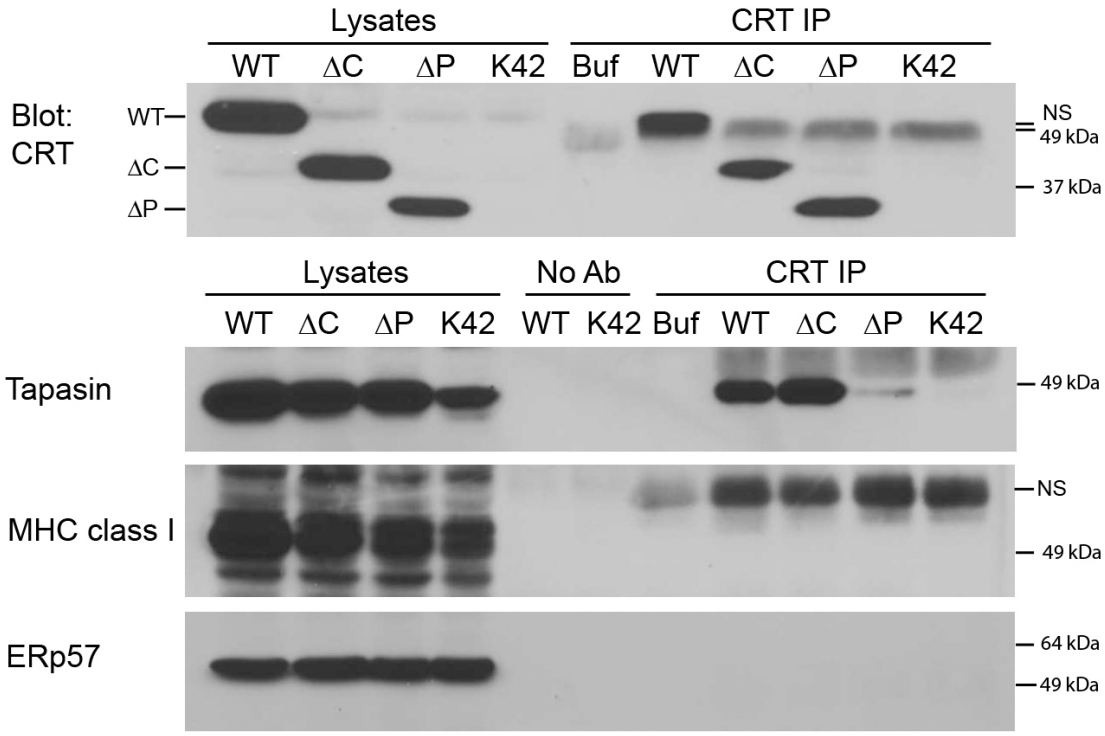

Figure 2.4. Calreticulin is required for the stabilization of the MHC class I – tapasin interaction within the PLC. The indicated cell lines were lysed in a digitonin lysis buffer. A rabbit anti-calreticulin antibody was used for the immunoprecipitation; lysates and samples were immunoblotted with goat anti-calreticulin, hamster anti-tapasin, or rabbit anti-ERp57 and anti-MHC class I antibodies. No antibody (No Ab) controls were performed by incubating indicated lysates with beads, and Buffer (Buf) indicates signals obtained with antibody alone (without lysates). NS indicates non-specific bands.

The mCRT(ΔC) truncation impacts ER retention of calreticulin

Truncating the acidic domain of calreticulin (mCRT(ΔC)) negatively impacted the stability of the PLC and steady-state levels of tapasin and MHC class I (Figures 2.3). The acidic domain of calreticulin is functional as a low affinity/high capacity calcium coordination site. Accordingly, calreticulin deficient cells have a reduced level of calcium storage capacity, which affects agonist-mediated calcium release from the ER [reviewed in (Michalak et al., 2009)]. Additionally, previous studies have suggested that the C-terminal domain of calreticulin, in part, mediates its ER retention (Sonnichsen et al., 1994). To verify the latter results, we assessed whether mCRT(ΔC) displayed impaired ER retention in our system. Immunoprecipitations were performed with an anti-

calreticulin antibody on supernatants of K42 cells expressing mCRT(WT), mCRT(ΔC) or mCRT(vec). Notably, the mCRT(ΔC) construct encodes a C-terminal KDEL motif, similar to mCRT(WT). Whereas mCRT(WT) was faintly detectable in the supernatant, mCRT(ΔC) was readily detectable (Figure 2.5, lane 4 compares to lane 5), in agreement with the previously published finding that the C-terminal domain of calreticulin is involved in the ER localization of calreticulin (Sonnichsen et al., 1994). Thus, inefficient ER retention of mCRT(ΔC) could in part explain the inefficiency of this construct in stabilizing interactions within the PLC and maintaining high steady state levels of MHC class I heavy chains and tapasin.

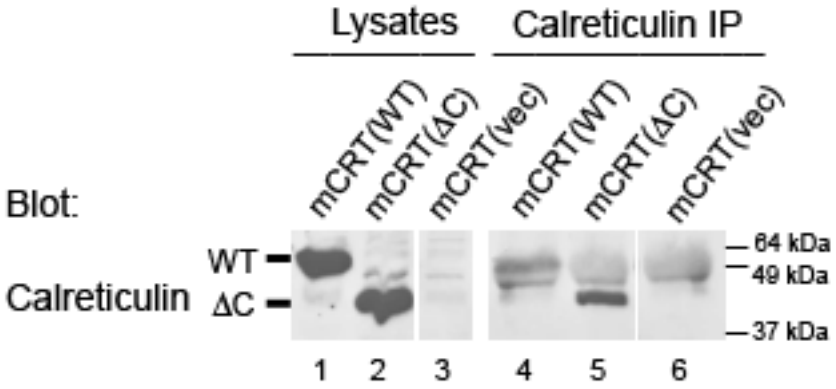

Figure 2.5. The C terminal domain of calreticulin mediates cellular retention of calreticulin. Immunoblotting analyses of indicated K42 cell lysates (lanes 1-3) and anti-calreticulin immunoprecipitations (IP) of cell supernatants (lanes 4-6). Indicated cells were incubated at 37 °C for forty-eight hours before the anti-calreticulin immunoprecipitation was performed on cell supernatants. Data are representative of a single analysis.

Point Mutations Targeting the ERp57 and Glycan Binding Sites of Calreticulin

Impact the Efficiencies of Calreticulin-Tapasin Binding, Stabilization of Tapasin and MHC Class I, and Calreticulin Recruitment to the PLC

Mutations of calreticulin at residues 92 (within the predicted glycan binding site of the globular domain, Figure 2.1B) and 244 (at the tip of the P domain) have previously been shown to strongly impact glycan and ERp57 binding, respectively (Kapoor et al., 2004; Martin et al., 2006); we assessed impacts of mutations at these sites upon MHC class I assembly. Following expression in *E. coli* and purification, mCRT(Y92A) and mCRT(Y92A/W244A) each eluted as a single major peak that was left-shifted compared with mCRT(WT) and mCRT(W244A) (Figure 2.6A). Native-PAGE revealed that the peak fraction of each protein was largely monomeric at 8 μM (37 °C, 0.5 mM $CaCl_2$). Under these conditions, the double mutant showed a small induction of a dimer and oligomeric species (Figure 2.6B). These findings indicate that mCRT(Y92A) and mCRT(Y92A/W244A) equilibrate between monomeric and dimeric/higher order forms during purification (likely due to the high concentrations achieved during purification), but that the equilibriums shift predominantly to monomers at a concentration of 8 μM. The T_m values of mCRT(Y92A) and mCRT(W244A), 45.90 +/- 0.31 °C and 46.59 +/- 0.46 °C, respectively, were slightly left-shifted relative to mCRT(WT) (47.96 +/- 0.21 °C), and that of mCRT(Y92A/W244A) was more strongly left-shifted (42.96 +/- 0.55 °C), indicating slightly lower resistance of the mutants to heat-induced structural changes (Figure 2.6C and Table 2.1). In the presence of G1M3, the T_m values for mCRT(Y92A) and mCRT(Y92A/W244A) did not significantly change, indicating these mutants are in fact deficient in glycan binding (Figure 2.6C and Table 2.1). Similar to mCRT(WT), the T_m value for mCRT(W244A) increased in the presence of G1M3 (50.74 +/- 0.03 °C) (Figure 2.6C and Table 2.1), verifying that this mutant binds glycans. ERp57 binding was strongly reduced with mCRT(W244A) and mCRT(Y92A/W244A) (Figure 2.6D; binding signals too low to allow for accurate K_D value estimation), whereas mCRT(Y92A) interacted with a K_D value of 0.67 μM, similar to that for mCRT(WT).

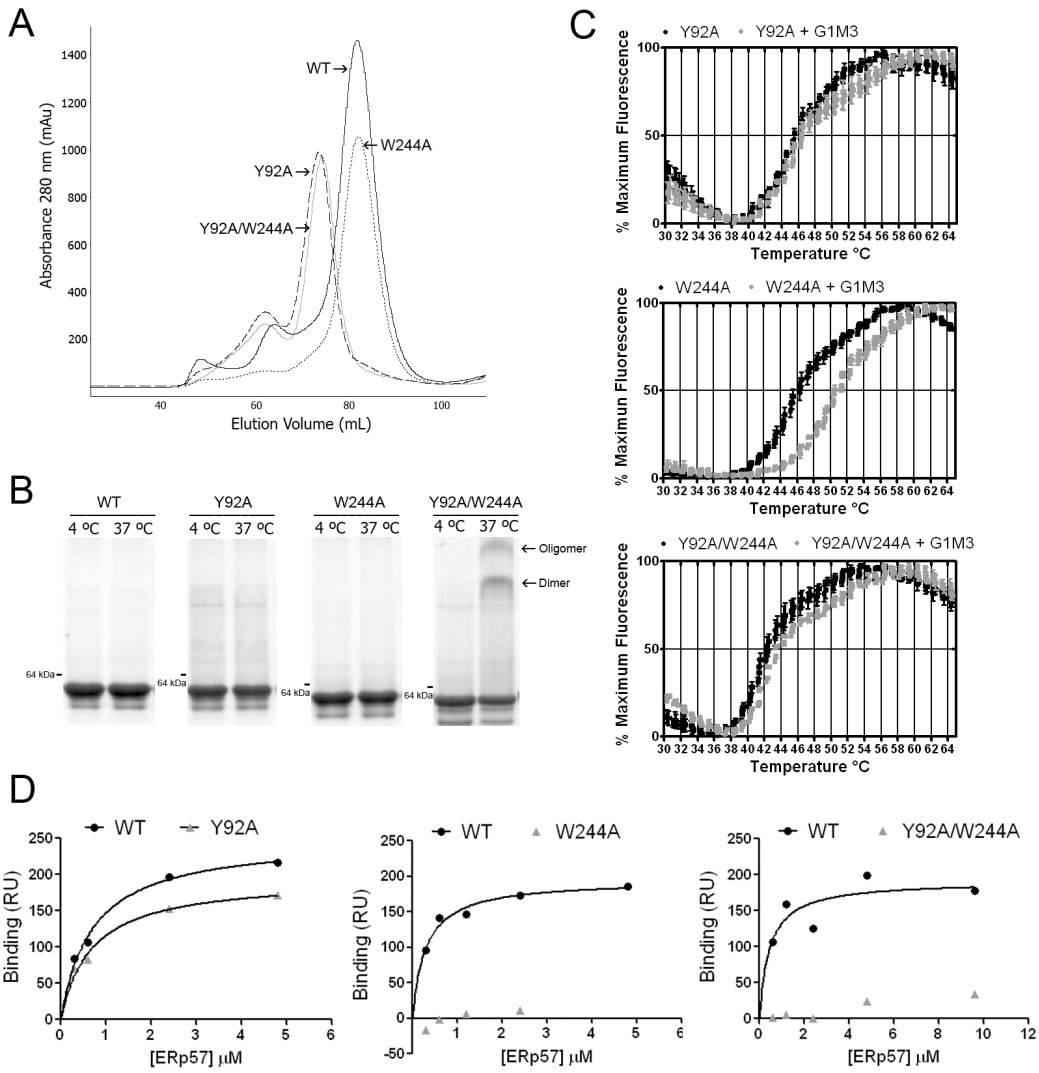

Figure 2.6. Y92A, W244A, and Y92A/W244A mutants of mCRT display expected impairments in glycan and/or ERp57 binding. A, representative gel-filtration chromatograms of mCRT(WT), mCRT(Y92A), mCRT(W244A), and mCRT(Y92A/W244A) following nickel affinity purification. B, native PAGE analyses of pooled peak fractions from A, following incubation at 4 or 37 °C for 1 h (8 μM protein in 1 mM $CaCl_2$). C and D, thermostability and glycan and ERp57 binding analyses of indicated mCRT constructs were performed as described in Fig. 2.2. Data are representative of two independent sets of analyses, except ERp57 binding to the mCRT(Y92A/W244A), for which one analysis was performed. Analyses shown in 2.6C were performed by Elise Jeffery, and analyses shown in 2.6D were performed by Syed Monem Rizvi.

With this knowledge of the conformational integrity and glycan and ERp57 binding phenotypes, mutants were expressed in K42 cells for further analyses. None of the mutants induced surface MHC class I to the same extent as mCRT(WT) (Figure 2.7A). Correlating with this result, and similar to the phenotypes seen with mCRT(ΔP), tapasin levels were reduced in the lysates of cells expressing mCRT(Y92A), mCRT(W244A), mCRT(Y92A/W244A), or the vector control (Figure 2.7B, lysate panels), despite the expression of the mutant calreticulin molecules at levels equal to or greater than mCRT(WT).

In anti-calreticulin-based immunoprecipitations, tapasin co-immunoprecipitation was essentially undetectable with each mutant, either in the presence or in the absence of NEM (Figure 2.7B, CRT IP, tapasin blot, and lanes 5–10). Anti-TAP1 immunoprecipitations revealed reduced incorporation of mCRT(Y92A) and mCRT(W244A) and low or undetectable mCRT(Y92A/W244A) incorporation (Figure 2.7C, CRT blot, and lanes 3– 6) despite expression of each mutant at a level similar to or greater than mCRT(WT). Correlating with lower steady-state MHC class I levels particularly in the context of mCRT(W244A) and mCRT(Y92A/W244A), and despite efficient tapasin incorporation into the PLC, reduced MHC class I incorporation into the PLC was also observed in K42 cells expressing each mutant (Figure 2.7C, MHC class I blot and lanes 3– 6).

Tyr-92 may be important for calreticulin binding to glycans of tapasin or MHC class I, as both proteins are glycosylated. To further examine the former possibility, K42 cells expressing or lacking mCRT(WT) were pre-treated with the drug tunicamycin to block protein glycosylation to a point at which deglycosylated tapasin was the major observable species (Figure 2.7D, tapasin blot and lanes 2 and 4). Under these conditions, the major species that co-immunoprecipitated with calreticulin was the glycosylated form of tapasin, whereas de-glycosylated tapasin was the minor species (Figure 2.7D, tapasin blot and lane 8). These results suggest that the tapasin glycan contributes at least in part to the observed interactions between calreticulin and tapasin. However, the observation of the de-glycosylated tapasin band as a minor species in the anti-calreticulin immunoprecipitation suggests that there are additional modes of direct or indirect calreticulin-tapasin interactions that are independent of the tapasin glycan.

Figure 2.7. Y92A (Y), W244A (W), and Y92A/W244A (Y/W) mutants of mCRT are impaired in mediating MHC class I assembly. A, flow cytometric analyses were performed with the three indicated MHC class I-specific antibodies. The -fold induction of mean fluorescence by each mCRT relative to parallel control vector infections is indicated. Data are the averages of two to three independent experiments from a single infection. A pair-wise student t-test was used for statistical analysis where three independent experiments were performed. Mean ± s.e.m. is shown. B–D, immunoprecipitated proteins (IP) (anti-calreticulin or anti-TAP1) or lysates were analyzed by immunoblotting with the indicated antibodies. Lysates were generated in the presence or absence of NEM (B) and from untreated cells or cells pre-treated with tunicamycin (Tun) (D). Data are representative of two independent analyses. In D, G = glycosylated tapasin, DG = deglycosylated tapasin. Control lanes are labeled as in Fig. 2.3.

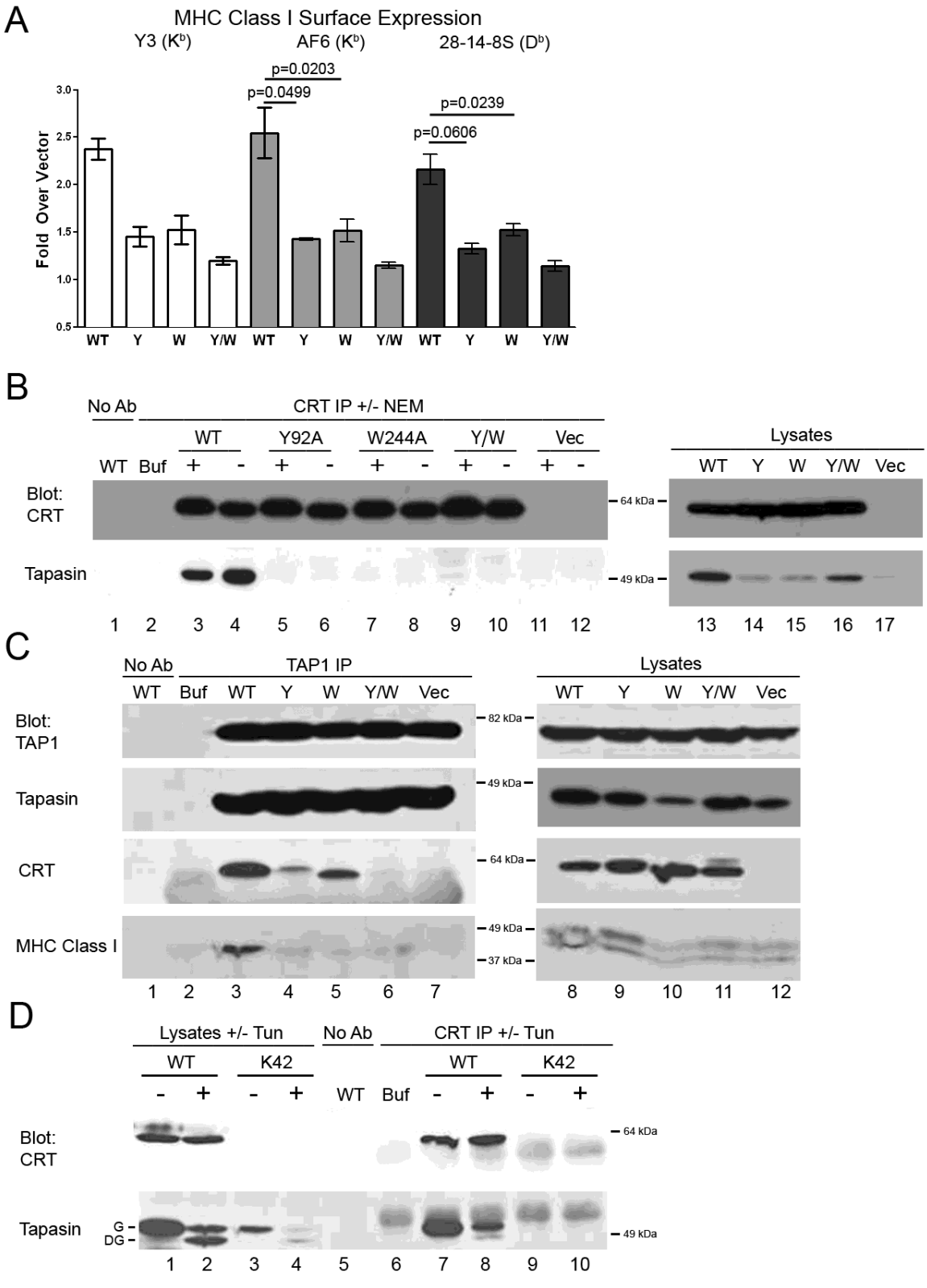
A
MHC Class I Surface Expression
Y3 (Kb)
AF6 (Kb)
28-14-8S (Db)
p=0.0203
p=0.0499
p=0.0239
p=0.0606
Fold Over Vector
3.0
2.5
2.0
1.5
1.0
0.5
WT Y W Y/W WT Y W Y/W WT Y W Y/W
B
No Ab
CRT IP +/- NEM
WT
Y92A
W244A
Y/W
Vec
WT Buf + - + - + - + - + -
Lysates
WT Y W Y/W Vec
Blot:
CRT
Tapasin
64 kDa
49 kDa
1 2 3 4 5 6 7 8 9 10 11 12 13 14 15 16 17
C
No Ab
TAP1 IP
WT Buf WT Y W Y/W Vec
Lysates
WT Y W Y/W Vec
Blot:
TAP1
Tapasin
CRT
MHC Class I
82 kDa
49 kDa
64 kDa
49 kDa
37 kDa
1 2 3 4 5 6 7 8 9 10 11 12
D
Lysates +/- Tun
No Ab
CRT IP +/- Tun
WT
K42
WT Buf - + - + - + - + - +
Blot:
CRT
Tapasin
G
DG
64 kDa
49 kDa
1 2 3 4 5 6 7 8 9 10

Trp-302 of calreticulin is in the vicinity of the glycan binding site of calreticulin (Kozlov et al., 2010) (Figure 2.1B) and impacts glycan binding (Gopalakrishnapai et al., 2006). Additionally, Trp-302 has been implicated in the *in vitro* chaperone activity of calreticulin (Martin et al., 2006). Similar to mCRT(Y92A), mCRT(W302A) protein displayed a gel-filtration profile whose major peak was slightly left-shifted relative to that of mCRT(WT) (Figure 2.8A), while remaining largely monomeric at 4 and 37 °C at a concentration of 8 μM (Figure 2.8B, right panel). In a thermostability assay, mCRT(W302A) displayed a T_m value of 44.82 +/- 0.55 °C, lower than that of mCRT(WT) (T_m = 47.96 +/- 0.21 °C), and the T_m value of mCRT(W302A) did not right-shift in the presence of G1M3 (Figure 2.8C and Table 2.1), indicating that the mutant has the expected deficiency in glycan binding. In Biacore assays, mCRT(W302A) was able to bind to ERp57 with a K_D value of 0.88 μM, similar to mCRT(WT) (Figure 2.8D).

In K42 cells, mCRT(W302A) was unable to restore surface MHC class I (Figure 2.8E). Steady-state levels of tapasin and MHC class I in the lysates of cells expressing mCRT(W302A) were reduced compared with those found in K42 cells expressing mCRT(WT) (Figure 2.8, F and G, lysate panels and lanes 8–10). Immunoprecipitations with anti-calreticulin revealed defects in tapasin binding by mCRT(W302A) (Figure 2.8F, CRT IP, tapasin blot, and compare lane 2 with lane 3). Immunoprecipitation with anti-TAP1 revealed impaired incorporation of mCRT(W302A) into the PLC (Figure 2.8G, TAP IP, CRT blot, and compare lane 2 with lane 3), and impaired MHC class I incorporation into the PLC in the context of mCRT(W302A) (Figure 2.8G, TAP IP, MHC class I blot, and compare lane 2 with lane 3).

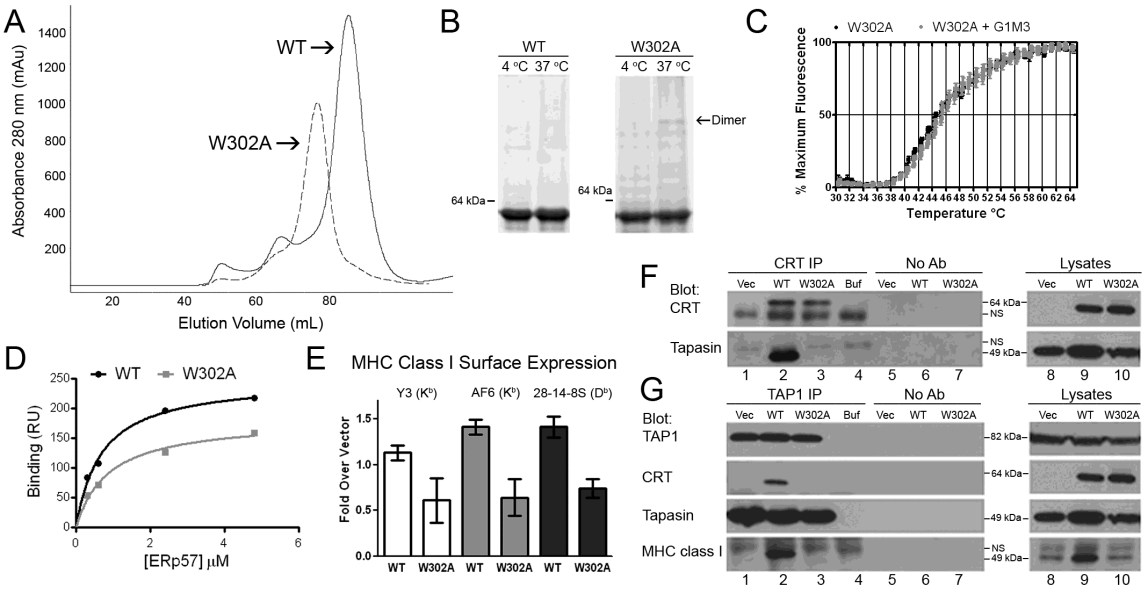

Figure 2.8. mCRT(W302A) is impaired in mediating MHC class I assembly. A, representative gel-filtration chromatograms of mCRT(WT) and mCRT(W302A) proteins following nickel affinity chromatography. B, native PAGE analysis of pooled peak fractions from A, following indicated incubations (in 0.5 mM $CaCl_2$). C and D, thermostability, glycan, and ERp57 binding analyses for mCRT(W302A) performed as described in Fig. 2.2. Thermostability data are representative of three independent analyses, and ERp57 binding data is based on a single analysis. E, flow cytometric analyses of the ability of mCRT(WT-FLAG) and mCRT(W302A-FLAG) to restore MHC class I expression in K42 cells were performed as described in Fig. 2.6A. Data are representative of three experiments from two infections. Significance of the reduction of cell surface MHC class I in the context of the W302A-FLAG construct used in Figure 2.8 is shown in (Jeffery et al., 2010). F and G, immunoprecipitated proteins (anti-calreticulin and anti-TAP1) or lysates were analyzed by immunoblotting with the indicated antibodies. Data are representative of two immunoprecipitations. Control lanes are labeled as indicated in Fig. 2.3. Analyses shown in Figure 2.8A-C and E-G were performed by Elise Jeffery. Analyses shown in Figure 2.8D were performed by Syed Monem Rizvi.

β2m is required for efficient calreticulin and ERp57 recruitment to the PLC

The findings described above indicated that calreticulin recruitment to the PLC was abrogated by mutations of the glycan and ERp57 binding sites of calreticulin. Previous studies have described that calreticulin recruitment to the PLC is also reduced in β2m-deficient human cells (Diedrich et al., 2001; Sadasivan et al., 1996). To further investigate requirements for calreticulin and ERp57 recruitment, $\beta2m^{-/-}$ mouse splenocytes were analyzed for their PLC compositions (Figure 2.9). Steady-state levels of

MHC class I H chains are not reduced in the lysates of β2m-deficient cells compared with wild-type cells (Figure 2.9, lanes 1 and 2, MHC class I H chain blot). However, the species that exists is entirely ER localized as assessed by Endo H digestion, whereas a minority of the H chains in wild-type lysates is ER localized (data not shown). Splenic cell lysates from wild-type C57BL/6 or $\beta2m^{-/-}$ mice were immunoprecipitated with anti-TAP1 (Figure 2.9). As expected based on previous results (Ortmann et al., 1994; Suh et al., 1994), MHC class I H chain recruitment was strongly impacted in cells lacking β2m compared with wild-type cells (Figure 2.9, class I H chain blot, lanes 6 and 7). Additionally, TAP–calreticulin association is essentially undetectable in cells lacking β2m compared with wild-type cells, as previously shown (Diedrich et al., 2001; Sadasivan et al., 1996) (Figure 2.9, CRT blot, lanes 6 and 7). Notably, ERp57 recruitment efficiency was also reduced in β2m-deficient cells (Figure 2.9, ERp57 blot, lanes 6 and 7). ERp57 is thought to be recruited to the PLC via heterodimeric interactions with tapasin (Dick et al., 2002; Peaper et al., 2005). However, it appears that β2m also aids in the recruitment of ERp57 (Figure 2.9, ERp57 blot), either via direct interactions, or indirectly. MHC class I H chains have been shown in some studies to interact directly with ERp57 (Kienast et al., 2007; Lindquist et al., 2001). It is thus also possible that β2m indirectly facilitates recruitment of MHC class I-associated ERp57 by stabilizing a conformation of MHC class I H chain that is better able to interact with ERp57.

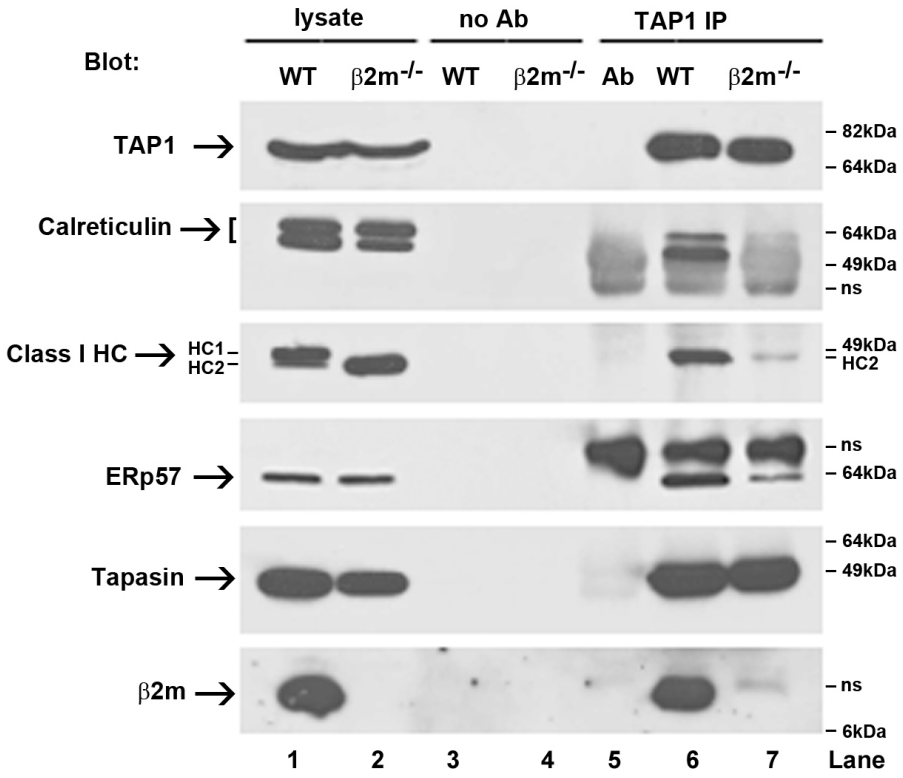

Figure 2.9. β2m$^{-/-}$ cells are deficient in recruiting CRT into the PLC. Anti-TAP1–immunoprecipitated proteins (IP) or lysates were analyzed by immunoblotting with the indicated Abs. Splenic lysates from wild-type (WT) or β2m$^{-/-}$ mice were used for the immunoprecipitations. Data are representative of one analysis for β2m, two analyses for class I H chain, two analyses for ERp57, three analyses for tapasin, and five analyses for CRT. Two bands are observed for CRT, most likely corresponding to a full-length version and a degradation product. Two species of MHC class I H chains are observed in the cell lysates (labeled as HC1 and HC2), most likely corresponding to differently glycosylated forms of H chains. Only HC2 is detectable in the immunoprecipitations and in β2m$^{-/-}$ cells. No Ab controls were performed by incubating indicated lysates with protein G beads, and Ab indicates signals obtained with Ab alone (without lysates). Ab-derived or other nonspecific bands are indicated as ns.

Various mCRT Mutants Induce the Activity of Calreticulin in Suppressing Protein Aggregation

Calreticulin has previously been shown to inhibit thermal aggregation of various non-glycosylated substrate proteins (Martin et al., 2006; Rizvi et al., 2004; Saito et al., 1999), a functional assay indicative of the polypeptide-binding activity of calreticulin. To assess this activity at 37 °C, listeriolysin O (LLO) was used as a substrate. LLO has been shown to aggregate at 37 °C and neutral pH (Schuerch et al., 2005), which was reproduced in the present study by gel-based aggregation assays and light scattering assays. By the gel-based assay, in the presence of 0.5 mM $CaCl_2$, mCRT(WT) was unable to significantly rescue LLO from precipitating at LLO:mCRT ratios up to 1:4 (Figure 2.10). Calcium depletion induced the aggregation suppression activity of mCRT(WT), as did the mCRT(ΔC) truncation, consistent with our previous findings with different substrates (Rizvi et al., 2004).

By the more sensitive light scattering assay, in 0.5 mM $CaCl_2$, mCRT(WT) had low activity until high stoichiometric ratios were achieved (1:16 LLO:mCRT(WT); data not shown). mCRT(ΔC) displayed induced activity relative to mCRT(WT) (for example, Figure 2.11A). mCRT(Y92A) and mCRT(Y92A/W244A) displayed strongly induced activities relative to mCRT(WT) in all analyses undertaken (for example, Figure 2.11, B and C). mCRT(W244A) and mCRT(W302A) also displayed higher or equal activities relative to mCRT(WT) in the majority of conditions tested (14 of 18 conditions analyzed over 4 independent experiments for W244A, and 19 of 24 conditions analyzed over 6 independent experiments for W302A; representative analyses shown in Figure 2.11, D and E). The W302A and W244A mutants of calreticulin have both previously been implicated as being impaired for rescue of aggregation of other substrates at 44 – 45 °C (Martin et al., 2006); our findings reflect different phenotypes of these two mutants in aggregation assays performed under a physiological non-stress condition.

Compared with mCRT(WT), lower activity of mCRT(ΔP) was observed in 9 analyses, and equal or higher activity was observed in 11 analyses of a total of 21 comparisons over 4 independent experiments (for example, Figure 2.11F). These variable results taken together with previous findings that the P domain of calnexin facilitates suppression of substrate aggregation (Brockmeier et al., 2009) prompted us to use gel-

based aggregation assays to further compare mCRT(ΔP) and mCRT(WT) activities. Because ATP is a factor that modulates the chaperone activity of calreticulin (Saito et al., 1999), aggregation suppression activities of mCRT(WT) and mCRT(ΔP) were measured in 0.5 mM $CaCl_2$ +/- 3 mM ATP. Both ATP and a 1:16 ratio of LLO to mCRT(WT) were required to partially inhibit LLO aggregation at 37 °C (in 0.5 mM $CaCl_2$) (Figure 2.11G, middle panel, and compare lane 3 with lanes 1 and 5). The addition of 3 mM ATP also markedly induced the aggregation suppression activity of mCRT(ΔP) (Figure 2.11G, top and middle panels, and compare lane 7 with lanes 1 and 9). This impact of ATP was readily apparent with mCRT(ΔP) even at a 1:8 ratio (Figure 2.11G, upper panel, and compare lane 7 with lanes 1 and 9), and ATP induced a more marked left-shift of the T_m value for mCRT(ΔP) compared with mCRT(WT) (Figure 2.11H and Table 2.1, T_m values of 45.49 +/- 0.13 and 46.24 +/- 0.02 °C, respectively, in the presence of ATP). Thus, the removal of the P-domain rendered calreticulin more susceptible to ATP-induced structural changes, thereby enhancing its ability to suppress aggregation of a misfolded protein under a physiological condition. Furthermore, several mutations that impaired mCRT function in MHC class I assembly induced its ability to suppress aggregation of a substrate protein *in vitro* under a physiological condition.

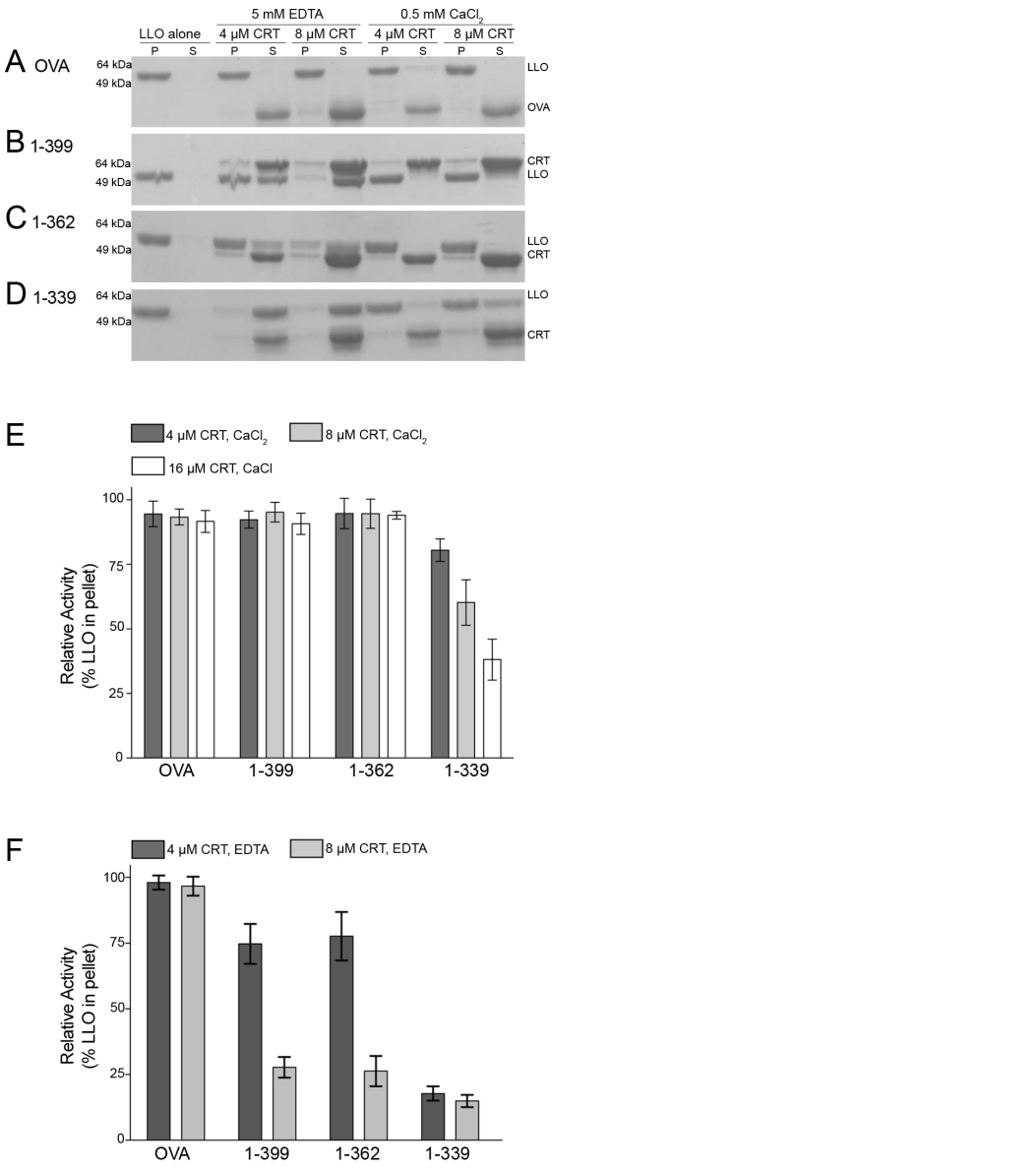

Figure 2.10. Relative aggregation suppression activities of full-length and C-terminal truncation mutants of mCRT under various conditions. (A-D) Representative SDS-PAGE gels of aggregation assays with indicated mCRT constructs and OVA as a control. OVA or mCRT at indicated concentrations were incubated with 4 μM LLO in the presence of 0.2-0.5 mM $CaCl_2$ or 5 mM EDTA at 37 °C for 1 hour. Following incubations, aggregated proteins were separated from soluble proteins by centrifugation, and proteins present in supernatants (S) and pellets (P) were resolved by SDS-PAGE and visualized by staining with coomassie blue dye. (E and F) Band intensities of LLO in the pellet after incubation in the presence of mCRT or OVA were quantified, and are represented as a percentage relative to LLO observed in the pellet in the absence of mCRT or OVA. For each condition, data represent results from 3 or more experiments, except under conditions of 16 μM $mCRT_{1\text{-}362}$, for which data represent quantifications from 2 experiments.

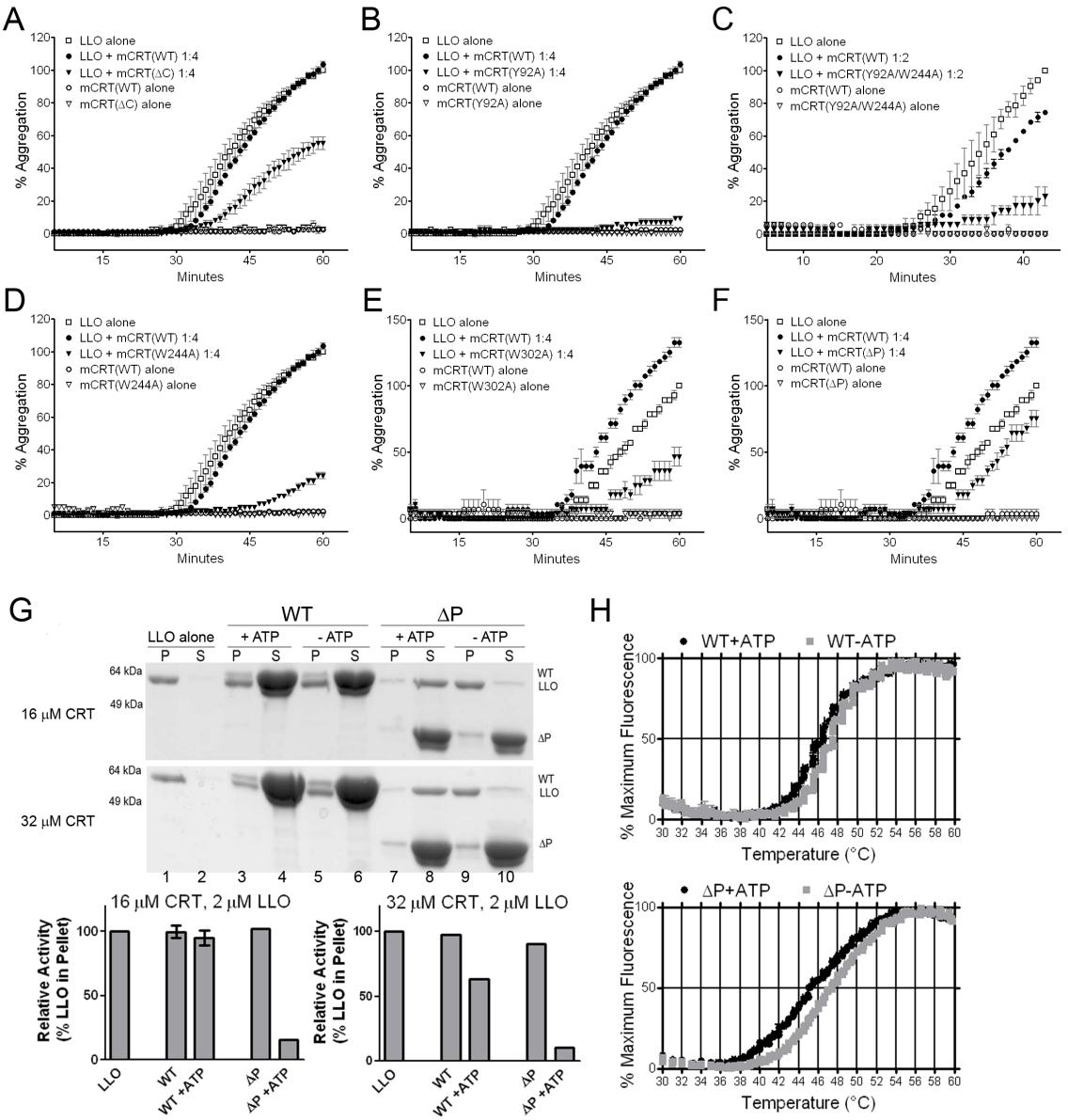

Figure 2.11. Aggregation suppression activities of calreticulin mutants *in vitro*. A–F, light scattering-based aggregation assays of the abilities of indicated mCRT constructs to suppress LLO (1 μM) aggregation at 37 °C in the presence of 0.5 mM $CaCl_2$. G, gel-based aggregation assays. LLO alone (4 μM) or LLO with indicated amounts mCRT(WT) or mCRT(ΔP) were incubated in the presence of 0.5 mM $CaCl_2$ ± 3 mM ATP at 37 °C for 1 h. Proteins present in supernatants (S) and pellets (P) were resolved by SDS-PAGE and visualized by staining with Coomassie Blue dye (top and middle panels). Lower panels, band intensities of LLO in the pellet were quantified and are represented as a percentage relative to LLO observed in the pellet in the absence of any mCRT. H, thermostability of mCRT(WT) or mCRT(ΔP) in the presence of 0.5 mM $CaCl_2$ ± 3 mM ATP as indicated, were measured as described in Fig. 2.2. Analyses shown in Figure 2.11H were performed by Elise Jeffery.

Discussion

In the N-terminally truncated calreticulin construct $mCRT_{33–362}$, essentially all protein was purified as dimers and higher order oligomers in the presence of 1 mM $CaCl_2$ (Figure 2.2, B and H), suggesting that structural changes involving this region of calreticulin may be responsible for inducing oligomer formation under heat-shock or calcium-depleting conditions. The C-terminal helix was also critical for maintaining calreticulin monomers (Figure 2.2, A and G); the predominant species induced by this truncation migrated in the void volume. Conformational alterations and self-association interfered with the ability of the truncated variants to bind glycan substrates. A loss of just 20 residues internal to the acidic domain or 33 N-terminal residues is sufficient to induce profound conformational alterations. A number of functional studies of calreticulin described in the literature that used calreticulin truncations lacking all or a subset of residues N- and C-terminal to the P domain (or truncation constructs containing only the regions N- or C-terminal to the P domain), may have to be re-interpreted in light of these findings.

The C terminal truncation mutant mCRT(ΔC) was not defective for tapasin binding (Figure 2.3B). However, mCRT(ΔC) was less efficient at being recruited into the TAP complex, did not stabilize tapasin and MHC class I heavy chains as efficiently as did mCRT(WT), and did not induce MHC class I surface expression as efficiently as did mCRT(WT) (Figure 2.3A and 2.3C). Ineffective ER retention of mCRT(ΔC) (Figure 2.5) may help explain the phenotypes observed in K42 cells expressing mCRT(ΔC). Secretion of mCRT(ΔC) from the ER would diminish the calreticulin available for PLC stabilization in the ER.

Truncation and point mutations of calreticulin that disrupted glycan binding [mCRT(Y92A) and mCRT(W302A)] or ERp57 binding [mCRT(ΔP) and mCRT(W244A)] were defective for binding tapasin, being recruited into the TAP complex, stabilizing tapasin and MHC class I heavy chains, and inducing MHC class I surface expression. For the Y92A and W244A mutations, binding deficiencies were more strongly apparent in the anti-CRT immunoprecipitations than in the anti-TAP1 immunoprecipitations, indicating that binding defects with these mutants may be partial rather than complete. Nevertheless, strong binding defects were apparent with these mutants as well as with mCRT(ΔP), mCRT(W302A), and mCRT(Y92A/W244A),

mutants for which tapasin or TAP binding were essentially undetectable. The Williams laboratory used a different set of mutants, Y111A for a glycan binding-deficient mutant, D241N for an ERp57 binding-deficient mutant (Y128A and D258N, respectively, in protein numbering that includes the signal sequence), and the double mutant Y111A/D241A, analyses of which suggested that calreticulin could be recruited into the PLC in the absence of interactions with both ERp57 and substrate oligosaccharides (Zhang et al., 2009). Previous studies have defined that trisaccharide interactions with calreticulin were essentially undetectable with the Y92F mutant (Y109F in mature protein numbering), whereas binding was detectable with Y111F (Y128F in mature protein numbering) (K_B = 11.21 x 10^4 M^{-1} for Y128F compared with a K_B of 58.8 x 10^4 M^{-1} for mCRT(WT)) (Kapoor et al., 2004). Thus, it is likely that the choice of mutant impacts the extent of the binding deficiency and forms the basis for the discrepancies in conclusions from the two studies. Additionally, antibodies used in the interactions analyses and the levels of calreticulin expression achieved are likely to determine the sensitivity with which binding differences can be elucidated.

Our mutational data are strongly supportive of a model in which calreticulin-ERp57 and calreticulin-glycan interactions are both important for the recruitment of calreticulin into the PLC and for the functional activity of calreticulin in stabilizing tapasin and MHC class I heavy chains. Although previous studies have suggested a role for MHC class I glycan-dependent interactions for the recruitment of calreticulin to the PLC, support for such a mode of binding comes from studies with glycosylation inhibitors, *in vitro* binding studies with purified MHC class I molecules and calreticulin, and glycan-deficient mutants of MHC class I molecules (Harris et al., 1998; Sadasivan et al., 1996; Wearsch et al., 2004). Support for an ERp57-dependent mode of calreticulin recruitment comes from the known tapasin-ERp57 interaction and its impact on calreticulin recruitment (Garbi et al., 2006; Peaper and Cresswell, 2008; Wearsch and Cresswell, 2007). The studies described here represent the first direct evidence for the involvement of the glycan and ERp57 binding sites of calreticulin for its recruitment into the PLC. Furthermore, based on the strong Tyr-92 and Trp-302 dependence of the tapasin-calreticulin binding (Figures 2.7 and 2.8), it was an open question whether calreticulin recruitment to the PLC involves tapasin's glycan, MHC class I's glycan, or both (Figure 2.12). Two models for the

recruitment of calreticulin into the PLC are shown in Figure 2.12 that were both consistent with the Figures 2.7 and 2.8. In both models, the tip of the P domain of calreticulin engages the b' domain of ERp57. In model A, glycans of MHC class I are bound by calreticulin, and a specific contact interface for tapasin binding is also present on calreticulin. This model is similar to that proposed following structural studies of tapasin-ERp57 complexes (Dong et al., 2009). Current support for model 2.12A comes from inhibitor-based data, which showed reduced calreticulin-MHC class I binding in castanospermine-treated cells, and from cells expressing mutant MHC class I molecules lacking an appropriate glycan, which displayed reduced calreticulin binding (Harris et al., 1998; Sadasivan et al., 1996). The treatments or mutations also impacted MHC class I-TAP binding, which leaves open the possibility of indirect impacts upon MHC class I-calreticulin binding. Further support for model 2.12A comes from detection of MHC class I – calreticulin assembly intermediates (Wearsch et al., 2011). In the additional/alternate model 2.12B, which is favored by the data in Figure 2.7D, calreticulin engages the glycan of tapasin.

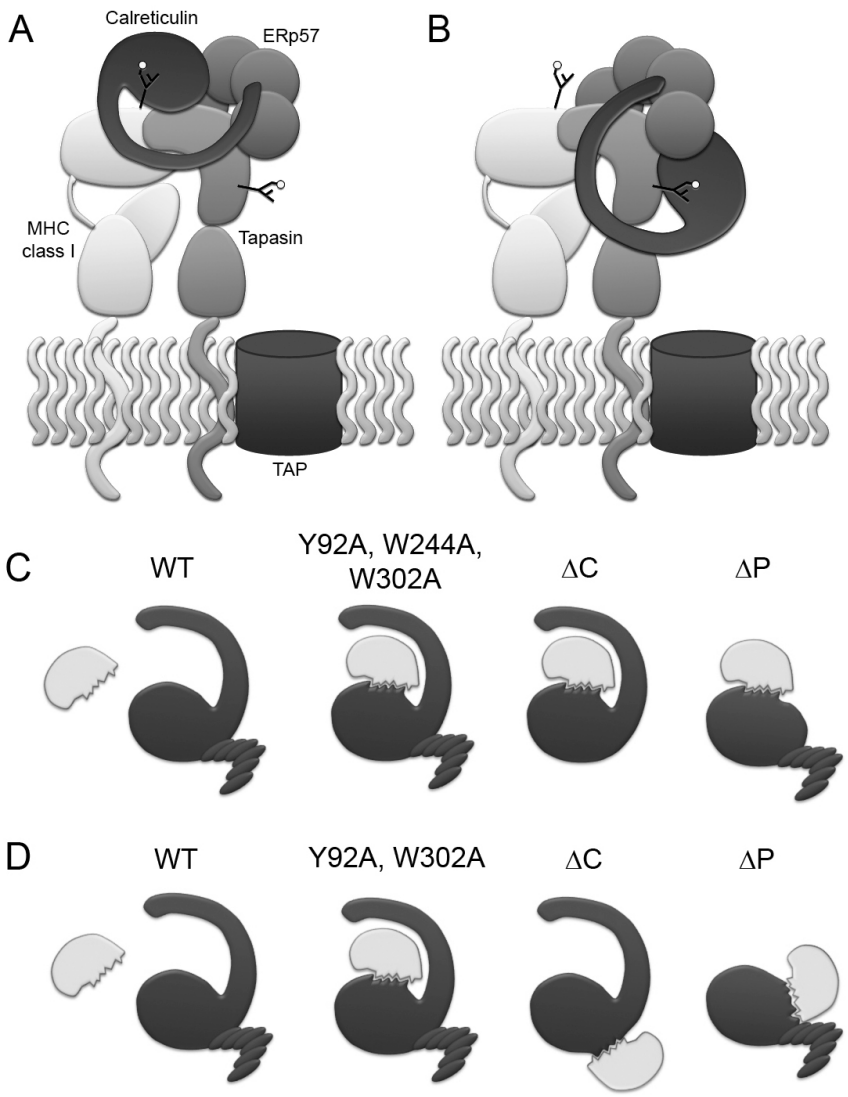

Figure 2.12. Modes of substrate recognition by calreticulin. A and B, two mechanisms to explain the central roles of tapasin, glycans, and ERp57 in calreticulin recruitment to the PLC and function within the PLC. In A, calreticulin binds to a MHC class I glycan, to ERp57 via the tip of its P domain, and to tapasin via a specific polypeptide binding site. In B, calreticulin binds to the glycan of tapasin, and to ERp57 via the tip of its P domain. A specific polypeptide-based interaction with MHC class I may also be relevant to this mode of recruitment. Interactions mediated by the acidic domain of calreticulin, which is also important for function, have to be further defined, and are not shown for simplicity. C and D, polypeptide binding sites on calreticulin are induced by mutations targeting distinct domains and residues on calreticulin, likely relating to the structural plasticity of calreticulin, which exposes single (C) or distinct hydrophobic sites (D) upon different truncations/mutations. Because mutations that induce the ability of calreticulin to suppress protein aggregation in vitro inhibit calreticulin recruitment to the PLC in cells, generic polypeptide binding sites *per se* are insufficient to recruit calreticulin to the PLC under non-stress conditions.

To further elucidate whether one or both models (Figure 2.12A or 2.12B) are relevant, in a subsequent study (Rizvi et al., 2011) we compared calreticulin recruitment mediated by a tapasin glycan mutant (N233Q) compared to wild type tapasin and by a MHC class I glycan mutant HLA-A2 (N86Q) compared to wild type HLA-A2 in the tapasin-deficient M553 cell line. Our findings support the model that tapasin's glycan is a relevant site that mediates calreticulin recruitment into the PLC.

Compared to wild type tapasin, the tapasin(N233Q) mutation significantly reduced the efficiency of calreticulin recruitment to tapasin under conditions where MHC class I heavy chain and β2m expression were low. ERp57 recruitment efficiency to tapasin was also reduced in cells expressing the tapasin(N233Q) mutation compared to cells expressing wild type tapasin (Rizvi et al., 2011). Calreticulin deficiency in cells reduced ERp57 recruitment into the PLC as well (data not shown). These data suggest that calreticulin bound to tapasin's glycan may initiate ERp57 recruitment into the PLC via a calreticulin P domain-ERp57 interaction. Once ERp57 is recruited to the PLC by the calreticulin P domain, ERp57 could bind and initiate conjugation with C95 of tapasin. Molecular modeling studies suggest that a calreticulin bound to tapasin's glycan cannot simultaneously contact the ERp57 molecule present within the same tapasin–ERp57 conjugate (S.J. Wijeyesakare and M. Raghavan, unpublished observations). Hence, we propose that once ERp57 forms a conjugate with tapasin, a conformational change is initiated that forces calreticulin to disengage from tapasin's glycan (Figure 2.13A) and repositions calreticulin for P-domain mediated ERp57 binding (Figure 2.13B). Calreticulin may equilibrate between the two conformational states (Figure 2.13A ⇔ 2.13B) where calreticulin recruitment is initially mediated by tapasin's glycan and once tapasin bound calreticulin recruits ERp57, calreticulin is repositioned to interact primarily with ERp57 and disengages from tapasin's glycan. The latter conformation (2.13B) appears to be the relevant one for recruitment of MHC class I molecules as the tapasin C95A mutant significantly affects the efficiency of MHC class I heavy chain and β2m recruitment to the PLC (Rizvi et al., 2011).

Experiments utilizing a deglycosylated heavy chain showed that the heavy chain glycan is not central to calreticulin recruitment into the PLC. This was suggested in experiments in murine cells (Figure 2.7), and confirmed in human cells (Rizvi et al.,

2011). The heavy chain glycan impacted the efficiency of H chain recruitment to the PLC, but does not impact calreticulin recruitment (Rizvi et al., 2011). On the other hand, β2m deficiency strongly impaired calreticulin recruitment into the PLC (Figure 2.9). These findings suggested a model involving tapasin, ERp57, calreticulin and β2m as intermediate PLCs into which MHC class I heavy chains are recruited (Figure 2.13C). Whether the MHC class I glycan participates in recruitment remains to be elucidated, although a recent study (Wearsch et al., 2011) alludes to this possibility.

Calreticulin is able to interact with MHC class I molecules in a glycan-independent manner under conditions of ER stress both in cells and *in vitro* (Rizvi et al., 2004), but whether such interactions also occur under physiological non-stress conditions is unclear. Mutations targeting diverse regions of calreticulin induced its ability to suppress aggregation of a non-glycosylated polypeptide (Figure 2.11), likely by providing increased exposure (at 37 °C in 0.5 mM $CaCl_2$) of either one or several hydrophobic surfaces that can participate in substrate binding (Figures 2.12, C and D), as suggested by the slight reduction in T_m values of the mutants (Figures 2.2, 2.6, and 2.8). However, calreticulin mutants with induced aggregation suppressive activities *in vitro* were impaired in their binding to tapasin and in their recruitment into the PLC under non-stress conditions (Figures 2.3, 2.7, 2.8, and 2.11). Thus, generic polypeptide-based associations involved in protein aggregation suppression mediated by calreticulin *per se* are insufficient for stable recruitment of calreticulin to PLC components in cells under non-stress conditions. However, based on the model discussed in Figure 2.13, it is likely that P domain based interactions are relevant to stabilize interactions within the PLC.

In summary, the work here provides greater insight into the assembly of the PLC. We show that MHC class I incorporation into the PLC is reduced in cells deficient in calreticulin. We also provide evidence that calreticulin recruitment into the PLC is mediated by ERp57 and glycan-based interactions, and calreticulin mutations affecting either the ERp57 or glycan binding site of calreticulin negatively affect MHC class I recruitment into the PLC. Additionally, we show that ERp57 recruitment into the PLC is negatively affected by the absence of calreticulin within the PLC. Finally, we find that β2m deficiency reduced the recruitment of both ERp57 and calreticulin into the PLC. Based on this study and a recently published study (Rizvi et al., 2011), we have

developed a model for PLC assembly (Figure 2.13). We propose that calreticulin is first recruited to TAP/tapasin via tapasin's glycan. ERp57 is then recruited into the PLC via the P domain of calreticulin. Once recruited by calreticulin, ERp57 forms a stable disulfide bond with tapasin. Lastly, β2m is recruited into the PLC intermediate. The PLC intermediate containing TAP, tapasin, ERp57, calreticulin and β2m functions to recruit MHC class I into the PLC. Details of the latter complex remain to be further clarified. Taken together, the findings here and in Rizvi et al. (2011) raise the possibility that although the glycan and ERp57 binding sites of calreticulin are important for its recruitment into the PLC or to components of the PLC, glycan-based and ERp57-based interactions of calreticulin may occur at distinct steps of PLC assembly.

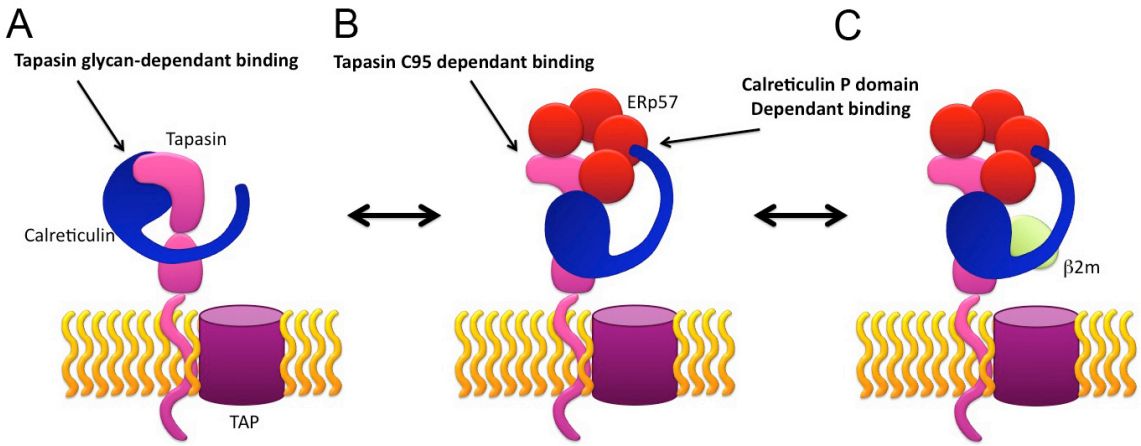

Figure 2.13. In a proposed model of the PLC, calreticulin equilibrates between tapasin glycan- and tapasin(C95)-associated forms. (A) Tapasin's glycan contributes to the recruitment of calreticulin. Such a subcomplex may facilitate ERp57 recruitment by transient interaction of ERp57 with the tip of calreticulin's P domain, thus bringing ERp57 into proximity to tapasin(C95). ERp57 becomes conjugated to tapasin(C95). This is shown to displace calreticulin from tapasin's glycan, and link calreticulin to the PLC via P domain-mediated interactions with tapasin(C95)-associated ERp57. This complex is unstable, as calreticulin and ERp57 recruitment to tapasin is reduced in β2m-/- cells (Figure 2.9). (C) β2m is recruited into the PLC, and this intermediate associates with MHC class I heterodimers, resulting in β2m and peptide dissociation from incoming heterodimers.

Materials and Methods

DNA Constructs

Expression of mCRT in Escherichia coli—Truncation mutants of mouse calreticulin (mCRT) were amplified from the pCMV-SPORT6 (ATCC, MGC-6209) vector using primers that allowed for subsequent ligation-independent cloning (LIC) into the pMCSG7 vector (Stols et al., 2002). The following oligonucleotide primers were used to terminate CRT at the indicated C-terminal amino acid positions: 399, 5 -TTA TCC ACT TCC AAT GTT ACA GCT CAT CCT TGG CTT-3 ; 362, 5'-TTA TCC ACT TCC AAT GTT ATT CCT CTT TAC GCT TCT TGT-3'; 339, 5'-TTA TCC ACT TCC AAT GTT ACT GCT TCT CGG CAG CCT TGG TTA CAC CCC-3'; and 318, 5'-TTA TCC ACT TCC AAT GTT AAT CAT TAG TGA TGA GGA AAT TGT C-3'. The following oligonucleotide primers were used to generate constructs at the N-terminal start sites: 1, 5'-TAC TTC CAA TCC AAT GCT GCC GCA GAC CCT GCC ATC- 3'; and 33, 5'-TAC TTC CAA TCC AAT GCT GTC CTC AGT TCT GGC AAG TTT TAC GGG-3'. Underlined bases represent those that are complementary to the sequence encoding mCRT, and additional 5' sequences were introduced for LIC.

Deletion of the P domain amino acids 187–283 and insertion of two glycine residues (mCRT(ΔP)) was achieved with the Finnzymes Phusion site-directed mutagenesis kit (New England Biolabs). The following primers were used to generate mCRT(ΔP): forward, 5'-GGA CCC GAT GCA AAT ATC TAT GCC TAT-3' and reverse, 5'-TCC CAG AAA GTC CCA ATC ATC CTC CAA-3'.

DNA constructs were sequenced and transformed into BL21 (DE3) cells for protein expression. All bacterially expressed mCRT constructs lacked the signal sequence and contained an N-terminal MHHHHHHSSGVDLGTENLYFQSNA fusion sequence for nickel affinity chromatography.

Cloning of mCRT Truncation Mutants into Retroviral Vectors— mCRT mutants were cloned into pMSCV-ires-GFP and pMSCV-puro retroviral vectors. pMSCV-puro constructs were created by ligation-dependent cloning, and LIC was used to generate pMSCV-ires-GFP vectors. The mCRT templates used were the corresponding mCRT in the pMSCV-ires-GFP vector (for ΔC x pMSCV-puro) or pCMV-SPORT6 (all other constructs). All constructs retained the mCRT signal sequence and KDEL ER retention

motifs.

Generation of LIC-competent Version of pMSCV-ires-GFP— The plasmid pMCSV-ires-GFP (Van Parijs et al., 2009) was used as the parent vector for construction of a LIC-competent variant. This was accomplished by inserting a unique sequence with a PmeI restriction site. LIC overhangs were then generated by treatment of the linearized vector with T4 DNA polymerase exonuclease activity. The inserted sequence was constructed by annealing two oligonucleotides to generate a fragment with overhangs complimentary to an EcoRI restriction site. The oligonucleotide sequences used were 5'-AATTAGAGAGTTTAAACTTCCAC-3' and 5'-AATTGTGGAAGTTTAAACTC-TCT-3'. The lyophilized oligonucleotides were resuspended in distilled water at a concentration of 20 μM. Prior to annealing these were phosphorylated using T4 polynucleotide kinase (New England Biolabs). The 20-μl reactions contained 2 μl of 10 mM ATP, 12.5 μl of 20 μM oligonucleotide, 2 μl of 10x reaction buffer, 1 μl of enzyme, and 2.5 μl of distilled water. Reactions were incubated for 1 h at 37 °C then shifted to 95 °C for an additional 10 min. The two oligonucleotide reactions were then mixed together at 95 °C and slow cooled to 37 °C. A 2.5-μl aliquot was then added to a 20-μl ligation reaction composed of 1 μl of 45 ng/μl EcoRI-cut pMCSV-ires-GFP, previously treated with calf intestinal phosphatase, 2 μl of 10x reaction buffer, and 13.5 μl of distilled water. The reaction was slow cooled from 37°C to 16°C, and 1 μl of 1 unit/μl of T4 DNA ligase (New England Biolabs) was added. Incubation was continued at 16 °C for ~16 h.

A 2-μl aliquot of the ligation reaction was used to transform 20 μl of competent XL1-Blue cells. These were plated on Lysogeny Broth (LB) agar with ampicillin (Amp) selection and incubated at 37 °C overnight. Colonies were picked and grown in 5 ml of LB-Amp, and plasmid DNA was isolated using Qiagen minispin columns. Positive clones were identified by restriction digestion with PmeI and ClaI and confirmed by DNA sequencing.

Primers for LIC of mCRT(WT), mCRT(ΔC) and mCRT(ΔP) into pMSCV-ires-GFP—The following primers were used: forward, 5'-GAA TTA GAG AGT TTC ACC ATG CTC CTT TCG GTG CCG CTC CTG CTT GGC-3', reverse for WT and ΔP: 5'-GG AAT TGT GGA AGT TTC TTA CAG CTC ATC CTT GGC TTG GCC AGG GGA TTC-3',

and reverse for ΔC, 5'-GG AAT TGT GGA AGT TTC TTA CAG CTC ATC CTT CG CTT CTC TGC AGC CTT GGT A-3'.

Procedures for LIC—LIC was performed to introduce mCRT sequences into the pMCSG7 and pMSCV-ires-GFP vectors. Overhangs of 15 bp were generated in the insert DNA by processing 0.2 pmol of the PCR product with 0.5 unit of LIC-qualified T4 DNA polymerase (Novagen) in the presence of 4 mM dCTP (for ligation with pMCSG7) or 4 mM dGTP (for ligation with pMSCV-ires-GFP) and 5 mM dithiothreitol, at 20-μl final reaction volume. Reactions were incubated for 30 min at 22 °C followed by 20 min at 75 °C. The pMCSG7 or pMSCV-ires-GFP vectors were linearized by restriction digestion with SspI (for pMCSG7) or PmeI (for pMSCV-ires-GFP) (New England Biolabs) at a concentration of 5 units/μg of DNA at 37 °C for 1.5 h. The protein was removed using a Qiagen PCR minispin kit. Linearized vector DNA was then processed by T4 DNA polymerase to yield single-stranded ends for annealing. Reactions, 60-μl total, were set up with 1.6 –2.0 μg of linear DNA and 3.75 units of LIC-qualified T4 polymerase (Novagen) in the presence of 4 mM dGTP (for pMCSG7) or 4 mM dCTP (for pMSCV-ires- GFP) and 5 mM dithiothreitol. Reactions were mixed on ice and incubated as described above for inserts. Insert and vector DNA were annealed in 96-well plates by combining 1 μl of processed vector and 2 μl of processed insert per well, followed by incubation in a PCR machine at 22 °C for 15 min with addition of 1 μl of 25 mM EDTA after 10 min of incubation. Annealed DNA was used to transform competent XL1-Blue cells. Positive clones were identified by PCR analysis. DNA sequences were verified at the University of Michigan DNA sequencing core. Purified plasmid DNA from positive clones was used to transform competent Rosetta cells (Novagen) or BL21 (DE3) cells for protein expression.

Primers for Cloning mCRT into pMSCV-puro—The following primers were used to clone untagged mCRT into the pMSCV-puro vector: forward, 5'-GA CTC GAG ATG CTC CTT TCG GTG-3; and reverse, 5'-GA GTT AAC CTA CAG CTC ATC CTT-3', which introduce 5' XhoI and 3' HpaI restriction sites. A FLAG-tagged CRT containing a C-terminal FLAG epitope tag was also generated in pMSCV-puro. The following primers were used: forward, 5'-GA CTC GAG ATG CTC CTT TCG GTG-3' and reverse 5'-GA GTT AAC CTA CAG CTC ATC CTT CTT ATC ATC GTC ATC CTT ATA ATC GGC

TTG GCC AGG GGA TTC TTC-3'. Underlined bases represent those that are complementary to the sequence encoding mCRT, with additional 5' sequences added to insert an XhoI restriction site upstream of the protein sequence, and a FLAG epitope tag inserted before the KDEL ER retention motif, and finally an HpaI restriction site downstream of the protein sequence. Following amplifications from appropriate templates, PCR products were digested with XhoI and HpaI (New England Biolabs). PCR reactions were cleaned using MinElute 96 UF PCR purification kits by Qiagen. The digested products were ligated into the pMSCV-puro vector digested with the same enzymes. Both mCRT retroviral constructs retained the mCRT signal sequence and KDEL ER retention motif.

Generation of Y92A, W244A, W302A, and Y92A/W244A Mutants of mCRT— mCRT(W244A) was obtained by site-directed mutagenesis of mCRT(WT) in pMSCV-puro (Finnzymes Phusion, New England Biolabs). mCRT(Y92A) and mCRT(Y92A/ W244A) were obtained by site-directed ligation-independent mutagenesis (Chiu et al., 2004) of mCRT(WT) and mCRT(W244A) constructs in pMSCV-puro. mCRT(W302A) was obtained by site-directed mutagenesis of mCRT in pCMV-SPORT6 (QuikChange II site-directed mutagenesis kit, Stratagene). mCRT(W302A) in pMSCV-puro was subsequently cloned using a 3' primer that introduced a FLAG epitope tag as described above. A corresponding FLAG-tagged mCRT(WT) was also generated. mCRT(Y92A), mCRT(W244A), mCRT(Y92A/W244A), and mCRT(W302A) were inserted into pMCSG7 from pMSCV-puro or pCMV- SPORT6 templates by LIC using the primers for an N-terminal start site at residue 1, and C-terminal end site at residue 399.

Site-directed Ligation-independent Mutagenesis to Create mCRT(Y92A) and mCRT(Y92A/W244A)—Procedures for site-directed ligation-independent mutagenesis were similar to those described in (Chiu et al., 2004). To create Y92A, full-length mCRT in the retroviral vector pMSCV-puro was used as a template for the following primers in two separate PCR reactions to create DNA fragments with complementary 5' overhangs, which are underlined: forward tailed, 5'-GGG GGC GGC GCC GTG AAG CTG TTT CCG AGT GGC TTG-3'; reverse short, 5'-ACA GTC GAT ATT CTG CTC ATG CTT CAC CG-3'; reverse tailed, 5'-CTT CAC GGC GCC GCC CCC ACA GTC GAT ATT CTG CTC-3'; and forward short, 5'-CTG TTT CCG AGT GGC TTG GAC CAG AAG-

3’. The PCR products were then incubated with DpnI (New England Biolabs) to digest template DNA, and this reaction was quenched with the addition of the following 2x site-directed ligation-independent mutagenesis buffer: 50 mM Tris, pH 8.8, 300 mM NaCl, 20 mM EDTA. The two products were then mixed and incubated for two cycles of 65 °C for 5 min and 30 °C for 15 min to hybridize the two fragments, and the product was transformed into competent XLI-Blue cells. Positive clones were identified through sequencing performed by the University of Michigan DNA Sequencing Core. The Y92A/W244A mutant was created with the same method as Y92A, except that the original template used was full-length mCRT containing the W244A mutation in pMSCV-puro.

Generation of mCRT(W244A) by Finnzymes Phusion Site-directed Mutagenesis Kit—The following primers were used to generate mCRT(W244A): forward, 5’-GCT GAA CCA CCA GTG ATT CAA AAT CCT GAA TAC-3’ and reverse, 5’-CTC TCC ATC CAT CTC TTC ATC CCA GTC CTC-3’.

Generation of the W302A Mutant Using the QuikChange II Site-directed Mutagenesis Kit—The following primers were used to generate mCRT(W302A): forward, 5’-G GGC CTA GAT CTC GCG CAG GTC AAG TCC GG-3’ and reverse, 5’-CC GGA CTT GAC CTG CGC GAG ATC TAG GCC C-3’.

Cloning Human ERp57 into pET33b—ERp57 was PCR-amplified from the pVL1392 vector (Silvennoinen et al., 2004) using primers that introduced 5’ NcoI and 3’ XhoI sites and deleted the signal sequence. The vector pET33b, which allows for insertion of a C-terminal His tag, and ERp57 inserts were both prepared by XhoI and NcoI digestion and ligated (Invitrogen). The following primers were used: forward, 5’-A TCC ATG GCC TCC GAC GTG CTA GAA CTC-3’ and reverse, 5’-AT CTC GAG GAG ATC CTC CTG TGC CTT C-3’.

Expression of LLO in E. coli—A listeriolysin O (LLO) W492A mutant LLO, which is described to have reduced cytotoxic activity (Michel et al., 1990), was used as a non-glycosylated calreticulin substrate. Wild-type LLO with a C-terminal histidine tag was mutated by PCR using the primer 5’-GCG AGA ACG GTA ATT GAT GAC C-3’ (Integrated DNA Technologies, Coralville, IA) to change Trp-492 to Ala. The PCR product was ligated into the pET29b plasmid (Novagen, WI), sequenced, transformed

into BL21 (DE3, Novagen), and purified as described below.

Generation of C95A, N33Q, C95A/N233A mutants of tapasin–The construction of retroviral vectors encoding wild-type and C95A human tapasin has been previously described (Rizvi and Raghavan, 2010). The N233Q mutants on the wild-type and tapasin(C95A) backgrounds were generated using the QuikChange site-directed mutagenesis kit (Stratagene). The MSCV-puro vector expressing wild-type or C95A tapasin was used as template and mutated using the following oligonucleotides: 5'-GGCCCATGGACCGGACAGGGGACCTTCTGGCTG-3' and 5'-CAGCCAGAAGGTCCCCTGTCCGGTCCATGGGCC-3'.

Protein Purifications

Purification of Calreticulin—Glycerol stocks of BL21 (DE3) cells expressing the calreticulin constructs were inoculated into a 25-ml terrific broth culture (with 50 μg/ml ampicillin) and incubated at 37 °C overnight. The starter culture was added to 1 liter of terrific broth with 50 μg/ml ampicillin and incubated at 37 °C until cell density measured by A_{600} was 0.8–0.9. Cultures were then incubated at room temperature for 1 h before inducing calreticulin protein expression with 200 μM isopropyl 1-thio-β-D-galactopyranoside. Bacterial cultures were incubated at room temperature for 16 –20 h before harvesting cells by centrifugation. Cell pellets were resuspended in 50 ml of 50 mM Tris with 0.33 mg/ml lysozyme and EDTA-free complete protease inhibitors (Roche Applied Science). Cells were lysed by sonication. Subsequently, 10 μg/ml DNase, 1% Triton X-100, 10 mM $MgCl_2$, and 1 mM $CaCl_2$ were added, and the cell lysis suspension was incubated at room temperature for 30 min. Cell debris was removed from samples by centrifugation, followed by vacuum filtration of the supernatant with a Steriflip having a 0.22-μm pore membrane (Millipore). The filtrate was then incubated with nickel-nitrilotriacetic acid-agarose beads (Qiagen) for 2– 4 h at 4 °C. The beads were washed with 10 mM imidazole in wash buffer (50 mM Tris, 150 mM NaCl, 1 mM $CaCl_2$, pH 7.5). Murine calreticulin was eluted from beads with 75 and 100 mM imidazole in wash buffer. Protein was concentrated to 0.5– 4.0 ml, by centrifugation using Centriplus centrifugal filter devices (Millipore) with molecular weight cut-offs of 10 or 30 kDa, and analyzed by gel-filtration chromatography.

Gel-filtration Analyses of Calreticulin—Purified concentrated calreticulin constructs

were analyzed by gel filtration at 4 °C using a Superdex 200 10/300 GL column or Highload 16/60 Superdex 200 (Amersham Biosciences). Buffer used was 20 mM Hepes, 150 mM NaCl, 10% glycerol, 1 mM CaCl2, pH 7.5. Following gel filtration, fractions corresponding to the various monomeric and oligomeric calreticulin species for each construct were pooled and concentrated by centrifugation using Centricon centrifugal filter devices (Millipore) with molecular weight cut-offs of 10 or 30 kDa. Protein concentration was determined measuring absorbance at 280 nm. Extinction coefficients were calculated from the protein amino acid sequence using ProtParam (www.expasy.ch) and are as follows (units are in M^{-1} cm^{-1}): $mCRT_{1–399}$, 82,975; $mCRT_{1–362}$, 82,975; $mCRT_{1–339}$(ΔC), 82,975; $mCRT_{1–318}$, 75,985; $mCRT_{33–362}$, 70,485; and mCRT(ΔP), 44,015.

Purification of LLO—BL21 E. coli cells expressing LLO were inoculated into LB broth with 60 μg/ml kanamycin. Cell cultures were expanded to log phase (A_{600} = 0.8–0.9), induced with 1 mM isopropyl 1-thio-β-D-galactopyranoside for 16 –20 h at room temperature, and the recombinant LLO was purified from bacterial lysates by nickel affinity chromatography. Buffers used throughout the purification procedure were pH 8.0 and contained 10% glycerol to minimize LLO aggregation. LLO was eluted from the nickel beads with 250 mM imidazole in wash buffer, and then stored in aliquots at -80 °C. Relative purity was consistently >95% by SDS-PAGE and SYPRO Red gel staining (Invitrogen). Prior to aggregation assays (described below), small aliquots of LLO were further purified by gel-filtration chromatography using a Superdex 200 10/300 column. Buffer used was 50 mM Hepes, 140 mM NaCl, 10% glycerol, pH 8.0. LLO concentration and extinction coefficient (77,240 M^{-1} cm^{-1}) were calculated as described above for mCRT.

Purification of ERp57—LB broth containing 50 μg/ml kanamycin was inoculated with BL21 *E. coli* cells expressing His-tagged ERp57. Cell cultures were expanded to log phase, induced with 250 μM isopropyl 1-thio- β -D-galactopyranoside for 3 h at 37 °C. ERp57 was purified by resuspending bacterial pellets in lysis buffer containing: 50 mM NaH_2PO4, 150 mM NaCl, 0.2 mg/ml lysozyme, 0.1% Triton X-100, 10 mM β-mercaptoethanol, 2.7 mM benzamidine, 5 μg/ml leupeptin, 7 μg/ml pepstatin, and 1.5 mM phenylmethylsulfonyl fluoride, pH 8.0. Cells were disrupted by sonication in lysis

buffer. Cell debris was removed from samples by centrifugation, followed by vacuum filtration of the supernatant with a Steriflip having a 0.22-μm pore membrane (Millipore). The filtrate was then incubated with nickel-nitrilotriacetic acid-agarose beads (Qiagen) for 3 h at 4 °C. The beads were washed with wash buffer (50 mM Tris, 300 mM NaCl, pH 8.0). ERp57 was eluted from beads with 10 and 20 mM imidazole in wash buffer. Protein was concentrated to ~6.5 ml, by centrifugation using Centriplus centrifugal filter devices (Millipore) with molecular weight cut-offs of 10 or 30 kDa, and further purified by Mono Q ion-exchange chromatography. A linear gradient from 150 mM to 1 M NaCl in 50 mM Tris (pH 7.4) was used to elute ERp57 from the column. The fractions of eluted protein containing ERp57 were dialyzed into 10 mM Tris, 150, mM NaCl (pH 7.4), concentrated, and stored at -80 °C after adding 10% glycerol.

Thermostability Analyses by Sypro Orange Binding

These analyses were undertaken as previously described (Lo et al., 2004; Malawski et al., 2006). Proteins (16 μM) were incubated in buffer (20 mM Hepes, 150 mM NaCl, and 1 mM $CaCl_2$, pH 7.5) and 1x Sypro Orange Stain (Invitrogen) diluted from a 5000 stock solution in the presence or absence of 48 μM Glcα1–3Manα1–2Manα1– 2Man-OH (G1M3, Alberta Research Council) in a total reaction volume of 10 μl. Thermal scans were performed using an ABI PRISM 7900HT Sequence Detection System using temperature increments of 1 °C starting at 25 °C. Within an experiment, each condition was analyzed in triplicate wells. Fluorescence emission was measured across different wavelength bins, and the bin with maximum fluorescence was chosen for further analysis. Fluorescence was normalized within wells as percent maximum fluorescence $((F_{obs} - F_{min})/(F_{max} - F_{min})*100)$ and plotted against the sample temperature.

Biacore-based Assays

CRT-ERp57 binding was assayed by surface plasmon resonance-based assays using a Biacore 2000 instrument, as previously described (Martin et al., 2006). Briefly, mCRT(WT) or mutants or the control protein bovine serum albumin were coupled to a Biacore CM5 chip (Amersham Biosciences) using amine-based coupling chemistry. ERp57 binding to each surface was monitored in 10 mM Hepes, 150 mM NaCl, 0.5 mM $CaCl_2$, 0.005% surfactant P-20, pH 7.5, at a flow rate of 5 μl/min at 25 °C over a 30-min period. Signals obtained from the bovine serum albumin surface were subtracted from

corresponding signals for each mCRT surface. Specific signals for mCRT binding were plotted as a function of ERp57 concentration, and non-linear curve fitting (1:1 specific binding model) was performed to derive K_D values using PRISM software.

Aggregation Assays

In gel-based assays, 2 or 4 μM LLO were incubated with purified mCRT constructs (4 – 32 μM), or OVA as a negative control, at 37 °C for 1 h. Assays were conducted in the presence of 0.2– 0.5 mM $CaCl_2$ with or without 5 mM EDTA or 3 mM ATP. Following incubation, aggregated proteins were separated from solution by microcentrifugation at maximum speed for 30 min at 4 °C. Supernatants containing non-aggregated protein were removed, and the pellets containing the aggregated protein were re-suspended in an equal volume of buffer. Proteins present in the supernatants and pellets were separated by SDS-PAGE and visualized with Coomassie Blue stain. Protein band intensity was quantified using ImageQuant (Amersham Biosciences) and used as a measure of aggregation suppression activity of calreticulin. A light scattering assay was also performed to compare the aggregation suppression activities of different calreticulin mutants. In this assay, 1 μM LLO was incubated in a 96-well plate with 1–16 μM of different mCRT in the presence of 0.5 mM $CaCl_2$. Plates were incubated in a BIO-TEK spectrophotometer pre-heated to 37 °C, and absorbance at 360 nm was monitored over a 60-min period (KC4 software). The absorbance signal for LLO alone was set to 100%.

Cell Cultures

Bosc cells were maintained in Dulbecco's modified Eagle's medium (Invitrogen) containing 4.5 g/liter glucose, L-glutamine, and 110 mg/liter sodium pyruvate, supplemented with 10% (v/v) fetal bovine serum (Invitrogen), 100 μg/ml streptomycin, and 100 units/ml penicillin (Invitrogen). Calreticulin-deficient (K42) cells (Gao et al., 2002) and a melanoma cell line M553 (Belicha-Villanueva et al., 2008) (obtained from N. Bangia, Roswell Park Cancer Institute) were maintained in RPMI medium 1640 (Invitrogen) supplemented with 10% (v/v) fetal bovine serum, 100 μg/ml streptomycin, and 100 units/ml penicillin.

Generation of Retroviral Supernatants

5.5 μg of pMSCV-ires-GFP or pMSCV-puro vector (encoding different mCRT or control vector lacking mCRT) DNA was mixed with 4 μg of pCL-EcoDNA and 0.5 μg of VSV-

G encoding plasmid, and added to a mixture of Opti-MEM (Invitrogen) and FuGENE 6 (Roche Applied Science). Following incubation for 20 min at room temperature, the mixture was added to Bosc cells that had been grown to 70% confluency in a 10-cm tissue culture dish. Medium was changed after 24 h, and after 48 h, supernatants containing retroviruses were harvested and used to infect K42 cells.

Mice

C57BL/6 and $\beta 2m^{-/-}$ mice were purchased from The Jackson Laboratory. All mice were maintained in a specific pathogen-free mouse facility. The mice were cared for according to the guidelines set by the University of Michigan Committee on Use and Care of Animals.

Flow Cytometry

For MHC class I surface analysis by flow cytometry, infected K42 cells were resuspended and washed in phosphate-buffered saline containing 1% fetal bovine serum (flow cytometry buffer). 2×10^5 cells were resuspended in 100 μl of flow cytometry buffer containing the MHC class I ascites fluid Y3 (1:100, anti-H2-K^b, ATCC HB-176), AF6 (anti-H2-K^b, ATCC HB-158, 1:50), 28-14-8S (1:50, anti-H2-D^b, ATCC HB-27), W6/32 (1:250), or anti-HA (Covance, 1:250) and incubated for 30 min to 1 hour on ice. Cells were washed once with buffer, then resuspended in 100 μl of buffer containing goat anti-mouse antibody conjugated to phycoerythrin (1:500) or to FITC (1:250), and incubated for 15 min to 1 hour on ice. Cells were washed three times, and data for each sample were collected on the FACSCanto flow cytometer (BD Biosciences). For pMSCV-ires-GFP-infected cells, levels of mCRT expression were normalized by gating on a subset of the GFP-positive population. For pMSCV-ires-GFP-derived cells, flow cytometric analyses were undertaken 37 and 71 h post-infection. For pMSCV-puro-derived cells, following selection and maintenance in media containing 1–2.5 μg/ml puromycin, cells were analyzed no earlier than 3 weeks post-infection. Analyses were performed using WinMDI version 2.8.

Immunoprecipitations

Splenocytes from wild-type (C57BL/6) and $\beta 2m^{-/-}$ mice were isolated, and the RBCs were lysed using red cell lysis buffer (Sigma-Aldrich R7757). The remaining splenocytes, K42 cells or K42 cells expressing mCRT constructs were harvested and

lysed in digitonin lysis buffer (10 mM Na_2HPO_4, 10 mM Tris, 130 mM NaCl, 1% digitonin, complete EDTA-free protease inhibitors, pH 7.5). Indicated immunoprecipitations additionally contained 20 mM N-ethylmaleimide in the lysis buffer. In some analyses, cells were incubated with 10 μg/ml tunicamycin to induce accumulation of de-glycosylated tapasin. Cells were lysed on ice for 1 h, followed by a 30-min centrifugation to remove cell debris. Supernatants of lysed cells or supernatance of medium collected from tissue culture plates were incubated with or without antibodies overnight at 4 °C. Samples were then centrifuged to remove precipitated proteins and incubated for 2 h with Protein G beads (Amersham Biosciences). Beads were washed three times with lysis buffer containing 0.1% digitonin. Samples were separated by 10% SDS-PAGE and transferred to Immobilon membranes (Millipore) for immunoblotting. Membranes were blocked in 5% milk in TBS for 1 h at room temperature, followed by an overnight incubation with primary antibody in TBS plus 0.05% Tween 20 (TTBS) at 4 °C. Membranes were washed for 2 h in TTBS, incubated for 30 min with secondary antibody, and washed again for 2 h at room temperature. Chemiluminescence was detected using the Amersham Biosciences ECL Plus kit.

The following antibodies were used to immunoisolate relevant proteins: rabbit anti-mouse TAP1 serum (1:15, kindly provided by Dr. Ted Hansen), rabbit anti-mCRT antibody (1:400, Abcam, catalog number ab2907), and rabbit anti-K^b antiserum (EX8, 1:100, kindly provided by Dr. Jonathan Yewdell). The following antibodies were used in immunoblotting analyses: goat anti-TAP1 antibody (1:2000, Santa Cruz Biotechnology, Inc., catalog number sc-11465), goat antibody specific to the N terminus of mCRT (1:2000, Santa Cruz Biotechnology, Inc., catalog number sc-7431), Hamster tapasin-specific Ab and rabbit anti-β2m serum were also obtained from T. Hansen and used at 1:3000 dilutions to detect murine tapasin and β2m, respectively, EX8 (1:7500), and rabbit anti-ERp57 (1:3000, Santa Cruz Biotechnology, Inc., catalog number 28823). Secondary antibodies (Jackson ImmunoResearch) were all conjugated to horseradish peroxidase: mouse anti-rabbit (light chain specific), bovine anti-goat, and goat anti-hamster.

Chapter 3

Influences of calreticulin, antigen uptake pathways, and innate signaling upon antigen cross-presentation

Abstract

Antigen cross-presentation involves the uptake and processing of exogenously derived soluble and cell-associated antigens by APCs via MHC class I. APCs load peptides derived from the exogenous antigens onto MHC class I molecules for presentation to CD8 T cells. Calreticulin has been suggested to mediate the cross-presentation of both soluble and cell-associated antigen. In this study, we examined roles for calreticulin in antigen cross-presentation using a number of models. Our findings indicate that soluble calreticulin does not enhance the cross-presentation of a peptide, fused, or bead associated antigen. Additionally, in a subcutaneous immunization context, cell-surface calreticulin of pre-apoptotic cells (induced by the drug thapsigargin) does not impact CD8 T cell proliferation or cytotoxicity in response to cell-associated antigen. Finally, although the ability of calreticulin to enhance intracellular MHC class I assembly does translate to induced transfer of MHC class I-peptide complexes from antigen donor cells to APC *in vitro*, this mode of antigen transfer is not relevant for the *in vivo* activation of naive CD8 T cells. Our findings indicate that known interactions between calreticulin and calreticulin-specific receptors are not sufficient to impact CD8 T cell activation against soluble or particulate antigens in association with calreticulin. Additionally, the ability of cell-surface calreticulin to facilitate phagocytic uptake of antigen donor cells does not translate to enhanced CD8 T cell activation against cell-associated antigen in subcutaneous immunizations of pre-apoptotic cells. Importantly, this study points to the redundancy of pathways for uptake of soluble and cell-associated antigen. Lastly, independent of calreticulin, we show that LPS or high doses of thapsigargin inhibits

the proliferation of CD8 T cells in response to cell-associated antigen. Overall, this study provides insight into mechanisms of cross-priming of CD8 T cells, particularly as relating to modes of antigen transfer and effects of innate stimuli.

Introduction

APCs present peptides bound to MHC class I or class II molecules to T cells; this process facilitates T cell development, homeostasis, peripheral tolerance and activation of antigen specific T cells. Typically, MHC class I molecules present peptides derived from endogenous antigens to CD8 T cells. However, exogenous antigens can also be presented by MHC class I molecules of professional APCs such as DCs by a process termed cross-presentation. APCs internalize extracellular soluble or cell-associated antigens and traffic the material to intracellular compartments that facilitate MHC class I presentation of the exogenously derived antigens [reviewed in (Amigorena and Savina, 2010)]. Cross-presentation is suggested to be critical for the maintenance of CD8 T cell peripheral tolerance and for generation of cytotoxic T cell responses against intracellular pathogens and tumor cells [reviewed in (Amigorena and Savina, 2010)].

Calreticulin is an ER-localized chaperone that aids in the intracellular assembly of nascent MHC class I molecules and other newly synthesized glycoproteins [reviewed in (Rutkevich and Williams, 2011)]. HSPs, like calreticulin, bind antigens. HSP-antigen complexes can be taken up by APCs and re-presented by APCs to CD8 T cells *in vitro* and *in vivo* (Basu et al., 2001; Basu and Srivastava, 1999; Binder and Srivastava, 2005; Nair et al., 1999). Furthermore, mice immunized with calreticulin derived from tumor cell lysates are protected against subsequent live tumor challenges (Basu and Srivastava, 1999). The protection is attributed to the ability of calreticulin to efficiently cross-present associated tumor peptides. Calreticulin cross-presents associated peptides more efficiently compared to the peptides alone *in vitro* and *in vivo* (Basu et al., 2001; Basu and Srivastava, 1999). Receptors that bind calreticulin such as CD91, scavenger receptor-A (SR-A) and scavenger receptor expressed by endothelial cells-1 (SREC-1) are thought to specifically bind to and endocytose calreticulin and associated cargo (Basu et al., 2001; Berwin et al., 2004; Berwin et al., 2003). These receptors are not exclusive to calreticulin as they bind other HSPs such as gp96, HSP90 and HSP70 (Basu et al., 2001; Berwin et al., 2003; Binder and Srivastava, 2004). Cross-presentation of soluble OVA is also

dependent on a receptor-specific interaction. Endocytosis and trafficking of OVA to a sub-cellular compartment that favors its cross-presentation is facilitated by the mannose receptor (Burgdorf et al., 2006). However, the idea that the mannose receptor is required for the efficient cross-presentation of OVA has been recently challenged (Segura et al., 2009), which highlights the possibility of redundancy in receptors that mediate uptake of soluble proteins for cross-presentation.

Calreticulin is also upregulated on the surface of apoptotic and pre-apoptotic cells; calreticulin acts as an "eat-me" signal on the cell surface (Gardai et al., 2005; Kuraishi et al., 2007; Obeid et al., 2007b). Cell-surface calreticulin, like soluble calreticulin, also binds CD91, facilitating the phagocytosis of cell-associated antigens (Gardai et al., 2005; Kuraishi et al., 2007; Obeid et al., 2007a). Recent studies show that cell-surface localized calreticulin contributes to the immunogenicity of tumor cells treated with specific chemotherapeutic drugs (Obeid et al., 2007b). Drug-induced surface calreticulin on pre-apoptotic tumor cells facilitates phagocytosis of treated tumor cells (Obeid et al., 2007b). Hence, calreticulin-dependent phagocytosis is hypothesized to play a role in developing the anti-tumor immune response (CD8 and CD4 T cell activation) [reviewed in (Kepp et al., 2011)]. Although calreticulin-mediated phagocytosis of pre-apoptotic and apoptotic cells is described by a number of groups (Gardai et al., 2005; Kuraishi et al., 2007; Obeid et al., 2007b), the direct association between calreticulin-mediated phagocytosis and enhanced proliferation or cytotoxicity of antigen-specific CD8 T cells has not been shown.

In this study, we examined the role of calreticulin in the cross-presentation of soluble and cell-associated antigens. To accomplish this, we formed OVA peptide-calreticulin complexes as well as fused full length OVA to calreticulin and examined the ability of calreticulin-specific receptors to enhance the cross-presentation of OVA peptide or OVA. Additionally, we used a calreticulin-deficient MEF cell line to examine the role played by calreticulin in the cross-presentation of cell-associated antigens. Thapsigargin treatment is known to induce cell surface calreticulin and phagocytosis of cells. Phagocytic uptake of MEFs by BMDC is partially facilitated by calreticulin (Peters and Raghavan, 2011). We used thapsigargin treated cells to assess whether enhanced calreticulin-dependant phagocytosis of antigen donor cells translates to enhanced CD8 T

cell proliferation and cytotoxcity. Finally, calreticulin deficient cells express a lower MHC class I levels compared to calreticulin sufficient cells because calreticulin helps facilitate MHC class I assembly (Gao et al., 2002). Thus, the calreticulin-deficient fibroblasts also allowed us to assess the contribution of trogocytosis [cell-cell MHC class I transfer (Dolan et al., 2006; Harshyne et al., 2001)] to *in vivo* priming of naïve CD8 T cells. In sum, this study sheds light into mechanisms of antigen transfer utilized for cross-priming naïve CD8 T cell responses against soluble and cell-associated antigens *in vitro* and *in vivo*.

RESULTS

Effects of calreticulin association upon the cross-presentation of a peptide

Calreticulin-peptide complexes form when peptides and calreticulin are mixed and heat shocked to 50 °C (Basu and Srivastava, 1999). To examine whether calreticulin-specific receptors enhance the cross-presentation of a calreticulin-associated peptide (Figure 3.1A), we heated calreticulin or bovine serum albumin (BSA) with a FITC labeled peptide derived from the model antigen OVA (amino acids 255-267: QLESIINFEKLTE-FITC) at 50 °C for 1 hour. Free peptide was removed using a centrifugal filter device, and the amount of peptide bound to calreticulin and BSA was examined. We observed that the peptide bound equally to both calreticulin and BSA (Figure 3.2A, left panel). We next incubated C57BL/6 BMDC with the peptide complexes or peptide alone, and then added to the culture a T cell hybridoma line (B3Z) whose TCR ligand is the $OVA_{258-265}$ epitope (SIINFEKL) bound to the murine MHC class I allele H2-K^b (Karttunen et al., 1992). We observed equal IL-2 levels in the culture supernatants when comparing responses to calreticulin-associated or BSA-associated peptide (Figure 3.2A, right panel) and equal IL-2 levels when comparing calreticulin-associated peptide to free peptide (Figure 3.2B). We also incubated the calreticulin- or BSA-peptide complexes with bone marrow-derived Mϕ (BM Mϕ), as Mϕ express a different set of receptors than DCs. Similar to the results seen with BMDC, calreticulin did not enhance the cross-presentation of a peptide-associated antigen compared to BSA when BM Mϕ were used as the APC (Figure 3.2C). Thus, the calreticulin-specific receptors that have been reported (Basu et al., 2001; Berwin et al., 2004; Berwin et al., 2003) are not sufficient to enhance the cross-presentation of the peptide used in this study.

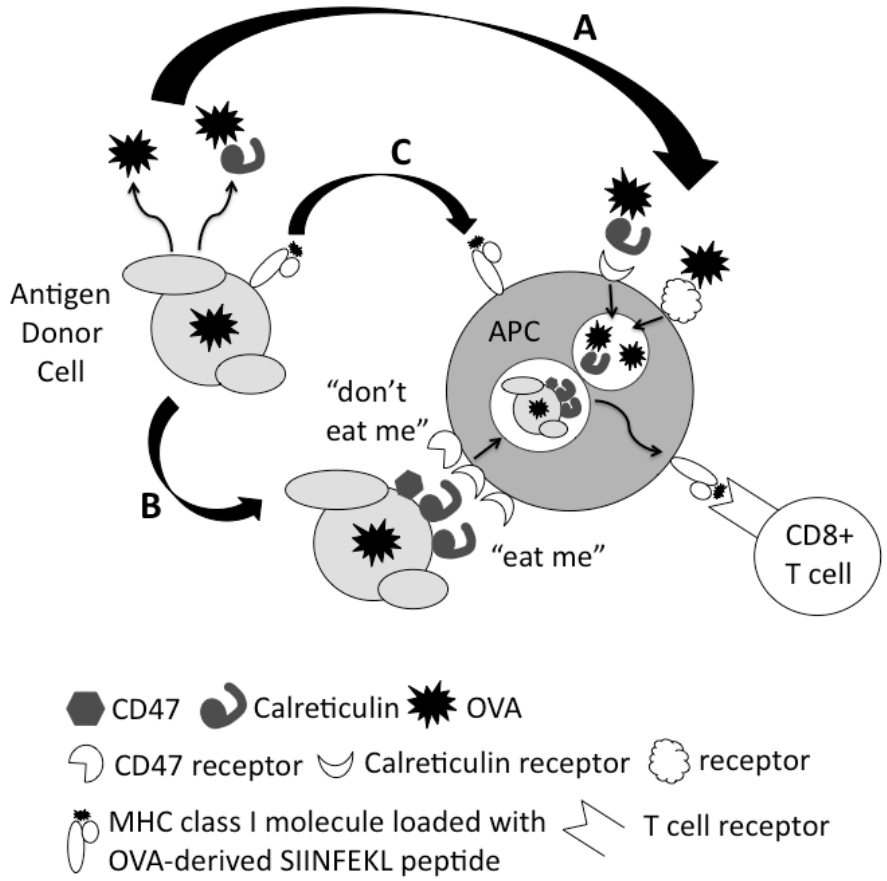

Figure 3.1: Hypothetical pathways by which calreticulin could enhance proliferation of naïve CD8 T cells. The figure depicts an APC displaying a MHC class I molecule loaded with an exogenously acquired OVA-derived peptide. Enhanced display of the OVA-derived peptide will lead to enhanced proliferation of naïve OT-I T cells, which are specific for H2-K^b complexes with the OVA-derived SIINFEKL peptide. The APC could generate or acquire H2-K^b-SIINFEKL complexes via three potential calreticulin-dependent mechanisms, which were tested in this study. (A) In the first pathway, calreticulin complexes with OVA might be cross-presented with higher efficiency compared to OVA alone; an OVA-calreticulin fusion protein and a peptide-calreticulin complex were generated in this study to test this possibility. (B) In the second pathway, cell-surface expression of calreticulin could enhance phagocytic uptake by APC of cells expressing OVA, thereby over-riding anti-phagocytic signals ("don't eat me" signals such as CD47), and leading to increased generation and display of the H2-K^b-SIINFEKL peptide. (C) In the third pathway, expression of calreticulin in a cell expressing OVA is expected to result in increased formation of H2-K^b-SIINFEKL complexes within the cell. Increased levels of H2-K^b-SIINFEKL complexes could then be transferred to the APC via trogocytocis (or could function *in trans* along with APC-derived co-stimulatory molecules) to lead to increased activation of OT-I T cells.

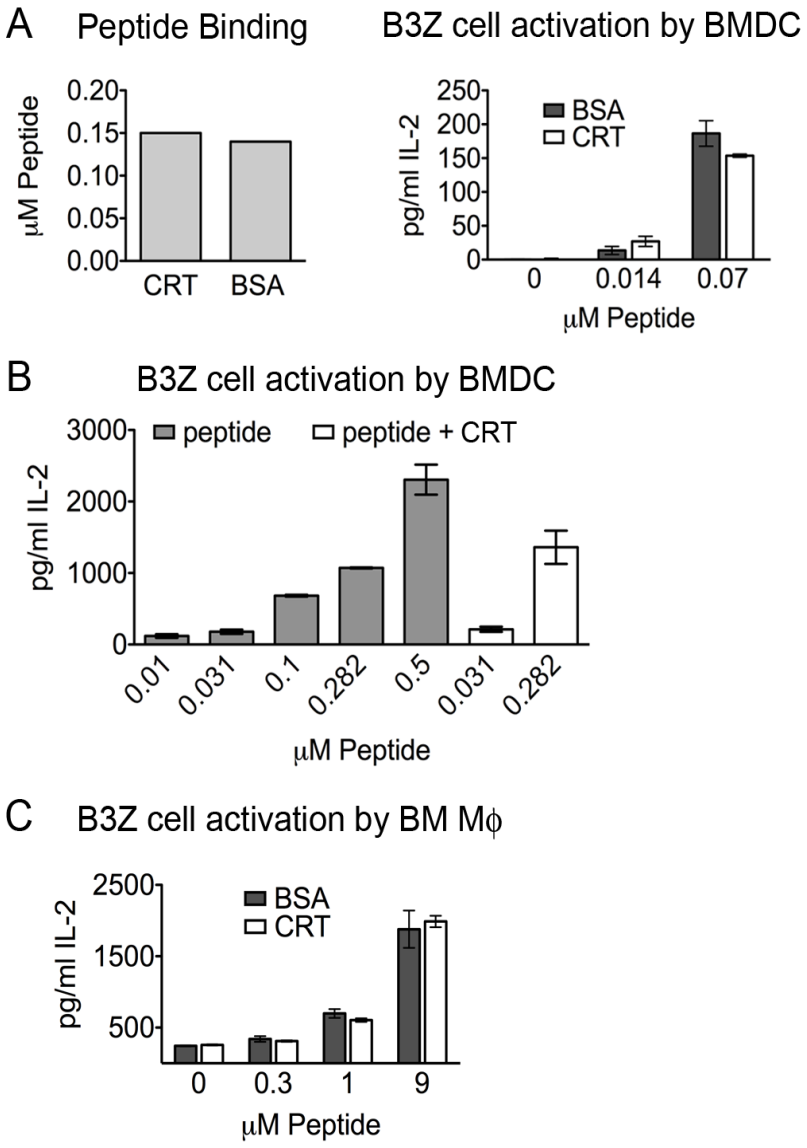

Figure 3.2. Calreticulin does not enhance cross-presentation of a peptide antigen. (A) 10 μM calreticulin (CRT) or bovine serum albumin (BSA) were incubated with 10 μM peptide (QLESIINFEKLTE-FITC). Free peptide was removed using a centrifugal filter device at 4 °C, and peptide still in complex with CRT or BSA was measured (left panel). CRT- or BSA-peptide complexes were incubated with BMDC and B3Z cells. IL-2 production was determined by ELISA of the supernatants after 24 hours (right). Peptide concentration is indicated; CRT or BSA were present at a final concentration of 1 μM. (B) Cross-presentation of free peptide or CRT-peptide complexes was measured as in *A*. (C) Cross-presentation of CRT- or BSA-peptide complexes was measured as in A, except that BM MΦ were used as APCs. Data are representative of two independent analyses for *A* (right panel), *B* and *C*. For *C,* peptide binding to CRT and BSA was not measured. Mean ± s.e.m. are shown.

Effects of calreticulin fusion and TLR4-deficiency upon the cross-presentation of OVA

The extended peptide used in Figure 3.2 does not have a high affinity for calreticulin, as similar amounts of peptide were recovered following heat shock with calreticulin or BSA (Figure 3.2A, left panel). The peptide-binding site of calreticulin and specificity of peptides that bind to calreticulin are poorly understood and defined. Hence, to assess the possibility that calreticulin could quantitatively enhance the cross-presentation of an associated soluble antigen (Figure 3.1A), we generated a fusion protein between full-length OVA and calreticulin [that linked OVA to the N-terminus of calreticulin (OVA-CRT)]. Both OVA-CRT and OVA were expressed in *E. coli* and contained a histidine tag for purification. Proteins were first purified over a nickel column and then further purified and analyzed on a size-exclusion column. OVA-CRT and OVA were both isolated predominantly as single peaks, results indicative of the homogeneity and stability of both proteins. The major peak of both proteins was isolated and used for subsequent experiments (Figure 3.3A).

To assess the cross-presentation efficiency of OVA-CRT compared to OVA, OVA-CRT or OVA were incubated with BMDC and CFSE labeled OT-I T cells [obtained from a transgenic mouse whose CD8 T cells express a TCR that recognizes the $OVA_{257-264}$ epitope (SIINFEKL) bound to the murine MHC class I allele H2-K^b (Hogquist et al., 1994)]. Levels of IL-2 in the supernatant were measured after 24 hours and OT-I T cell proliferation was measured after 3 days. No significant differences were observed in levels of IL-2 produced by the OT-I T cells in response to OVA or OVA-CRT, and proliferation of the OT-I T cells was found to be very similar (Figure 3.3B). To assess binding of OVA and OVA-CRT to BMDC, both proteins were labeled with allophycocyanin. Higher level of fluorescence incorporation was observed for OVA-CRT compared to OVA, and correspondingly, binding to BMDC was enhanced for OVA-CRT compared to OVA (Figure 3.3C and 3.3D). Due to the difficulty in achieving equivalent labeling of OVA-CRT and OVA, it remains unclear whether calreticulin fusion to OVA confers a specific BMDC uptake advantage.

To evaluate the *in vivo* response to the soluble proteins, CFSE labeled OT-I T cells were injected intravenously (i.v.) into wild-type (WT) recipient mice. Twenty-four

hours later, mice were immunized subcutaneously (s. c.) with equimolar amounts of *E. coli* derived OVA or OVA-CRT. Three days after the immunization, proliferation of the OT-I T cells from the draining lymph node (dLN) was assessed. Percentages of proliferating OT-I T cells (Figure 3.3E) and percentages of OT-I T cells recovered (Figure 3.3F) were similar in response to OVA, whether or not OVA was fused to calreticulin

In the experiments described thus far, lipopolysaccharide (LPS) contamination was of concern because the recombinant proteins used in these experiments are of *E. coli* origin. LPS is an agonist for TLR4 (Poltorak et al., 1998). It was conceivable that LPS contamination could mask potentiating effects of calreticulin. To address this concern, $TLR4^{-/-}$ recipient mice (Hoshino et al., 1999) were used, previously characterized for their inability to respond to LPS. OVA-CRT did not induce a greater CD8 T cell response compared to OVA alone even when $TLR4^{-/-}$ mice were used as recipients (Figure 3.3E, left panel and 3.3F). We concluded that there was no specific advantage for OT-I T cell proliferation when OVA was fused to calreticulin compared to OVA alone, even in the absence of LPS signaling. It is however noteworthy that percentages of OT-I T cells recovered in response to OVA and OVA-CRT were somewhat reduced in $TLR4^{-/-}$ mice compared to WT mice (Figure 3.3F). This reduction was not surprising as TLR4 engagement can provide signal 2 (Figure 1.3), which enhances CD8 T cell activation. These results are also consistent with previous findings that TLR signaling enhances *in vitro* cross-presentation of soluble antigen (Burgdorf et al., 2008). However, the difference in OT-I T cell recovery is small at the tested antigen doses, indicating that TLR4 signaling is non-essential for *in vivo* cross-presentation of soluble antigen.

Figure 3.3: Calreticulin fusion does not enhance cross-presentation of OVA**.**
(A) Gel-filtration chromatogram of *E. coli*-derived OVA or the OVA-calreticulin (OVA-CRT) fusion protein (left). SDS-PAGE analysis of pooled fractions from left panel; proteins were loaded in equimolar amounts (right) and coomassie stained. (B) Indicated proteins were incubated with BMDC for 3 hours. BMDC were fixed and CFSE labeled OT-I T cells were added. IL-2 levels in supernatants were determined by ELISA (left panel; 24 hour time point). OT-I T cell proliferation was measured at 72 hours in response to 44 μM OVA or OVA-CRT. The solid grey profile indicates the condition where no antigen (no Ag) was added. Data are representative of two independent analyses. (C, D) OVA-CRT and OVA were labeled with allophycocyanin. (C) Labeling intensity was determined by fluorescence imaging of the proteins after separation by SDS-PAGE (inset). Fluorescence intensity was quantified for the indicated proteins. (D) Binding of fluorescent proteins to BMDC was assessed by flow cytometry. BMDC were incubated with labeled proteins on ice before being analyzed by flow cytometry. BMDC not incubated with proteins are depicted as a grey filled (unlab). Representative of two independent experiments performed with the same labeled proteins. (E, F) WT or $TLR4^{-/-}$ recipient mice were injected i.v. with CFSE labeled OT-I T cells. Twenty-four hours later, mice received s.c. injections of the indicated antigen (100 μl of a 220 nM solution). OT-I T cell proliferation was measured 3 days later in the dLN (inguinal). (E) The % of proliferating OT-I T cells averaged from the mice of one experiment is shown in the left panel. Two to three mice were used in all groups. The right panel depicts proliferation in WT recipient mice. (F) Quantification of the percentage of OT-I T cells of all CD8 T cells recovered in *E*. Data for *E* and *F* are representative of three out of four independent analyses for WT recipients and a single analysis with $TLR4^{-/-}$ recipients. Similar results were obtained in comparisons of OVA and OVA-CRT-induced OT-I proliferation in WT and $TLR2/4^{-/-}$ recipient mice (data not shown). (G) Compilation of the % of proliferating OT-I T cells (left panel) and of the % of OT-I T cells as a function of all CD8 T cells (right panel) from 4 independent experiments performed with WT recipient mice. Two experiments contained 2 doses of antigen and two experiments contained 1 antigen dose. Antigen doses ranged from 0.22 μM – 22 μM, using 100 μl. Each point represents the mean of 2-3 mice for that condition. Mean ± s.e.m. are shown. A two-tailed pair-wise student t-test was used for statistical analyses in G. Analyses shown in Figure 3.3E-G were performed by Lianjun Shen.

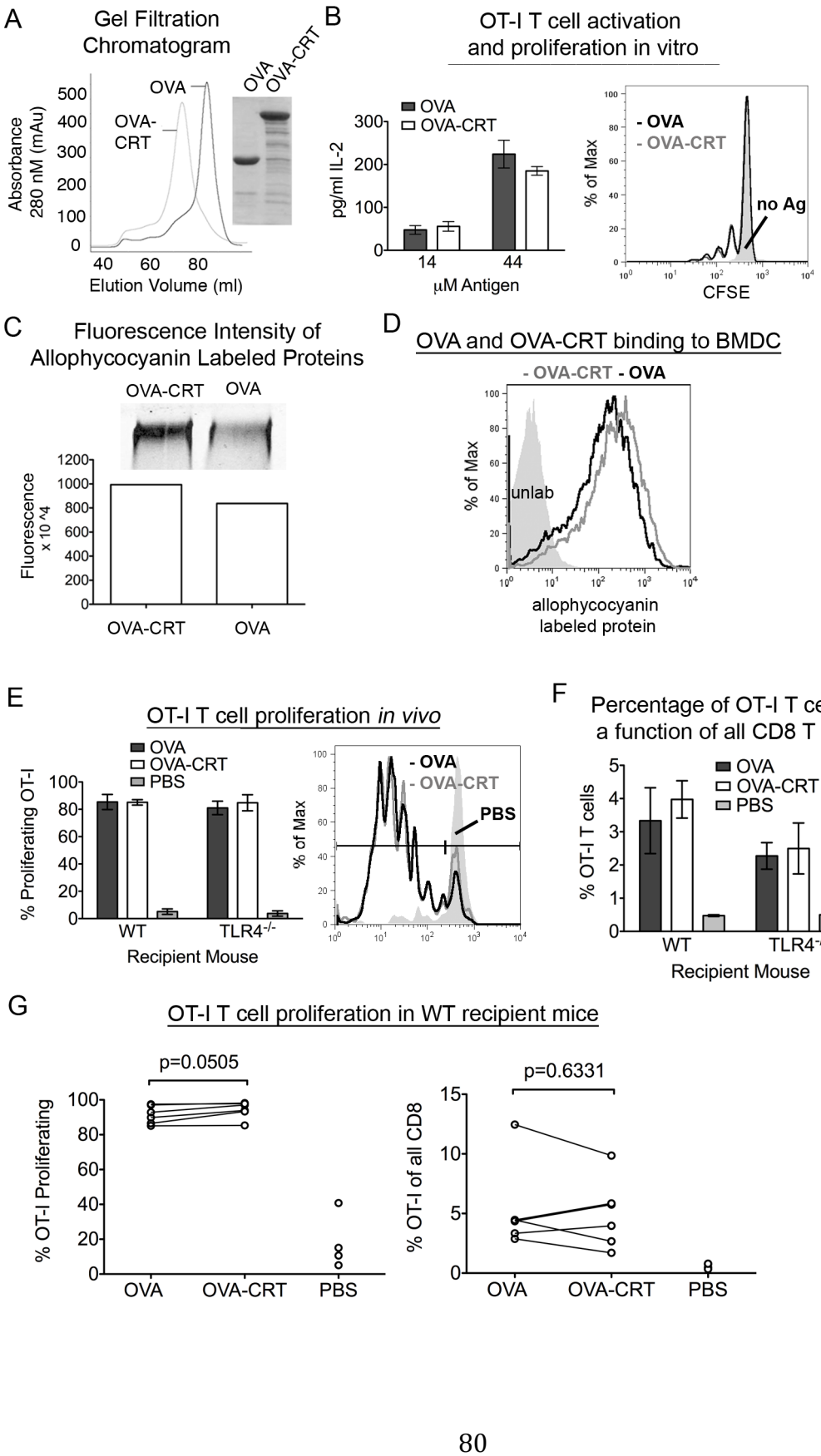
A
Gel Filtration Chromatogram
OVA
OVA-CRT
Absorbance 280 nM (mAu)
Elution Volume (ml)
B
OT-I T cell activation and proliferation in vitro
OVA
OVA-CRT
pg/ml IL-2
μM Antigen
- OVA
- OVA-CRT
no Ag
% of Max
CFSE
C
Fluorescence Intensity of Allophycocyanin Labeled Proteins
OVA-CRT
OVA
Fluorescence x 10 ^4
D
OVA and OVA-CRT binding to BMDC
- OVA-CRT - OVA
unlab
% of Max
allophycocyanin labeled protein
E
OT-I T cell proliferation in vivo
OVA
OVA-CRT
PBS
% Proliferating OT-I
WT
TLR4-/-
Recipient Mouse
- OVA
- OVA-CRT
PBS
% of Max
F
Percentage of OT-I T cells as a function of all CD8 T cells
% OT-I T cells
G
OT-I T cell proliferation in WT recipient mice
p=0.0505
% OT-I Proliferating
p=0.6331
% OT-I of all CD8

Cross-presentation efficiencies of glycosylated and non-glycosylated OVA

Cross-presentation of soluble OVA is suggested to be facilitated by the mannose receptor (Burgdorf et al., 2006). OVA purified from *E. coli* is not glycosylated, as *E. coli* lack eukaryotic glycosylation machinery. However, we found that non-glycosylated OVA isolated from *E. coli* was cross-presented *in vivo* (Figure 3.3), indicating that the mannose receptor may not be essential for the cross-presentation of soluble OVA. This result prompted us to assess the cross-presentation efficiency of OVA purified from *E. coli* and OVA obtained from Sigma [OVA (Sigma)], which is glycosylated as it is isolated from chicken eggs. This comparison would allow us to further determine the importance of OVA uptake through the mannose receptor upon the cross-priming of OT-I T cells.

To assess the cross-presentation efficiency of OVA purified from *E. coli* [OVA (*E. coli*)] compared to OVA (Sigma), OVA (*E. coli*) and OVA (Sigma) were incubated with BMDC for 3 hours. After 3 hours, the cells were fixed and B3Z cells (a T cell line that is specific for the same OVA epitope for which OT-I T cells are specific (Karttunen et al., 1992)) were added to the cultures. IL-2 levels induced by OVA (Sigma) were similar compared to IL-2 levels induced by OVA (*E. coli*) at a number of OVA doses tested (Figure 3.4A). However, at an OVA dose of 0.9-2.6 mg, we observed a significant ($p=0.0018$) increase in IL-2 levels produced in response to OVA (Sigma) compared to OVA (*E. coli*) (Figure 3.4A). We next assessed the ability of s.c. delivered OVA (*E. coli*) and OVA (Sigma) to induce proliferation of CFSE labeled OT-I T cells *in vivo*. Using WT mice as recipients, the percentages of proliferating OT-I T cells were similar in response to OVA (Sigma) compared to OVA (*E. coli*) (Figure 3.4B; $p=0.8583$). We concluded that glycosylated OVA does have a slight cross-presentation advantage compared to non-glycosylated OVA *in vitro* using BMDC as APC, as at one OVA dose range, OVA (Sigma) was cross-presentated more efficiently than OVA (*E. coli*) (Figure 3.4A). However, glycosylated OVA does not have a cross-presentation advantage compared to non-glycosylated OVA *in vivo*. Taken together, the data in Figure 3.4 suggest that the mannose receptor is non-essential for the cross-presentation of soluble OVA.

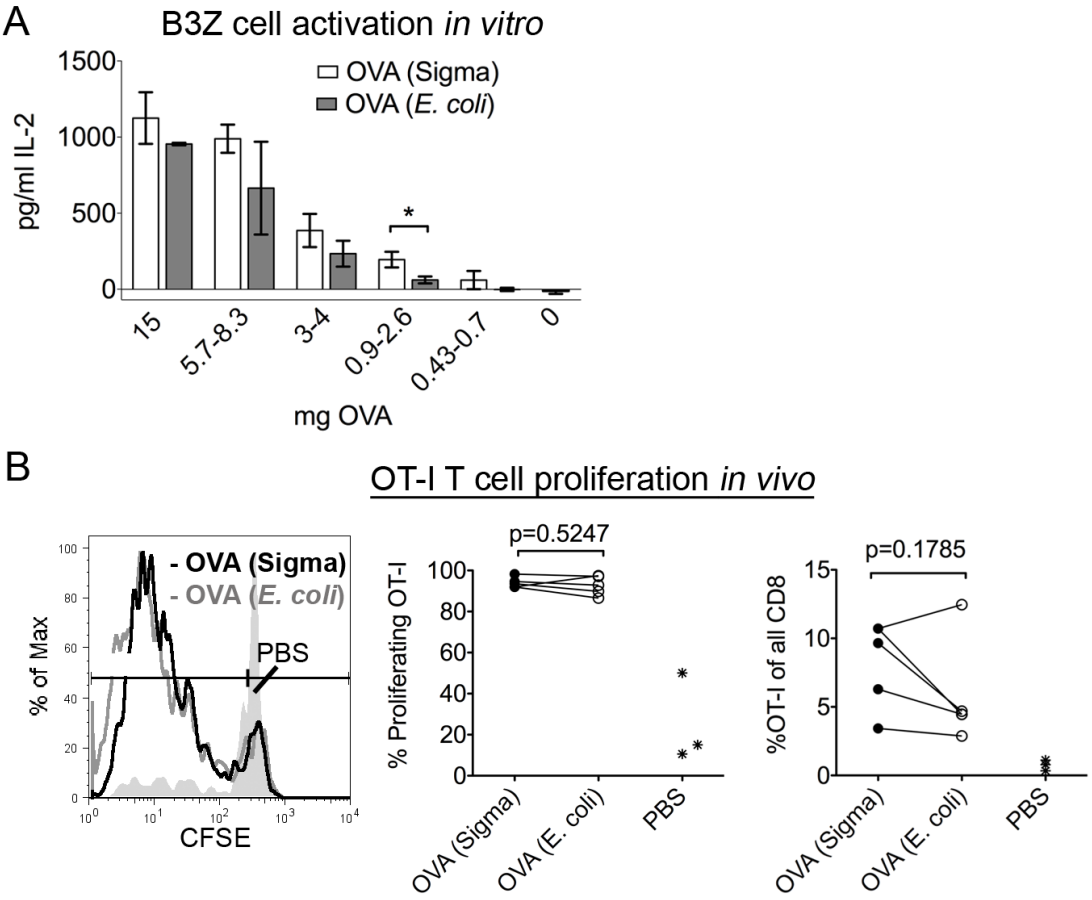

Figure 3.4: Glycosylated and non-glycosylated OVA are cross-presented with the same efficiency. (A) Indicated proteins were incubated with BMDC for 3 hours. BMDC were fixed B3Z cells were added. IL-2 levels in supernatants were determined by ELISA (24 hour time point). Within one experiment, each condition was performed in triplicate and averaged. Reported here is the average of two, three, six, eight and five independent experiments performed with 15, 5.7-8.3, 3-4, 0.9-2.6, and 0.43-0.7 mg OVA, respectively, and each experiment contained one to two doses within a dose range. *p=0.0018. (B) WT recipient mice were injected i.v. with CFSE labeled OT-I T cells. Twenty-four hours later, mice received s.c. injections of the indicated antigen (2.5-100 μg). OT-I T cell proliferation was measured 3-5 days later in the dLN (inguinal). Left panel: A representative proliferation profile is presented in response to 2.5 μg OVA. Middle and right panels: Two to three mice are averaged to generate each data point, which represents the % of proliferating OT-I T cells (middle) or the % of OT-I T cells as a function of all CD8 T cells recovered (right). Three independent experiments are represented. In one experiment, 2 different OVA (*E. coli*) preps were used in 2 different groups of mice. In another experiment, two doses (10 μg and 100 μg) of OVA were used in 2 different groups of mice. Mean ± s.e.m. is shown in *A*. A two-tailed pair-wise student t-test was used for statistical analysis in *A* and *B*. Analyses shown in Figure 3.4B were performed by Lianjun Shen.

Effects of calreticulin upon the cross-presentation of bead-associated OVA

We next hypothesized that calreticulin may have a role in inducing the cross-presentation of a particulate antigen as calreticulin has been shown to function as an "eat-me" signal when present on the surface of cells (Gardai et al., 2005; Kuraishi et al., 2007; Obeid et al., 2007b; Peters and Raghavan, 2011). Additionally, it is possible that the soluble antigens tested thus far (calreticulin-peptide complex and OVA-calreticulin fusion protein) may lack the avidity needed bind to and be efficiently internalized by calreticulin specific receptors. To test the effect of calreticulin on a particulate antigen, OVA or an equimolar mixture of OVA and calreticulin (OVA+CRT) were conjugated to 1.5 μm iron oxide beads, and cross-presentation efficiencies were assessed *in vitro* and *in vivo*. Levels of OVA conjugated to beads were quantified with a fluorescent Ab. Comparable amounts of OVA were conjugated in the OVA and OVA+CRT bead preparations (Figure 3.5A). Similar to Figure 3.3B, OVA or OVA+CRT beads were next incubated with BMDC and CFSE labeled OT-I T cells. Again, there was no difference in the levels of IL-2 generated or in the proliferation of the OT-I T cells induced in response to OVA or OVA+CRT beads (Figure 3.5B). Similar results were obtained *in vivo* with WT or TLR2/4$^{-/-}$ recipient mice (Takeuchi et al., 1999) (Figure 3.5C). These results echoed our findings using the soluble OVA-CRT fusion protein. Taken together, we concluded that extracellular calreticulin, in a soluble or particulate context, does not enhance the cross-presentation of an associated antigen.

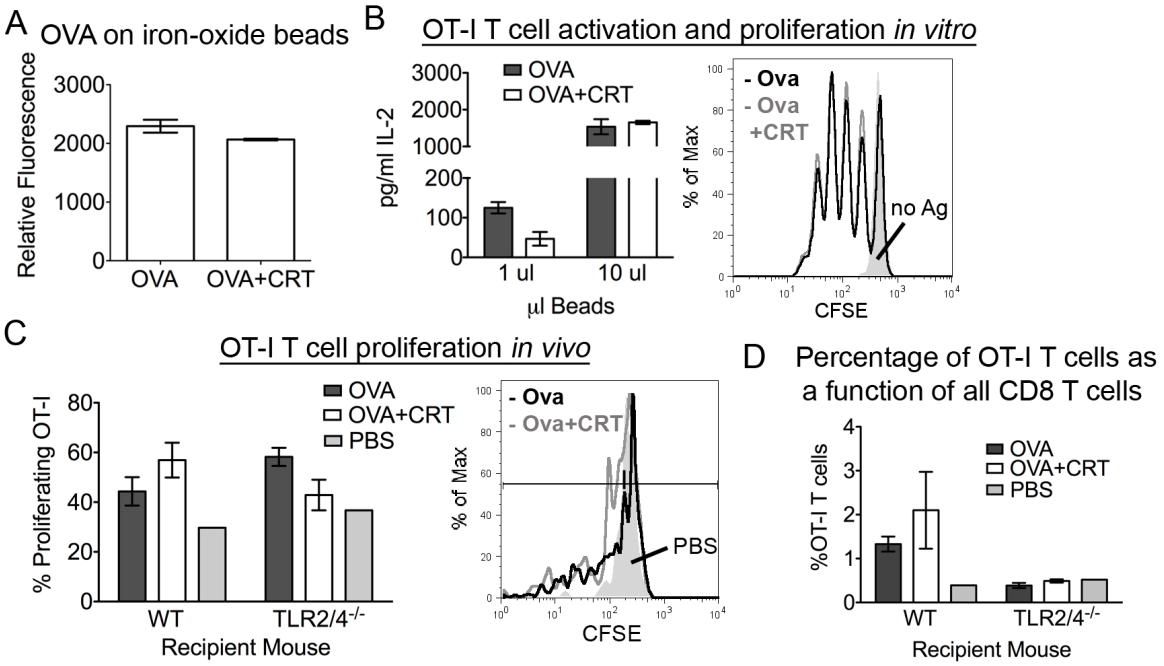

Figure 3.5: Calreticulin on the surface of a particulate antigen does not influence CD8 T cell proliferation. (A) OVA alone or with calreticulin (OVA+CRT) were conjugated to iron-oxide beads. Levels of OVA conjugated to the beads were quantified using a fluorescence-based assay. (B) The indicated beads were incubated with BMDC for 3 hours. BMDC were fixed and CFSE labeled OT-I T cells were added. IL-2 production was determined by ELISA of the supernatants at 24 hours (left panel). OT-I T cell proliferation was measured after 72 hours in response to 10 µl OVA or OVA+CRT beads. The solid grey profile indicates the condition where no antigen (no Ag) was added (right panel). Data are representative of three independent analyses. Comparing proliferation of OT-I T cells in response to 10 µl OVA or OVA+CRT, a p-value of 0.3105 was obtained using a two-tailed pair-wise student t-test. (C, D) OT-I T cell proliferation and recovery were measured in WT or TLR2/4$^{-/-}$ mice in response to 50 µl beads on day 3. (C) Average proliferation values for 2-3 mice per group (except PBS, where 1 mouse was used) are shown in the left panel. A representative proliferation prolife from WT recipients in response to OVA beads, OVA+CRT beads or PBS (filled in grey) is shown on the right panel. (D) Quantification of the percentage of OT-I T cells of all CD8 T cells recovered in *C*. Data are representative of two independent analysesfor *C*. Mean ± s.e.m. are shown. Analyses shown in Figure 3.5C and 3.5D were performed by Lianjun Shen.

Calreticulin expression in thapsigargin-treated cells cells does not enhance the cross-presentation of cell-associated OVA *in vitro*

We next tested the ability of cell-surface calreticulin to enhance the cross-presentation of a cell-associated antigen, via the induction of cellular phagocytic uptake (Figure 3.1B). The drug thapsigargin depletes ER calcium by inhibiting the sarco-ER Ca^{2+}-ATPase pumps (Thastrup et al., 1990). We showed recently that short treatments of MEF with thapsigargin induce cell surface expression of calreticulin, and phagocytosis of treated MEF was enhanced in a manner that was partially dependent on calreticulin (Jeffery et al., 2010; Peters and Raghavan, 2011). To test whether thapsigargin-induced cell surface calreticulin could thereby quantitatively enhance CD8 T cell proliferation in response to a cell-associated antigen, a MEF cell line (K42) derived from a calreticulin-deficient mouse embryo (Gao et al., 2002; Mesaeli et al., 1999) was used. K42 cells were infected with a retrovirus encoding WT calreticulin or one lacking calreticulin [to generate K42(WT CRT) and K42($CRT^{-/-}$) cells, respectively (Del Cid et al., 2010).] Calreticulin protein expression was confirmed by immunoblotting analyses (Figure 3.6A, inset). To assess the ability of thapsigargin to induce surface calreticulin, K42(WT CRT) and K42($CRT^{-/-}$) (as a specificity control) cells were incubated with either 200 nM or 5 μM thapsigargin for 5 hours. The cells then harvested and triple stained for analysis by flow cytometry. The cells were stained with anti-calreticulin (in the presense or absence of the calreticulin peptide used as the immunogen to generate the calreticulin-specific antibody in order to account for any non-specific binding of the antibody), annexin V (AnnV) and 7-aminoactinomycin D (7AAD). Annexin V binds PS, a surface marker of apoptotic cells. 7AAD is not permeable to live or early apoptotic cells. However, 7AAD does stain late apoptotic/secondary necrotic cells and thus allows us to assess surface calreticulin expression only on cells that have maintained membrane integrity. Cell-surface calreticulin was significantly up-regulated in response to both 200 nM or 5 μM thapsigargin on pre-apoptotic K42(WT CRT) cells (AnnV-7AAD-) (Figure 3.6A). Staining was specific for calreticulin, as surface calreticulin was not detectable on K42($CRT^{-/-}$) cells. Both cell types were largely pre-apoptotic immediately after treatment, and most cells reached secondary necrosis by 30 hours post treatment [Figure 3.6B and (Peters and Raghavan, 2011)].

K42(WT CRT) and K42($CRT^{-/-}$) cells were infected with a retrovirus encoding a truncated, cytosolically-expressed form of OVA and GFP utilizing a bicistronic IRES-GFP element in the retroviral vector (Van Parijs et al., 2009). The OVA/GFP expressing K42(WT CRT) and K42($CRT^{-/-}$) cells were sorted to match the two cell types for GFP intensity (Figure 3.7A), and GFP expression was found to be stably maintained thereafter (and assessed prior to each experiment). Thapsigargin-treated OVA-expressing K42($CRT^{-/-}$) or K42(WT CRT) cells were used as an antigen source for *in vitro* experiments with BMDC as the APC. Five hours after thapsigargin treatment, cells were washed and then mixed with BMDC and CFSE labeled OT-I T cells. The five-hour time point was used because cell-surface calreticulin is significantly detectable only in pre-apoptotic thapsigargin-treated cells (Peters and Raghavan, 2011), and the majority of MEFs are pre-apoptotic at this time point (Figure 3.6B). Levels of IFNγ and OT-I T cell proliferation were measured after 5 days. The OT-I T cells did not produce IFNγ or proliferate in presence of antigen donor cells alone when no BMDC were present (Figure 3.7B; K42 + OT-I alone and 3.7C; grey fills). This finding indicates that the cells expressing OVA were not able to directly activate the OT-I T cells. BMDC are necessary for OT-I T cell activation in a primary response, likely due to the requirement for co-stimulatory molecules that are provided by BMDC. In the samples containing both BMDC and thapsigargin-treated cells, slightly higher levels of IFNγ were detected in response to OVA derived from thapsigargin-treated K42(WT CRT) cells compared to thapsigargin-treated K42($CRT^{-/-}$) cells at the higher of the two target cell doses tested (Figure 3.7B). However, we observed no significant difference in proliferation of the OT-I T cells in response to OVA derived from thapsigargin-treated K42(WT CRT) cells compared to thapsigargin-treated K42($CRT^{-/-}$) cells (Figures 3.7C and 3.7D). As an alternative protocol, thapsigargin-treated OVA-expressing K42($CRT^{-/-}$) or K42(WT CRT) cells were incubated with BMDC for 60 min, a time point at which calreticulin-dependent phagocytic uptake of thapsigargin treated cells was observed (Peters and Raghavan, 2011). CD11c+ cells were subsequently purified and added to OT-I T cells; proliferation was then assessed. The result did not change based on the altered protocol (Figure 3.7E). The use of purified CD11c+ cells eliminates possible activation of OT-I cells *in trans* (by antigen donor cell derived MHC-peptide signals in combination with

APC derived co-stimulation). Thus, thapsigargin-induced surface calreticulin on pre-apoptotic cells enhances phagocytosis of cells (Peters and Raghavan, 2011), but the enhancement in phagocytosis does not translate to enhanced cross-presentation of cell-associated antigen by BMDC (Figure 3.7).

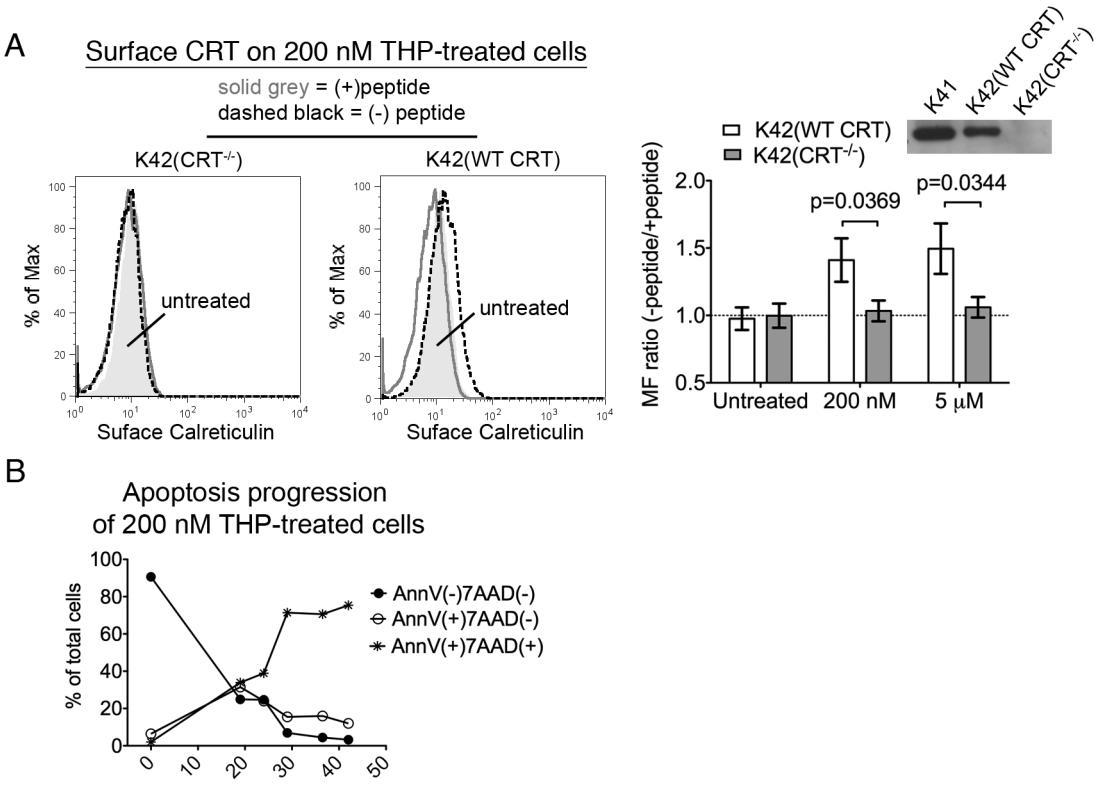

Figure 3.6: 200 nM and 5 μM thapsigargin induce cell-surface calreticulin in MEF. Calreticulin$^{-/-}$ MEF (K42) were infected with a retrovirus expressing wild-type calreticulin or empty vector [K42(WT CRT) and K42(CRT$^{-/-}$), respectively]. (A) Immunoblotting analyses of indicated cell lysates were undertaken with an antibody directed against calreticulin [inset; wild-type MEF (K41) were used as a positive control]. K42(WT CRT) or K42(CRT$^{-/-}$) cells were treated with 200 nM or 5 μM thapsigargin (THP) for 5 hrs. Cells were then stained with anti-calreticulin or anti-calreticulin pre-incubated with the calreticulin-derived peptide used as the immunogen and used to affinity purify the Ab (KEQFLDGDAWTNRWVESKHK). All cells were also stained with annexinV (AnnV) and 7-aminoactinomycin D (7AAD) to measure PS exposure and cell membrane permeability, respectively; the cells were then analyzed by flow cytometry. The ratio of the mean fluorescence (MF) of the samples in the absence over the presence of the peptide is reported here for the AnnV$^-$7AAD$^-$ population (right panel) and a representative histogram of cells treated with 200 nM thapsigargin is shown (left panel). Cells were gated on the AnnV$^-$7AAD$^-$ population for the histogram. Untreated cells are shown in filled grey. (B) K42(WT CRT) or K42(CRT$^{-/-}$) cells were treated with 200 nM THP. At the indicated time points post-treatment, the cells were labeled with AnnV and 7AAD. The percentage AnnV single positive (apoptotic), AnnV/7AAD double positive (secondary necrotic) and double negative (live/pre-apoptotic) cells are shown. Data are a compilation of 7 and 6 experiments for 200 nM and 5 mM thapsigargin treatments, respectively for *A*. For *B*, the 0 time point is a compilation of 4 independent experiments and the rest of the time points are from a single experiment. A two-tailed pair-wise student t-test was used for statistical analysis. Mean ± s.e.m. are shown.

Figure 3.7: Calreticulin expression in thapsigargin-treated cells does not enhance CD8 T cell proliferation *in vitro*. K42(WT CRT) or K42($CRT^{-/-}$) cells were infected with a retrovirus expressing cytosolic OVA and GFP, and GFP-positive cells were sorted and stably maintained. (A) K42(WT CRT) or K42($CRT^{-/-}$) cells expressing OVA were analyzed for GFP expression. (B, C) K42(WT CRT) or K42($CRT^{-/-}$) cells expressing OVA were treated with 200 nM THP for 5 hrs. The K42 cells were washed three times and incubated with BMDC and CFSE labeled OT-I T cells. Five days later, IFNγ production was determined by ELISA of the supernatants (B), and proliferation of OT-I T cells was measured (C). For the IFNγ ELISA, K42 + OT-I alone indicates samples in which BMDC were not added. SIINFEKL indicates samples containing BMDC + OT-I and the OVA-derived peptide, SIINFEKL. BMDC + OT-I alone indicates samples in which no target cells or peptide was added. Data are representative of 2 independent experiments. For the proliferation analysis, THP-treated K42(WT CRT) cells expressing OVA incubated with OT-I T cells alone (no BMDC) are shown in grey (filled in). Data are representative of 2 replicates per condition. (D) Compilation of four independent experiments comparing the proliferation of OT-I T cells in response to K42(WT CRT) or K42($CRT^{-/-}$) cells expressing OVA and treated with 200 nM THP. Each point represents the average proliferation of 2 replicates per condition and is an independent experiment. (E) K42(WT CRT) or K42($CRT^{-/-}$) cells expressing OVA were treated with 200 nM THP for 5 hrs. The K42 cells were washed three times and incubated with BMDC for 1 hour. CD11c+ cells were MACS purified and incubated with CFSE labeled OT-I T cells. Proliferation of OT-I T cells was measured 5 days later. Data are representative of 2 replicates per condition and of 2 independent experiments. A two-tailed pair-wise student t-test was used for statistical analysis. Mean ± s.e.m. are shown.

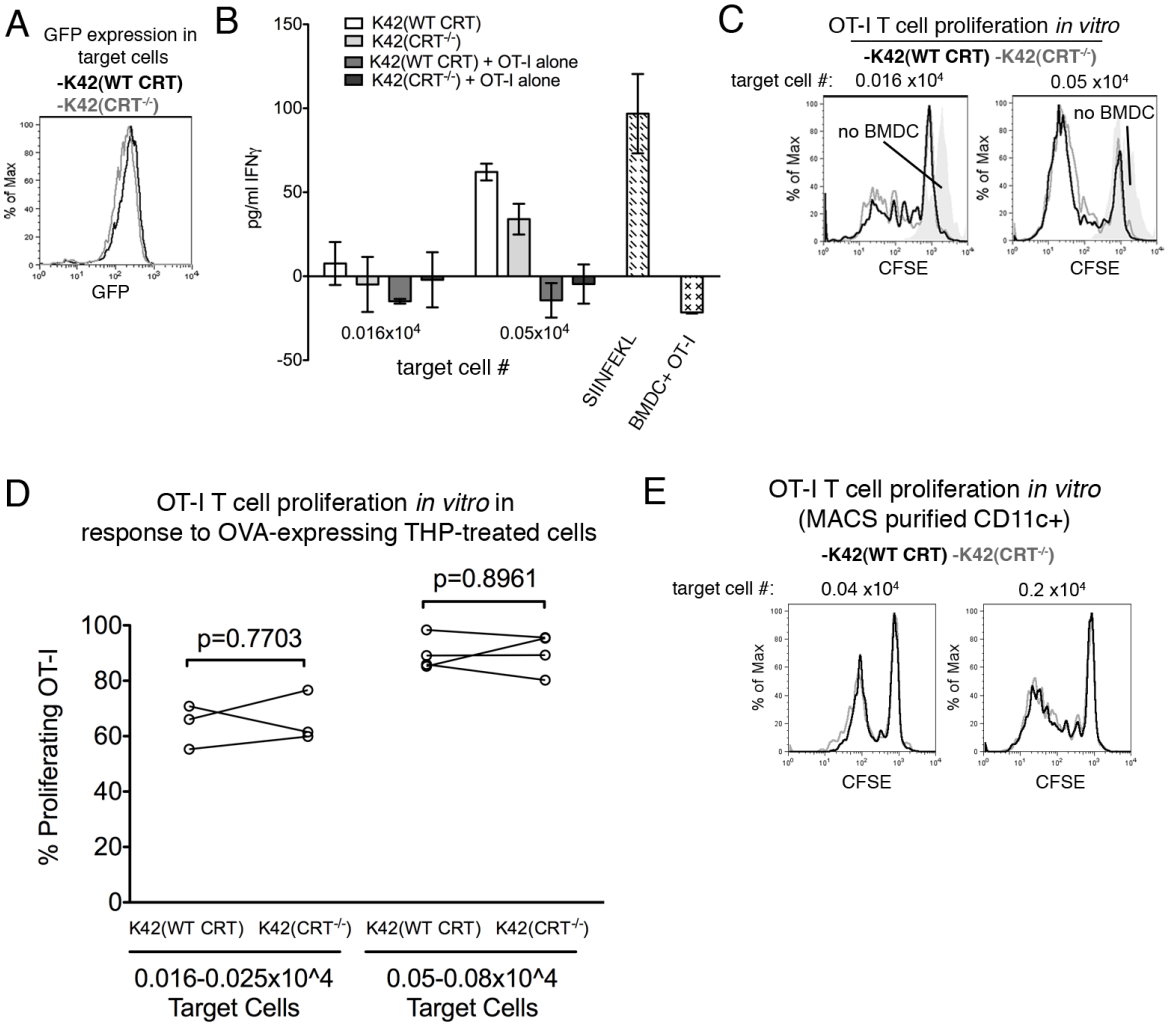
A
GFP expression in target cells
-K42(WT CRT)
-K42(CRT-/-)
% of Max
GFP
B
K42(WT CRT)
K42(CRT-/-)
K42(WT CRT) + OT-I alone
K42(CRT-/-) + OT-I alone
pg/ml IFNγ
0.016x10^4
0.05x10^4
target cell #
SIINFEKL
BMDC+ OT-I
C
OT-I T cell proliferation in vitro
-K42(WT CRT) -K42(CRT-/-)
target cell #: 0.016 x10^4
0.05 x10^4
no BMDC
% of Max
CFSE
D
OT-I T cell proliferation in vitro in response to OVA-expressing THP-treated cells
p=0.8961
p=0.7703
% Proliferating OT-I
K42(WT CRT)
K42(CRT-/-)
0.016-0.025x10^4 Target Cells
0.05-0.08x10^4 Target Cells
E
OT-I T cell proliferation in vitro (MACS purified CD11c+)
-K42(WT CRT) -K42(CRT-/-)
target cell #: 0.04 x10^4
0.2 x10^4
% of Max
CFSE

Calreticulin expression in antigen donor cells does not enhance the proliferation or cytotoxicity of CD8 T cells *in vivo* in response to cell-associated antigen

The *in vivo* counterpart of the cell-associated antigen experiment was undertaken as described above for the fusion protein, following injection of thapsigargin-treated OVA-expressing K42(WT CRT) or K42($CRT^{-/-}$) cells s.c. into the flank of the recipient mice. Four days after the injection of antigen donor cells, proliferation of the adoptively transferred CFSE labeled OT-I T cells was measured by flow cytometry. At a dose of 200 nM thapsigargin, there was no difference in proliferation in response to OVA from K42(WT CRT) or K42($CRT^{-/-}$) cells (Figures 3.8A and 3.8B). Surprisingly however, OT-I T cell proliferation was strongly inhibited when the K42 cells [both K42(WT CRT) and K42($CRT^{-/-}$)] were treated with 5 μM thapsigargin [Figures 3.8A and 3.8B; data not shown for K42($CRT^{-/-}$)]. We have recently shown that conditioned media from MEFs treated with 5 μM thapsigargin induces IL-6 production in BMDC in the absense of any other stimuli. The sterile induction of IL-6 is not observed in response to conditioned media from MEFs treated with 200 nM thapsigargin. Direct treatment of BMDC with thapsigargin was also able to induce sterile IL-6 production in BMDC. Sterile IL-6 production by BMDC in response to the conditioned media was attributed to the direct effects of thapsigargin sequestered within the treated cell membranes and subsequently partitioned into the conditioned media (Peters and Raghavan, 2011). Hence, drug sequestered in K42 cells treated with 5 μM thapsigargin may have directly activated APC *in vivo*, inducing inhibition of OT-I T cells. Further studies are needed to understand the inhibition of OT-I T cells in response to K42 cells treated with 5 μM thapsigargin. Nevertheless, similar levels of OT-I T cell proliferation was observed in response to K42(WT CRT) and K42($CRT^{-/-}$) cells expressing OVA treated with 200 nM thapsigargin (Figure 3.8B, left panel). Similar percentages of OT-I T cells were recovered from mice immunized with K42(WT CRT) and K42($CRT^{-/-}$) thapsigargin treated cells as well (Figure 3.8B, right panel).

The *in vivo* experiments described thus far measure proliferation of OT-I T cells in response to soluble, bead-associated and cell-associated OVA. However, proliferation may not be indicative of effector function. Additionally, although widely used, the OT-I cell adoptive transfer protocol could represent a non-physiological mode of expansion of

CD8 T cells (in the absence of adequate CD4 T cell help). To evaluate the effector function of endogenous CD8 T cells in response to different forms of cell-associated antigen, an *in vivo* cytotoxicity assay was performed. Recipient WT mice were immunized s.c. with PBS, or 200 nM thapsigargin-treated K42(WT CRT) or K42($CRT^{-/-}$) cells expressing OVA. Seven days later, two different groups of target splenocytes labeled with two different dilutions of CFSE dye were simultaneously injected i.v. into the recipient mice. One group of target cells was pulsed with the OVA-derived SIINFEKL peptide, and these target cells were labeled with a high concentration of CFSE. The second group of target cells was pulsed with a non-specific peptide that, similar to SIINFEKL, binds the mouse MHC class I allele H2-K^b and is derived from listeriolysin O (LLO; a protein expressed by the bacterium *Listeria monocytogenes*) (Goldszmid et al., 2009). This second group of target cells was labeled with a low concentration of CFSE. The two populations of target cells were injected at a 1:1 ratio into the immunized mice, with a total of $3.6x10^6$ target cells injected. The spleens of the recipient mice were harvested and analyzed by flow cytometry for persistence of labeled cells 18 hours after the injection of the target cells. The percentage of SIINFKEL pulsed target cells recovered from the mouse that was immunized with PBS remained about 50. However, target cells isolated from mice immunized with $5x10^5$ K42(WT CRT) or K42($CRT^{-/-}$) cells showed a reduction in the percentage of SIINFEKL pulsed target cells (Figure 3.8C). Thus, effector cells specific to the OVA-derived peptide (and not the LLO-derived peptide) were generated in mice that had been immunized with K42 cells expressing OVA. Reduction of the SIINFEKL pulsed target cells was not observed at the lower immunizing cells dose of $5x10^4$ K42 cells (Figure 3.8C). The reduction of SIINFEKL pulsed target cells was similar between mice immunized with $5x10^5$ K42(WT CRT) or K42($CRT^{-/-}$) cells (Figure 3.8C).

The draining lymph nodes of the recipient mice were also harvested (at the same time as the spleens) to assess the activation of the endogenous antigen specific CD8 T cells. The cells of the lymph nodes were incubated with SIINFEKL peptide for 48 hours. IFNγ production was then measured from the supernatants. The levels of IFNγ produced by CD8 T cells was similar between mice immunized with $5x10^5$ K42(WT CRT) or K42($CRT^{-/-}$) cells expressing OVA (Figure 3.8D). These findings indicate that

thapsigargin-induced cell-surface calreticulin on K42 cells (Figure 3.6) does not lead to enhanced cytotoxicity of endogenous antigen specific CD8 T cells (Figure 3.8).

Figure 3.8: Calreticulin expression in thapsigargin-treated cells does not enhance CD8 T cell proliferation or cytotoxicity *in vivo*. (A) Recipient WT mice were injected i.v. with CFSE labeled OT-I T cells. Twenty-four hours later, the mice received PBS, $5x10^5$ THP-treated K42(WT CRT) and K42($CRT^{-/-}$) (left panel; 200 nM THP) or THP-treated K42(WT CRT) (right panel; 5 μM THP) OVA expressing cells s.c. Proliferation was measured 4 days later in the dLN (inguinal). The control immunization with PBS is depicted in filled grey. Data are representative of 2-3 mice per group. (B) Quantification of proliferating OT-I T cells and the percentage of OT-I T cells as a function of all CD8 T cells recovered in response to 200 nM and 5 μM THP. Panels comparing K42(WT CRT) to K42($CRT^{-/-}$): For both panels, each point represents the average OT-I T cell proliferation from 2-3 mice and is an independent experiment. Three independent experiments are represented; mice received $2.5\text{-}5x10^5$ THP-treated antigen donor cells. One experiments contained 2 cell doses, and two experiments contained 1 cell dose. Panels comparing 200 nM to 5 μM THP: In the left panel, each point represents the average OT-I T cell proliferation from 2-3 mice and is an independent experiment. Five independent experiments are represented; mice received $0.1\text{-}50x10^5$ THP-treated antigen donor cells. Only two experiments compared 200 nM to 5 μM THP. In the right panel, four independent experiments are represented; mice received $2.5\text{-}10x10^5$ THP-treated antigen donor cells. Only two experiments compared 200 nM to 5 μM THP. (C) Recipient WT mice were injected s.c. with PBS, or 200 nM THP-treated K42(WT CRT) and K42($CRT^{-/-}$) cells expressing OVA. Seven days post-immunization, mice were injected i.v. with PKH26 labeled target cells pulsed with the OVA-derived SIINFEKL peptide (high CFSE labeling) or the listeriolysin O derived VAYGRQVYL non-specific peptide (low CFSE labeling). Spleens were recovered 18 hours later to assess killing of target cells by flow cytometry; the PKH26 dye and a congenic marker (CD45.1) identified the target cells. The percentage of SIINFEKL loaded target cells recovered is depicted in the graph. Each circle is representative of the percentage of target cells recovered from one mouse. Representative of two independent experiments. (D) Draining lymph nodes (inguinal) were harvested at the same time as spleens and incubated *in vitro* with 10 μM SIINFEKL for 72 hours. IFNγ production was determined by ELISA of the supernatants. Representative of two independent experiments. For *B*, A two-tailed pair-wise student t-test was used for statistical analysis. Mean ± s.e.m. are shown in *C* and *D*. Analyses shown in Figure 3.8A and 3.8B were in part performed by Lianjun Shen.

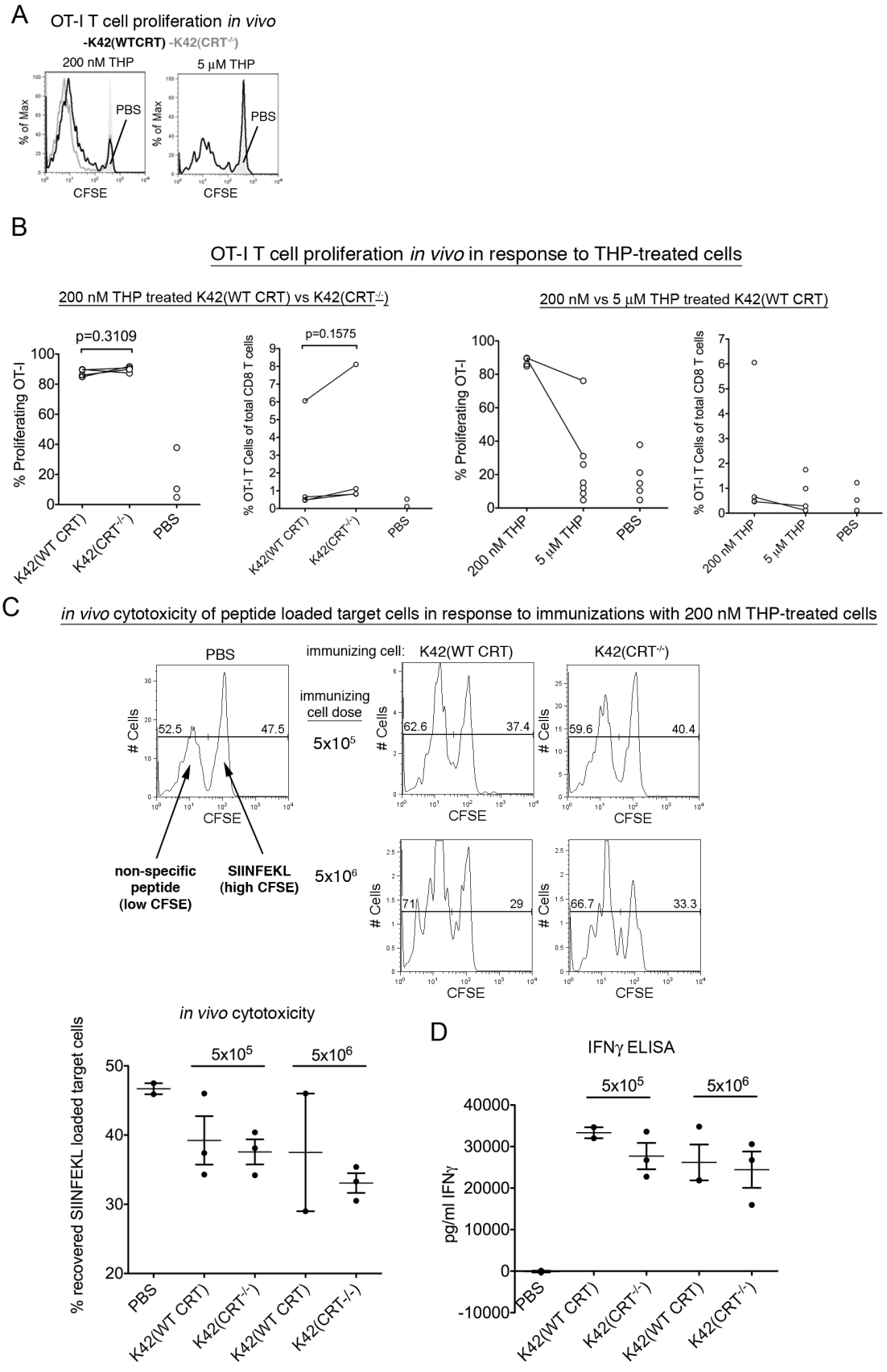
A
OT-I T cell proliferation *in vivo*
-K42(WTCRT) -K42(CRT-/-)
200 nM THP
5 μM THP
PBS
% of Max
CFSE
B
OT-I T cell proliferation *in vivo* in response to THP-treated cells
200 nM THP treated K42(WT CRT) vs K42(CRT-/-)
200 nM vs 5 μM THP treated K42(WT CRT)
p=0.3109
p=0.1575
% Proliferating OT-I
% OT-I T Cells of total CD8 T cells
K42(WT CRT)
K42(CRT-/-)
PBS
200 nM THP
5 μM THP
C
in vivo cytotoxicity of peptide loaded target cells in response to immunizations with 200 nM THP-treated cells
PBS
immunizing cell: K42(WT CRT)
K42(CRT-/-)
immunizing cell dose
5x10^5
5x10^6
Cells
CFSE
52.5
47.5
62.6
37.4
59.6
40.4
71
29
66.7
33.3
non-specific peptide (low CFSE)
SIINFEKL (high CFSE)
in vivo cytotoxicity
% recovered SIINFEKL loaded target cells
D
IFNγ ELISA
pg/ml IFNγ

Calreticulin expression in antigen donor cells enhances CD8 T cell proliferation *in vitro*

We considered the possibility that pre-assembled MHC class I molecules of antigen donor cells could contribute to CD8 T cell proliferation (Figure 3.1C), thus accounting for the non-critical role of cell-surface calreticulin in inducing CD8 T cell proliferation (Figures 3.7 and 3.8). Calreticulin facilitates intracellular assembly of MHC class I molecules (Gao et al., 2002), and correspondingly, K42(WT CRT) cells expressing OVA have higher levels of H2-K^b and H2-K^b-SIINFEKL complexes compared to K42($CRT^{-/-}$) cells expressing OVA (Figure 3.9A and 3.9B). If pre-assembled MHC class I molecules of antigen donor cells contribute to CD8 T cell proliferation *in vitro* or *in vivo*, we would expect to see some enhancement in proliferation in response to antigen derived from WT cells compared to calreticulin-deficient cells. This effect may not have been apparent with thapsigargin-treated cells as thapsigargin treatment abrogates the calreticulin-dependent optimization of MHC class I assembly (Jeffery et al., 2010).

To further address possible contributions of pre-assembled MHC class I to CD8 T cell proliferation, MEFs were UV-irradiated immediately prior to use in OT-I T cell assays [in order to prevent their uncontrolled proliferation; cell death progression in UV-treated cells had comparable kinetics to that for thapsigargin-treated cells (Figure 3.10A compared to Figure 3.6B)]. In contrast to findings with thapsigargin treated MEF (Figure 3.7D), OT-I T cells proliferated to a greater extent and secreted more IFNγ in response to OVA-expressing UV-treated K42(WT CRT) cells compared to OVA-expressing UV treated K42($CRT^{-/-}$) cells *in vitro* (Figures 3.11A; first panel and 3.11B & 3.11C; top panels). The difference in proliferation was significant at the higher of the two cell doses assessed (Figure 3.11D).

We showed recently that UV-treated MEF do not induce cell-surface calreticulin at a level detectable by flow cytometry and that calreticulin does not enhance phagocytic uptake of UV-treated MEF (Peters and Raghavan, 2011). These findings were confirmed in the present study by measuring cell-surface calreticulin at various time points post UV-treatment. It is noteworthy that these analyses were undertaken in the absence of calcium. Cell-surface calreticulin induction was not detectable by flow cytometry at any of the time-points that were tested (Figure 3.10B). Calreticulin is reported to bind PS in a

calcium dependant manner (Paidassi et al., 2011; Tarr et al., 2010), and it is possible that use of AnnexinV in our staining protocol or the absence of calcium during staining interfered with expression or detection of calreticulin. Under these conditions, phagocytic uptake of K42(WT CRT) or K42($CRT^{-/-}$) cells was also very similar at multiple time-points tested (Figure 3.10C-3.10E; phagocytic uptake was measured 17 hours post UV-treatment). Although conditions used for OT-I T cell proliferation and phagocytosis were different (MEFs were irradiated immediately or 17 hours prior to the assay, respectively), these findings suggested that the observed calreticulin-dependent increase in OT-I T cell proliferation (Figure 3.11D) could not be attributed mainly to increased calreticulin-dependent phagocytic uptake of antigen donor cells.

To further test for possible involvement of intracellular calreticulin-dependent enhancement of MHC class I assembly, we examined the ability of MHC-mismatched BMDC (Balb/c mice-derived) to activate OT-I T cells. In this setting, Balb/c BMDC cannot cross-present OVA from the apoptotic donor cell to OT-I T cells because Balb/c BMDC lack the appropriate MHC class I allele (H2-K^b). Thus, the primary mechanism of OT-I T cell activation by Balb/c BMDC would involve the trogocytic transfer of H2-K^b-SIINFEKL complexes from the antigen donor cell to Balb/c BMDC, or activation *in trans* mediated by MEF-derived H2-K^b-SIINFEKL together with BMDC-derived co-stimulatory molecules. Indeed, when Balb/c BMDC were used as APC, differences in IFNγ secreted by OT-I T cells and OT-I T cell proliferation induced by OVA-expressing UV-treated K42(WT CRT) and K42($CRT^{-/-}$) cells persisted (Figure 3.11A; middle panel and Figure 3.11B; lower panel). Proliferation of OT-I T cells was also examined using BMDC from $\beta2m^{-/-}$ mice (B6 background) and similar results were obtained (Figure 3.11C, lower panel). The analyses of Figure 3.11C used K42(WT CRT) and K42($CRT^{-/-}$) cells from a different OVA-GFP-expressing virus infection compared to that shown in Figure 3.11B. GFP and MHC class I expression profiles for antigen donor cells used in 3.11B are shown in Figures 3.7A and Figure 3.8A, respectively. MHC class I and GFP expression profiles for antigen donor cells used for the experiment shown in Figure 3.11C are depicted in Figures 3.9B and 3.9C, respectively.

Two experiments were performed comparing Balb/c to B6 BMDC, and two experiments were performed comparing B6($\beta2m^{-/-}$) and B6(WT) BMDC. Combining

these four experiments to perform statistical analyses, we found that OT-I T cells proliferated to a significantly higher extent in response to UV-treated OVA-expressing K42(WT CRT) cells compared to K42($CRT^{-/-}$) cells when either B6 BMDC or Balb/c and B6($\beta 2m^{-/-}$) BMDC were used (Figure 3.11E). Although OT-I T cells secreted less IL-2 in response to K42 cells using BMDC from Balb/c mice compared to B6 mice, there was no statistically significant difference in OT-I T cell proliferation in response to OVA derived from K42(WT CRT) cells using B6 BMDC compared to Balb/c and B6($\beta 2m^{-/-}$) BMDC (Figure 3.11E). The same result was observed when comparing K42($CRT^{-/-}$) antigen donor cells incubated with the different BMDC preparations (Figure 3.11E). Notably, OT-I T cells did not proliferate in response to K42 cells expressing OVA when BMDC were not present (Figure 3.11B and 3.11C, grey filled profiles). These findings suggested that 1) the positive effect of calreticulin on OT-I T cell proliferation in the UV-treated antigen donor cell context was attributable to the ability of intracellular calreticulin of K42(WT CRT) cells to facilitate MHC class I assembly and 2) OT-I T cell proliferation observed in a syngeneic *in vitro* experimental set-up (using B6 BMDC) largely derives from pre-assembled H2-K^b-SIINFEKL complexes rather than *de novo* assembly of MHC class I via cross-presentation of antigen from phagocytosed antigen donor cells.

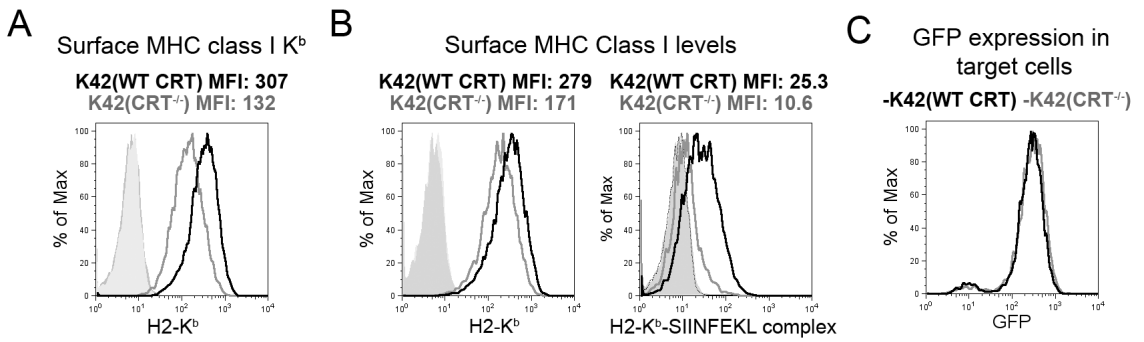

Figure 3.9: MHC class I or GFP expression in antigen donor cells used in the analyses of Figures 3.11. (A) and (B, left panel) OVA-expressing K42(WT CRT) or K42($CRT^{-/-}$) cells were labeled with an Ab against H2-K^b, or secondary alone (filled grey). Analyses shown in A and B are data from separate infections of K42(WT CRT) or K42($CRT^{-/-}$) cells with retroviruses encoding GFP and OVA. Cells characterized in panel A were used for experiments shown in Figure 3.11A and 3.11B. Cells characterized in panels B and C were used for the experiment shown in 3.11C. (B, right panel) Cells were labeled with an Ab against H2-K^b-SIINFEKL [non-OVA expressing cells are shown as controls; K42(WT CRT) in filled grey and K42($CRT^{-/-}$) as a dotted line]. (C) GFP expression was measured by flow cytometry in cells used for experiments shown in 3.11C.

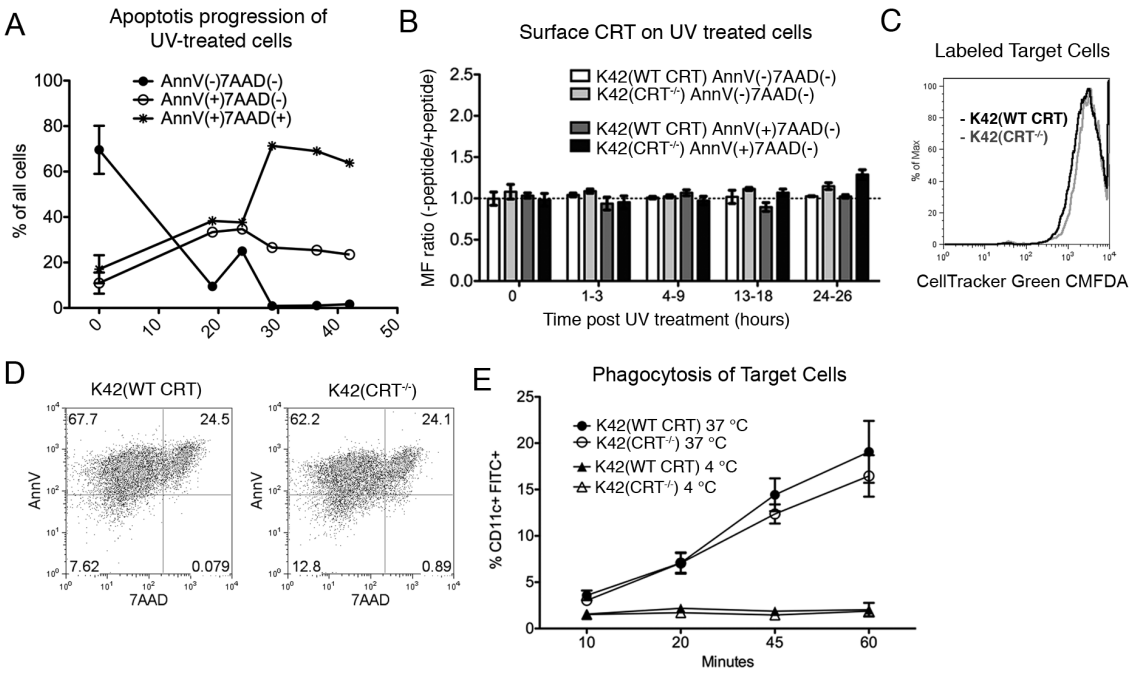

Figure 3.10: UV treatment of WT MEF does not induce cell-surface calreticulin or enhanced phagocytosis compared to calreticulin-deficient MEF**.** (A) K42(WT CRT) cells were exposed to UV. At the indicated time points post-treatment, the cells were labeled with AnnV and 7AAD. The percentage AnnV single positive (apoptotic), AnnV/7AAD double positive (secondary necrotic) and double negative (live/pre-apoptotic) cells are shown. (B) K42(WT CRT) or K42(CRT$^{-/-}$) cells were exposed to UV and allowed to progress through apoptosis for the indicated time points. Cells were harvested and stained with anti-calreticulin or anti-calreticulin pre-incubated with the calreticulin-derived peptide used as the immunogen and used to affinity purify the Ab. All cells were also stained with AnnV and 7AAD; the cells were then analyzed by flow cytometry. The ratio of the mean fluorescence (MF) of the samples in the absence over the presence of the peptide is reported here. (C) K42(WT CRT) or K42(CRT$^{-/-}$) cells were labeled with CellTracker Green CMFDA. Fluorescence intensity of the labeled cells was measured using the FITC channel. (D) K42(WT CRT) or K42(CRT$^{-/-}$) cells were exposed to UV and allowed to undergo apoptosis for 17 hrs. AnnV and 7AAD binding was measured after this time. (E) Labeled apoptotic cells were incubated with BMDC for the indicated time points at either 37 °C or 4 °C. The acquisition of K42 cells by CD11c+ cells was measured and plotted as a function of time. These experiments were performed in the absence of calcium. For (A), the 0 time point is a compilation of 3 independent experiments and the rest of the time points are from a single experiment. Data are representative of 4 experiments for (B). Three to six independent analyses are averaged for each time point reported for (E). Mean ± s.e.m. are shown.

Figure 3.11: Calreticulin expression in antigen donor cells enhances CD8 T cell proliferation *in vitro* (A, B) K42(WT CRT) or K42($CRT^{-/-}$) OVA-expressing cells were exposed to UV light, following which cells were immediately incubated with CFSE labeled OT-I T cells and either B6 or Balb/c BMDC. Levels of IL-2 were measured 24 hours later (A) and proliferation of OT-I T cells was measured 5 days later (B). In *A*, K42 + OT-I alone indicated samples that did not contain BMDC. Data are representative of 2 independent experiments. In *B*, UV-treated K42(WT CRT) OVA-expressing cells incubated with OT-I T cells alone (no BMDC) are shown in grey (filled). Data are representative of 2 replicates per condition. (C) Analyses similar to *B*, but comparing OT-I T cell proliferation induced in the presence of B6 or B6($\beta2m^{-/-}$) BMDC. Data are representative of 2 replicates per condition. (D, E) Compilation of four independent experiments comparing the proliferation of OT-I T cells in response to OVA-expressing, UV-treated K42(WT CRT) or K42($CRT^{-/-}$) cells using (D) B6 BMDC or (E) B6, Balb/c and $\beta2m^{-/-}$ BMDC ($0.4\text{-}0.6x10^4$ antigen donor cells were used in *E*). Each point represents the average proliferation of 2 replicates per condition and is an independent experiment within the group. For *E*, a similar analysis was performed at the $0.05\text{-}0.08x10^4$ target cell dose comparing OT-I T cell proliferation in response to K42(WT CRT) to K42($CRT^{-/-}$) cells using Balb/c and $\beta2m^{-/-}$ BMDC. This analysis yielded a p value of 0.0033. Two-tailed pair-wise student t-tests were used for all statistical analysis. Mean ± s.e.m. are shown.

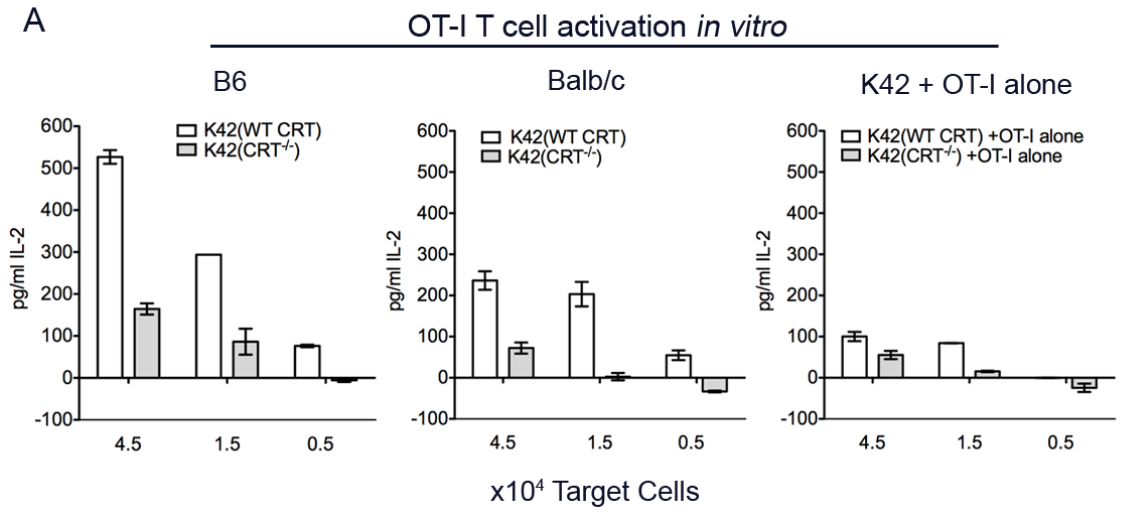
A
OT-I T cell activation *in vitro*
B6
Balb/c
K42 + OT-I alone
K42(WT CRT)
K42(CRT-/-)
K42(WT CRT) +OT-I alone
K42(CRT-/-) +OT-I alone
pg/ml IL-2
600
500
400
300
200
100
0
-100
4.5
1.5
0.5
x10⁴ Target Cells

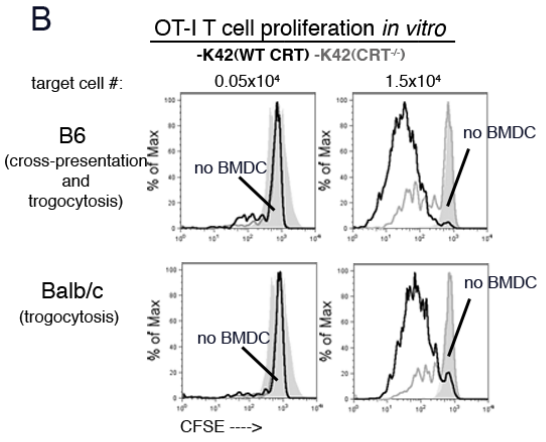
B
OT-I T cell proliferation *in vitro*
-K42(WT CRT) -K42(CRT-/-)
target cell #:
0.05x10⁴
1.5x10⁴
B6
(cross-presentation and trogocytosis)
Balb/c
(trogocytosis)
no BMDC
% of Max
CFSE --->

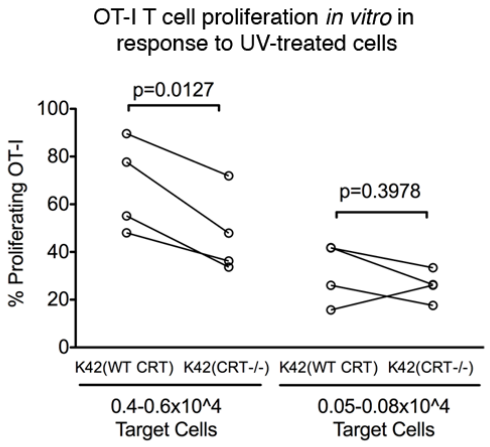
D
OT-I T cell proliferation *in vitro* in response to UV-treated cells
p=0.0127
p=0.3978
% Proliferating OT-I
100
80
60
40
20
0
K42(WT CRT)
K42(CRT-/-)
0.4-0.6x10^4 Target Cells
0.05-0.08x10^4 Target Cells

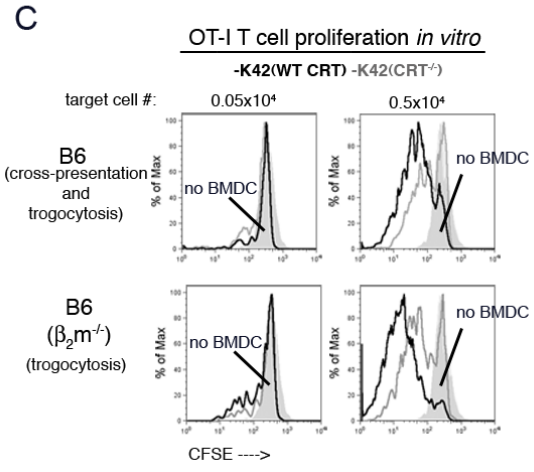
C
OT-I T cell proliferation *in vitro*
-K42(WT CRT) -K42(CRT-/-)
target cell #:
0.05x10⁴
0.5x10⁴
B6
(cross-presentation and trogocytosis)
B6
(β2m-/-)
(trogocytosis)
no BMDC
% of Max
CFSE --->

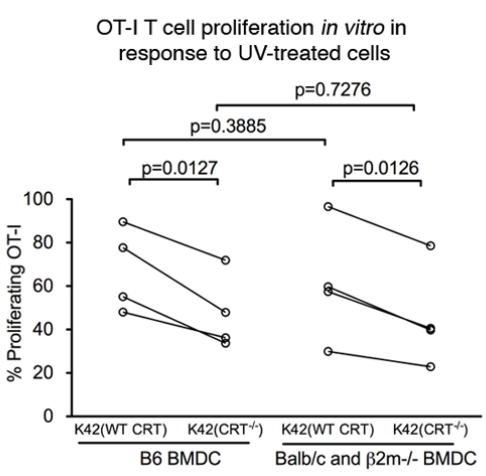
E
OT-I T cell proliferation *in vitro* in response to UV-treated cells
p=0.7276
p=0.3885
p=0.0127
p=0.0126
% Proliferating OT-I
100
80
60
40
20
0
K42(WT CRT)
K42(CRT-/-)
B6 BMDC
Balb/c and β2m-/- BMDC

MHC class I molecules of subcutaneously delivered antigen donor cells are non-essential for CD8 T cell proliferation *in vivo*

We next examined whether pre-assembled MHC class I of antigen donor cells also contribute significantly to CD8 T cell proliferation *in vivo*, which could account for the non-critical role of cell-surface calreticulin in inducing CD8 T cell proliferation (Figures 3.7 and 3.8). CFSE labeled OT-I T cells were adoptively transferred into B6 recipient mice. Twenty-four hours later, we immunized the mice s.c. with K42(WT CRT) or K42($CRT^{-/-}$) cells expressing OVA that had been UV-treated immediately prior to immunizations. There was no statistical difference in the proliferation of the OT-I T cells in the two groups of mice (Figures 3.12A and 3.12B). Similar percentages of OT-I T cells were recovered from mice immunized with K42(WT CRT) and K42($CRT^{-/-}$) UV treated cells as well (Figure 3.12B, right panel). These findings suggested that unlike the *in vitro* situation with BMDC, during a primary response, pre-assembled MHC class I molecules did not contribute significantly to CD8 T cell proliferation *in vivo* in response to cell-associated antigen. To extend and verify the latter possibility, OT-I T cell proliferation efficiencies were compared following immunizations with WT MEF or MEF deficient in H2-K^b, H2-D^b and β2m (3KO) (Lybarger et al., 2003). 3KO cells lack H2-K^b (Figure 3.12C, left panel). Therefore, trogocytic transfer or direct activation by MEFs (*in trans* with APC) cannot contribute to the CD8 T cell response. WT and 3KO MEF were infected with the retrovirus encoding OVA and GFP, and sorted cells expressing similar levels of GFP were obtained (Figure 3.12C, right panel). If trogocytosis or direct activation by MEFs contributes significantly to antigen transfer *in vivo*, we would expect impaired OT-I T cell proliferation in response to OVA derived from UV-treated 3KO cells compared to WT cells. Interestingly, we found that OT-I T cells responded similarly to OVA derived from WT and 3KO cells (Figures 3.12D and 3.12E). These findings suggest that trogocytosis or activation *in trans* are not significant mechanisms of CD8 T cell activation *in vivo* in a primary response to s.c. antigen, or that other redundant pathways for antigen transfer are present.

Figure 3.12: MHC class I molecules of subcutaneously delivered antigen donor cells are non-essential for *in vivo* proliferation of CD8 T cells. (A) Recipient B6 mice were injected i.v. with CFSE labeled OT-I T cells. Twenty-four hours later, the mice received s.c. immunization of UV-treated K42(WT CRT) or K42($CRT^{-/-}$) cells expressing OVA. Proliferation was measured 4 days later in the dLN. PBS control is depicted in filled grey. Data are representative of 2-4 mice per group. (B) Left panel: quantification of proliferating OT-I T cells in response to 1-2.5 $x10^5$, 5-10 $x10^5$, or 50-100 $x10^5$ UV-treated antigen donor cells. Two experiments are reported for the 50-100 $x10^5$ dose range. Each point represents the average proliferation of 2-4 mice per group. Six independent experiments are shown, with multiple doses performed within an experiment. Right panel: the percentage of OT-I T cells as a function of all CD8 T cells. (C-E) WT or 3KO cells were infected with a retrovirus expressing cytosolic OVA and GFP. MHC class I (C, left panel) or GFP expression (C, right panel) were compared on sorted cells. (D) OT-I T cell proliferation was assessed *in vivo* as described in A, with the difference that recipient mice received s.c. immunizations of $0.6x10^6$ UV-treated WT or 3KO OVA-expressing cells. Data are representative of 3 mice per group, except the PBS condition, where 1 mouse was used. (E) Quantification of proliferating OT-I T cells in response to 0.5-$0.6x10^6$ UV-treated antigen donor cells. Each point represents the proliferation of OT-I T cells from an individual mouse and 2 independent experiments are depicted. Two-tailed pair-wise student t-tests were used for all statistical analysis. Mean ± s.e.m. are shown. Analyses shown in Figure 3.12B were in part performed by Lianjun Shen.

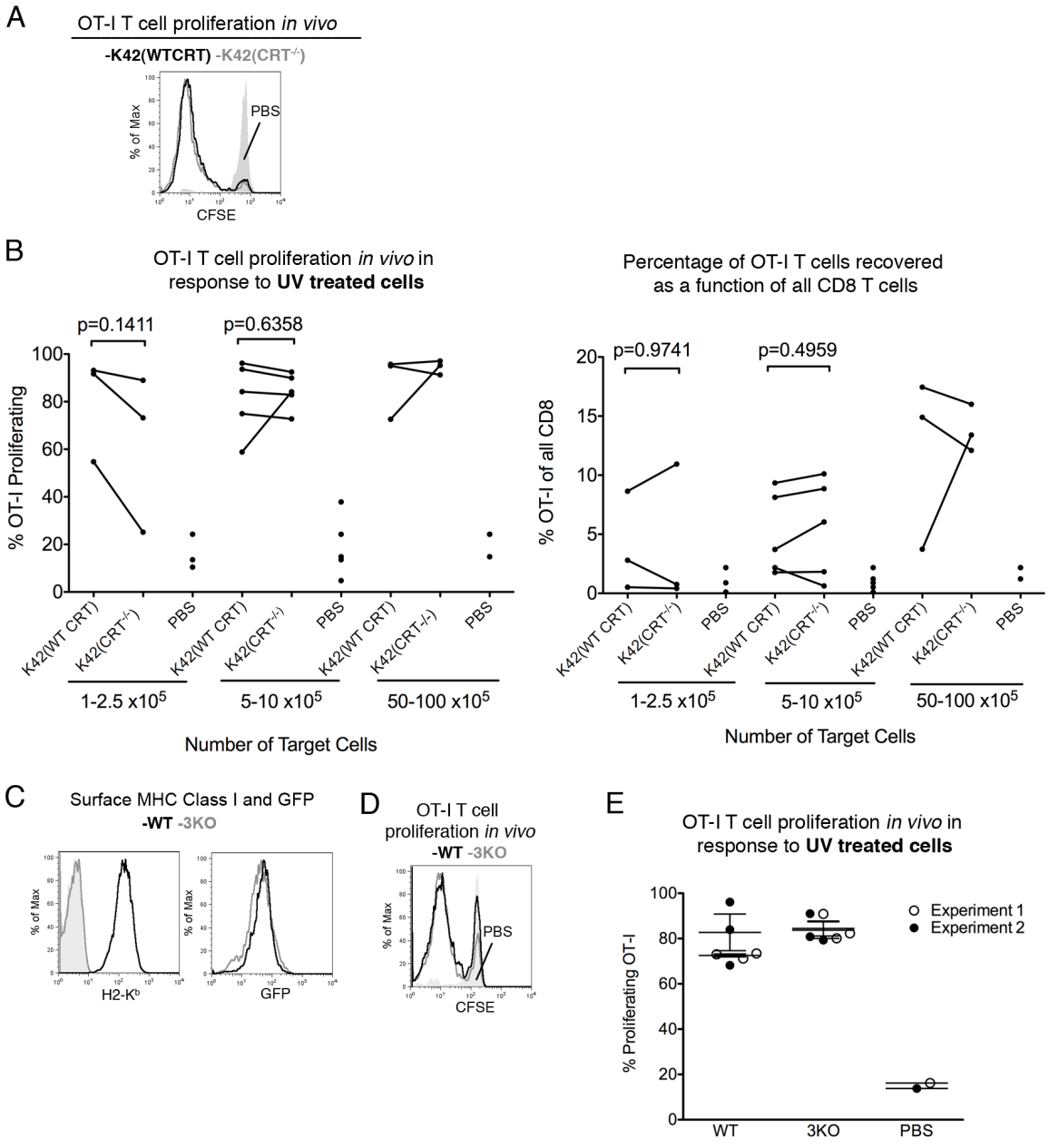
A
OT-I T cell proliferation *in vivo*
-K42(WTCRT) -K42(CRT-/-)
% of Max
PBS
CFSE
B
OT-I T cell proliferation *in vivo* in response to **UV treated cells**
p=0.1411
p=0.6358
% OT-I Proliferating
K42(WT CRT)
K42(CRT-/-)
PBS
1-2.5 x10^5
5-10 x10^5
50-100 x10^5
Number of Target Cells
Percentage of OT-I T cells recovered as a function of all CD8 T cells
p=0.9741
p=0.4959
% OT-I of all CD8
C
Surface MHC Class I and GFP
-WT -3KO
H2-Kb
GFP
D
OT-I T cell proliferation *in vivo*
-WT -3KO
E
OT-I T cell proliferation *in vivo* in response to **UV treated cells**
% Proliferating OT-I
Experiment 1
Experiment 2
WT
3KO
PBS

LPS treatment of antigen donor cells inhibits CD8 T cell proliferation against cell-associated antigen *in vivo*

As noted above, we have recently shown that thapsigargin induces the secretion of sterile IL-6 by BMDC *in vitro*. Thus, observed inhibition of CD8 T cell proliferation *in vivo* in response to antigen donor cells treated with 5 μM thapsigargin (Figure 3.8) prompted us to further investigate the role of innate signaling in CD8 T cell proliferation. To investigate the possibility that innate signaling could inhibit CD8 T cell proliferation in response to s.c. delivered cell-associated antigen, we examined the effects of LPS treatment of antigen donor cells on CD8 T cell proliferation *in vivo*. K42(WT CRT) cells expressing OVA were exposed to UV-irradiation and subsequently mixed with 0, 1, 10 or 100 ng LPS. The UV-treated cells and the varying amounts of LPS were injected s.c. into WT recipient mice that had received CFSE labeled OT-I T cells 24 hours prior. Proliferation was then assessed. Similar to the 5 μM thapsigargin treatment of antigen donor cells, LPS inhibited proliferation of the OT-I T cells in a dose-dependent manner. LPS was inhibitory at levels as low as 1 ng per mouse (Figures 3.13A and 3.13B).

In this set of experiments, insufficient CD4 T cell help may be available for the OT-I CD8 T cells due to the large numbers of OT-I T cells transferred in the adoptive transfer experiment. It is possible that the LPS-induced inhibition of CD8 T cell proliferation resulted from the lack of sufficient CD4 T cell help. Therefore, a similar experiment was undertaken as described above with the addition of OT-II T cells [obtained from a transgenic mouse whose CD4 T cells express a TCR that recognizes the $OVA_{323-399}$ epitope ISQAVHAAHAEINEAGR bound to the murine MHC class II allele $I\text{-}A^d$ (Barnden et al., 1998)]. OT-I T cell proliferation was inhibited by 10 ng LPS (Figure 3.13C), as previously observed (Figure 3.13B), in the absence of OT-II T cells in response to antigen donor cells treated with UV. When unlabeled OT-II T cells were injected along with the CFSE labeled OT-I T cells at a CD8:CD4 T cell ratio of 1:2, LPS induced inhibition of OT-I T cell proliferation in response to antigen donor cells was still observed (Figure 3.13C). The observed inhibition of CD8 T cells proliferation indicates that LPS interferes with CD8 T cell responses against cell-associated antigen even when CD4 T cell help is present. We also assessed the percentage of OT-I T cells recovered of

all CD8 T cells recovered. This type of analysis revealed the extent of LPS induced inhibition of OT-I T cells (Figure 3.13D). Also, in the absence of LPS, OT-I T cells proliferated to a lower extent in the presence of OT-II T cells (Figure 3.13C). Accordingly, a lower percentage of OT-I T cells were recovered from mice that received both OT-I and OT-II T cells (Figure 3.13D). The reduction may be explained by competition for lymph node space or antigen. Compared to mice that receive only OT-I T cells, OT-II T cells may compete with OT-I T cells in mice that receive both cell types. Nevertheless, our findings indicate that antigen donor cells treated with inducers of innate signaling (5 μM thapsigargin or LPS) inhibit the proliferation of CD8 T cells *in vivo* against cell-associated antigen (Figure 3.8B and 3.13).

Figure 3.13: LPS inhibits OT-I T cell proliferation *in vivo* against a cell-associated antigen in the presence or absence of CD4 T cell help. (A) Recipient mice were injected i.v. with CFSE labeled OT-I T cells. Twenty-four hours later, the mice received s.c. immunizations of $2.5x10^5$ UV-treated K42(WT CRT) cells expressing OVA mixed with 0, 1, 10 or 100 ng LPS. Proliferation was measured 4 days later in the dLN. PBS control is depicted in filled grey. Data are representative of 2-3 mice per treatment. (B) Quantification of OT-I T cell proliferation in response to UV, UV + 1-10 ng LPS and UV + 40 μg LPS treatments of antigen donor cells. Each point represents the average OT-I T cell proliferation from 2-6 mice (except for one experiment, which had 1 mouse in the PBS group) and is an independent experiment. Four independent experiments are represented; mice received $2.5\text{-}5x10^5$ antigen donor cells. Two experiments compared UV treatment of cells to UV + 1-10 ng LPS (unfilled and filled triangles), one experiment compared UV treatment of cells to UV + 40 μg LPS (unfilled squares), and one experiment contained all three conditions (unfilled circles). (C) Recipient mice were injected i.v. with CFSE labeled OT-I T cells alone or a 1:2 ratio of CFSE labeled OT-I T cells and unlabeled OT-II T cells (the same number of OT-I T cells were injected in both groups of mice). Twenty-four hours later, the mice received s.c. immunizations of $5x10^5$ UV-treated K42(WT CRT) cells expressing OVA mixed with 0 or 10 ng LPS (no LPS and + LPS, respectively). Proliferation was measured 4 days later in the dLN. PBS control is depicted in filled grey. Data are representative of 2-3 mice per treatment. Quantification of the percentage of proliferating OT-I T cells is depicted in the right panel; each circle represents the proliferation of OT-I T cells from an individual mouse. (D) Quantification of the percentage of OT-I T cells of all CD8 T cells recovered in *C*. Each circle represents the proliferation of OT-I T cells from an individual mouse. (C, D) One experiment was performed. A two-tailed pair-wise student t-test was used for statistical analysis. Mean ± s.e.m. are shown.

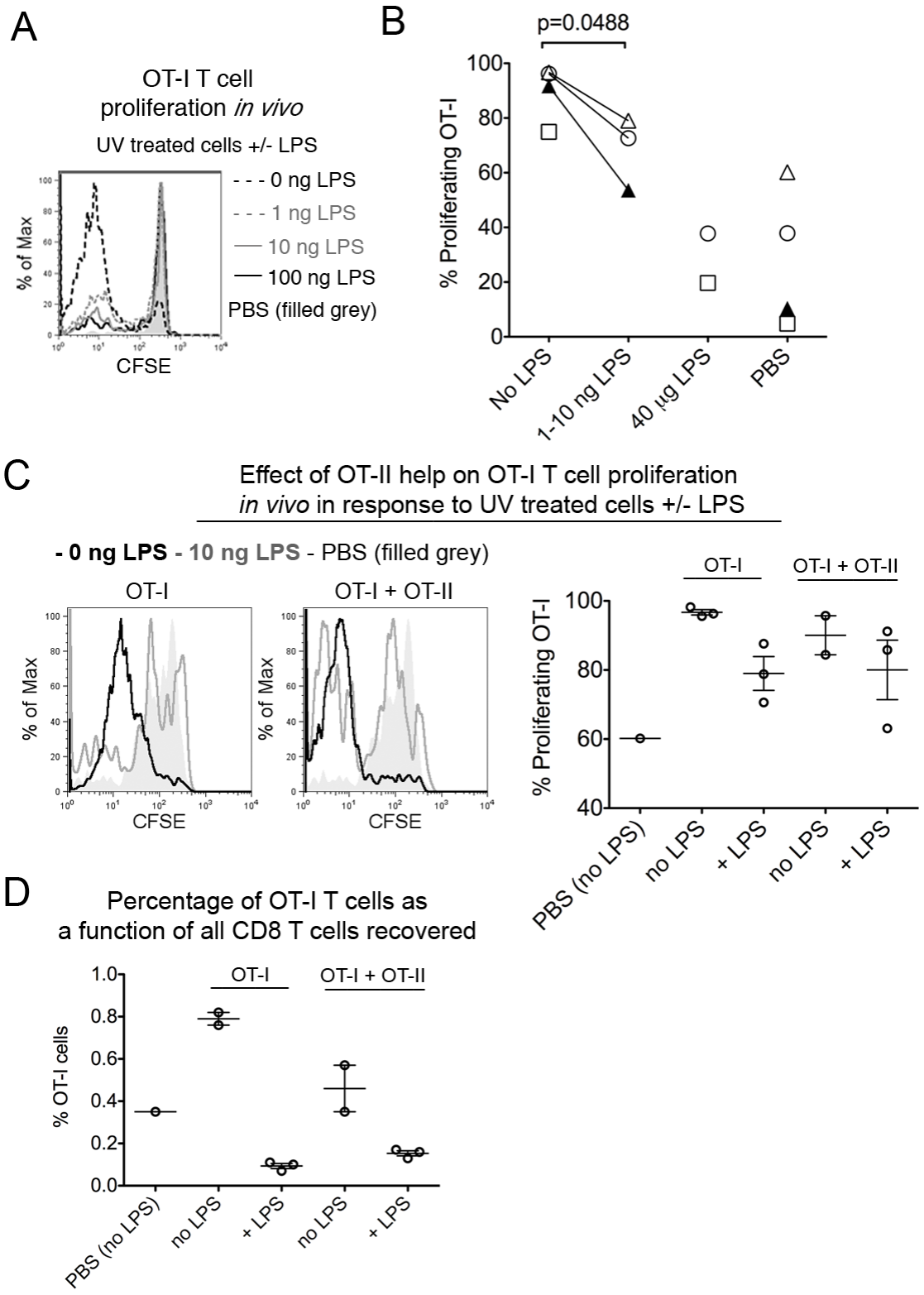
A
OT-I T cell
proliferation *in vivo*
UV treated cells +/- LPS
- - - 0 ng LPS
- - - 1 ng LPS
10 ng LPS
100 ng LPS
PBS (filled grey)
% of Max
CFSE
B
p=0.0488
% Proliferating OT-I
No LPS
1-10 ng LPS
40 μg LPS
PBS
C
Effect of OT-II help on OT-I T cell proliferation
in vivo in response to UV treated cells +/- LPS
- 0 ng LPS - **10 ng LPS** - PBS (filled grey)
OT-I
OT-I + OT-II
% of Max
CFSE
% Proliferating OT-I
PBS (no LPS)
no LPS
+ LPS
D
Percentage of OT-I T cells as
a function of all CD8 T cells recovered
% OT-I cells

Discussion

In this study, we set out to examine three different pathways by which calreticulin could have an impact on CD8 T cell proliferation. The first pathway involves the ability of extracellular, soluble calreticulin to enhance the cross-presentation of an associated antigen (Figure 3.1A). We imagine a scenario where calreticulin in complex with an antigen (pathogen derived or self) escapes a cell in response to calcium perturbations (Peters and Raghavan, 2011) or pathogen-induced cell lysis, thus gaining access to the extracellular environment. Using a Mϕ cell line as the APC, a previous study has shown that calreticulin enhances the cross-presentation of an associated peptide to a T cell line compared to the peptide alone (Basu et al., 2001). We were not able to replicate this finding using a different peptide and BMDC as the APC (Figure 3.2). This discrepancy maybe due to differences in peptide affinity for calreticulin. The polypeptide- and peptide-binding site of calreticulin and specificity of peptides that bind to CRT are poorly understood and defined. Hence, to bypass the need to identify a high affinity calreticulin-specific peptide, we generated a fusion protein containing calreticulin and OVA. We show that calreticulin was not able to enhance the cross-presentation of the fused OVA *in vitro* or *in vivo* (Figure 3.3). We concluded that calreticulin-specific receptors such as CD91 did not target calreticulin to sub-cellular compartments favorable for cross-presentation or that calreticulin receptors are absent on BMDC.

In the *in vivo* experiments, we injected the soluble antigens subcutaneously in the flanks of the recipient mice. It remains possible that CD91 expression is low on relevant APCs in the draining lymph node examined (inguinal lymph node). Peritoneal cells and the RAW264.7 Mϕ cell line express high levels of CD91 (Basu et al., 2001; Pawaria and Binder, 2011). The expression of CD91 enables peritoneal Mϕ and RAW264.7 cells to cross-present HSP-associated peptides to CD8 T cells by engaging the HSPs directly (Basu et al., 2001). Thus, if CD91 expression were low on APC residing in the inguinal lymph node, we would not expect calreticulin to enhance the cross-presentation of a fused antigen. Interestingly, gp96-chaperoned peptide is cross-presented with a higher efficiency compared to peptide alone or albumin-chaperoned peptide when administered intradermally in mice. In this study, 6 hours after the administration of antigen, axillary and inguinal draining lymph nodes were harvested, and CD11c+ cells were isolated for

an *in vitro* activation assay of B3Z cells (Binder and Srivastava, 2004). The ability of gp96 to efficiently chaperone the peptide was shown to be dependant on the CD91 receptor, indicating that it is possible that APCs in the inguinal lymph node express sufficient levels of CD91 to mediate HSP uptake and re-presentation. The caveat to the experiments is that the axillary and inguinal lymph nodes described above were mixed. Thus, the observed effect could have been due primarily to APCs in the axillary lymph node. Further studies are necessary to assess CD91 expression on the relevant cross-presenting APCs in the inguinal lymph node to better understand the results obtained in this study concerning the cross-presentation of soluble calreticulin associated OVA.

We hypothesized that calreticulin associated antigens are cross-presented efficiently because the antigens are targeted to APCs via calreticulin-specific receptors. However, it may be possible that calreticulin has a role in protecting unstable peptides or proteins from degradation *in vivo*. The protection would allow more time for the peptide or protein to be phagocytosed by an APC before it degrades. The relatively high stability of OVA may have rendered calreticulin non-critical for antigen stability in our study. It may also be possible that calreticulin enhances cross-presentation by altering the cytokine milieu. Calreticulin is reported to induce CD91 phosphorylation, which results in the activation of a number of NF-κB-dependent and –independent cytokines (Pawaria and Binder, 2011). However, if inflammatory cytokines were induced *in vivo* by calreticulin-CD91 interactions in response to the OVA-CRT immunization, the presence of the cytokines did not lead to greater CD8 T cell proliferation in response to OVA-CRT compared to OVA (Figure 3.3). However, the cytokines produced in response to the calreticulin-CD91 interaction may have a more significant role in shaping the T-helper response, as has been recently assessed (Pawaria and Binder, 2011). The T-helper response may in turn affect the CD8 T cell response. The impact of CD4 T cell help on CD8 T cell proliferation was untested in our study using soluble proteins.

OVA-CRT and OVA are taken up by BMDCs through pinocytosis or receptor-mediated endocytosis. Figure 3.3 indicates that either pinocytosis is dominant over receptor-mediated endocytosis, or that there exist other receptors that mediate the uptake of OVA which render calreticulin-specific receptors non-essential. The mannose receptor is reported to be critical for the phagocytosis and trafficking of glycosylated OVA to

early endosomes conducive for cross-presentation (Burgdorf et al., 2007). However, this model was called into question by findings demonstrating that steady state DC are able to cross-present glycosylated OVA independently of the mannose receptor (Segura et al., 2009). The latter finding was subsequently also refuted due to the non-physiologically high levels of antigen used in the study (Burgdorf et al., 2010). OVA used in Figure 3.3 is not expected to be taken up by the mannose receptor (as it is isolated from *E. coli* and non-glycosylated). However, we show that non-glycosylated OVA (*E. coli*) and glycosylated OVA (Sigma) induce similar levels of OT-I T cell proliferation *in vivo*. We used 2.5-100 μg OVA per mouse; this amount is well below the amount used to show a dependence on the mannose receptor *in vivo* (500 μg) (Burgdorf et al., 2010). Our data suggest that the mannose receptor is non-essential for the cross-presentation of soluble OVA *in vivo* in the context of a s.c. administration of antigen. Notably, OVA was injected i.v. in the studies described above (Burgdorf et al., 2010; Segura et al., 2009). Ours is the first study to examine the impact of glycosylation upon the cross-presentation of a soluble antigen. Taken together, Figure 3.3 and Figure 3.4 demonstrate that there are redundant receptor pathways for soluble antigen uptake that render calreticulin-specific receptors and the mannose receptor non-essential for the cross-presentation of calreticulin-OVA or OVA, respectively. However, a closer examination of mannose receptor expression on APCs in the inguinal lymph node is warranted.

It remains possible that the soluble OVA-CRT construct may not have been able to bind calreticulin-specific receptors with a high enough avidity to impact the cross-presentation of OVA. Alternatively, OVA may have masked the calreticulin-receptor binding site on calreticulin. To address this issue, CRT and OVA or OVA alone were conjugated to iron oxide beads and cross-presentation efficiencies were assessed. OVA and CRT are not fused in this system. Thus, CRT-receptor interactions should not be inhibited. We show that CRT was not able to enhance the cross-presentation of the bead-associated OVA compared to beads with OVA alone, both *in vitro* and *in vivo* (Figure 3.5). CRT has been reported to be an "eat me" signal on the surface of apoptotic cells (Gardai et al., 2005; Kuraishi et al., 2007). The findings of Figure 3.5 suggest that CRT does not work independently in a phagocytic context, but rather might work with one or more "eat me" signals such as PS. Hence, CRT in isolation is not sufficient to enhance

cross-presentation of a particulate antigen. However, it is also possible that phagocytic uptake of the iron oxide beads was instrinsically high in the absence of calreticulin, rendering calreticulin ineffective at uptake.

The second pathway we examined involves the ability of cell surface calreticulin to enhance the uptake of cell-associated antigens (calreticulin is an "eat-me" signal in this scenario; Figure 3.1B). Calreticulin is upregulated on apoptotic and pre-apoptotic cells (Gardai et al., 2005; Kuraishi et al., 2007; Obeid et al., 2007b) and has been identified as an "eat-me" signal (Gardai et al., 2005; Kuraishi et al., 2007; Peters and Raghavan, 2011). It is hypothesized that the pro-phagocytic property of calreticulin contributes towards the immunogenicity of tumor cells treated with cell-surface calreticulin inducing chemotherapeutic agents [reviewed in (Chaput et al., 2007; Martins et al., 2010)]. Ours is the first study to examine whether cell-surface calreticulin on antigen donor cells is able to quantitatively impact CD8 T cell proliferation. Increased CD8 T cell proliferation would be expected if surface-calreticulin positively impacted the phagocytosis of antigen donor cells by APC and phagocytic transfer were the dominant mode of antigen transfer to APCs. We show that even though thapsigargin-induced surface calreticulin plays a role in the phagocytosis of pre-apoptotic cells (Peters and Raghavan, 2011), enhanced phagocytosis does not influence the proliferation or cytotoxicity of CD8 T cells *in vitro* or *in vivo* in response to pre-apoptotic antigen donor MEFs treated with thapsigargin (Figure 3.7 and 3.8). Studies examining the immunogenicity of drug-treated tumor cells attribute immunogenicity to HMGB1 and ATP release from the tumor cells and to the phagocytic role of calreticulin [reviewed in (Kepp et al., 2011)]. Thapsigargin treated cells do not release either ATP or HMGB1 (Peters and Raghavan, 2011). Thus, it is possible that calreticulin-mediated phagocytosis of antigen donor cells in the absence of HMGB1 or ATP release does not have an effect on the immunogenicity of the antigen donor cells (CD8 T cell activation against cell-associated antigens), as previously suggested (Kepp et al., 2011). Additionally, uptake of apoptotic cells delivered s.c. is mediated by CD169+ Mϕ via uptake through PS on the apoptotic cell in draining lymph nodes (Asano et al., 2011). The cells we used were largely pre-apoptotic at the time of immunization, but became apoptotic 20 hours post treatment (Figure 3.6). It is thus possible that PS, and not calreticulin, mediated the uptake of the drug-treated antigen

donor cells as they progressed through apoptosis. The phagocytic kinetics of pre-apoptotic MEFs treated with thapsigargin are not characterized *in vivo*, but may warrant further studies. We conclude that enhanced calreticulin mediated uptake of antigen donor cells (Peters and Raghavan, 2011) is not sufficient to enhance the cross-priming of CD8 T cells in the context of thapsigargin drug treatment of antigen donor cells. As noted above, cytokines induced by calreticulin-mediated CD91 signaling (Pawaria and Binder, 2011) may impact the CD4 T cell response, which was not examined. The CD4 T cell response may in turn mediate the anti-tumor response observed against tumor cells treated with surface calreticulin-inducing chemotherapeutic drugs. Alternatively, the CD4 T cells may help in shaping an effective anti-tumor CD8 T cell response. Neither possibility was examined in this study, but both warrant further investigation.

Calreticulin helps facilitate endogenous assembly of MHC class I (Del Cid et al., 2010; Gao et al., 2002). Hence, the third pathway we examined by which calreticulin could impact CD8 T cell proliferation involved the cell-cell transfer of MHC class I molecules from antigen donor cell to APC (trogocytosis; Figure 3.1C). Increased transfer, and thus increased activation of CD8 T cells, is expected to be induced by calreticulin as calreticulin expressing cells express a higher level of surface MHC class I compared to calreticulin-deficient cells (Del Cid et al., 2010; Gao et al., 2002). Trogocytic transfer contributes to CD8 T cell proliferation in response to s.c. delivered dead cells (Dolan et al., 2006). Trogocytosis has also been shown to be important in activating memory CD8 T cells in a viral infection (Wakim and Bevan, 2011). Interestingly, the same study was not able to find a role for trogocytosis in the activation of naïve CD8 T cells. If trogocytic transfer were the dominant form of antigen transfer in our system, calreticulin-dependant phagocytosis might not significantly impact CD8 T cell proliferation (Figure 3.7 and 3.8). We show that trogocytic transfer (and/or activation by MEF and BMDC *in trans*) is the dominant form of antigen transfer *in vitro* (Figure 3.11). However, trogocytic transfer does not contribute to the proliferation of naïve CD8 T cells *in vivo* (Figure 3.12), consistent with published findings (Wakim and Bevan, 2011). We conclude that trogocytic transfer of antigen is not relevant for the proliferation of naïve CD8 T cells in response to s.c. delivered UV-treated cells. Additionally, trogocytic transfer can explain the non-essential role of calreticulin-mediated phagocytosis *in vitro* but not *in vivo*.

Interestingly, treatment of antigen donor cells with 5 μM thapsigargin inhibited CD8 T cell proliferation *in vivo* (Figure 3.8B), an unexpected finding. LPS treatment of antigen donor cells also inhibited CD8 T cell proliferation in a dose-dependant manner (Figure 3.13B). The secreted endogenous factor HMGB1, proposed to be a TLR4 ligand (Park et al., 2004), is suggested to contribute to the immunogenic cell death of drug-treated tumor cells (Apetoh et al., 2007). Additionally, TLR4-deficiency impairs the ability of chemotherapeutic drugs to induce immunogenic forms of cell death (Apetoh et al., 2007; Tesniere et al., 2010). Thus, it was surprising that LPS inhibited the cross-priming of CD8 T cells *in vivo* in response to cell-associated antigen. However, HMGB1 and LPS have different mechanisms for activating cells (Park et al., 2003; Park et al., 2004), which could explain the discrepancy of the effects of TLR4. APC are known to secrete immunosuppressive factors when exposed to a combination of apoptotic cells and LPS. The immunosuppressive factors are thought to be a mechanism to regulate inflammation and inflammatory cytokine production (Byrne and Reen, 2002). Monocytes stimulated with LPS secrete significantly more IL-10 and TFGβ in response to apoptotic neutrophils compared to unstimulated monocytes (Byrne and Reen, 2002). BMDC exposed to LPS-coated apoptotic cells secrete higher levels of TGF-β compared to BMDC exposed to uncoated apoptotic cells (Torchinsky et al., 2009). Hence, an immunoinhibitory cytokine milieu produced by APC in response to a combination of innate signaling [thapsigargin (Peters and Raghavan, 2011) or LPS] and dying antigen donor cells may have resulted in the inhibition of CD8 T cell proliferation (Figure 3.8 and 3.13). LPS-mediated inhibition of antigen-specific CD8 T cell proliferation appears to be unique to CD8 T cell responses against cell-associated antigen. First, we did not observe a significant decrease in CD8 T cell proliferation in response to soluble, bacterially derived recombinant OVA in WT mice compared to $TLR4^{-/-}$ mice (Figure 3.3). Inhibition would be expected in WT mice if LPS signaling negatively affected CD8 T cell responses against soluble antigen. Second, similar findings have been published using Poly(I:C) as the innate ligand (Frleta et al., 2009); Poly(I:C) inhibited the cross-priming of CD8 T cells against dead cell-associated antigens but not soluble antigen. In that study, CD4 T cell help was not able to rescue the observed inhibition of CD8 T cell proliferation, which is supported by data in our study (Figure 3.13C and 3.13D).

However, it is also possible that we observed the inhibition in CD8 T cell proliferation because the relevant APC became depleted *in vivo* in response to LPS (or 5 μM thapsigargin), as has been previously observed in response to i.v. LPS (Qiu et al., 2009). Alternatively, the relevant APC may have matured in response to the LPS prior to the arrival of the cell-associated antigen into the dLN. The maturation of APC would inhibit the cross-presentation of cell-associated antigen, as mature APC have a diminished capacity for phagocytosis compared to immature APCs. Delayed cross-presentation kinetics is observed when antigen donor cells are injected intradermally (i.d.) compared to intravenous (i.v.) injection (days vs. hours). Furthermore, the administration of Poly I:C one day after the injection of antigen donor cells inhibits cross-priming if the antigen donor cells are administered i.d. but enhances cross-priming if the antigen donor cells are administered i.v (Bouvier et al. 2011). In our study, it is possible that APCs in the dLN matured in response to the LPS before the arrival of antigen donor cells. However, apoptotic cells injected s.c. in the footpads of mice drain to the popliteal lymph nodes within hours (Asano et al., 2011). Further studies are needed to fully understand the kinetics of antigen-uptake of thapsigargin treated cells when administered s.c. in the flanks of mice (as was performed in our *in vivo* studies) and the mechanism of inhibition of CD8 T cell proliferation in response to cell-associated antigen in the presence of innate stimuli. Lastly, it is also possible that thapsigargin or LPS induced OT-I T cell proliferation earlier than on day 4 (proliferation was assessed on day 4) by activating relevant APCs. The OT-I T cell population may have expanded and contracted within 4 days. Indeed, the level of inflammation present influences the contraction of CD8 T cells (Badovinac et al., 2004). Thus, assessing CD8 T cell proliferation at earlier time points may help elucidate the effects of innate stimuli on CD8 T cell activation.

In summary, we have examined three pathways by which calreticulin could influence CD8 T cell responses against cell-associated antigen. First, we show that calreticulin-specific receptors are non-essential for the cross-presentation of a stable calreticulin-associated soluble antigen. Second, we show that thapsigargin induced surface calreticulin on antigen donor cells does not impact CD8 T cell proliferation. Third, the ability of calreticulin to facilitate surface MHC class I assembly on antigen donor cells leads to enhanced CD8 T cell proliferation *in vitro* (either due to activation *in*

trans or to trogocytic transfer of MHC class I-peptide complexes). However, MHC class I transfer does not have a role *in vivo* in activating naïve CD8 T cells. Finally, independent of calreticulin, LPS and high dose thapsigargin treatments of antigen donor cells inhibit CD8 T cell proliferation in response to cell-associated antigens. Further studies are needed to understand the mechanisms underlying this inhibition, which has relevance in understanding mechanisms of peripheral tolerance in the context of an infection or inflammatory setting.

Materials and Methods

Mice

C57BL/6J (WT or B6 in text; CD45.2), B6.SJL-*Ptprc*^{a} *Pepc*^{b}/BoyJ (WT or B6 in text; CD45.1), Balb/cJ (Balb/c in text), B6.129P2-*B2m*^{tm1Unc}/J [B6(β2m$^{-/-}$) or β2m$^{-/-}$ in text], C57BL/6-Tg(TcraTcrb)1100Mjb/J (OT-I in text), and C57BL/6-Tg(TcraTcrb)425Cbn/J (OT-II in text) mice were purchased from The Jackson Laboratory. OT-I transgenic mice were used directly (CD45.2) or bred with B6.SJL-Ptprca Pep3b/Boy mice (The Jackson Laboratory) to yield CD45.1 T cells. TLR2$^{-/-}$ and TLR4$^{-/-}$ mice (Hoshino et al., 1999; Takeuchi et al., 1999) were provided by Dr. S. Akira at the Laboratory of Host Defense, Osaka University, Osaka, Japan. TLR2/4$^{-/-}$ mice were generated by crossing TLR2$^{-/-}$ with TLR4$^{-/-}$ mice. TLR4$^{-/-}$ mice were backcrossed onto the B6 background six times before being bred with TLR2$^{-/-}$ mice. All mice were maintained in specific pathogen-free conditions at the University of Michigan or the University of Massachusetts Medical School mouse facilities. The mice were cared for according to the guidelines set by the University Committee on Use and Care of Animals (UCUCA). Recipient mice for *in vivo* experiments were used at 5 to 10 weeks of age.

Cell culture, purification and labeling

Cell lines

The B3Z hybridoma T cell line (Karttunen et al., 1992) and calreticulin-deficient MEF (K42), WT MEF (K41) and 3KO (H2-K^{b}, H2-D^{b} and β2m deficient) MEF cell lines (Gao et al., 2002; Lybarger et al., 2003; Mesaeli et al., 1999) were maintained in RPMI+ [RPMI medium 1640 (Invitrogen) supplemented with 10% (v/v) fetal bovine serum, 100 μg/ml streptomycin, and 100 units/ml penicillin (Invitrogen)]. L-cells were maintained in MEM (Invitrogen) supplemented with 10% (v/v) fetal bovine serum (Gibco), non-

essential amino acids, 1 mM sodium pyruvate, and 100 μg/ml streptomycin, 100 units/ml penicillin (Invitrogen). Cells were maintained in an incubator kept at 37 °C with 5% CO_2.

BMDC

DCs were generated from the bone marrow of B6, Balb/c or B6(β2m$^{-/-}$) mice. Bone marrow was flushed from the femur and tibia with RPMI+. The red blood cells were lysed using red cell lysis buffer (Sigma), and the cells were re-suspended in RPMI medium supplemented with 10% (v/v) fetal bovine serum (Gibco), 100 μg/ml streptomycin, 100 units/ml penicillin (Invitrogen), 1 mM HEPES (Gibco), 0.1 mM MEM Non-Essential Amino Acids (Gibco), 1 mM Sodium pyruvate, 50 μM β-mercaptoethanol and granulocyte Mϕ colony-stimulating factor (GM-CSF). The bone marrow obtained from one mouse was plated into two 24-well plates (Corning). The medium was replaced on days 2 and 4, and the cells were harvested for *in vitro* experiments on day 5 or 6.

BM Mϕ

Mϕ were generated from the bone marrow of B6 mice. Bone marrow was flushed from the femur and tibia with RPMI+. The red blood cells were lysed using red cell lysis buffer (Sigma), and the cells were resuspended in DMEM (Invitrogen) medium supplemented with 20% (v/v) fetal bovine serum (Gibco), 30% (v/v) L-cell conditioned medium, 100 μg/ml streptomycin, 100 units/ml penicillin (Invitrogen), 2 mM GlutaMAX (Gibco), and 50 μM β-mercaptoethanol. The bone marrow obtained from one mouse was plated into x5 150 mm plates. The medium was replaced on days 2, 4 and 6. On day 7, medium without L-cell conditioned medium was added and Mϕ were harvested for assays on day 8 with ice-cold PBS.

Purification of CD8+ and CD4+ T cells

Spleens were extracted from OT-I or OT-II transgenic mice. The red blood cells were lysed using red cell lysis buffer (Sigma), and the $CD8^+$ or $CD4^+$ cells were isolated by positive selection using anti-CD8a (Ly-2) or anti-CD4 (L3T4) microbeads (MACS, Miltenyi Biotec), respectively, following the manufacturer's suggested protocol.

CFSE labeling

MACS purified CD8+ T cells from OT-I transgenic mice were labeled with CFSE for proliferation analyses. CD8+ T cells were washed once with PBS, centrifuged, and re-suspended in PBS + 5 μM CFSE. The cells were incubated at 37 °C for 10 min. The cells

were washed once with medium, re-suspended in RPMI+ and incubated at 37 °C, 5% CO_2 for 1 hour. The cells were then centrifuged and re-suspended in an appropriate volume of RPMI+ for *in vitro* experiments or PBS for *in vivo* experiments. On average, 3-5x10^6 live, CFSE labeled, CD8+ OT-I T cells were recovered from one spleen, where trypan blue staining assessed viability.

PKH26 labeling

Splenocytes were labeled with PKH26 (Sigma) for *in vivo* cytoxicity analysis. Splenocytes were extracted from B6 CD45.1 mice. The red blood cells were lysed using red cell lysis buffer (Sigma). Splenocytes were washed in PBS and labeled with 2-4 μM PKH26 according to the manufacturer's instructions. After cells were washed, they were labeled with 1 or 0.1 μM CFSE as described above.

DNA constructs

Expression of calreticulin, OVA, and OVA-calreticulin in Escherichia coli

Mouse calreticulin (accession number BC003453) was amplified from the pCMV-SPORT6 (ATCC, MGC-6209) vector using primers that allowed for subsequent ligation-independent cloning (LIC) into the pMCSG7 vector (Stols et al., 2002). The following primers were used: forward, 5' TAC TTC CAA TCC AAT GCT GCC GCA CAT CCT TGG CTT 3' and reverse, 5' TTA TCC ACT TCC AAT GTT ACA GCT CAT CCT TGG CTT 3'. Underlined bases represent those that are complementary to the sequence encoding calreticulin, and additional 5' sequences were introduced for LIC.

Chicken egg OVA (accession number V00383) was amplified for LIC. The following primers were used: forward: 5' TAC TTC CAA TCC AAT GCT ATG GGC TCC ATC GGC G 3' and reverse, 5' TTA TCC ACT TCC AAT GTT AAG GGG AAA CAC ATC TGC 3'. Underlined bases represent those that are complementary to the sequence encoding OVA, and additional 5' sequences were introduced for LIC.

The OVA-calreticulin fusion protein was constructed using a 2-step amplification process resulting in a full length OVA molecule fused to the N-terminus of full length calreticulin by a flexible linker (gly-gly-ser-gly-gly). The reverse OVA primer was complementary to the forward calreticulin primer, allowing for the fusion of the two PCR products in a second PCR reaction. OVA was amplified using the following primers: 5' TAC TTC CAA TCC AAT GCT ATG GGC TCC ATC GGC G 3' and reverse, 5' *GGC*

AGG GTC TGC GGC **TCC TCC TGA TCC ACC** AGG GGA AAC ACA TCT 3'. Calreticulin was amplified using the following primers: forward, 5' AGA TGT GTT TCC CCT **GGT GGA TCA GGA GGA** *GCC GCA GAC CCT GCC* 3' and reverse, 5' TTA TCC ACT TCC AAT GTT *ACA GCT CAT CCT TGG CTT* 3'. Underlined bases represent those that are complementary to the sequence encoding OVA, bold bases represent the introduced linker sequences (gly-gly-ser-gly-gly), italicized bases represent those that are complementary to calreticulin, and additional sequences were introduced for LIC. Both PCR products were run on a 0.8% agarose gel and gel-purified (Qiagen). Both products were then used together as templates in a second PCR reaction using the forward OVA primer and reverse calreticulin primer, which allowed for subsequent LIC of the OVA-calreticulin fusion into the pMCSG7 vector.

LIC was performed to introduce calreticulin, OVA, and OVA-calreticulin sequences into the pMCSG7 vector as described in Chapter 2.

DNA constructs were sequenced and transformed into BL21 (DE3) cells for protein expression. All bacterially expressed constructs lacked their signal sequence and contained an N-terminal MHHHHHHSSGVDLGTENLYFGSNA fusion sequence for nickel affinity chromatography.

Cloning WT calreticulin into pMSCV-puro

This was performed as described in Chapter 2.

pMSCV-IRES-GFP encoding OVA

The pMSCV-IRES-GFP retroviral vector was created as previously described (Van Parijs et al., 1999) and was modified to express OVA upstream of the IRES-GFP reporter. Briefly, OVA contains a secretion signal sequence beginning at amino acid 21 and ending at residue 47 (Robinson et al., 1986). Linker primers (5' OVA BglII-del 50 and 3' OVA EcoRI) were designed to truncate the amino terminus and delete the secretion signal sequence from OVA as well as introduce an in-frame start codon at amino acid position 50 of the protein. Linker primers were engineered with BglII and EcoRI sites for cloning the truncated OVA into pMSCV-IRES-GFP upstream of the IRES-GFP reporter. Resultant clones from ligation of OVA into pMSCV-IRES-GFP were confirmed through DNA sequencing.

Linker Primer sequences:

5’ OVA BglII-del 50: 5’-GGAGATCTACCATGCAGGACACAGATAAATAAGG-3’

3’ OVA EcoRI: 5’-GCGAATTCTTAAGGGGAAACACATCTGCCAAA-3’

Protein purification

OVA, and OVA-calreticulin were all purified as previously described for calreticulin in Chapter 2. Gel-filtration analyses were performed as described in Chapter 2. Extinction coefficients were calculated from the protein amino acid sequence using ProtParam (www.expasy.ch) and are as follows (units are M^{-1} cm^{-1}): OVA, 33,265; OVA-calreticulin, 114,750.

Generation of calreticulin-peptide and BSA-peptide complexes

10 μM calreticulin or BSA were incubated with 10 or 100 μM peptide (QLESIINFEKLTE-FITC; University of Michigan Protein Structure Facility) for 1 hour at 50 °C. Free peptide was removed by centrifugal filter (Centricon-30, Millipore). Peptide bound to calreticulin or BSA was measured using a VICTOR plate reader (fluorimeter; PerkinElmer) against a peptide standard.

OVA and OVA-CRT allophycocyanin conjugation

Allophycocyanin was conjugated to OVA and OVA-CRT following manufacturer’s instructions at a 1:1 molar ratio (Lightning-Link Conjugation Kit, Innova Biosciences). To measure fluorescence intensity, OVA and OVA-CRT were separated by SDS-PAGE and fluorescence was measured using a fluorescence imager (Typhoon TRIO, GE Healthcare). Quantification was performed using ImageQuant5.2 software.

Generation of retroviral supernatants and infections

This was performed as described in Chapter 2.

Flow Cytometry

OVA and OVA-CRT binding to BMDC

$1x10^5$ BMDC were incubated with 1.3 μg OVA-CRT or 0.6 μg OVA that were allophycocyanin labeled in a total reaction volume of 100 μl for 30 minutes on ice. Cells were washed twice with flow cytometry buffer and analyzed by flow cytometry.

Detection of cell-surface calreticulin and MHC class I

The presence of cell-surface calreticulin was analyzed and performed as previously described (Jeffery et al., 2010; Peters and Raghavan, 2011). The staining of surface MHC

class I was carried out as described in Chapter 2. In addition, an allophycocyanin labeled anti-mouse H2-K^b-SIINFEKL Ab (1:300, eBioscience) was used in this study.

Detection of proliferating OT-I T cells

dLN (inguinal) were harvested; a single cell suspension was obtained and plated in a 96-well plate. Cells were lysed in red cell lysis buffer (Sigma). These cells were washed once with flow cytometry buffer (2% FBS in PBS) and then incubated for 10 min with unconjugated murine IgG (Jackson ImmunoResearch) to bind and block F_c receptors. Cells from draining lymph nodes or from *in vitro* cell cultures were stained with a rat anti-mouse CD8a Ab conjugated to allophycocyanin (BD Pharmingen, 1:400) or anti-CD8a Ab conjugated to PerCP (eBioscience) and mouse anti-mouse CD45.1 or CD45.2 Ab conjugated to PE or allophycocyanin for *in vivo* experiments (BD Pharmingen, 1:300 and eBioscience). Either CD45.1 or CD45.2 OT-I mice were utilized for *in vivo* adoptive transfers into WT strains (CD45.2 or CD45.1, respectively); the appropriate antibody was used to discriminate between donor and recipient cells. The cells were incubated with the Ab for 20 min, washed twice with flow cytometry buffer and then analyzed by flow cytometry. CFSE labeled OT-I T cells were analyzed in the FITC channel. All centrifugations in the 96-well plate were performed for 1 minute at 2,000 rpm.

Detection of PKH26 labeled target splenocytes

Spleens were harvested and processed as described for dLN above. Cells were stained with anti-CD45.1 conjugated to allophycocyanin as described for dLN above. PKH26 labeling was analyzed in the PE channel.

Phagocytosis assay

K42(WT CRT) and K42($CRT^{-/-}$) cells were labeled with CellTracker™ Green CMFDA (5-chloromethylfluorescein diacetate) according to the manufacturer's instructions (Invitrogen). Cells were harvested with PBS + 5 mM EDTA and $2x10^5$ cells were plated per well in a 96-well plate in RPMI+. The plate was exposed to a UV light box for 3 min and incubated at 37 °C for 17 hours. $1x10^5$ B6 BMDC were added to the wells, incubated at 37 °C or on ice and then harvested at various time points with PBS + 5 mM EDTA. Samples were fixed with 1% formaldehyde for 7 min at room temperature at various indicated time points. Once the last time point was collected and fixed, cells were washed with flow cytometry buffer. Cells were incubated with a hamster anti-mouse CD11c Ab

conjugated to allophycocyanin (BD Pharmingen, 1:400) for 20 min on ice, washed 2 times with flow cytometry buffer and then analyzed by flow cytometry.
All samples were read on the FACSCanto flow cytometer (BD Biosciences). Analysis was performed using FlowJo 8.8.6 (Treestar Inc.).

***In vitro* antigen cross-presentation assays**

Assays using peptide antigen

3-5x10^4 BMDC and 2-3x10^4 B3Z cells were plated in a 96 well plate. Calreticulin-peptide complexes, BSA-peptide complexes, or peptide alone were added to the wells. At 24 hours, supernatant IL-2 levels were measured by ELISA.

Assays using soluble or bead-associated antigen

4-5x10^5 BMDC were plated in a 96 well plate. Soluble proteins were then added to the wells. The cells were incubated at 37 °C for 3 hours. BMDC were fixed with 1% formaldehyde for 7 min at room temperature. The wells were then washed two times with 200 μl PBS and once with RPMI+. Medium was aspirated from the wells, and a suspension of 4-5x10^5 B3Z or 1-3x10^5 CFSE labeled OT-I T cells in 250 μl RPMI+ was added to the wells. At 24 hours, supernatant IL-2 levels were measured by ELISA, and proliferation of OT-I T cells was measured at 72 hours by flow cytometry. OVA (Sigma) was obtained from Sigma (A5503).

Assays using cell-associated antigen

Target cell fibroblasts expressing OVA were either exposed to UV-irradiation or treated with thapsigargin. For thapsigargin treatments, cells in 10 cm plates were incubated with 7 ml of 200 nM or 5 μM thapsigargin in RPMI+ for 5 hours. The cells were washed 3 times with 7 ml PBS and harvested with PBS + 5 mM EDTA. Untreated or thapsigargin-treated cells were plated in a 96-well plate. Apoptosis was induced in the untreated cells by exposing the 96-well plate to UV on a UV-box for 3 min. 2x10^5 BMDC and 0.4-0.7x10^5 CFSE labeled OT-I T cells were added to the wells immediately after the treatments. For assays with MACS-purified cells, target cells were incubated with BMDC in the 96-well plate at 37 °C for 1 hour. The cells were then harvested with 5 mM EDTA + PBS and CD11c+ cells were isolated by positive selection using anti-CD11c Ab according to the manufacturer's instructions (MACS, Miltenyi Biotec). 0.7x10^5 CD11c+ cells were incubated with 0.4-0.7x10^5 CFSE labeled OT-I T cells. The OT-I T cells were

analyzed by flow cytometry on day 5 post incubation. At 24 hours, supernatant IL-2 levels were measured by ELISA. Where indicated, IFNγ was measured on day 5 by ELISA.

***In vivo* antigen cross-presentation assays using OT-I T cells**

CD8+ OT-I T cells were MACS purified from CD45.1 or CD45.2 mice and transferred i.v. into CD45.2 or CD45.1 recipient mice, respectively. Where indicated, unlabeled OT-II CD4+ T cells were co-administered with OT-I T cells. One day later, mice were immunized s.c. in either the left or right flank with the indicated concentration/number of soluble or cell-associated antigen in 100 μL PBS. Three to four days later, dLN (inguinal) were harvested and analyzed as described above. For cell-associated antigen immunizations, UV-irradiated or thapsigargin-treated cells (as described above) were harvested immediately after treatment with 5 mM EDTA + PBS. Cells were washed 3 times with PBS and counted. The indicated numbers of target cells were re-suspended in 100 μl PBS (LPS was added where indicated) and used for the immunizations.

***In vivo* cytotoxicity of endogenous CD8 T cells**

WT mice were immunized s.c. in the right flank with the indicated number of antigen donor cells in 100 μL PBS. Seven days post-immunization, mice were injected i.v. with PKH26 (Sigma) labeled target cells pulsed with SIINFEKL (1 μM CFSE labeled cells) or VAYGRQVYL (0.1 μM CFSE labeled cells). Spleens were recovered 18 hours later to assess killing of target cells by flow cytometry. dLN were also recovered and incubated with SIINFEKL. IFNγ was measured 48 hours later by ELISA.

ELISA

IL-2 and IFNγ

96-well plates were coated with purified anti-mouse IL-2 Ab (BD Pharmingen, catalog # 554424) or anti-mouse IFNγ Ab (BD Pharmingen, catalog # 551216) overnight at room temperature. After blocking with 10% calf serum for 3 hours, cell culture supernatants were incubated in the plate for 1 hour at 37 °C. The plates were washed 3 times with 0.05% Tween-20 in PBS and a biotinylated anti-mouse IL-2 Ab (BD Pharmingen, catalog # 554426) or anti-mouse IFNγ Ab (BD Pharmingen, catalog # 554410) was added for an overnight incubation at room temperature. The plates were washed 3 times, and

streptavidin conjugated to HRP (BD Pharmingen, catalog # 554066) was added to the plates for 20 min at room temperature. The plates were again washed 3 times, and the assay was developed using a TMB substrate reagent set (BD OptEIA, catalog # 555214).

Chapter 4

Conclusions

The studies undertaken in this thesis explored the role of calreticulin in the context of MHC class I assembly and cross-presentation. In Chapter 2, we examined specific interactions required for calreticulin recruitment into the MHC class I PLC. We also documented the effects of calreticulin deficiency on MHC class I heavy chain and tapasin stability. In Chapter 3, we examined roles of calreticulin in the cross-priming of CD8 T cell responses against peptide, soluble, bead-associated, and cell-associated antigen. Data from both chapters further our understanding of MHC class I assembly and antigen presentation.

Interactions between calreticulin and components of the PLC

In Chapter 2, calreticulin was shown to require ERp57 and glycan based interactions for recruitment into the PLC and stabilization of the PLC. We proposed a model for calreticulin recruitment into the PLC that involves glycan- and ERp57-based interactions, where the glycan-based interaction is mediated at least in part by the glycan of tapasin (Figure 2.13). Our study reinforced the proposed model for calreticulin recruitment into the PLC involving glycan- and ERp57-based interactions (Dong et al., 2009) and demonstrated critical roles for the glycan and ERp57 binding sites in the formation of the PLC. However, in our model, the glycan of tapasin rather than that of the MHC class I heavy chain impacted the recruitment of calreticulin into the PLC (Dong et al., 2009). Our study enabled us to put forth a new model for interactions that mediate MHC class I assembly in the PLC (Figure 2.13).

When components of the PLC (tapasin, calreticulin, ERp57, and MHC class I) were reconstituted *in vitro,* calreticulin–glycan and calreticulin–Erp57 based interactions were found to be crucial for tapasin-mediated peptide loading onto MHC class I, and MHC class I glycans were suggested to be important for the functional effects of

calreticulin (Wearsch et al., 2011). Soluble MHC class I purified from baculovirus-infected insect cell lysates was used in these assays. However, the glycosylation status of MHC class I was not directly tested. The same glycan-binding mutant of calreticulin used in our study (Y92A) and a mutant of ERp57 that is deficient in calreticulin binding were used in the assay. A model for PLC assembly was proposed that involved the formation of a calreticulin–MHC class I complex independent of the PLC, via glycan-based interactions. The calreticulin–MHC class I complex was suggested to be subsequently recruited into the PLC via calreticulin–Erp57 mediated interactions. The model for calreticulin-mediated MHC class I recruitment into the PLC is partially based on results utilizing a transient siRNA transfection to knock-down β2m in cells. Upon siRNA knock down of β2m, calreticulin and MHC class I decreased their association with TAP as a function of time, whereas tapasin did not (Wearsch et al., 2011). The dissociation of calreticulin from TAP suggested that calreticulin is not recruited into the PLC in the absence of MHC class I heterodimers. We have similarly reported that calreticulin is not recruited into the PLC in β2m-deficient cells (Figure 2.9). However, calreticulin and β2m (but not MHC class I heavy chains) *are* recruited into the PLC in cells that lack heavy chain expression and in cells that express a deglycosylated MHC class I heavy chain, although with a lower efficiency than cells expressing wild-type heavy chains (Rizvi et al., 2011). Hence, the siRNA knock down of β2m may negatively affect the recruitment of MHC class I heavy chains and calreticulin into the PLC independently, as β2m expression and recruitment into the PLC (but not MHC class I heavy chain) facilitates calreticulin recruitment into the PLC. Further studies are needed to fully understand the sequence of events that result in the formation of the PLC. One of the most interesting questions our study raises is: what is the role of MHC class I heavy chain independent recruitment of β2m into the PLC? Understanding the interactions within the proposed (Figure 2.13) PLC intermediate (consisting of TAP, tapasin, ERp57, calreticulin and β2m) and the role of this intermediate may help in elucidating the mechanism by which the PLC facilitates the generation and export of stable MHC class I molecules to the cell surface.

The effects of calreticulin deficiency on tapasin stability and PLC assembly are quite striking. Within the PLC, the MHC class I heterodimer was previously the only recognized substrate for calreticulin. Calreticulin is proposed to bind MHC class I via glycan-based interactions, and in the absence of calreticulin, MHC class I steady state levels are reduced [(Figure 2.3C) and reviewed in (Wearsch and Cresswell, 2008)]. In this thesis, we have shown that calreticulin also preferentially interacts with glycosylated rather than deglycosylated tapasin in cells (Figure 2.7D). Additionally, similar to MHC class I, steady-state levels of tapasin are substantially diminished in cells that lack calreticulin or that express a glycan binding deficient mutant of calreticulin (Figure 2.7B, tapasin lysates). Thus, as tapasin is highly dependant on calreticulin for its stability, we propose that tapasin is a second substrate of calreticulin within the PLC, a novel role for calreticulin. Additionally, in contrast to the previous model that newly synthesized MHC class I molecules can bind to TAP in calreticulin-deficient cells (Gao et al., 2002), our data suggest that MHC class I recruitment into the PLC is strongly impaired in calreticulin deficient cells (Figure 2.3C and 2.7C). Thus, calreticulin is key to the overall stability of the PLC.

Role of the calreticulin P domain in substrate binding

In Chapter 2, we assessed the interactions that mediated calreticulin recruitment into the PLC. To demonstrate the critical role of the ERp57 binding site of calreticulin, two constructs were examined: mCRT(ΔP) and mCRT(W244A). The entire P domain of calreticulin is removed in mCRT(ΔP) and a single residue in calreticulin critical for calreticulin binding to ERp57 is mutated in mCRT(W244A). Calreticulin binding to ERp57 is strongly reduced with both constructs (Figures 2.2N and 2.2D). However, there are notable differences between cells expressing mCRT(ΔP) and mCRT(W244A). In anti-TAP immunoprecipitations, mCRT(ΔP) co-immunoprecipitation is not detected whereas mCRT(W244A) is detected, albeit at a lower level than mCRT(WT) (Figure 2.3C compared to 2.7C). Surface MHC class I induction appears lower in cells expressing mCRT(ΔP) compared to mCRT(W244A) as well. The fold increase of surface MHC class I in cells expression mCRT(ΔP) compared to mCRT($CRT^{-/-}$) is close to 1 whereas the fold increase is closer to 1.5 in cells expressing mCRT(W244A) (Figure 2.3A compared to 2.7A). Additionally, the level of surface MHC class I induction in cells

expressing the calreticulin double mutant deficient in glycan and ERp57 binding mCRT(Y92A/W244A) is lower than the induction in cells expressing mCRT(W244A), suggesting that the mCRT(W244A) mutant is not entirely impaired for MHC class I assembly (Figure 2.7A). Taken together, the enhanced activity of mCRT(W244A) compared to mCRT(ΔP) suggests that in addition to recruiting ERp57 into the PLC, the P domain of calreticulin may have another role within the MHC class I assembly complex.

Whereas mCRT(W244A) displayed enhanced aggregation suppression activity against a polypeptide substrate compared to mCRT(WT), the data with mCRT(ΔP) were variable (Figure 2.11). Additionally, the P domains of calnexin and calreticulin facilitate suppression of aggregation of polypeptide substrates (Brockmeier et al., 2009; Pocanschi et al., 2011), supporting the hypothesis that the calreticulin P domain may have a role in polypeptide-based substrate binding within the PLC, a role independent of ERp57 recruitment. Calreticulin binds ERp57 via residues in the b' domain of ERp57 (Russell et al., 2004) (Figure 4.1). Based on data in Chapter 2, we hypothesized that calreticulin also interacts with the glycan of tapasin. However, docking of calreticulin onto the solved crystal structure of ERp57-tapasin revealed that calreticulin could not simultaneously bind both the glycan of tapasin and the b' domain of ERp57. Thus, association of calreticulin with the glycan and ERp57 of the tapasin-ERp57 complex may be sequential rather than simultaneous. MHC class I molecules are preferentially recruited to the ERp57 associated form of tapasin (Rizvi et al., 2011). A number of orientations of calreticulin relative to tapasin-ERp57 were possible. This is further compounded by the possibility of multiple relative orientations of the globular domain of calreticulin relative to its P domain. Further studies are needed to understand how calreticulin and MHC class I are oriented upon the tapasin-ERp57 complex. It is likely that the P domain has a role in tethering together this complex. Based on the finding that MHC class I-deficient cells recruit β2m into an intermediate PLC (Rizvi et al., 2011), it is possible that the P domain interacts with the β2m component of MHC class I heterodimers. Further studies are needed to better understand modes of PLC construction. We propose a model in which the flexible P domain wraps around a substrate during calreticulin interaction with the PLC, and that the P domain interaction with β2m is important for the stabilization of PLC intermediates consisting of TAP, ERp57, tapasin, β2m and calreticulin. The P domain

may also wrap around MHC class I heterodimers upon their recruitment, which could have a small, but significant role in the overall stability of the PLC.

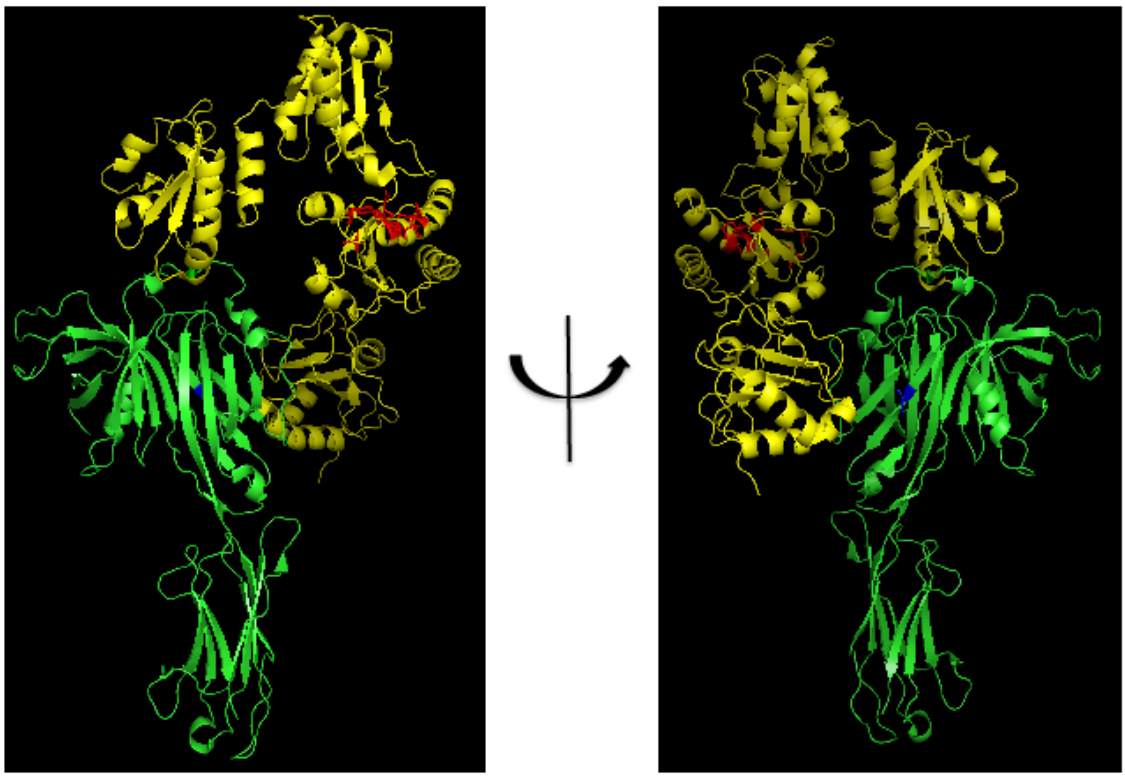

Figure 4.1. Tapasin-ERp57 crystal structure and depiction of calreticulin binding site on ERp57. A. Crystal structure of ERp57 (yellow) and tapasin (green) (PDB ID 3F8U) (Dong et al., 2009). Residues in ERp57 that mediate calreticulin binding are depicted in red (Russell et al., 2004). Asn233, the glycosylation site in tapasin, is depicted in blue. Docking of calreticulin onto this structure reveals that calreticulin cannot simultaneously contact its ERp57 binding site (red) and the glycan of tapasin (blue). Thus, we predict that interactions involving calreticulin binding the glycan of tapasin and the tapasin-associated ERp57 must involve distinct steps of PLC formation. MHC class I molecules are predominantly recruited to the ERp57 associated form of tapasin, and how calreticulin orients itself in this complex remains to be further elucidated. Docking of calreticulin was performed by Sanjeeva J. Wijeyesakere.

Role for the acidic domain in the ER retention of calreticulin

Expression of mCRT(ΔC) resulted in the secretion of calreticulin from cells (Figure2.5). The mCRT(ΔC) construct contained the KDEL retrieval motif of full length calreticulin, suggesting that the KDEL motif is not sufficient for the ER localization of calreticulin, consistent with published findings (Sonnichsen et al., 1994). Interestingly, a KDEL retrieval motif was insufficient to prevent the secretion of IL-6 from human hepatoma cells (Rose-John et al., 1993). However, appending the 14 C-terminal residues (including KDEL) of PDI to the C-terminus of cytosolic IL-6 resulted in complete ER retention. Notably, there was a string of 5 acidic amino acids in the sequence appended to IL-6. The ability of the acidic residues of PDI to aid in the retention of IL-6 suggests that ER retention mediated by acidic residues may not be unique to calreticulin. Indeed, the removal of the KDEL motif from PDI does not drastically affect the ER retention of PDI (Mazzarella et al., 1990). A matrix of interactions between ER proteins mediated by acidic residues is suggested to retain soluble proteins in the ER (Sonnichsen et al., 1994).

Higher order plants express two distinct families of calreticulin isoforms: a calreticulin1/calreticulin2 group and a calreticulin3 group (Persson et al., 2003). Calreticulin1 and calreticulin2 isoforms share a higher sequence homology with each other compared to calreticulin3. All three isoforms are upregulated in response to ER stress. Notably, the C terminal domains of calreticulin1 and calreticulin2 contain a large number of acidic residues, suggesting these isoforms have a role in ER calcium homeostasis. However, the C terminal domain calreituclin3 contains a high number of positively charged residues. The globular and P domains of all three isoforms are not significantly different. Recently, calreticulin3, UGGT and a putative HDEL retrieval receptor ERD2b were implicated in the quality control of EFR, a plant innate immune receptor (Li et al., 2009). The gene that encodes ERD2b is a homolog of the (H/K)DEL receptor in yeast, ERD2. The second homolog for ERD2 in *Arabidopsis*, ERD2a, has been shown to function as an ER retrieval receptor in yeast expressing a non-functional mutant of ERD2 (Lee et al., 1993). However, ERD2b had not previously been assessed for its function as an ER retrieval receptor. Calreticulin1 and calreticulin2 played a small role in quality control, but could not substitute for calreticulin3 in the folding of EFR. Interestingly, mutations in ERD2b affect ER retention of calreticulin3 but not of

calreticulin1 or calreticulin2. It is surprising that ER retention of calreticulin1 and calreticulin2 are not affected by mutations in ERD2b, as both isoforms also express a HDEL retrieval motif similar to calreticulin3. We speculate that in addition to the HDEL retrieval motif, the acidic domains of calreticulin1 and calreticulin2 play a role in the ER retention of these two isoforms of calreticulin either directly or via interactions with factors distinct from ERD2b. However, as the C domain of calreticulin3 is positively charged, calreticulin3 is dependant on HDEL receptor mediated retrieval for its ER localization. Thus, data accumulated in the literature as well as our data (Figure 2.5) all point to a poorly described novel mechanism for the ER retention of soluble ER proteins that contain positively charged residues in their C terminus. This mode of retention likely functions cooperatively with (K/H)DEL retrieval mechanisms, ensuring the proper ER localization of the protein.

Although substrate binding may be highly redundant between the three isoforms of plant calreticulin, the C domain has been shown to play a crucial role in ER quality control mediated by calreticulin towards some substrates. As mentioned above, calreticulin3, but not calreticulin1 or calreticulin2, was able to chaperone EFR, a plant innate immune receptor (Li et al., 2009). In another study of *Arabidopsis*, calreticulin2 was shown to be a regulator of a different component of plant innate immunity (Qiu et al., 2012). In a third study, calreticulin3, but not calreticulin1 or calreticulin2 was shown to mediate the retention of a mutant surface receptor (Jin et al., 2009). Additionally, swapping the acidic C domain of calreticulin1 for the positively charged C domain of calreticulin3 enabled calreticulin1 to retain the mutant receptor. Calreticulin3 with the C domain of calreticulin1 lost its ability to mediate retention. Thus, the C domain of calreticulin3 was crucial in conferring substrate specificity (Jin et al., 2009). The different substrate specificities of the plant calreticulin isoforms suggest that the C terminal domain of calreticulin is able to influence calreticulin targeting to specific substrates.

Substrate specificities of calnexin and calreticulin

Different substrates display varying dependence on calreticulin or calnexin (Molinari et al., 2004). The molecular basis for these differences is incompletely understood since both proteins have identical glycan binding specificities and similar ERp57 interacting characteristics. One factor that is suggested to influence substrate

specificity is the topological environment of calnexin and calreticulin. A calreticulin construct engineered to contain a transmembrane domain was shown to associate with substrates with a pattern that matched the pattern seen for calnexin. Conversely, a soluble version of calnexin associated with substrates that were normally calreticulin-associated (Danilczyk et al., 2000). However, soluble calnexin was not able to induce MHC class I assembly in calreticulin deficient cells [data not shown and (Gao et al., 2002)], suggesting that the membrane bound constraint of calnexin is not the only factor that inhibits the ability of calnexin to mediate PLC assembly. However, the soluble calnexin construct used in Gao et al. 2002 partially truncates the P domain of calnexin. Thus, the finding that soluble calnexin was not able to induce MHC class I assembly needs to be re-examined in the context of a correct soluble calnexin construct. The length of the calreticulin P domain is shorter than the calnexin P domain (Figure 4.2). If one role of the P domain is to encompass a substrate bound to calreticulin or calnexin, having a longer or shorter P domain could drastically alter substrate specificities. Finally, although calnexin has a C terminal acidic domain, it is located in the cytosol. The luminal location of the calreticulin acidic domain may determine calreticulin substrate specificity in a manner similar to that observed for different plant calreticulin isoforms.

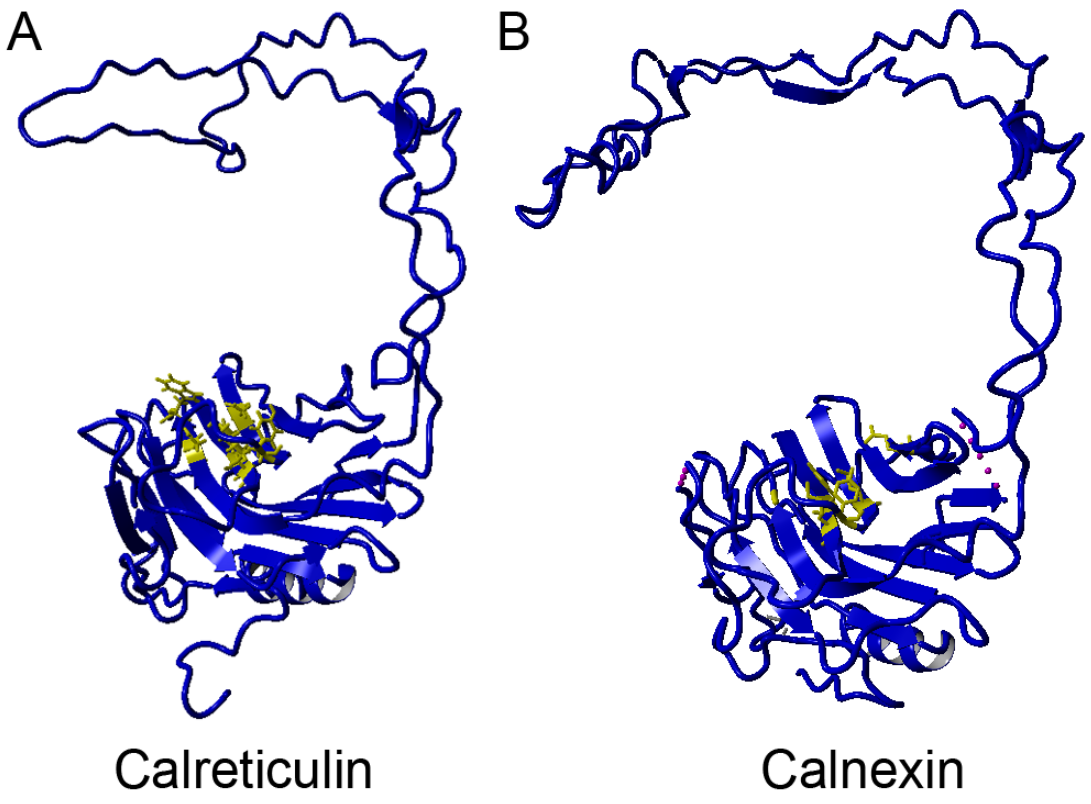

Figure 4.2. Structural models of calreticulin and calnexin. A. Model of calreticulin (described in Figure 1.6). B. Crystal structure of the luminal domains of calnexin (PDB ID IJHN) (Schrag et al., 2001). Putative glycan-binging residues of calreticulin and calnexin are depicted in yellow. The longer P domain of calnexin, the luminal location of the acidic domain of calreticulin, or the presence of a transmembrane domain in calnexin may account for the differing substrate specificities of the two proteins.

A role for calreticulin in MHC class I quality control outside the PLC

The calreticulin mutants generated in this thesis provide insight into functions of calreticulin outside the PLC. Calreticulin lacking the KDEL motif [mCRT(ΔKDEL)] was recently shown to be both recruited into the PLC and secreted from cells (Howe et al., 2009). Additionally, mCRT(ΔKDEL) did not restore surface expression of MHC class I at a level induced by mCRT(WT) (Howe et al., 2009). Reduced surface expression of MHC class I was attributed to a novel role for calreticulin in MHC class I assembly that is independent of the PLC. Calreticulin was shown to have a role in the retrieval of sub-optimally loaded MHC class I molecules from the golgi back to the ER. In this thesis, we show that mCRT(ΔC) is recruited into the PLC (Figure 2.3C). However, cells expressing

mCRT(ΔC) have low levels of surface MHC class I (Figure 2.3A) and are unable to reduce the acquisition rate of EndoH resistance by MHC class I heavy chains to levels seen in cells expressing mCRT(WT) (data not shown). The phenotype of mCRT(ΔC) is likely due to the inability of mCRT(ΔC) to retrieve sub-optimally folded MHC class I molecules from the golgi, as mCRT(ΔC) itself is defective in being retained in the ER [(Figure 2.5) and (Sonnichsen et al., 1994)]. Hence, we provide further evidence for a secondary role for calreticulin outside of PLC formation and related to retrieval of MHC class I molecules from post-ER compartments.

Although the mode of the calreticulin-MHC class I interaction relevant for retrieval was only speculated upon in Howe et al. (2009), data from our group suggest that glycan based interactions are relevant. In Chapter 2, we showed that cells expressing glycan binding-deficient mutants of calreticulin [mCRT(Y92A) or mCRT(W302A)] did not rescue MHC class I surface expression to levels in cells expressing mCRT(WT) (Figure 2.7 and 2.8). Both mutants of calreticulin displayed enhanced *in vitro* aggregation suppression activities of a polypeptide substrate (Figure 2.11). Additionally, mCRT(W302A) was unable to reduce the rate of EndoH resistance acquisition by MHC class I heavy chains when expressed in calreticulin deficient cells (Jeffery et al., 2010). However, a calreticulin mutant deficient in suppressing the aggregation of a polypeptide substrate *in vitro* [mCRT(L139A)] was able to restore surface levels of MHC class I and reduce the acquisition rate of EndoH resistance by MHC class I heavy chains to the same level as cells expressing mCRT(WT) (Jeffery et al., 2010).

We speculate that under steady state conditions, the glycan binding site of calreticulin is involved two aspects of MHC class I heavy chain quality control. The first is recruitment of calreticulin into the PLC for stabilization of tapasin and MHC class I. The second is the retrieval of MHC class I molecules loaded with sub-optimal peptides from the golgi into the ER. This retrieval is mediated via the KDEL motif of calreticulin (Howe et al., 2009). Although tapasin has been dubbed the "peptide editor" of the PLC [reviewed in (Peaper and Cresswell, 2008)], our data blur the lines of whether or not calreticulin could also be included in that category. Tapasin displaces low affinity peptides bound to the MHC class I peptide binding groove and facilitates the exchange for high affinity peptides (Howarth et al., 2004). Tapasin is also believed to have the

ability to detect the presence of empty MHC class I heterodimers or those loaded with sub-optimal peptides and prevent the export of these unstable MHC class I molecules from the ER. Calreticulin has not been shown to displace peptides within the MHC class I peptide binding groove, but calreticulin does slow the rate of transport of MHC class I molecules out of the ER and prevents the export of MHC class I molecules loaded with sub-optimal peptides. Thus, calreticulin and tapasin may have redundant roles, with both being important in maintaining complete quality control of MHC class I assembly. Additionally, the redundant roles may be spatially distinct – ER retention of MHC class I molecules by tapasin and golgi retrieval of MHC class I molecules by calreticulin.

Insights into the calreticulin/calnexin cycle

ERp57, an oxidoreductase that is a member of the PDI family, aids in the folding of nascent proteins. However, unlike other members of the PDI family, ERp57 shows a preference for glycoprotein substrates [reviewed in (Rutkevich and Williams, 2011)]. This preference is thought to be due to the ability of ERp57 to interact with the P domain of calreticulin and calnexin, both of which contain binding sites for glycoprotein substrates. Inhibiting the formation of monoglucosylated glycoproteins in cells reduced the ability of ERp57 to aid in the isomerization of some, but not all, of its substrates. Some ERp57 substrates are not dependant on the calreticulin/calnexin cycle (Jessop et al., 2007). In our proposed model for calreticulin recruitment into the PLC, calreticulin recruits ERp57 to its substrate (tapasin) by first binding to tapasin via glycan-based interactions [(Figure 2.13) and (Rizvi et al., 2011)]. This model was partially based on our observation of reduced ERp57 recruitment to TAP/tapasin in calreticulin deficient cells (data now shown). Hence, to our knowledge, ours is the first study to demonstrate the unique requirement for calreticulin for ERp57 binding to a known ERp57 substrate, tapasin. Although calnexin also contains a glycan-binding site similar to calreticulin, calnexin expression is not sufficient to recruit ERp57 to tapasin in calreticulin deficient cells (data not shown).

Our studies also open the possibility of other requirements for the efficient folding of glycoprotein substrates by calreticulin and ERp57. A PLC intermediate containing TAP, tapasin, ERp57, calreticulin and β2m is detected in cells devoid of detectable MHC class I heavy chain (Rizvi et al., 2011). Additionally, calreticulin and ERp57 recruitment

into the PLC are undetectable and reduced, respectively, in β2m-/- cells (Figure 2.9). The impaired recruitment of calreticulin and ERp57 suggest that β2m is necessary to stabilize the tapasin-ERp57-calreticulin complex. Hence, it is possible that polypeptide based binding between calreticulin and β2m contribute to stability of the sub-complex of the PLC.

Relevance of aggregation assays as a measure of polypeptide binding by calreticulin

Aggregation assays were used to measure polypeptide binding by calreticulin in Chapter 2. In these assays, calcium depletion of calreticulin dramatically enhances activity (Figure 2.10), and correspondingly calcium depletion induces calreticulin oligomerization [Figure 2.2D and (Rizvi et al., 2004)]. Under physiological non-stress conditions however calreticulin is largely monomeric (Rizvi et al., 2004). Thus, it is possible that aggregation assays reflect the use of polypeptide binding sites of calreticulin that are stress-induced rather than constitutive. Further studies are needed to understand locations and functions of polypeptide binding sites of calreticulin under non-stress conditions.

Immune implications of calcium depletion induced secretion of calreticulin

It is interesting that calreticulin and PDI are also secreted in response to ER calcium depletion (Peters and Raghavan, 2011), a finding that also indicates calcium sensitivity of ER retention. The secretion of specific ER proteins in response to forms of ER stress that induce calcium perturbations in the ER may be one mechanism of immune marking cells under ER stress. For example, cell-surface calreticulin appears to be a marker for the phagocytic uptake of viable cells under conditions of ER stress mediated by perturbations in ER calcium (Peters and Raghavan, 2011). The clearance of cells under ER stress may be one mechanism of suppressing steady-state levels of inflammation, as ER stress induction in cells results in the secretion of factors that induce ER stress, activation and secretion of IL-6 in Mϕ (Mahadevan et al., 2011).

As mCRT(ΔC) is secreted under steady-state conditions, it would be interesting to ask whether mCRT(ΔC) is expressed on the cell surface. Such analyses would indicate whether surface receptor(s) for calreticulin are present on the cell-surface during steady-state conditions. Additionally, if mCRT(ΔC) is partially localized on the surface of cells under steady-state conditions, the phagocytic uptake of cells expressing mCRT(WT

CRT) or mCRT(ΔC) can be compared to determine whether calreticulin, independent of any other apoptotic-associated pro-phagocytic markers, is sufficient to mediate the uptake of cells. The calreticulin "eat me" signal could be countered by "don't eat me" signals on viable cells (such as CD47) (Gardai et al., 2005). However, it is also possible that surface levels and/or clustering of CD47 are altered on cells, following ER stress induction. Future directions may include investigating the role of surface calreticulin in the context of ER stress. Based on our current knowledge about the pro-phagocytic role of cell-surface calreticulin (Gardai et al., 2005; Kuraishi et al., 2007; Obeid et al., 2007b; Peters and Raghavan, 2011) and ER stress associated inflammation (Mahadevan et al., 2011), we hypothesize that calreticulin upregulation on the surface of cells under ER stress mediates the removal of the cells to suppress ER stress associated inflammation.

Effect of thapsigargin and LPS treatments on the cross-presentation of cell-associated antigen

In Chapter 3, we examined the role that calreticulin plays in the cross-presentation of associated antigen. We showed that calreticulin does not enhance the cross-presentation of a fused or bead-associated antigen. Additionally, enhancement in phagocytic uptake of cells treated with thapsigargin that is partially dependant on calreticulin does not translate to induced cross-priming of CD8 T cell responses against cell-associated antigen. CD8 T cells proliferated and were activated to similar levels in response to antigen derived from wild-type or calreticulin-deficient thapsigargin treated cells. Although we did not find a positive role for calreticulin in the various cross-presentation models examined, our work contributes to the understanding of various aspects of CD8 T cell activation driven by cell-derived antigen.

We have previously shown that conditioned media from MEFs treated with thapsigargin induces sterile IL-6 production and synergizes with LPS to induce a greater secretion of IL-1β and IL-12p70 in BMDC (Peters and Raghavan, 2011). Consistent with the hypothesis that MEFs treated with thapsigargin are activating towards APCs (Mahadevan et al., 2011; Peters and Raghavan, 2011), we find greater OT-I T cell proliferation induced by OVA-expressing thapsigargin-treated MEFs compared to UV treatment of MEFs (Figure 3.7C compared to 3.11B, upper panel). Furthermore, compared to mice immunized with OVA-expressing UV-treated MEFs, mice immunized

with OVA-expressing MEFs treated with 200 nM thapsigargin generally induced higher numbers of OT-I T cells in the draining lymph node (Figure 4.1). Enhanced OT-I T cell numbers were independent of calreticulin expression in the antigen donor cell. Madadevan et al. (2011) argue that pro-inflammatory cytokines produced by Mϕ in response to unknown secreted factors from ER-stressed cells support tumor growth and metastasis, as tumor growth and metastasis are supported by an inflammatory environment [reviewed in (Grivennikov et al., 2010)]. However, enhanced immunogenicity of tumor cells is observed upon treatment of tumor cells with thapsigargin and cisplatin compared to cisplatin alone (Tesniere et al., 2010). Hence, although thapsigargin may induce ER stress (and thus inflammation), under certain contexts the inflammatory consequences of thapsigargin treatment could be exploited to induce a more potent anti-tumor immune response.

It is important to note that the immunostimulatory effect of the conditioned media on BMDC in our prior studies was attributed to the release of thapsigargin sequestered in the membrane of treated cells into the conditioned media, as direct treatment of BMDC with thapsigargin induced secretion of a similar profile of inflammatory cytokines (Peters and Raghavan, 2011). Interestingly, immunizing mice with 5 μM thapsigargin treated cells inhibited the proliferation of antigen-specific CD8 T cell responses against cell-associated antigen (Figure 3.8B). The inhibition was to a level similar to that induced by LPS treatment of antigen donor cells (Figure 3.13B). The time at which APCs are stimulated with adjuvant (before or after encountering antigen donor cells) can drastically affect CD8 T cell responses against cell-associated antigen (Bouvier et al., 2011). If an APC matures prior to encountering cell-associated antigen, cross-presentation of the cell-associated antigen will be extremely inefficient. On the other hand, if APC maturation occurs after the uptake of cell-associated antigen, cross-presentation of the cell associated antigen will be enhanced. In our experiments, it is possible that excess drug released by K42 cells treated with 5 μM thapsigargin reached the dLN prior to the antigen donor cells, thus promoting a pro-inflammatory response but simultaneously inhibiting cross-presentation via inhibition of antigen uptake.

Our data support a model in which cross-presentation of cell-associated is slightly enhanced if APCs encounter antigen donor cells and activating signals at the same time.

First, 200 nM thapsigargin treatment of cells does not enhance the proliferation of OT-I T cells against cell-associated antigen compared to the UV-treatment of cells (Figure 4.3A). However, thapsigargin treatment of antigen donor cells did appear to have slightly enhanced the percentage of OT-I T cells recovered (Figure 4.3B). If drug was not secreted to a level necessary to activate APCs before the arrival of treated MEFs, the APC would encounter residual drug or secreted factors that induce activation upon the arrival or phagocytosis of the antigen donor cells. Second, thapsigargin treatment of cells with either 5 μM or 200 nM thapsigargin greatly enhanced the cross-presentation of cell-associated antigen *in vitro* compared to UV treatment of cells (Figure 3.7C compared to 3.11B, and data not shown). In this assay, BMDCs have instant access to antigen donor cells. However, it is possible that BMDCs respond differently than the relevant APC *in vivo*.

We found that LPS induced inhibition of CD8 T cell responses against cell-associated antigen, even at low doses (Figure 3.13B). Whereas the thapsigargin treated cells were washed multiple times before injection, the LPS was added to the cells directly prior to injection. Thus, LPS was free to drain with the PBS to the dLN. It is likely that the LPS matured the APC before the arrival of the MEFs. Thus, even low levels of LPS were able to inhibit proliferation, as the antigen donor cells did not sequester LPS. These findings are extremely relevant for the generation of cell-based vaccines. Adjuvants have the ability to enhance CD8 T cell responses against cell-associated antigen, but the timing of their delivery and the timing of the arrival of cell-associated antigen into the draining lymph node need to be considered. This is especially important since the draining of cells to dLN is highly dependent on mode of antigen delivery (Bouvier et al., 2011).

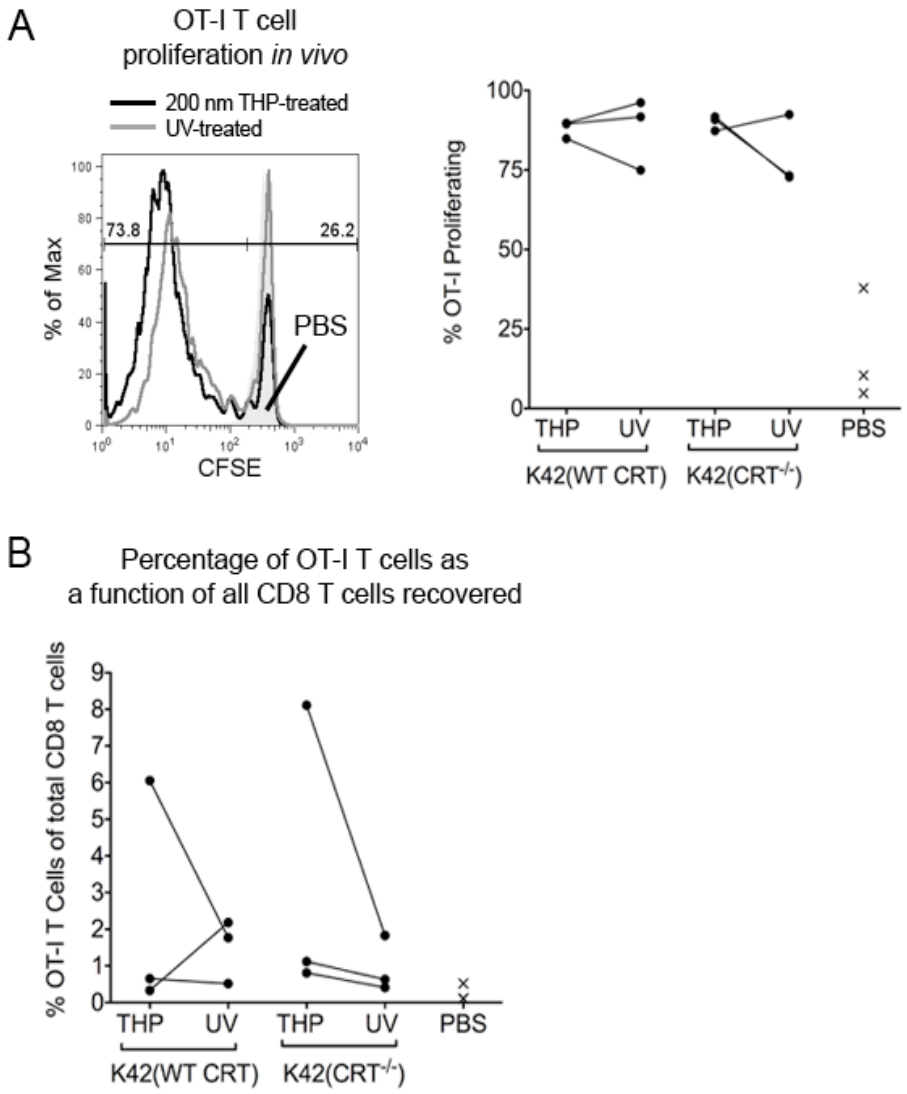

Figure 4.3. Compared to UV treatment of MEFs, thapsigargin treatment of MEFs may induce greater recovery of OT-I T cells. Recipient mice were injected i.v. with CFSE labeled OT-I T cells. Twenty-four hours later, the mice received PBS, 2.5-5x10^5 THP-treated or UV-treated K42(WT CRT) and K42($CRT^{-/-}$) OVA expressing cells s.c. (A) Proliferation was measured 4 days later in the dLN (inguinal). Left panel: The control immunization with PBS is depicted in filled grey. Data are representative of 2-3 mice per group. Right panel: Quantification of proliferating OT-I T cells. Each point represents the average OT-I T cell proliferation from 2-3 mice and is an independent experiment. Three independent experiments are represented. (B) The percentage of OT-I T cells as a function of all CD8 T cells recovered is depicted. Each point represents the average OT-I T cell proliferation from 2-3 mice and is an independent experiment.

Roles for calreticulin in inducing immunogenicity of dying cells

Although surface calreticulin mediates the uptake of thapsigargin treated cells by BMDC *in vitro* (Peters and Raghavan, 2011), we did not observe enhanced activation of CD8 T cell responses against OVA-expressing K42(WT CRT) cells compared to K42($CRT^{-/-}$) cells *in vitro* or *in vivo* (Figure 3.7 and 3.8). It possible that calreticulin in isolation of other danger signals is not sufficient to impact CD8 T cell proliferation. The laboratories of Kroemer and Zitvogel have proposed that HMGB1 and ATP release, and induction of surface calreticulin on drug-treated cells are necessary for immunogenicity of antigen donor cells [reviewed in (Kepp et al., 2011)]. The idea that all three are required for immunogenicity is partially supported by another group. The laboratory of Agostinis has recently shown that tumor cells treated with photodynamic therapy, which induces reactive oxygen species mediated ER stress, are as immunogenic as mitoxantrone treated cells (Garg et al., 2012). Mitoxantrone, an anthralcylin, has been suggested by Kroemer's group to be immunogenic due to its ability to induce surface calreticulin on tumor cells and induce the secretion of ATP and HMGB1 (Apetoh et al., 2007; Ghiringhelli et al., 2009; Obeid et al., 2007b). Garg et al. (2012) show that photodynamic therapy of tumor cells induces ATP secretion and surface calreticulin on tumor cells. HMGB1 secretion and the requirement for calreticulin for immunogenicity were not assessed in the study. Thus, in Chapter 3, calreticulin mediated phagocytosis may have not translated to an enhanced CD8 T cell response, as neither ATP nor HMGB1 are secreted from thapsigargin treated cells (Peters and Raghavan, 2011).

The proposed roles of HMGB1 and ATP in tumor cell immunogenicity are for pro-IL-1β synthesis and NLRP3 inflammasone activation to mediate IL-1β secretion, respectively [reviewed in (Kepp et al., 2011)]. The proposed role of surface calreticulin is to mediate uptake of tumor cells. As calreticulin is upregulated prior to PS in response to anthracyclins, it was suggested that calreticulin-mediated uptake of tumor cells may induce differential processing of antigen donor cells compared to PS-mediated uptake [reviewed in (Kepp et al., 2011)]. It is possible that the high innate stimulating activity of thapsigargin-treated cells [(Peters and Raghavan, 2011) and Figure 4.3 may have masked potentiating activities of calreticulin. It is possible that with certain drug treatments, calreticulin, HMGB1 or ATP are not necessary for immunogenicity, as APC can become

directly activated in response to residual drug or via factors secreted from drug treated tumor cells under ER stress (Mahadevan et al., 2011; Peters and Raghavan, 2011). As thapsigargin may have masked potentiating influences of calreticulin, it is important to examine high activity drug treatments or effects of other cell surface calreticulin-inducing drug treatments upon T cell activation.

Calreticulin-mediated uptake may be more crucial for drug treatments that do not directly activate APCs or in an immunosuppressive environment typical of tumor cells. However, as drug treated cells will eventually upregulate PS, why is calreticulin-mediated uptake so crucial for immunogenicity? As mentioned above (Kepp et al., 2011), it has been suggested that while PS-mediated uptake may induce "silent" removal of the apoptotic cells, calreticulin may induce an immunogenic uptake of cells. This hypothesis has not yet been proven. Ours is the first study to directly test this concept, but clearly more studies are needed in other drug treatment contexts for more a more complete understanding of how calreticulin contributes to tumor cell immunogenicity. Assessing the trafficking of cells and stability of cell-associated antigen within an APC after PS- or calreticulin-mediated uptake is crucial in further understanding why surface calreticulin is immunogenic. PS-mediated uptake by APC traffics cell-associated antigen to lysosomes, which degrade antigen quickly (Peng and Elkon, 2011). It is possible that calreticulin-mediated uptake traffics cell-associated antigen to early endosomes, which are conducive for cross-presentation (Burgdorf et al., 2007).

Impacts of trogocytic transfer on CD8 T cell proliferation

It may be important to note that chemotherapeutic drugs that induce cell surface calreticulin on tumor cells may have secondary impacts on MHC class I presentation that can affect CD8 T cell activation. Reduced levels of calreticulin in the PLC lead to the reduced steady-state levels of tapasin and MHC class I and reduced levels of surface MHC class I (Figure 2.3 and 2.7). Accordingly, while thapsigargin treatment induces cell-surface calreticulin, cell-surface MHC class I is diminished (Jeffery et al., 2010). Hence, the trogocytic transfer of MHC class I molecules from drug-treated cells to APC is expected to be reduced as well. Although we did not find a role for trogocytic transfer in the proliferation of naïve of CD8 T cells, such transfer may have a much more significant role in the proliferation of memory CD8 T cells (Wakim and Bevan, 2011).

Studies examining the role of surface calreticulin in the immunogenicity of tumor cells focus on a mouse model in which naïve anti-tumor CD8 T cells are generated (Obeid et al., 2007b). However, memory CD8+ T cells generated against established tumors are likely to exist in human patients with solid tumors. The expansion of anti-tumor memory CD8 T cells may be partially dependant on trogocytic transfer of MHC class I molecules from drug-treated tumor cells. However, if drug-treated tumor cells express diminished levels of cell surface MHC class I, the expansion of memory CD8 T cell may be compromised. Examining the ability of drug-treated tumor cells to activate naïve *and* memory CD8 T cells is then of further interest, as relevant modes of antigen transfer may differ between the two sets of CD8 T cells.

Modes of antigen transfer relevant to cross-presentation

Our data indicate that mannose receptor-mediated uptake is not critical for the cross-presentation of soluble OVA, as discussed in Chapter 3. A number of other endocytic receptors have also been implicated in the cross-presentation of antigen. LOX-1, SREC-I, and SR-A have all been suggested to mediate uptake and cross-presentation of HSP-associated antigens (Berwin et al., 2004; Berwin et al., 2003; Delneste, 2004). In terms of mechanism, the C-type lectin receptor DC-SIGN is shown to traffic antigen to early endosomes, which were favorable for cross-presentation (Tacken et al., 2011). Notably, receptors that mediate uptake of antigen may become downregulated on activated APCs. For example, another C-type lectin receptor, CLEC9A, expressed on human DCs mediates uptake and cross-presentation of antigen. However, expression of the receptor is reduced after DC maturation induced by TLR ligands (Schreibelt et al., 2012). As calreticulin is non-essential for the cross-presentation of fused and bead-associated OVA (Figure 3.4 and 3.5), there is likely a high level of redundancy in the receptors that mediate uptake and cross-presentation of soluble or particulate antigen. However, APC maturation may induce a loss of receptor redundancy. Upon the down-regulation or internalization of redundant receptors, receptors that remain on the cell surface could become crucial for cross-presentation.

Nevertheless, the uptake of antigen may is not the only factor that determines the fate of an exogenous antigen. Peptidoglycan (PGN) is a ligand for the nucleotide-binding

oligomerization domain-like (Nod-like) receptors. Nod-like receptors are cytosol localized innate immune receptors that can induce NF-κb activation. Although DCs exposed to LPS and PGN phagocytose antigen donor cells to similar levels, PGN inhibits the cross-presentation of cell-associated antigen whereas LPS does not inhibit cross-presentation (Wagner and Cresswell, 2012). It is worth noting that a conventionally derived source of LPS inhibited cross-presentation, whereas cross-presentation was not inhibited by highly purified LPS. It is possible that contaminants were present in the LPS that we used in our cross-presentation assay, which could have inhibited cross-presentation in a manner independent of LPS. Nonetheless, a network of signals enables an APC to successfully cross-present and prime naïve and memory CD8 T cells. Phagocytic/endocytic receptors and innate signaling may drastically change depending on the environment and antigen source (soluble vs. cell-associated). Understanding the impacts that each have on cross-presentation is crucial if cross-presentation is to be harnessed for vaccine design or for the treatment of established tumors.

We found trogocytic transfer of antigen to be relevant *in vitro* but not *in vivo* for inducing the proliferation of naïve CD8 T cells in response to cell-associated antigen (Figure 3.11 and 3.12). Trogocytic transfer may be relevant for expanding memory CD8 T cells, but not naïve CD8 T cells (Wakim and Bevan, 2011). However, we found that naïve OT-I T cells were activated primarily by trogocytic transfer of antigen *in vitro* (Figure 3.11). Thus, it is possible that naïve CD8 T cells could be activated via trogocytic transfer of antigen onto APCS under certain conditions *in vivo*. The APCs that phagocytose antigen may not have a role in directly activating CD8 T cells. Rather, a secondary APC subset could acquire MHC class I-peptide complexes from APCs that cross-presented antigen. The secondary APC subset could be the relevant subset that primes naïve CD8 T cells (Qu et al., 2009). In this scenario, trogocytic transfer of antigen from one APC subset to another mediates activation of CD8 T cells. In our *in vivo* model, it is possible that APCs capable of acquiring MHC class I-peptide complexes were not present in the dLN or did not have access to antigen, thus rendering trogocytic transfer undetectable (Figure 3.12).

APCs relevant for cross-presentation

As discussed in Chapters 1 and 3, if specific receptor mediated uptake is crucial for the cross-presentation of certain antigens, elucidating relevant APC subset *in vivo* is vital. Receptor expression, antigen processing capacity and lymph node localization of APCs can drastically affect the ability of an APC to cross-prime CD8 T cells. A number of studies have been undertaken to identify relevant cross-presenting APCs *in vivo* in a number of different dLNs (Asano et al., 2011; del Rio et al., 2007; Desch et al., 2011). We have not yet investigated which APC subsets are relevant for uptake and presentation of pre-apoptotic cell derived antigen following subcutaneous immunizations. Thus, we used BMDC for *in vitro* cross-presentation assays, which limited our ability to accurately assess the role of calreticulin in the cross-presentation of antigen *in vitro*. For *in vitro* assays, it may be more relevant to immunize mice and use dLN to activate CD8 T cells *ex vivo*. dLN from immunized mice can also be re-stimulated *in vitro* with relevant antigens to assess memory responses (Figure 3.8D). Although these alternatives may not allow for complete cellular and molecular dissection of antigen presentation events *in vitro,* they may offer more physiologically relevant insights into processes relevant to priming of CD8 T cells by cell-associated antigens.

In summary, the work described in this thesis led to the development of a novel model for PLC formation and elucidated novel roles for calreticulin in MHC class assembly. This work also contributed to a better understanding of general cellular processes including mechanisms of ER retention and the calnexin/calreticulin chaperone cycle. We also assessed factors that influence CD8 T cell proliferation, including calreticulin, innate signaling, and antigen transfer. Although this work contributes towards a better understanding about how calreticulin functions in a cell, more research is needed to better understand the immunogenic role of calreticulin.

Bibliography

Amigorena, S., and A. Savina. 2010. Intracellular mechanisms of antigen cross presentation in dendritic cells. *Curr Opin Immunol* 22:109-117.

Apetoh, L., F. Ghiringhelli, A. Tesniere, M. Obeid, C. Ortiz, A. Criollo, G. Mignot, M.C. Maiuri, E. Ullrich, P. Saulnier, H. Yang, S. Amigorena, B. Ryffel, F.J. Barrat, P. Saftig, F. Levi, R. Lidereau, C. Nogues, J.P. Mira, A. Chompret, V. Joulin, F. Clavel-Chapelon, J. Bourhis, F. Andre, S. Delaloge, T. Tursz, G. Kroemer, and L. Zitvogel. 2007. Toll-like receptor 4-dependent contribution of the immune system to anticancer chemotherapy and radiotherapy. *Nat Med* 13:1050-1059.

Asano, K., A. Nabeyama, Y. Miyake, C.H. Qiu, A. Kurita, M. Tomura, O. Kanagawa, S. Fujii, and M. Tanaka. 2011. CD169-positive macrophages dominate antitumor immunity by crosspresenting dead cell-associated antigens. *Immunity* 34:85-95.

Badovinac, V.P., B.B. Porter, and J.T. Harty. 2004. CD8+ T cell contraction is controlled by early inflammation. *Nat Immunol* 5:809-817.

Bangia, N., P.J. Lehner, E.A. Hughes, M. Surman, and P. Cresswell. 1999. The N-terminal region of tapasin is required to stabilize the MHC class I loading complex. *Eur J Immunol* 29:1858-1870.

Barnden, M.J., J. Allison, W.R. Heath, and F.R. Carbone. 1998. Defective TCR expression in transgenic mice constructed using cDNA-based alpha- and beta-chain genes under the control of heterologous regulatory elements. *Immunol Cell Biol* 76:34-40.

Basu, S., R.J. Binder, T. Ramalingam, and P.K. Srivastava. 2001. CD91 is a common receptor for heat shock proteins gp96, hsp90, hsp70, and calreticulin. *Immunity* 14:303-313.

Basu, S., and P.K. Srivastava. 1999. Calreticulin, a peptide-binding chaperone of the endoplasmic reticulum, elicits tumor- and peptide-specific immunity. *J Exp Med* 189:797-802.

Belicha-Villanueva, A., S. McEvoy, K. Cycon, S. Ferrone, S.O. Gollnick, and N. Bangia. 2008. Differential contribution of TAP and tapasin to HLA class I antigen expression. *Immunology* 124:112-120.

Berwin, B., Y. Delneste, R.V. Lovingood, S.R. Post, and S.V. Pizzo. 2004. SREC-I, a type F scavenger receptor, is an endocytic receptor for calreticulin. *J Biol Chem* 279:51250-51257.

Berwin, B., J.P. Hart, S. Rice, C. Gass, S.V. Pizzo, S.R. Post, and C.V. Nicchitta. 2003. Scavenger receptor-A mediates gp96/GRP94 and calreticulin internalization by antigen-presenting cells. *EMBO J* 22:6127-6136.

Binder, R.J., and P.K. Srivastava. 2004. Essential role of CD91 in re-presentation of gp96-chaperoned peptides. *Proc Natl Acad Sci U S A* 101:6128-6133.

Binder, R.J., and P.K. Srivastava. 2005. Peptides chaperoned by heat-shock proteins are a necessary and sufficient source of antigen in the cross-priming of CD8+ T cells. *Nat Immunol* 6:593-599.

Bjorkman, P.J., M.A. Saper, B. Samraoui, W.S. Bennett, J.L. Strominger, and D.C. Wiley. 1987. Structure of the human class I histocompatibility antigen, HLA-A2. *Nature* 329:506-512.

Blander, J.M., and R. Medzhitov. 2006. Toll-dependent selection of microbial antigens for presentation by dendritic cells. *Nature* 440:808-812.

Bouvier, I., H. Jusforgues-Saklani, A. Lim, F. Lemaitre, B. Lemercier, C. Auriau, M. Nicola, S.. Leroy, H.K. Law, A. Bandiera, J.J. Moon, P. Bouso, and M.L. Albert. 2011. Immunization route dictates cross-priming efficiency and impacts the optimal timing of adjuvant delivery. *Front Immun* 2:1-18.

Bratton, D.L., V.A. Fadok, D.A. Richter, J.M. Kailey, L.A. Guthrie, and P.M. Henson. 1997. Appearance of phosphatidylserine on apoptotic cells requires calcium-mediated nonspecific flip-flop and is enhanced by loss of the aminophospholipid translocase. *J Biol Chem* 272:26159-26165.

Brockmeier, A., U. Brockmeier, and D.B. Williams. 2009. Distinct contributions of the lectin and arm domains of calnexin to its molecular chaperone function. *J Biol Chem* 284:3433-3444.

Burgdorf, S., A. Kautz, V. Bohnert, P.A. Knolle, and C. Kurts. 2007. Distinct pathways of antigen uptake and intracellular routing in CD4 and CD8 T cell activation. *Science* 316:612-616.

Burgdorf, S., and C. Kurts. 2008. Endocytosis mechanisms and the cell biology of antigen presentation. *Curr Opin Immunol* 20:89-95.

Burgdorf, S., V. Lukacs-Kornek, and C. Kurts. 2006. The mannose receptor mediates uptake of soluble but not of cell-associated antigen for cross-presentation. *J Immunol* 176:6770-6776.

Burgdorf, S., C. Scholz, A. Kautz, R. Tampe, and C. Kurts. 2008. Spatial and mechanistic separation of cross-presentation and endogenous antigen presentation. *Nat Immunol* 9:558-566.

Burgdorf, S., V. Schuette, V. Semmling, K. Hochheiser, V. Lukacs-Kornek, P.A. Knolle, and C. Kurts. 2010. Steady-state cross-presentation of OVA is mannose receptor-dependent but inhibitable by collagen fragments. *Proc Natl Acad Sci U S A* 107:E48-49; author reply E50-41.

Byrne, A., and D.J. Reen. 2002. Lipopolysaccharide induces rapid production of IL-10 by monocytes in the presence of apoptotic neutrophils. *J Immunol* 168:1968-1977.

Chaput, N., S. De Botton, M. Obeid, L. Apetoh, F. Ghiringhelli, T. Panaretakis, C. Flament, L. Zitvogel, and G. Kroemer. 2007. Molecular determinants of immunogenic cell death: surface exposure of calreticulin makes the difference. *J Mol Med* 85:1069-1076.

Chiu, J., P.E. March, R. Lee, and D. Tillett. 2004. Site-directed, Ligase-Independent Mutagenesis (SLIM): a single-tube methodology approaching 100% efficiency in 4 h. *Nucleic Acids Res* 32:e174.

Cresswell, P., A.L. Ackerman, A. Giodini, D.R. Peaper, and P.A. Wearsch. 2005. Mechanisms of MHC class I-restricted antigen processing and cross-presentation. *Immunol Rev* 207:145-157.

Danilczyk, U.G., M.F. Cohen-Doyle, and D.B. Williams. 2000. Functional relationship between calreticulin, calnexin, and the endoplasmic reticulum luminal domain of calnexin. *J Biol Chem* 275:13089-13097.

Del Cid, N., E. Jeffery, S.M. Rizvi, E. Stamper, L.R. Peters, W.C. Brown, C. Provoda, and M. Raghavan. 2010. Modes of calreticulin recruitment to the major histocompatibility complex class I assembly pathway. *J Biol Chem* 285:4520-4535.

del Rio, M.L., J.I. Rodriguez-Barbosa, E. Kremmer, and R. Forster. 2007. CD103- and CD103+ bronchial lymph node dendritic cells are specialized in presenting and cross-presenting innocuous antigen to CD4+ and CD8+ T cells. *J Immunol* 178:6861-6866.

Delneste, Y. 2004. Scavenger receptors and heat-shock protein-mediated antigen cross-presentation. *Biochem Soc Trans* 32:633-635.

den Haan, J.M., S.M. Lehar, and M.J. Bevan. 2000. CD8(+) but not CD8(-) dendritic cells cross-prime cytotoxic T cells in vivo. *J Exp Med* 192:1685-1696.

Desch, A.N., G.J. Randolph, K. Murphy, E.L. Gautier, R.M. Kedl, M.H. Lahoud, I. Caminschi, K. Shortman, P.M. Henson, and C.V. Jakubzick. 2011. CD103+ pulmonary dendritic cells preferentially acquire and present apoptotic cell-associated antigen. *J Exp Med* 208:1789-1797.

Dick, T.P., N. Bangia, D.R. Peaper, and P. Cresswell. 2002. Disulfide bond isomerization and the assembly of MHC class I-peptide complexes. *immunity* 16:87-98.

Diedrich, G., N. Bangia, M. Pan, and P. Cresswell. 2001. A role for calnexin in the assembly of the MHC class I loading complex in the endoplasmic reticulum. *J Immunol* 166:1703-1709.

Dolan, B.P., K.D. Gibbs, Jr., and S. Ostrand-Rosenberg. 2006. Dendritic cells cross-dressed with peptide MHC class I complexes prime CD8+ T cells. *J Immunol* 177:6018-6024.

Dong, G., P.A. Wearsch, D.R. Peaper, P. Cresswell, and K.M. Reinisch. 2009. Insights into MHC class I peptide loading from the structure of the tapasin-ERp57 thiol oxidoreductase heterodimer. *Immunity* 30:21-32.

Ellgaard, L., P. Bettendorff, D. Braun, T. Herrmann, F. Fiorito, I. Jelesarov, P. Guntert, A. Helenius, and K. Wuthrich. 2002. NMR structures of 36 and 73-residue fragments of the calreticulin P-domain. *J Mol Biol* 322:773-784.

Ernst, B., D.S. Lee, J.M. Chang, J. Sprent, and C.D. Surh. 1999. The peptide ligands mediating positive selection in the thymus control T cell survival and homeostatic proliferation in the periphery. *Immunity* 11:173-181.

Erwig, L.P., and P.M. Henson. 2008. Clearance of apoptotic cells by phagocytes. *Cell Death Differ* 15:243-250.

Fadel, M.P., E. Dziak, C.M. Lo, J. Ferrier, N. Mesaeli, M. Michalak, and M. Opas. 1999. Calreticulin affects focal contact-dependent but not close contact-dependent cell-substratum adhesion. *J Biol Chem* 274:15085-15094.

Frickel, E.M., R. Riek, I. Jelesarov, A. Helenius, K. Wuthrich, and L. Ellgaard. 2002. TROSY-NMR reveals interaction between ERp57 and the tip of the calreticulin P-domain. *Proc Natl Acad Sci U S A* 99:1954-1959.

Frleta, D., C.I. Yu, E. Klechevsky, A.L. Flamar, G. Zurawski, J. Banchereau, and A.K. Palucka. 2009. Influenza virus and poly(I:C) inhibit MHC class I-restricted presentation of cell-associated antigens derived from infected dead cells captured by human dendritic cells. *J Immunol* 182:2766-2776.

Gabathuler, R., G. Reid, G. Kolaitis, J. Driscoll, and W.A. Jefferies. 1994. Comparison of cell lines deficient in antigen presentation reveals a functional role for TAP-1 alone in antigen processing. *J Exp Med* 180:1415-1425.

Gao, B., R. Adhikari, M. Howarth, K. Nakamura, M.C. Gold, A.B. Hill, R. Knee, M. Michalak, and T. Elliott. 2002. Assembly and antigen-presenting function of

MHC class I molecules in cells lacking the ER chaperone calreticulin. *Immunity* 16:99-109.

Garbi, N., P. Tan, A.D. Diehl, B.J. Chambers, H.G. Ljunggren, F. Momburg, and G.J. Hammerling. 2000. Impaired immune responses and altered peptide repertoire in tapasin-deficient mice. *Nat Immunol* 1:234-238.

Garbi, N., S. Tanaka, F. Momburg, and G.J. Hammerling. 2006. Impaired assembly of the major histocompatibility complex class I peptide-loading complex in mice deficient in the oxidoreductase ERp57. *Nat Immunol* 7:93-102.

Gardai, S.J., D.L. Bratton, C.A. Ogden, and P.M. Henson. 2006. Recognition ligands on apoptotic cells: a perspective. *J Leukoc Biol* 79:896-903.

Gardai, S.J., K.A. McPhillips, S.C. Frasch, W.J. Janssen, A. Starefeldt, J.E. Murphy-Ullrich, D.L. Bratton, P.A. Oldenborg, M. Michalak, and P.M. Henson. 2005. Cell-surface calreticulin initiates clearance of viable or apoptotic cells through trans-activation of LRP on the phagocyte. *Cell* 123:321-334.

Garg, A.D., D.V. Krysko, T. Verfaillie, A. Kaczmarek, G.B. Ferreira, T. Marysael, N. Rubio, M. Firczuk, C. Mathieu, A.J. Roebroek, W. Annaert, J. Golab, P. de Witte, P. Vandenabeele, and P. Agostinis. 2012. A novel pathway combining calreticulin exposure and ATP secretion in immunogenic cancer cell death. *EMBO J*

Ghiringhelli, F., L. Apetoh, A. Tesniere, L. Aymeric, Y. Ma, C. Ortiz, K. Vermaelen, T. Panaretakis, G. Mignot, E. Ullrich, J.L. Perfettini, F. Schlemmer, E. Tasdemir, M. Uhl, P. Genin, A. Civas, B. Ryffel, J. Kanellopoulos, J. Tschopp, F. Andre, R. Lidereau, N.M. McLaughlin, N.M. Haynes, M.J. Smyth, G. Kroemer, and L. Zitvogel. 2009. Activation of the NLRP3 inflammasome in dendritic cells induces IL-1beta-dependent adaptive immunity against tumors. *Nat Med* 15:1170-1178.

Goldrath, A.W., and M.J. Bevan. 1999. Low-affinity ligands for the TCR drive proliferation of mature CD8+ T cells in lymphopenic hosts. *Immunity* 11:183-190.

Goldszmid, R.S., I. Coppens, A. Lev, P. Caspar, I. Mellman, and A. Sher. 2009. Host ER-parasitophorous vacuole interaction provides a route of entry for antigen cross-presentation in Toxoplasma gondii-infected dendritic cells. *J Exp Med* 206:399-410.

Gopalakrishnapai, J., G. Gupta, T. Karthikeyan, S. Sinha, E. Kandiah, E. Gemma, S. Oscarson, and A. Surolia. 2006. Isothermal titration calorimetric study defines the substrate binding residues of calreticulin. *Biochem Biophys Res Commun* 351:14-20.

Grandea, A.G., 3rd, T.N. Golovina, S.E. Hamilton, V. Sriram, T. Spies, R.R. Brutkiewicz, J.T. Harty, L.C. Eisenlohr, and L. Van Kaer. 2000. Impaired assembly yet normal trafficking of MHC class I molecules in Tapasin mutant mice. *Immunity* 13:213-222.

Grivennikov, S.I., F.R. Greten, and M. Karin. 2010. Immunity, inflammation, and cancer. *Cell* 140:883-899.

Hammer, G.E., F. Gonzalez, M. Champsaur, D. Cado, and N. Shastri. 2006. The aminopeptidase ERAAP shapes the peptide repertoire displayed by major histocompatibility complex class I molecules. *Nat Immunol* 7:103-112.

Harris, M.R., Y.Y. Yu, C.S. Kindle, T.H. Hansen, and J.C. Solheim. 1998. Calreticulin and calnexin interact with different protein and glycan determinants during the assembly of MHC class I. *J Immunol* 160:5404-5409.

Harshyne, L.A., S.C. Watkins, A. Gambotto, and S.M. Barratt-Boyes. 2001. Dendritic cells acquire antigens from live cells for cross-presentation to CTL. *J Immunol* 166:3717-3723.

Hogquist, K.A., S.C. Jameson, W.R. Heath, J.L. Howard, M.J. Bevan, and F.R. Carbone. 1994. T cell receptor antagonist peptides induce positive selection. *Cell* 76:17-27.

Hoshino, K., O. Takeuchi, T. Kawai, H. Sanjo, T. Ogawa, Y. Takeda, K. Takeda, and S. Akira. 1999. Cutting edge: Toll-like receptor 4 (TLR4)-deficient mice are hyporesponsive to lipopolysaccharide: evidence for TLR4 as the Lps gene product. *J Immunol* 162:3749-3752.

Hoves, S., J.A. Trapani, and I. Voskoboinik. 2010. The battlefield of perforin/granzyme cell death pathways. *J Leukoc Biol* 87:237-243.

Howarth, M., A. Williams, A.B. Tolstrup, and T. Elliott. 2004. Tapasin enhances MHC class I peptide presentation according to peptide half-life. *Proc Natl Acad Sci U S A* 101:11737-11742.

Howe, C., M. Garstka, M. Al-Balushi, E. Ghanem, A.N. Antoniou, S. Fritzsche, G. Jankevicius, N. Kontouli, C. Schneeweiss, A. Williams, T. Elliott, and S. Springer. 2009. Calreticulin-dependent recycling in the early secretory pathway mediates optimal peptide loading of MHC class I molecules. *EMBO J* 28:3730-3744.

Ireland, B.S., U. Brockmeier, C.M. Howe, T. Elliott, and D.B. Williams. 2008. Lectin-deficient calreticulin retains full functionality as a chaperone for class I histocompatibility molecules. *Mol Biol Cell* 19:2413-2423.

Jeffery, E., L.R. Peters, and M. Raghavan. 2010. The polypeptide binding conformation of calreticulin facilitates its cell surface expression under conditions of ER stress. *J Biol Chem*

Jessop, C.E., S. Chakravarthi, N. Garbi, G.J. Hammerling, S. Lovell, and N.J. Bulleid. 2007. ERp57 is essential for efficient folding of glycoproteins sharing common structural domains. *EMBO J* 26:28-40.

Jin, H., Z. Hong, W. Su, and J. Li. 2009. A plant-specific calreticulin is a key retention factor for a defective brassinosteroid receptor in the endoplasmic reticulum. *Proc Natl Acad Sci U S A* 106:13612-13617.

Jorgensen, C.S., L.R. Ryder, A. Steino, P. Hojrup, J. Hansen, N.H. Beyer, N.H. Heegaard, and G. Houen. 2003. Dimerization and oligomerization of the chaperone calreticulin. *Eur J Biochem* 270:4140-4148.

Jung, S., D. Unutmaz, P. Wong, G. Sano, K. De los Santos, T. Sparwasser, S. Wu, S. Vuthoori, K. Ko, F. Zavala, E.G. Pamer, D.R. Littman, and R.A. Lang. 2002. In vivo depletion of CD11c+ dendritic cells abrogates priming of CD8+ T cells by exogenous cell-associated antigens. *Immunity* 17:211-220.

Kapoor, M., L. Ellgaard, J. Gopalakrishnapai, C. Schirra, E. Gemma, S. Oscarson, A. Helenius, and A. Surolia. 2004. Mutational analysis provides molecular insight into the carbohydrate-binding region of calreticulin: pivotal roles of tyrosine-109 and aspartate-135 in carbohydrate recognition. *Biochemistry* 43:97-106.

Karttunen, J., S. Sanderson, and N. Shastri. 1992. Detection of rare antigen-presenting cells by the lacZ T-cell activation assay suggests an expression cloning strategy for T-cell antigens. *Proc Natl Acad Sci U S A* 89:6020-6024.

Kepp, O., L. Galluzzi, I. Martins, F. Schlemmer, S. Adjemian, M. Michaud, A.Q. Sukkurwala, L. Menger, L. Zitvogel, and G. Kroemer. 2011. Molecular determinants of immunogenic cell death elicited by anticancer chemotherapy. *Cancer Metastasis Rev* 30:61-69.

Kienast, A., M. Preuss, M. Winkler, and T.P. Dick. 2007. Redox regulation of peptide receptivity of major histocompatibility complex class I molecules by ERp57 and tapasin. *Nat Immunol* 8:864-872.

Kieper, W.C., and S.C. Jameson. 1999. Homeostatic expansion and phenotypic conversion of naive T cells in response to self peptide/MHC ligands. *Proc Natl Acad Sci U S A* 96:13306-13311.

Koller, B.H., P. Marrack, J.W. Kappler, and O. Smithies. 1990. Normal development of mice deficient in beta 2M, MHC class I proteins, and CD8+ T cells. *Science* 248:1227-1230.

Kozlov, G., C.L. Pocanschi, A. Rosenauer, S. Bastos-Aristizabal, A. Gorelik, D.B. Williams, and K. Gehring. 2010. Structural basis of carbohydrate recognition by calreticulin. *J Biol Chem* 285:38612-38620.

Kuraishi, T., J. Manaka, M. Kono, H. Ishii, N. Yamamoto, K. Koizumi, A. Shiratsuchi, B.L. Lee, H. Higashida, and Y. Nakanishi. 2007. Identification of calreticulin as a marker for phagocytosis of apoptotic cells in Drosophila. *Exp Cell Res* 313:500-510.

Kurts, C., B.W. Robinson, and P.A. Knolle. 2010. Cross-priming in health and disease. *Nat Rev Immunol* 10:403-414.

Lee, H.I., S. Gal, T.C. Newman, and N.V. Raikhel. 1993. The Arabidopsis endoplasmic reticulum retention receptor functions in yeast. *Proc Natl Acad Sci U S A* 90:11433-11437.

Lehner, P.J., M.J. Surman, and P. Cresswell. 1998. Soluble tapasin restores MHC class I expression and function in the tapasin-negative cell line .220. *Immunity* 8:221-231.

Lev, A., P. Dimberu, S.R. Das, J.C. Maynard, C.V. Nicchitta, J.R. Bennink, and J.W. Yewdell. 2009. Efficient cross-priming of antiviral CD8+ T cells by antigen donor cells is GRP94 independent. *J Immunol* 183:4205-4210.

Li, J., C. Zhao-Hui, M. Batoux, V. Nekrasov, M. Roux, D. Chinchilla, C. Zipfel, and J.D. Jones. 2009. Specific ER quality control components required for biogenesis of the plant innate immune receptor EFR. *Proc Natl Acad Sci U S A* 106:15973-15978.

Li, Z., W.F. Stafford, and M. Bouvier. 2001. The metal ion binding properties of calreticulin modulate its conformational flexibility and thermal stability. *Biochemistry* 40:11193-11201.

Lin, M.L., Y. Zhan, A.I. Proietto, S. Prato, L. Wu, W.R. Heath, J.A. Villadangos, and A.M. Lew. 2008. Selective suicide of cross-presenting CD8+ dendritic cells by cytochrome c injection shows functional heterogeneity within this subset. *Proc Natl Acad Sci U S A* 105:3029-3034.

Lindquist, J.A., G.J. Hammerling, and J. Trowsdale. 2001. ER60/ERp57 forms disulfide-bonded intermediates with MHC class I heavy chain. *FASEB J* 15:1448-1450.

Liu, J., K.Y. Chen, and E.C. Ren. 2011. Structural insights into the binding of hepatitis B virus core peptide to HLA-A2 alleles: towards designing better vaccines. *Eur J Immunol* 41:2097-2106.

Lo, M.C., A. Aulabaugh, G. Jin, R. Cowling, J. Bard, M. Malamas, and G. Ellestad. 2004. Evaluation of fluorescence-based thermal shift assays for hit identification in drug discovery. *Anal Biochem* 332:153-159.

Luckashenak, N., S. Schroeder, K. Endt, D. Schmidt, K. Mahnke, M.F. Bachmann, P. Marconi, C.A. Deeg, and T. Brocker. 2008. Constitutive crosspresentation of tissue antigens by dendritic cells controls CD8+ T cell tolerance in vivo. *Immunity* 28:521-532.

Lybarger, L., X. Wang, M.R. Harris, H.W.t. Virgin, and T.H. Hansen. 2003. Virus subversion of the MHC class I peptide-loading complex. *Immunity* 18:121-130.

Mahadevan, N.R., J. Rodvold, H. Sepulveda, S. Rossi, A.F. Drew, and M. Zanetti. 2011. Transmission of endoplasmic reticulum stress and pro-inflammation from tumor cells to myeloid cells. *Proc Natl Acad Sci U S A* 108:6561-6566.

Malawski, G.A., R.C. Hillig, F. Monteclaro, U. Eberspaecher, A.A. Schmitz, K. Crusius, M. Huber, U. Egner, P. Donner, and B. Muller-Tiemann. 2006. Identifying protein construct variants with increased crystallization propensity--a case study. *Protein Sci* 15:2718-2728.

Mantegazza, A.R., A. Savina, M. Vermeulen, L. Perez, J. Geffner, O. Hermine, S.D. Rosenzweig, F. Faure, and S. Amigorena. 2008. NADPH oxidase controls phagosomal pH and antigen cross-presentation in human dendritic cells. *Blood* 112:4712-4722.

Martin, V., J. Groenendyk, S.S. Steiner, L. Guo, M. Dabrowska, J.M. Parker, W. Muller-Esterl, M. Opas, and M. Michalak. 2006. Identification by mutational analysis of amino acid residues essential in the chaperone function of calreticulin. *J Biol Chem* 281:2338-2346.

Martins, I., O. Kepp, L. Galluzzi, L. Senovilla, F. Schlemmer, S. Adjemian, L. Menger, M. Michaud, L. Zitvogel, and G. Kroemer. 2010. Surface-exposed calreticulin in the interaction between dying cells and phagocytes. *Ann N Y Acad Sci* 1209:77-82.

Mazzarella, R.A., M. Srinivasan, S.M. Haugejorden, and M. Green. 1990. ERp72, an abundant luminal endoplasmic reticulum protein, contains three copies of the active site sequences of protein disulfide isomerase. *J Biol Chem* 265:1094-1101.

Mesaeli, N., K. Nakamura, E. Zvaritch, P. Dickie, E. Dziak, K.H. Krause, M. Opas, D.H. MacLennan, and M. Michalak. 1999. Calreticulin is essential for cardiac development. *J Cell Biol* 144:857-868.

Michalak, M., J. Groenendyk, E. Szabo, L.I. Gold, and M. Opas. 2009. Calreticulin, a multi-process calcium-buffering chaperone of the endoplasmic reticulum. *Biochem J* 417:651-666.

Michel, E., K.A. Reich, R. Favier, P. Berche, and P. Cossart. 1990. Attenuated mutants of the intracellular bacterium Listeria monocytogenes obtained by single amino acid substitutions in listeriolysin O. *Mol Microbiol* 4:2167-2178.

Miles, J.J., A.M. Bulek, D.K. Cole, E. Gostick, A.J. Schauenburg, G. Dolton, V. Venturi, M.P. Davenport, M.P. Tan, S.R. Burrows, L. Wooldridge, D.A. Price, P.J. Rizkallah, and A.K. Sewell. 2010. Genetic and structural basis for selection of a ubiquitous T cell receptor deployed in Epstein-Barr virus infection. *PLoS Pathog* 6:e1001198.

Molinari, M., K.K. Eriksson, V. Calanca, C. Galli, P. Cresswell, M. Michalak, and A. Helenius. 2004. Contrasting functions of calreticulin and calnexin in glycoprotein folding and ER quality control. *Mol Cell* 13:125-135.

Murshid, A., J. Gong, and S.K. Calderwood. 2010. Heat shock protein 90 mediates efficient antigen cross presentation through the scavenger receptor expressed by endothelial cells-I. *J Immunol* 185:2903-2917.

Nair, S., P.A. Wearsch, D.A. Mitchell, J.J. Wassenberg, E. Gilboa, and C.V. Nicchitta. 1999. Calreticulin displays in vivo peptide-binding activity and can elicit CTL responses against bound peptides. *J Immunol* 162:6426-6432.

Nakamura, K., E. Bossy-Wetzel, K. Burns, M.P. Fadel, M. Lozyk, I.S. Goping, M. Opas, R.C. Bleackley, D.R. Green, and M. Michalak. 2000. Changes in endoplasmic reticulum luminal environment affect cell sensitivity to apoptosis. *J Cell Biol* 150:731-740.

Nakamura, K., A. Zuppini, S. Arnaudeau, J. Lynch, I. Ahsan, R. Krause, S. Papp, H. De Smedt, J.B. Parys, W. Muller-Esterl, D.P. Lew, K.H. Krause, N. Demaurex, M.

Opas, and M. Michalak. 2001. Functional specialization of calreticulin domains. *J Cell Biol* 154:961-972.

Nanney, L.B., C.D. Woodrell, M.R. Greives, N.L. Cardwell, A.C. Pollins, T.A. Bancroft, A. Chesser, M. Michalak, M. Rahman, J.W. Siebert, and L.I. Gold. 2008. Calreticulin enhances porcine wound repair by diverse biological effects. *Am J Pathol* 173:610-630.

Obeid, M., T. Panaretakis, N. Joza, R. Tufi, A. Tesniere, P. van Endert, L. Zitvogel, and G. Kroemer. 2007a. Calreticulin exposure is required for the immunogenicity of gamma-irradiation and UVC light-induced apoptosis. *Cell Death Differ* 14:1848-1850.

Obeid, M., A. Tesniere, F. Ghiringhelli, G.M. Fimia, L. Apetoh, J.L. Perfettini, M. Castedo, G. Mignot, T. Panaretakis, N. Casares, D. Metivier, N. Larochette, P. van Endert, F. Ciccosanti, M. Piacentini, L. Zitvogel, and G. Kroemer. 2007b. Calreticulin exposure dictates the immunogenicity of cancer cell death. *Nat Med* 13:54-61.

Oldenborg, P.A., A. Zheleznyak, Y.F. Fang, C.F. Lagenaur, H.D. Gresham, and F.P. Lindberg. 2000. Role of CD47 as a marker of self on red blood cells. *Science* 288:2051-2054.

Oliver, J.D., H.L. Roderick, D.H. Llewellyn, and S. High. 1999. ERp57 functions as a subunit of specific complexes formed with the ER lectins calreticulin and calnexin. *Mol Biol Cell* 10:2573-2582.

Ortmann, B., M.J. Androlewicz, and P. Cresswell. 1994. MHC class I/beta 2-microglobulin complexes associate with TAP transporters before peptide binding. *Nature* 368:864-867.

Paidassi, H., P. Tacnet-Delorme, M. Verneret, C. Gaboriaud, G. Houen, K. Duus, W.L. Ling, G.J. Arlaud, and P. Frachet. 2011. Investigations on the C1q-calreticulin-phosphatidylserine interactions yield new insights into apoptotic cell recognition. *J Mol Biol* 408:277-290.

Park, J.S., J. Arcaroli, H.K. Yum, H. Yang, H. Wang, K.Y. Yang, K.H. Choe, D. Strassheim, T.M. Pitts, K.J. Tracey, and E. Abraham. 2003. Activation of gene expression in

human neutrophils by high mobility group box 1 protein. *Am J Physiol Cell Physiol* 284:C870-879.

Park, J.S., D. Svetkauskaite, Q. He, J.Y. Kim, D. Strassheim, A. Ishizaka, and E. Abraham. 2004. Involvement of toll-like receptors 2 and 4 in cellular activation by high mobility group box 1 protein. *J Biol Chem* 279:7370-7377.

Pawaria, S., and R.J. Binder. 2011. CD91-dependent programming of T-helper cell responses following heat shock protein immunization. *Nat Commun* 2:521.

Peaper, D.R., and P. Cresswell. 2008. Regulation of MHC class I assembly and peptide binding. *Annu Rev Cell Dev Biol* 24:343-368.

Peaper, D.R., P.A. Wearsch, and P. Cresswell. 2005. Tapasin and ERp57 form a stable disulfide-linked dimer within the MHC class I peptide-loading complex. *EMBO J* 24:3613-3623.

Peng, Y., and K.B. Elkon. 2011. Autoimmunity in MFG-E8-deficient mice is associated with altered trafficking and enhanced cross-presentation of apoptotic cell antigens. *J Clin Invest* 121:2221-2241.

Persson, S., M. Rosenquist, K. Svensson, R. Galvao, W.F. Boss, and M. Sommarin. 2003. Phylogenetic analyses and expression studies reveal two distinct groups of calreticulin isoforms in higher plants. *Plant Physiol* 133:1385-1396.

Peters, L.R., and M. Raghavan. 2011. Endoplasmic Reticulum Calcium Depletion Impacts Chaperone Secretion, Innate Immunity, and Phagocytic Uptake of Cells. *J Immunol*

Peterson, J.R., A. Ora, P.N. Van, and A. Helenius. 1995. Transient, lectin-like association of calreticulin with folding intermediates of cellular and viral glycoproteins. *Mol Biol Cell* 6:1173-1184.

Pocanschi, C.L., G. Kozlov, U. Brockmeier, A. Brockmeier, D.B. Williams, and K. Gehring. 2011. Structural and functional relationships between the lectin and arm domains of calreticulin. *J Biol Chem* 286:27266-27277.

Poltorak, A., X. He, I. Smirnova, M.Y. Liu, C. Van Huffel, X. Du, D. Birdwell, E. Alejos, M. Silva, C. Galanos, M. Freudenberg, P. Ricciardi-Castagnoli, B. Layton, and B.

Beutler. 1998. Defective LPS signaling in C3H/HeJ and C57BL/10ScCr mice: mutations in Tlr4 gene. *Science* 282:2085-2088.

Procko, E., and R. Gaudet. 2009. Antigen processing and presentation: TAPping into ABC transporters. *Curr Opin Immunol* 21:84-91.

Qiu, C.H., Y. Miyake, H. Kaise, H. Kitamura, O. Ohara, and M. Tanaka. 2009. Novel subset of CD8{alpha}+ dendritic cells localized in the marginal zone is responsible for tolerance to cell-associated antigens. *J Immunol* 182:4127-4136.

Qiu, Y., J. Xi, L. Du, S. Roje, and B.W. Poovaiah. 2012. A dual regulatory role of Arabidopsis calreticulin-2 in plant innate immunity. *Plant J* 69:489-500.

Qu, C., V.A. Nguyen, M. Merad, and G.J. Randolph. 2009. MHC class I/peptide transfer between dendritic cells overcomes poor cross-presentation by monocyte-derived APCs that engulf dying cells. *J Immunol* 182:3650-3659.

Raghavan, M., N. Del Cid, S.M. Rizvi, and L.R. Peters. 2008. MHC class I assembly: out and about. *Trends Immunol* 29:436-443.

Ravichandran, K.S. 2011. Beginnings of a good apoptotic meal: the find-me and eat-me signaling pathways. *Immunity* 35:445-455.

Rizvi, S.M., N. Del Cid, L. Lybarger, and M. Raghavan. 2011. Distinct functions for the glycans of tapasin and heavy chains in the assembly of MHC class I molecules. *J Immunol* 186:2309-2320.

Rizvi, S.M., L. Mancino, V. Thammavongsa, R.L. Cantley, and M. Raghavan. 2004. A polypeptide binding conformation of calreticulin is induced by heat shock, calcium depletion, or by deletion of the C-terminal acidic region. *Mol Cell* 15:913-923.

Rizvi, S.M., and M. Raghavan. 2006. Direct peptide-regulatable interactions between MHC class I molecules and tapasin. *Proc Natl Acad Sci U S A* 103:18220-18225.

Rizvi, S.M., and M. Raghavan. 2010. Mechanisms of function of tapasin, a critical major histocompatibility complex class I assembly factor. *Traffic* 11:332-347.

Robinson, A., C. Meredith, and B.M. Austen. 1986. Isolation and properties of the signal region from ovalbumin. *FEBS Lett* 203:243-246.

Rose-John, S., H. Schooltink, H. Schmitz-Van de Leur, J. Mullberg, P.C. Heinrich, and L. Graeve. 1993. Intracellular retention of interleukin-6 abrogates signaling. *J Biol Chem* 268:22084-22091.

Russell, S.J., L.W. Ruddock, K.E. Salo, J.D. Oliver, Q.P. Roebuck, D.H. Llewellyn, H.L. Roderick, P. Koivunen, J. Myllyharju, and S. High. 2004. The primary substrate binding site in the b' domain of ERp57 is adapted for endoplasmic reticulum lectin association. *J Biol Chem* 279:18861-18869.

Rutkevich, L.A., and D.B. Williams. 2011. Participation of lectin chaperones and thiol oxidoreductases in protein folding within the endoplasmic reticulum. *Curr Opin Cell Biol* 23:157-166.

Sadasivan, B., P.J. Lehner, B. Ortmann, T. Spies, and P. Cresswell. 1996. Roles for calreticulin and a novel glycoprotein, tapasin, in the interaction of MHC class I molecules with TAP. *Immunity* 5:103-114.

Saito, Y., Y. Ihara, M.R. Leach, M.F. Cohen-Doyle, and D.B. Williams. 1999. Calreticulin functions in vitro as a molecular chaperone for both glycosylated and non-glycosylated proteins. *EMBO J* 18:6718-6729.

Saveanu, L., O. Carroll, M. Weimershaus, P. Guermonprez, E. Firat, V. Lindo, F. Greer, J. Davoust, R. Kratzer, S.R. Keller, G. Niedermann, and P. van Endert. 2009. IRAP identifies an endosomal compartment required for MHC class I cross-presentation. *Science* 325:213-217.

Savina, A., A. Peres, I. Cebrian, N. Carmo, C. Moita, N. Hacohen, L.F. Moita, and S. Amigorena. 2009. The small GTPase Rac2 controls phagosomal alkalinization and antigen crosspresentation selectively in CD8(+) dendritic cells. *Immunity* 30:544-555.

Schafer, A., and D.H. Wolf. 2009. Sec61p is part of the endoplasmic reticulum-associated degradation machinery. *EMBO J* 28:2874-2884.

Schrag, J.D., J.J. Bergeron, Y. Li, S. Borisova, M. Hahn, D.Y. Thomas, and M. Cygler. 2001. The Structure of calnexin, an ER chaperone involved in quality control of protein folding. *Mol Cell* 8:633-644.

Schreibelt, G., L.J. Klinkenberg, L.J. Cruz, P.J. Tacken, J. Tel, M. Kreutz, G.J. Adema, G.D. Brown, C.G. Figdor, and I.J. de Vries. 2012. The C type lectin receptor CLEC9A mediates antigen uptake and (cross-)presentation by human blood BDCA3+ myeloid dendritic cells. *Blood*

Schuerch, D.W., E.M. Wilson-Kubalek, and R.K. Tweten. 2005. Molecular basis of listeriolysin O pH dependence. *Proc Natl Acad Sci U S A* 102:12537-12542.

Segura, E., A.L. Albiston, I.P. Wicks, S.Y. Chai, and J.A. Villadangos. 2009. Different cross-presentation pathways in steady-state and inflammatory dendritic cells. *Proc Natl Acad Sci U S A* 106:20377-20381.

Sijts, E.J., and P.M. Kloetzel. 2011. The role of the proteasome in the generation of MHC class I ligands and immune responses. *Cell Mol Life Sci* 68:1491-1502.

Sille, F.C., A. Visser, and M. Boes. 2005. T cell priming by tissue-derived dendritic cells: new insights from recent murine studies. *Cell Immunol* 237:77-85.

Silvennoinen, L., J. Myllyharju, M. Ruoppolo, S. Orru, M. Caterino, K.I. Kivirikko, and P. Koivunen. 2004. Identification and characterization of structural domains of human ERp57: association with calreticulin requires several domains. *J Biol Chem* 279:13607-13615.

Sonnichsen, B., J. Fullekrug, P. Nguyen Van, W. Diekmann, D.G. Robinson, and G. Mieskes. 1994. Retention and retrieval: both mechanisms cooperate to maintain calreticulin in the endoplasmic reticulum. *J Cell Sci* 107 (Pt 10):2705-2717.

Spiro, R.G., Q. Zhu, V. Bhoyroo, and H.D. Soling. 1996. Definition of the lectin-like properties of the molecular chaperone, calreticulin, and demonstration of its copurification with endomannosidase from rat liver Golgi. *J Biol Chem* 271:11588-11594.

Stols, L., M. Gu, L. Dieckman, R. Raffen, F.R. Collart, and M.I. Donnelly. 2002. A new vector for high-throughput, ligation-independent cloning encoding a tobacco etch virus protease cleavage site. *Protein Expr Purif* 25:8-15.

Suh, W.K., M.F. Cohen-Doyle, K. Fruh, K. Wang, P.A. Peterson, and D.B. Williams. 1994. Interaction of MHC class I molecules with the transporter associated with antigen processing. *Science* 264:1322-1326.

Tacken, P.J., W. Ginter, L. Berod, L.J. Cruz, B. Joosten, T. Sparwasser, C.G. Figdor, and A. Cambi. 2011. Targeting DC-SIGN via its neck region leads to prolonged antigen residence in early endosomes, delayed lysosomal degradation, and cross-presentation. *Blood* 118:4111-4119.

Takeuchi, O., K. Hoshino, T. Kawai, H. Sanjo, H. Takada, T. Ogawa, K. Takeda, and S. Akira. 1999. Differential roles of TLR2 and TLR4 in recognition of gram-negative and gram-positive bacterial cell wall components. *Immunity* 11:443-451.

Tarr, J.M., P.J. Young, R. Morse, D.J. Shaw, R. Haigh, P.G. Petrov, S.J. Johnson, P.G. Winyard, and P. Eggleton. 2010. A mechanism of release of calreticulin from cells during apoptosis. *J Mol Biol* 401:799-812.

Tesniere, A., F. Schlemmer, V. Boige, O. Kepp, I. Martins, F. Ghiringhelli, L. Aymeric, M. Michaud, L. Apetoh, L. Barault, J. Mendiboure, J.P. Pignon, V. Jooste, P. van Endert, M. Ducreux, L. Zitvogel, F. Piard, and G. Kroemer. 2010. Immunogenic death of colon cancer cells treated with oxaliplatin. *Oncogene* 29:482-491.

Testori, A., J. Richards, E. Whitman, G.B. Mann, J. Lutzky, L. Camacho, G. Parmiani, G. Tosti, J.M. Kirkwood, A. Hoos, L. Yuh, R. Gupta, and P.K. Srivastava. 2008. Phase III comparison of vitespen, an autologous tumor-derived heat shock protein gp96 peptide complex vaccine, with physician's choice of treatment for stage IV melanoma: the C-100-21 Study Group. *J Clin Oncol* 26:955-962.

Thastrup, O., P.J. Cullen, B.K. Drobak, M.R. Hanley, and A.P. Dawson. 1990. Thapsigargin, a tumor promoter, discharges intracellular Ca2+ stores by specific inhibition of the endoplasmic reticulum Ca2(+)-ATPase. *Proc Natl Acad Sci U S A* 87:2466-2470.

Torchinsky, M.B., J. Garaude, A.P. Martin, and J.M. Blander. 2009. Innate immune recognition of infected apoptotic cells directs T(H)17 cell differentiation. *Nature* 458:78-82.

Tsan, M.F., and B. Gao. 2009. Heat shock proteins and immune system. *J Leukoc Biol* 85:905-910.

Van Parijs, L., Y. Refaeli, J.D. Lord, B.H. Nelson, A.K. Abbas, and D. Baltimore. 1999. Uncoupling IL-2 signals that regulate T cell proliferation, survival, and Fas-mediated activation-induced cell death. *Immunity* 11:281-288.

Van Parijs, L., Y. Refaeli, J.D. Lord, B.H. Nelson, A.K. Abbas, and D. Baltimore. 2009. Retraction. Uncoupling IL-2 signals that regulate T cell proliferation, survival, and Fas-mediated activation-induced cell death. *Immunity* 30:611.

Verhoven, B., R.A. Schlegel, and P. Williamson. 1995. Mechanisms of phosphatidylserine exposure, a phagocyte recognition signal, on apoptotic T lymphocytes. *J Exp Med* 182:1597-1601.

Wagner, C.S., and P. Cresswell. 2012. TLR and Nucleotide-Binding Oligomerization Domain-like Receptor Signals Differentially Regulate Exogenous Antigen Presentation. *J Immunol* 188:686-693.

Wakim, L.M., and M.J. Bevan. 2011. Cross-dressed dendritic cells drive memory CD8(+) T-cell activation after viral infection. *Nature* 471:629-632.

Ware, F.E., A. Vassilakos, P.A. Peterson, M.R. Jackson, M.A. Lehrman, and D.B. Williams. 1995. The molecular chaperone calnexin binds Glc1Man9GlcNAc2 oligosaccharide as an initial step in recognizing unfolded glycoproteins. *J Biol Chem* 270:4697-4704.

Wearsch, P.A., and P. Cresswell. 2007. Selective loading of high-affinity peptides onto major histocompatibility complex class I molecules by the tapasin-ERp57 heterodimer. *Nat Immunol* 8:873-881.

Wearsch, P.A., and P. Cresswell. 2008. The quality control of MHC class I peptide loading. *Curr Opin Cell Biol* 20:624-631.

Wearsch, P.A., C.A. Jakob, A. Vallin, R.A. Dwek, P.M. Rudd, and P. Cresswell. 2004. Major histocompatibility complex class I molecules expressed with

monoglucosylated N-linked glycans bind calreticulin independently of their assembly status. *J Biol Chem* 279:25112-25121.

Wearsch, P.A., D.R. Peaper, and P. Cresswell. 2011. Essential glycan-dependent interactions optimize MHC class I peptide loading. *Proc Natl Acad Sci U S A* 108:4950-4955.

Wijeyesakere, S.J., A.A. Gafni, and M. Raghavan. 2011. Calreticulin is a thermostable protein with distinct structural responses to different divalent cation environments. *J Biol Chem* 286:8771-8785.

Wolf, P.R., and H.L. Ploegh. 1995. How MHC class II molecules acquire peptide cargo: biosynthesis and trafficking through the endocytic pathway. *Annu Rev Cell Dev Biol* 11:267-306.

Zhang, N., and M.J. Bevan. 2011. CD8(+) T cells: foot soldiers of the immune system. *Immunity* 35:161-168.

Zhang, Y., G. Kozlov, C.L. Pocanschi, U. Brockmeier, B.S. Ireland, P. Maattanen, C. Howe, T. Elliott, K. Gehring, and D.B. Williams. 2009. ERp57 does not require interactions with calnexin and calreticulin to promote assembly of class I histocompatibility molecules, and it enhances peptide loading independently of its redox activity. *J Biol Chem* 284:10160-10173.